

$\omega$ -ALKYNYL FATTY ACIDS: SURROGATES TO STUDY PROTEIN  
ADDITION BY ENDOGENOUSLY GENERATED  
LIPID ELECTROPHILES

By

William Norris Beavers Jr.

Dissertation

Submitted to the Faculty of the  
Graduate School of Vanderbilt University  
in partial fulfillment of the requirements

for the degree of

DOCTOR OF PHILOSOPHY

in

Chemistry

August, 2015

Nashville, Tennessee

Approved:

Lawrence J. Marnett, Ph.D.

Brian O. Bachmann, Ph.D.

H. Alex Brown, Ph.D.

Sean S. Davies, Ph.D.

Ned A. Porter, Ph.D.

## DEDICATION

To my wife Liz, and our daughters Pearson, Kate, and Nora. None of this would have been possible without your unconditional love and endless support.

## ACKNOWLEDGEMENTS

First I would like to thank my mentor Larry Marnett. Larry has provided me with every resource necessary to be a successfully scientist. I have been able to do any experiment I can dream. He has also shown a lot of patience. We have suffered many set backs and delays getting to the point where we are currently with this project, but he has always been patient when others might have chosen to “cut our losses”, and move in a different direction. Larry has also struck the delicate balance between pushing me hard to succeed, and giving me the freedom to drive my project in a direction I saw fit; allowing me to make mistakes and fix those mistakes. It has made the process full of learning pains at times, but I feel well prepared for future scientific challenges.

I would like to thank the other members of my committee as well. Brian Bachmann, Alex Brown, Sean Davies, and Ned Porter have spent many hours discussing my project with me, reading my reports, and critiquing my presentations. Your comments and suggestions have been invaluable to me in my preparation to become an independent scientist.

Vanderbilt has created a culture where a chemistry graduate student can easily find assistance in other departments. I would like to thank the many members of the Vanderbilt community who have taken time to discuss various aspects of my project with me including Aaron Bowman, Alan Brash, Cathy Clarke, Simona Codreanu, Josh Fessel, David Harrison, Annet Kirabo, Dan Liebler, Stokes Peebles, Jack Roberts, Claus Schneider, and Bing Zhang.

The Marnett laboratory has a long-standing relationship with the Porter laboratory. As such, I have spent a lot of time in the Porter laboratory. First I would like to further thank Ned for taking the time to discuss various aspects of radical chemistry with me. Keri Tallman has generated an arsenal of tools that I have been fortunate to have access to, and would like to thank her greatly for the steady supply of these probes as well as all of our conversations on various aspects of my project. I would also like to thank Connor Lamberson, Libin Xu, and Huiyong Yin for help and discussions over the years.

I have been fortunate to work with the various fantastic core facilities around campus. I would like to thank Don Stec of the small molecule NMR core. I would like to thank Rob Carnahan and Matt Goff of the Vanderbilt Antibody and Protein Resource. I would like to thank Wade Calcutt, Julie Coleman, Dave Hachey, Salisha Hill, and Kristie Rose of the Mass Spectrometry Resource Center. An extra thank you is deserved by Kristie Rose, for without her hard work and expertise, there is no way we would have made as much progress on this project as we have.

I have also had the opportunity to get a lot of teaching experience. I would like to thank Larry for giving me the opportunity to guest lecture in his Foundations of Chemical Biology course. I have also been fortunate to work with the Vanderbilt Program for Talented Youth. I would like to thank Michelle Sulikowski and Brittany Allison for first introducing me to the program. I would also like to thank all of those at PTY who have helped with the courses I was a part of including Sarah DeLisle, David Dunn, Megan Parker-Peters, and Gem

Thomerson. It was a fantastic experience to design and implement courses to get young, gifted students interested in science as a career.

The administrative staff at Vanderbilt has been extremely helpful. Leigh Clayton, Stephen Doster, Sandra Ford, Celeste Gouldman, Magda Paszewska, Amanda Renick-Beech, Leigh Thompson, and Mary Veazy have made my life much easier through their help with scheduling, submitting paperwork, and submitting grants. Anne Lara deserves a special thank you. Without Anne's help, I would have been lost trying to accomplish anything. She is truly the factor that allows the Marnett laboratory to interface with the rest of the world efficiently.

I have been fortunate to work with some fantastic colleagues during my time in the Marnett lab. Thank you to all of the lemmings for comments and discussions about my project. I would also like to thank Chris Aluise, Jeannie Camarillo, Brenda Crews, Kelsey Duggan, Kebreab Ghebreselasie, Phil Kingsley, Shalley Kudalkar, Joe Manna, Michelle Mitchener, Yuki Shimozu, Sarah Shuck, Jody Ullery, Orrette Wauchope, James Wepy, and Matt Windsor specifically for work that we have done together or conversations we have had during my time in the lab. I want to thank Colleen Lawrence, who was my mentor when I first joined the lab, and introduced me to alkynyl lipid electrophiles. I would also like to thank Jim Galligan. Jim joined the laboratory shortly after Colleen left, and has helped with my day-to-day mentorship on the things needed to be successful. I have also had the opportunity to mentor several talented rotation students during my time in the Marnett laboratory. Thank you to Esha Dalvie and Nick Shelburne for being eager to learn and work hard, and also

being patient with me as I learned to mentor young scientists. Finally, I would like to thank our lemming from afar, Carol Rouzer. Larry once told me, “Carol improves everything she touches”. This statement could not be truer. Carol, I thank you for all of your comments and patience over the years as I have struggled with learning manuscript and grant writing.

I have had ample funding to pursue my project and attend scientific conferences without restriction. I would like to thank the Vanderbilt Institute for Chemical Biology Fellowship and the Hercules Fellowship from the Department of Chemistry for funding the start of my graduate career. I would like to thank the Vanderbilt Center in Molecular Toxicology Training Grant from the National Institute of Environmental Health Sciences (T32 ES007028) for two years of funding. Finally, I would like to thank the American Heart Association for two years of fellowship funding (13PRE17270009).

I have had many great mentors that have helped me grow, mature, and develop a desire for an academic life over the years. I would like to thank Joe Spicer, my high school chemistry teacher, and Mike Krepich, my high school Latin teacher for being wonderful role models during my formative years. I would like to thank my mentor at Old Dominion University, Craig Bayse, and my mentor at Northeastern University, Sunny Zhou, for helping me develop as a young scientist. I would like to thank Paul Morrison, Jim Lee, and Loren Walensky at the Dana-Farber Cancer Institute. The experience I gained working with them prepared me to be successful in graduate school.

I have an outstanding support network of family and friends, and am fortunate that there are too many to name here individually. They have always believed in me, even when my own faith has wavered, and for that I am truly grateful. I would like to specifically thank my parents. I watched my Dad get up every morning and go to a job he did not enjoy to support his family, and never complained about it. In thirty-three years, I can count on one hand the number of sick days he took, which has been a strong influence on how I approach work every morning. My Mom always encouraged us to explore and pushed us academically. She spent hours exploring in the woods and helping us with homework as children. During the summers she would indulge our curiosities with countless trips to the museums in Washington, D.C. (several hours of driving, in terrible traffic, with three rowdy boys in the back seat). These interactions with my parents have contributed greatly to my choice to pursue science as a career. I truly love coming into lab every day. What I enjoy most is that I get to be curious, learn new things every day, and think about things nobody else has.

Finally, I have to thank the people who have provided me with the daily support that I needed to make it through graduate school. I do not think I can put into words how much I appreciate the love and support my wife Liz and daughters Pearson, Kate, and Nora have given me. You have kept me motivated when I would have otherwise lost focus. You have kept me grounded when my ego would have swelled. You have been my escape when I needed one. I love you very much. Thank you.

## TABLE OF CONTENTS

	Page
DEDICATION.....	ii
ACKNOWLEDGEMENTS.....	iii
LIST OF TABLES .....	x
LIST OF FIGURES .....	xi
LIST OF ABBREVIATIONS .....	xv
Chapter	
I. INTRODUCTION.....	1
Immune Response, Inflammation, and Disease .....	1
Macrophages .....	1
Inflammation and disease .....	4
Oxidation of Polyunsaturated Fatty Acids.....	9
Polyunsaturated fatty acids .....	9
Radical mechanism of lipid oxidation .....	10
Autoxidation .....	11
Cyclooxygenases .....	15
Lipoxygenases .....	18
Lipid Electrophiles.....	21
Generation of lipid electrophiles.....	21
Reactivity of lipid electrophiles .....	24
Cellular consequences of lipid electrophile adduction .....	26
Studying lipid electrophiles in disease models .....	29
Exogenously generated lipid electrophiles.....	30
Endogenously generated lipid electrophiles.....	34
Dissertation Aims.....	37
II. $\omega$ -ALKYNYL LIPID SURROGATES FOR POLYUNSATURATED FATTY ACIDS: FREE RADICAL AND ENZYMATIC OXIDATIONS .....	40
Introduction .....	40
Materials and Methods .....	42
Results.....	53
Discussion .....	69



III. ENDOGENOUSLY GENERATED LIPID ELECTROPHILES TARGET MITOCHONDRIAL PROTEINS IN ACTIVATED RAW264.7 MACROPHAGES .....	76
Introduction .....	76
Materials and Methods .....	79
Results .....	88
Discussion .....	115
IV. PATHWAYS OF PEROXIDATION: STUDIES TO DETERMINE ROUTES OF LIPID OXIDATION AND ELECTROPHILE FORMATION.....	125
Introduction .....	125
Materials and Methods .....	130
Results .....	136
Discussion .....	149
Future Directions .....	156
V. SUMMARY/FUTURE VISIONS.....	157
Summary .....	157
Future Visions .....	164
Rotenone generation of lipid electrophile protein adducts.....	164
Identification of the site of modification of Sod2 .....	168
<i>a</i> LA <i>in vivo</i> .....	171
REFERENCES .....	174

## LIST OF TABLES

Table		Page
II-1	Kinetic comparison of AA and <i>a</i> AA with COX and LOX enzymes .....	56
II-2	<sup>1</sup> H-NMR chemical shifts and coupling constants of the COX-2 <i>a</i> AA metabolite with <i>m/z</i> = 315.2 .....	63
II-3	<sup>1</sup> H-NMR chemical shifts and coupling constants of the COX-2 <i>a</i> AA metabolite with <i>m/z</i> = 331.2 .....	63
III-1	Wikipathway enrichment for the 192 proteins in the most differentially expressed class as determined by Webgestalt .....	103
III-2	Wikipathway enrichment for the 76 proteins in the most differentially adducted class as determined by Webgestalt .....	106
IV-1	<i>R/S</i> ratios for esterified hydroxy polyunsaturated fatty acids .....	138
IV-2	Comparison of protein adduction and esterified HODEs and HETEs in macrophages with indomethacin and giripladib treatment.....	153

## LIST OF FIGURES

Figure	Page
I-1	Reactive species generated by leukocyte activation ..... 3
I-2	Common fatty acids ..... 9
I-3	Radical mechanism of lipid oxidation..... 10
I-4	General mechanism of PUFA oxidation..... 11
I-5	Autoxidation products of LA..... 13
I-6	Autoxidation of AA generates F <sub>2</sub> $\alpha$ -isoprostanes ..... 15
I-7	COX metabolism of AA..... 17
I-8	5-LOX metabolism of AA ..... 21
I-9	Structures of some commonly studied lipid electrophiles ..... 22
I-10	Adducts formed on amino acids by lipid electrophiles ..... 25
I-11	Analysis of lipid electrophile adducted proteins using click chemistry, affinity purification, and UV-cleavable biotin..... 33
II-1	Autoxidation products of LA, aLA, AA, and aAA..... 53
II-2	Chiral analysis of 13- <i>c,t</i> -HODE..... 54
II-3	s15-LOX-1 metabolism of LA, aLA, AA, and aAA..... 57
II-4	Soybean 15-LOX metabolite profiles of LA and aLA ..... 59
II-5	Comparison of the metabolite profiles of aLA and LA with s15-LOX-1 ..... 60
II-6	COX-2 <i>in vitro</i> metabolite profiles of aAA and AA ..... 61
II-7	<sup>1</sup> H- <sup>1</sup> H-COSY spectrum of the COX-2 aAA metabolite with <i>m/z</i> = 315.2..... 64
II-8	<sup>1</sup> H- <sup>1</sup> H-COSY spectrum of the COX-2 aAA metabolite with <i>m/z</i> = 331.2..... 65

II-9	Michaelis-Menten plots and relevant kinetic parameters for COX-2 metabolism of AA and aAA.....	67
II-10	Activated macrophages generate aAA metabolites .....	68
II-11	Proposed mechanism of COX-2 oxygenation of aAA.....	71
III-1	Click chemistry scheme for protein adduction .....	89
III-2	Extent of aLA incorporation into phospholipid pools.....	90
III-3	Total amounts of aLA and LA in RAW264.7 macrophages before and after aLA incorporation .....	91
III-4	aAA is biosynthesized from aLA .....	92
III-5	Total amounts of aAA and AA in RAW264.7 macrophages before and after aLA incorporation .....	93
III-6	KLA activation induces lipid electrophile protein adduction .....	94
III-7	SILAC workflow.....	96
III-8	Analysis of expression and adduction changes during KLA-activation of macrophages.....	98
III-9	Frequency counts for proteome and adductome replicates.....	99
III-10	Spearman correlation coefficients relating the proteome and adductome replicates to each other.....	101
III-11	Complex V of the electron transport chain is the most differentially expressed pathway in activated macrophages.....	104
III-12	Complex V of the electron transport chain is the most differentially adducted pathway in activated macrophages.....	106
III-13	MitoTEMPO modulates KLA-induced protein adduction, while TEMPOL does not .....	108
III-14	MitoTEMPO modulates the amount of adducted protein affinity purified in aLA-incorporated macrophages .....	109
III-15	Western blot confirmation of protein targets of lipid electrophile adduction.....	111

III-16	Activity changes associated with lipid electrophile adduction of mitochondrial proteins.....	113
III-17	Superoxide dismutase 1 and 2 expression in mitochondrial and cytosolic isolates.....	114
III-18	Absolute Sod2 activity in unactivated and activated RAW264.7 macrophage mitochondria .....	115
IV-1	Enzymatic and autoxidation products of LA.....	126
IV-2	Kinetic and thermodynamic autoxidation products of LA.....	128
IV-3	Quantification of positional and geometric isomers of esterified hydroxy polyunsaturated fatty acids .....	137
IV-4	Chiral standards and cell extracts of LA oxidation products .....	139
IV-5	Chiral standards and cell extracts of AA oxidation products.....	140
IV-6	Chiral analysis of abundant $\omega$ -alkynyl fatty acid metabolites .....	140
IV-7	Click blot and PG analysis for MitoTEMPO treated macrophages .....	141
IV-8	Click blot and PG analysis for indomethacin treated macrophages .....	142
IV-9	Click blot and PG analysis for COX-inhibited macrophages with and without PG supplementation .....	144
IV-10	Click blot and PG analysis for giripladib treated macrophages .....	145
IV-11	Quantification of esterified HODEs in indomethacin and giripladib treated macrophages .....	147
IV-12	Quantification of esterified HETEs in indomethacin and giripladib treated macrophages .....	148
IV-13	Inhibitor effects on PG synthesis and protein adduction by lipid electrophiles in macrophages .....	155
V-1	Rotenone induced protein adduction in RAW264.7 macrophages .....	165
V-2	Rotenone does not activate RAW264.7 macrophages.....	166

V-3	MitoTEMPO reduces lipid electrophile protein adduction induced by rotenone .....	167
V-4	Rotenone induces lipid electrophile protein adducts in HEK-293 cells .....	169
V-5	Sod2 is adducted by lipid electrophiles in rotenone treated HEK-293 cells .....	170
V-6	Expression and purification of Sod2-His <sub>6</sub> .....	171
V-7	Subcellular fractionation of Sod2-His <sub>6</sub> .....	171
V-8	Lipid electrophile protein adduction in <i>a</i> LA-incorporated mice treated with AngII .....	173

## LIST OF ABBREVIATIONS

1-AG	1-arachidonylglycerol
2-AG	2-arachidonylglycerol
5-LOX	arachidonate 5-lipoxygenase
8-LOX	arachidonate 8-lipoxygenase
9-LOX	linoleate 9-lipoxygenase
12-LOX	arachidonate 12-lipoxygenase
13-LOX	linoleate 13-lipoxygenase
15d-PGJ <sub>2</sub>	15-deoxy- $\Delta^{12,14}$ -prostaglandin J <sub>2</sub>
15-LOX	arachidonate 15-lipoxygenase
a11-8,9-HEET	$\omega$ -alkynyl 11-hydroxy-8,9-epoxy eicosatrienoic acid
a11-HETE	$\omega$ -alkynyl 11-hydroxy eicosatetraenoic acid
AA	arachidonic acid
aAA	$\omega$ -alkynyl arachidonic acid
AD	Alzheimer's disease
aF <sub>2</sub> $\alpha$ -isoP	$\omega$ -alkynyl F <sub>2</sub> $\alpha$ -isoprostane
aHETE	$\omega$ -alkynyl hydroxy eicosatetraenoic acid
aHNE	$\omega$ -alkynyl 4-hydroxy-2-nonenal
aHODE	$\omega$ -alkynyl hydroxy octadecadienoic acid
aHPETE	$\omega$ -alkynyl hydroperoxy eicosatetraenoic acid
aLA	$\omega$ -alkynyl linoleic acid
ALS	amyotrophic lateral sclerosis
AngII	angiotensin II

aONE	$\omega$ -alkynyl 4-oxo-2-nonenal
aPG	$\omega$ -alkynyl prostaglandin
aPGD <sub>2</sub>	$\omega$ -alkynyl prostaglandin D <sub>2</sub>
aPGE <sub>2</sub>	$\omega$ -alkynyl prostaglandin E <sub>2</sub>
aPGG <sub>2</sub>	$\omega$ -alkynyl prostaglandin G <sub>2</sub>
ATP	adenosine triphosphate
BHT	butylated hydroxy toluene
BODIPY	boron-dipyrromethene
BSA	bovine serum albumin
COX	cyclooxygenase
COX-1	cyclooxygenase 1
COX-2	cyclooxygenase 2
cPLA <sub>2</sub>	cytosolic phospholipase A <sub>2</sub>
DAMP	damage-associated molecular pattern
DMEM	Dulbecco's modified Eagle medium + glutamax
DMSO	dimethyl sulfoxide
DNA	deoxyribonucleic acid
ESI	electrospray ionization
ETC	electron transport chain
F <sub>2</sub> $\alpha$ -isoP	F <sub>2</sub> $\alpha$ -isoprostane
FLAP	arachidonate 5-lipoxygenase activating protein
GAPDH	glyceraldehyde-3-phosphate dehydrogenase
GRP78	78 kDa glucose-regulated protein



GSH	glutathione
hCOX2	human cyclooxygenase 2 (purified)
HEK-293	human embryonic kidney 293 cells
HETE	hydroxy eicosatetraenoic acid
HHT	12-hydroxy heptadecatrienoic acid
Hmox1	heme oxygenase-1
HNE	4-hydroxy-2-nonenal
HODE	hydroxy octadecadienoic acid
HPETE	hydroperoxy eicosatetraenoic acid
HPLC	high-performance liquid chromatography
HPODE	hydroperoxy octadecadienoic acid
HSA	human serum albumin
HSP90	heat shock protein 90
IFN $\gamma$	interferon gamma
I $\kappa$ B	inhibitor of nuclear factor kappa-light-chain-enhancer of activated B cells
IKK	inhibitor of nuclear factor kappa-light-chain-enhancer of activated B cells kinase
IKK- $\alpha$	inhibitor of nuclear factor kappa-light-chain-enhancer of activated B cells kinase, alpha subunit
IKK- $\beta$	inhibitor of nuclear factor kappa-light-chain-enhancer of activated B cells kinase, beta subunit
IKK- $\gamma$	inhibitor of nuclear factor kappa-light-chain-enhancer of activated B cells kinase, gamma subunit
IL-1 $\beta$	interleukin-1 beta

IL-6	interleukin-6
IL-10	interleukin-10
IL-12	interleukin-12
In•	radical initiator
iNOS	inducible nitric oxide synthase
IsoP	isoprostane
Keap1	Kelch-like ECH-associated protein 1
KETE	oxo eicosatetraenoic acid
KLA	Kdo <sub>2</sub> -lipid A
KODE	oxo octadecadienoic acid
L•	lipid radical
LA	linoleic acid
LC/MS/MS	liquid chromatography tandem mass spectrometry
LDL	low-density lipoprotein
lk12LOX	porcine leukocyte-type 12-lipoxygenase
LOO•	lipid peroxy radical
LOX	lipoxygenase
LPS	lipopolysaccharide
LTA <sub>4</sub>	leukotriene A <sub>4</sub>
LTB <sub>4</sub>	leukotriene B <sub>4</sub>
LTC <sub>4</sub>	leukotriene C <sub>4</sub>
LTC <sub>4</sub> S	leukotriene C <sub>4</sub> synthase
LTD <sub>4</sub>	leukotriene D <sub>4</sub>

LTE <sub>4</sub>	leukotriene E <sub>4</sub>
MeOAMVN	2,2'-azobis(4-methoxy-2,4-dimethylvaleronitrile)
mRNA	messenger ribonucleic acid
MS	mass spectrometry
MudPIT	multidimensional protein identification technology
<i>m/z</i>	mass to charge ratio
NF- $\kappa$ B	nuclear factor kappa-light-chain-enhancer of activated B cells
NMBHA	N-methyl benzohydroxamic acid
NMR	nuclear magnetic resonance
NP-HPLC	normal-phase high-performance liquid chromatography
Nrf2	nuclear factor erythroid 2-related factor 2
NSAID	nonsteroidal anti-inflammatory drug
Nu	nucleophile
oCOX1	ovine cyclooxygenase 1
ONE	4-oxo-2-nonenal
PAMP	pathogen-associated molecular pattern
PBS	phosphate buffered saline
PD	Parkinson's disease
PG	prostaglandin
PGA <sub>2</sub>	prostaglandin A <sub>2</sub>
PGD <sub>2</sub>	prostaglandin D <sub>2</sub>
PGE <sub>2</sub>	prostaglandin E <sub>2</sub>

PGF <sub>2α</sub>	prostaglandin F <sub>2α</sub>
PGG <sub>2</sub>	prostaglandin G <sub>2</sub>
PGH <sub>2</sub>	prostaglandin H <sub>2</sub>
PGI <sub>2</sub>	prostacyclin
PGJ <sub>2</sub>	prostaglandin J <sub>2</sub>
PIN1	peptidyl-prolyl <i>cis/trans</i> isomerase A1
plt12LOX	human platelet-type 12-lipoxygenase
PPh <sub>3</sub>	triphenyl phosphine
PRR	pattern recognition receptor
PUFA	polyunsaturated fatty acid
r15LOX1	rabbit reticulocyte 15-lipoxygenase 1
RNS	reactive nitrogen species
ROS	reactive oxygen species
RP-HPLC	reverse-phase high-performance liquid chromatography
s15-LOX-1	soybean arachidonate 15-lipoxygenase-1
SCX	strong cation exchange
SDS-PAGE	sodium dodecyl sulfate polyacrylamide gel electrophoresis
SIRT3	sirtuin 3
SN	substantia nigra
Sod1	superoxide dismutase 1
Sod2	superoxide dismutase 2
SRM	selected reaction monitoring

TBTA	tris[(1-benzyl-1 <i>H</i> -1,2,3-triazol-4-yl)methyl]amine
TCEP	tris(2-carboxyethyl)phosphine
TFE	2,2,2-trifluoroethanol
TNF $\alpha$	tumor necrosis factor alpha
TXA <sub>2</sub>	thromboxane A <sub>2</sub>

## Chapter I

### INTRODUCTION

#### Immune Response, Inflammation, and Disease

##### *Macrophages*

As the sesquicentennial anniversary of Dr. Élie Metchnikoff's discovery of the macrophage approaches<sup>4</sup>, macrophages have become one of the most highly studied immune cells in the human body. In 2014 nearly 10,000 publications listed in PubMed contained the keyword macrophage. Dr. Metchnikoff was studying nutrient uptake in cells when he noticed a cell type that would engulf particulates. He coined the term phagocytes, or "eating cell" as a name for these cells<sup>5</sup>. Dr. Metchnikoff was not the first to observe this phenomenon. Dr. Robert Koch noted anthrax inside granulomas, but misinterpreted what he saw as the bacterium invading the host cell, and not the host cell engulfing the bacterium<sup>5</sup>. Dr. Metchnikoff noticed that these cells were also involved in the first line of host defense (innate immunity), as they would phagocytose yeast cells that were foreign to the host. These new cells "ate" different amounts of material and he named them accordingly: microphages or "little eaters" later to be renamed neutrophils and macrophages or "big eaters"<sup>5</sup>. Dr. Metchnikoff, along with Dr. Paul Ehrlich received the 1908 Nobel Prize in

Physiology or Medicine for their discoveries of innate immunity and adaptive immunity respectively<sup>5</sup>.

Since their discovery, macrophages have been identified in nearly every body system. They have various names depending on the tissue type including Kupfer cells in the liver<sup>6</sup>, microglia in the central nervous system<sup>7</sup>, osteoclasts in bones<sup>8</sup>, Langerhans cells in skin and mucosa<sup>9</sup>, alveolar macrophages in lungs<sup>10</sup>, monocytes, or macrophages in an early differentiation stage, are abundant in the bone marrow and blood<sup>11</sup>, histiocytes in the lymph nodes<sup>12</sup>, Hofbauer cells in the placenta<sup>13</sup>, and many more. Macrophages are a critical component of the immune system, with functions as varied as their names and locations. The functions of macrophages begin in early embryo development with the removal of apoptotic cells allowing formation of organs and limbs, and continues to protect the organism until death<sup>14</sup>.

Macrophages are primarily involved in innate immunity, but can also participate in adaptive immunity<sup>10, 15</sup>. Innate immunity is the nonspecific host response to a variety of pathogenic stimuli, generating an acute inflammatory response (M1-polarization) through a series of pattern recognition receptors (PRR)<sup>16</sup>. The PRRs have evolved to recognize molecules unique to broad classes of pathogens, and easily distinguished from host molecules called pathogen-associated molecular patterns (PAMPs)<sup>17</sup>. One example of a PAMP is lipopolysaccharide (LPS), which is on the outer coat of all Gram-negative bacteria, and initiates inflammatory signaling through toll-like receptor 4, a macrophage PRR<sup>18, 19</sup>. PAMP signaling stimulates phagocytosis to engulf the

pathogen; generates reactive oxygen species (ROS)<sup>20</sup> and reactive nitrogen species (RNS)<sup>21</sup> to kill the pathogen; and synthesizes a variety of chemokines and cytokines, including prostaglandins (PGs)<sup>22</sup> leukotrienes<sup>23</sup>, interleukin-1 beta (IL-1 $\beta$ )<sup>24</sup>, interferon gamma (IFN $\gamma$ )<sup>25</sup>, interleukin-6 (IL-6)<sup>24</sup>, interleukin-12 (IL-12)<sup>26</sup>, and tumor necrosis factor alpha (TNF $\alpha$ )<sup>27</sup>. These chemokines and cytokines activate and recruit neighboring leukocytes by signaling that a pathogen has been detected, exacerbating the immune response (Figure 1)<sup>15, 28, 29</sup>.

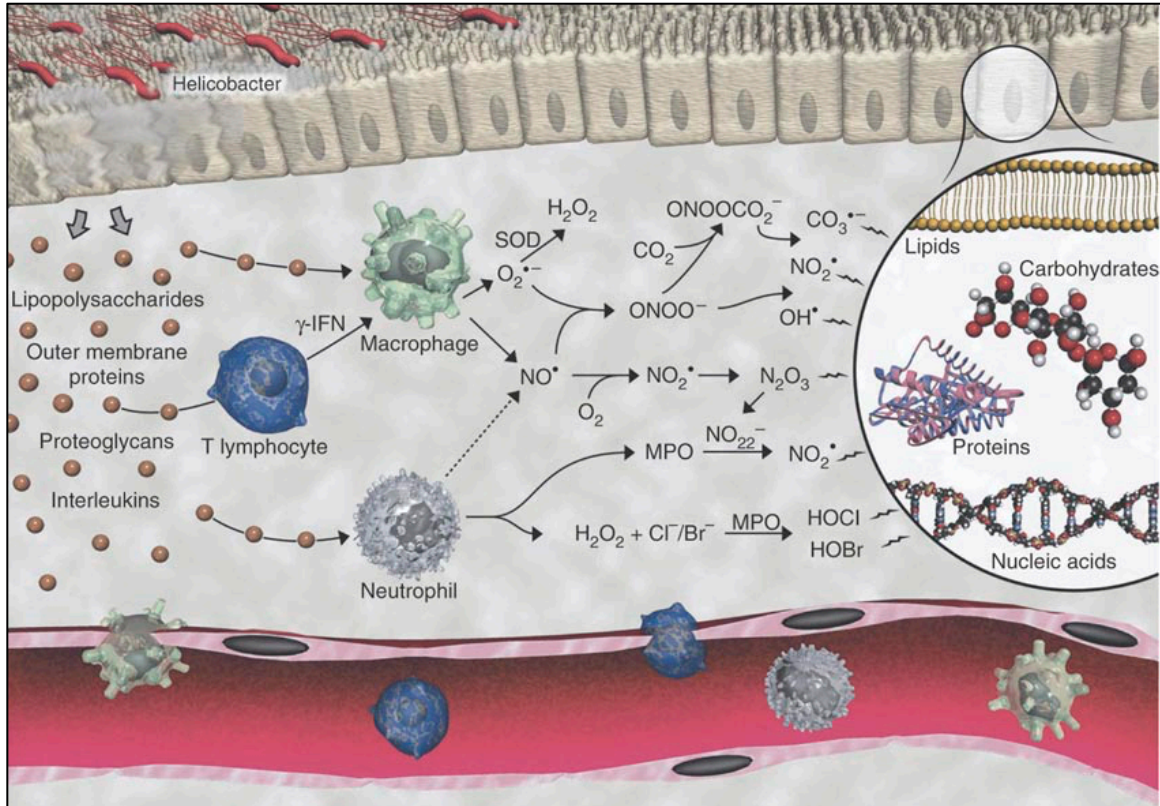


**Figure 1.** Reactive species generated by leukocyte activation. Leukocyte activation by PAMPs as well as pro-inflammatory cytokines and chemokines results in the production of reactive oxygen species and reactive nitrogen species. These highly reactive molecules can damage both host and pathogen cellular macromolecules including carbohydrates, proteins, and nucleic acids. Reprinted by permission from Macmillan Publishers Ltd: Taghizadeh, K, *et al. Nature Protocols* (2008), 3; 1287. Copyright 2008<sup>1</sup>.



Even though largely considered a pro-inflammatory cell, macrophages also play a role in resolving inflammation and repairing tissue damage<sup>30, 31</sup>. Macrophages have another set of PRRs that recognize and respond to damage-associated molecular patterns (DAMPs), molecules associated with host tissue damage. Unlike PAMPs, DAMPs initiate a noninfectious inflammatory signal (M2-polarization), meaning it is not designed to kill an invading pathogen, but to repair damaged tissue by engulfing and recycling damaged cells<sup>32, 33</sup>. M2-polarized macrophages also emit a host of cytokines and small molecules including interleukin-4<sup>30</sup>, interleukin-10 (IL-10)<sup>26, 34</sup>, interleukin-13<sup>30</sup>, interleukin-1 receptor antagonist<sup>35</sup>, transforming growth factor beta<sup>36</sup>, and PGs<sup>37</sup>.

### ***Inflammation and disease***

Due to their prominent role in inflammatory responses, many macrophage studies have been focused on inflammatory signaling pathways. Inflammation is a complex process involving a variety of cells types<sup>38</sup>. The process of inflammation starts with some initiating factor, which can range from cellular injury to invasion by a pathogen, discussed in depth above. In addition, many environmental factors can induce inflammatory signaling including cigarette smoke<sup>39, 40</sup> and non-nutrient transition metals<sup>41, 42</sup>. The cardinal signs of inflammation were first described by Celsus nearly two millennia ago. Calor (heat), rubor (redness), tumor (swelling), and dolor (pain), are relatively simplistic, but the molecular processes underlying these signs are anything but simple<sup>43</sup>. Inflammation involves signaling cascades with multiple redundancies as

well as feed back and feed forward mechanisms. Both proteins and small molecules are generated that play prominent roles in cellular signaling and cellular consequences both intended and unintended<sup>44</sup>.

One of the major inflammatory signaling pathways is the nuclear factor kappa-light-chain-enhancer of activated B cells (NF- $\kappa$ B) pathway, named after the ultimate transcriptional regulator of the pathway<sup>45</sup>. When a PRR recognizes a molecule associated with a pathogen, a series of phosphorylation events is induced, resulting in the phosphorylation of the inhibitor of NF- $\kappa$ B (I $\kappa$ B) kinase (IKK) complex<sup>46-48</sup>. The IKK complex consists of two catalytic subunits, IKK- $\alpha$  and IKK- $\beta$ , and one regulatory subunit, IKK- $\gamma$ <sup>49</sup>. I $\kappa$ B binds the two subunits of NF- $\kappa$ B, preventing them from translocating to the nucleus and initiating transcription<sup>50, 51</sup>. IKK phosphorylates I $\kappa$ B, targeting it for proteasomal degradation, releasing NF- $\kappa$ B to the nucleus to induce transcription<sup>52, 53</sup>. NF- $\kappa$ B regulates the synthesis of many pro-inflammatory enzymes that generate chemokines including cyclooxygenase-2 (COX-2)<sup>54</sup> and inducible nitric oxide synthase (iNOS)<sup>55</sup> as well as the pro-inflammatory cytokines TNF $\alpha$ <sup>56</sup> and IL-6<sup>57</sup>. NF- $\kappa$ B signaling also results in the up regulation of many of the anti-apoptotic, pro-survival proteins including B-cell lymphoma-extra large<sup>58</sup>, B-cell lymphoma-2 related protein<sup>59</sup>, cellular inhibitors of apoptosis<sup>60</sup>, and superoxide dismutase 2 (Sod2)<sup>61, 62</sup>.

Inflammatory signaling has many feed back loops that help to regulate signaling, preventing a transition to chronic inflammation. One of the major anti-inflammatory signaling pathways is the Kelch-like ECH-associated protein 1 (Keap1) and nuclear factor erythroid 2-related factor 2 (Nrf2) pathway<sup>63, 64</sup>. Under

normal cellular conditions, Keap1 binds to the transcription factor Nrf2, facilitating its ubiquitination by Cullin-3, leading to its turnover and preventing translocation to the nucleus<sup>65, 66</sup>. Keap1 is cysteine rich, and ROS generated during inflammatory signaling can bind to cysteines<sup>67</sup>. Cysteine modification results in Keap1 conformational changes that prevent ubiquitination of Nrf2, allowing its release and translocation to the nucleus. Nrf2 binds to the antioxidant response elements of its target genes, inducing transcription of genes that facilitate survival of oxidative stress<sup>68-70</sup>. Target genes of Nrf2 include heme oxygenase-1 (Hmox1) to generate the anti-inflammatory CO<sup>71</sup>, glutamate-cysteine ligase to synthesize the cellular antioxidant glutathione (GSH)<sup>72</sup>, and glutathione S-transferase to catalyze the conjugation of GSH to reactive electrophiles resulting in detoxification<sup>73</sup>.

Many diseases can be linked to inflammation playing a role in etiology or progression including cancer, neurodegenerative diseases, and cardiovascular disease. Virchow first noted the linkage between cancer and leukocyte infiltration, years before the discovery of the macrophage<sup>74</sup>. Studies have confirmed a link between inflammation and cancer through the presence of macrophages in the tumor microenvironment, and the dependence on macrophages for tumor survival<sup>75-77</sup>. Human breast cancer and ovarian cancer cells become more invasive when co-incubated with macrophages. Invasiveness is reduced to control levels when TNF $\alpha$  signaling is reduced by treatment with TNF $\alpha$  antibodies<sup>78</sup>. A mouse model for hepatocellular carcinoma shows that inhibition of NF- $\kappa$ B signaling or TNF $\alpha$  signaling increases tumor cell apoptosis<sup>79</sup>. Human

mammary tumor cells are four-fold more motile when they are within 20  $\mu\text{m}$  of a macrophage<sup>80</sup>. IKK- $\beta$  knockout mice showed a 75% reduction in tumors over wild-type mice when treated with azoxymethane, a known pro-carcinogen for colorectal cancer<sup>81</sup>. All of these studies strongly indicate a correlation between macrophage infiltration, inflammation, and various forms of cancer.

Many neurodegenerative diseases have been linked to inflammation as well, including Alzheimer's disease (AD)<sup>82</sup>, Amyotrophic Lateral Sclerosis (ALS) or Lou Gehrig's Disease<sup>83</sup>, and Parkinson's Disease (PD)<sup>84</sup>. Accumulation of amyloid-beta peptide, a hallmark of AD, has been shown to induce ROS in microglia leading to increased inflammation in the brain<sup>85</sup>. Superoxide dismutase 1 (Sod1) transcript expression increases, but protein expression is reduced in sporadic ALS (90% of patients)<sup>86</sup>. Sod1 is an important ROS defense protein, converting superoxide anion, a molecule generated in high amounts and a precursor to most ROS, to the much less reactive  $\text{H}_2\text{O}_2$ . A contributing factor to familial ALS (10% of patients) is mutations in the Sod1 gene. Identified mutations linked to ALS include A4V<sup>87</sup>, H46R<sup>88</sup>, and G93A<sup>89</sup>. PD results from neuronal death in the substantia nigra (SN)<sup>90</sup>. Significantly higher levels of resting microglia are present in the SN of the mature brain compared to other regions. The increased numbers of microglia make the SN particularly susceptible to ROS and RNS generation<sup>91</sup>. Nitric oxide generation, a direct result of inflammatory signaling has been implicated in the SN neuronal death of PD<sup>92</sup>. These studies show that inflammation mediated ROS production is a major contributor to neurodegenerative diseases.

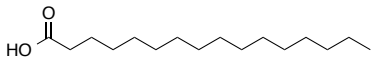
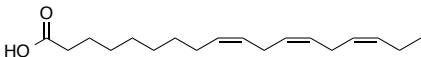
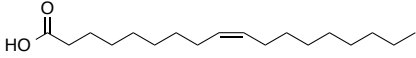
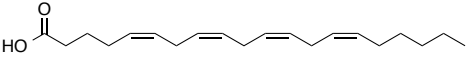
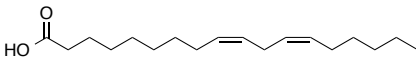
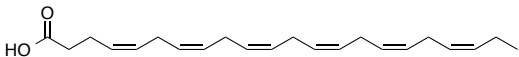
Atherosclerosis has long been associated with chronic inflammation and leukocytes<sup>38, 93</sup>. It was first discovered that macrophages are a major component of atherosclerotic plaques in porcine aorta<sup>94</sup>. Accumulation of lipoprotein causes monocytes, progenitors of macrophages, to infiltrate the intima of blood vessels. They begin to ingest large amounts of lipid and protein and differentiate to a special class of macrophages called foam cells. Foam cell formation is visualized as fatty streaks in early atherosclerotic lesions, and foam cells make up most of the mass of a mature atherosclerotic lesion<sup>95</sup>. As the lesion grows, other leukocytes are recruited<sup>96</sup>. If M1-polarized macrophages are recruited, then the lesion will grow, as will the risk of rupture, resulting in myocardial infarction or stroke<sup>97, 98</sup>. This recruitment is through C-C chemokine receptor 2, which when knocked out make mice resistant to atherosclerosis<sup>99</sup>. Both cyclooxygenases (COXs)<sup>100</sup> and lipoxygenases (LOXs)<sup>101</sup>, enzymes that generate lipid mediators of inflammation, are over expressed in atherosclerotic lesions. However, M2-polarized macrophage recruitment will result in the repair of the lesion<sup>102</sup>.

The study of inflammatory signaling has led to an appreciation of the many potent small molecule signals generated by cells involved. One major class of molecules generated during inflammation is oxidized polyunsaturated fatty acids (PUFAs). A diverse class of these species are generated during inflammation with a larger ranges of cellular consequences reported.

## Oxidation of Polyunsaturated Fatty Acids

### *Polyunsaturated fatty acids*

Fatty acids, named because they are composed of a carboxylic acid and a hydrophobic tail, can be saturated, monounsaturated, and polyunsaturated. These terms refer to the number of double bonds in the fatty acids, with saturated having zero, monounsaturated having one, and polyunsaturated having two or more. Fatty acids are named generically X:Y ( $\omega$ -Z) where X is the number of carbons in the fatty acid, Y is the number of double bonds, and Z is the number of carbons between the last double bond and the end of the hydrophobic tail (Figure 2). Most of double bonds in fatty acids are in the *cis* conformation, with a single methylene group separating multiple double bonds in PUFAs. The number and orientation of these double bonds have a tremendous influence on signaling action as well as the chemistry of oxidation.

 <p>Palmitic Acid 16:0</p>	 <p>alpha Linolenic Acid 18:3(<math>\omega</math>-3)</p>
 <p>Oleic Acid 18:1(<math>\omega</math>-9)</p>	 <p>Arachidonic Acid 20:4(<math>\omega</math>-6)</p>
 <p>Linoleic Acid 18:2(<math>\omega</math>-6)</p>	 <p>Docosahexanoic Acid 22:6(<math>\omega</math>-3)</p>

**Figure 2.** Common fatty acids. Common unsaturated: palmitic acid; monounsaturated: oleic acid; and polyunsaturated fatty acids: linoleic acid, alpha linolenic acid, arachidonic acid and docosahexanoic acid.

### Radical mechanism of lipid oxidation

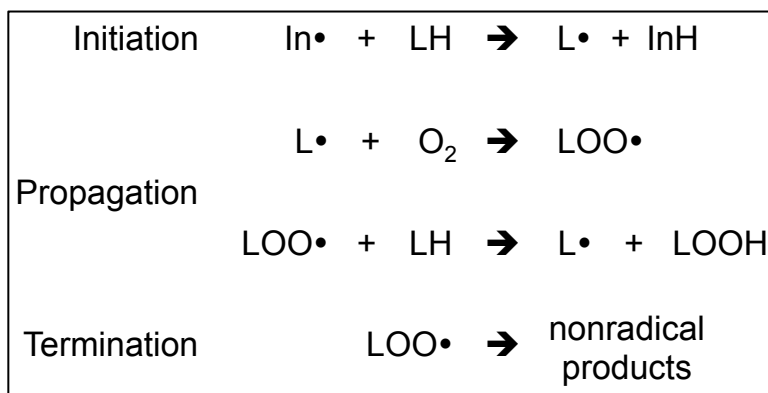


**Figure 3.** Radical mechanism of lipid oxidation. General scheme for the radical mechanism of lipid (LH) oxidation. First the reaction is initiated by some initiating species (In•) generating a lipid radical (L•). Reaction of the lipid radical with molecular oxygen to form a lipid peroxy radical (LOO•). The peroxy radical can function as the initiator for another lipid molecule, propagating the reaction. Finally, termination of the peroxy radical to nonradical products.

PUFA oxidation follows the common radical mechanism of initiation, propagation, and termination (Figure 3). As mentioned above, most PUFAs have at least one *bis*-allylic position (Figure 4). The hydrogen atoms at the *bis*-allylic position are easily abstractable and the resulting pentadienyl radical is delocalized across five carbons. This hydrogen abstraction results from the action of a cellular oxidant as is the case for autoxidation, or in a more controlled fashion by enzymes such as the COXs and LOXs. The resulting radical reacts with molecular oxygen forming a peroxy radical that can propagate the chain reaction, and/or terminate to nonradical products depending on microenvironment conditions<sup>103-105</sup>.

## Autoxidation

Non-enzymatic abstraction of the *bis*-allylic hydrogen is called autoxidation, which is uncontrolled lipid peroxidation. As expected with an uncontrolled reaction, a much more diverse array of lipid peroxidation products will be formed. While autoxidation can occur with both mono and polyunsaturated fatty acids, I will focus on linoleic acid (LA) and arachidonic acid (AA) here.

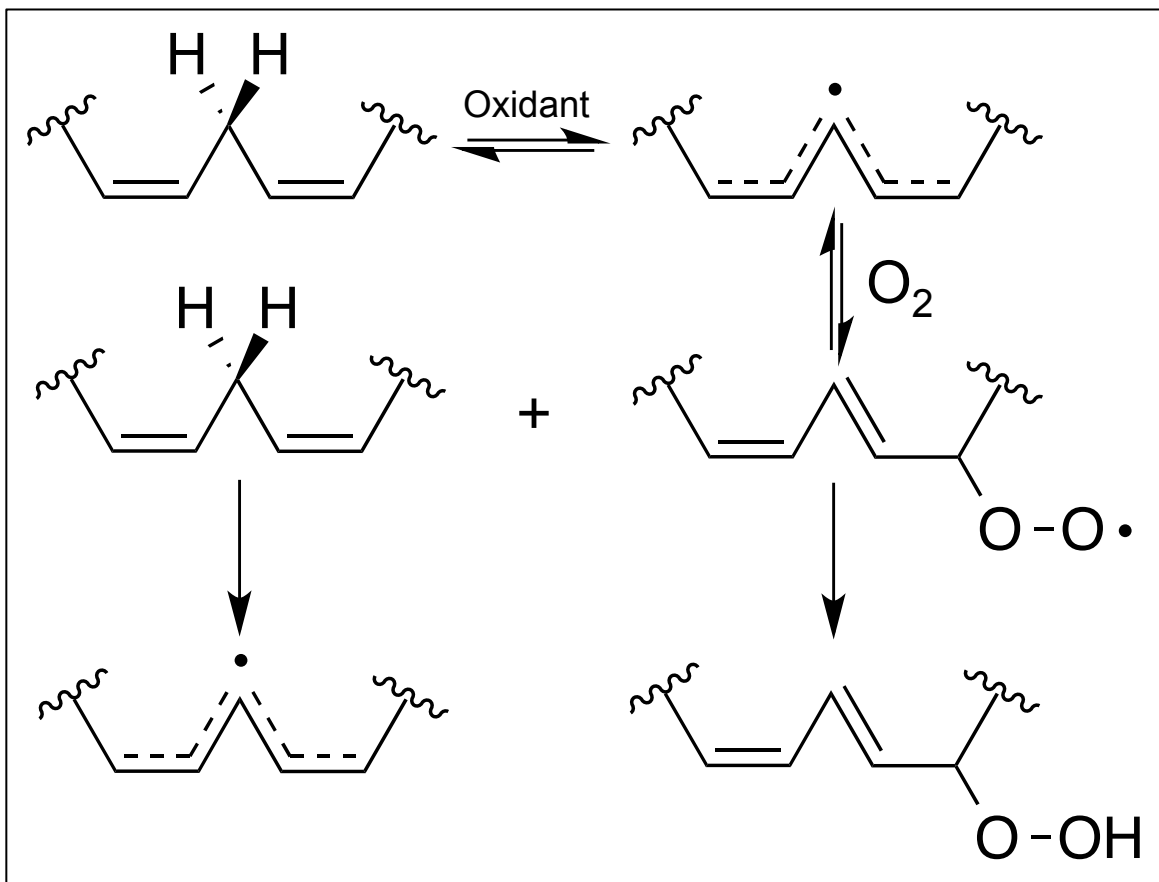


**Figure 4.** General mechanism of PUFA oxidation. First an oxidant abstracts a *bis*-allylic hydrogen resulting in a pentadienyl radical (initiation). The pentadienyl radical can react with molecular oxygen forming the peroxy radical. The peroxy radical can then abstract a *bis*-allylic hydrogen from an adjacent PUFA, generating a new pentadienyl radical (propagation), but also terminating itself to the hydroperoxide (termination).



The autoxidation of LA is one of the simpler PUFA oxidation profiles to study due to its structure. With only two double bonds, LA only has one set of abstractable hydrogen atoms. Oxygen can add to the 9-, 11-, or 13- carbons generating a conjugated diene peroxy radical for 9- and 13- positional isomers or a *bis*-allylic peroxy radical for the 11- positional isomer<sup>106</sup>. Oxygen addition is a reversible process, and the peroxy radical can be regenerated<sup>107</sup>. The rate constant for the reverse reaction of the 11-peroxy radical is orders of magnitude greater than the rate constant for the formation of both the *Z,E*-9-peroxy radical and *Z,E*-13-peroxy radical. These rate constants indicate that unless trapped immediately, the 11-peroxy radical will decompose quickly, giving all 9- or 13-peroxy radicals<sup>108</sup>. 11-Hydroperoxy octadecadienoic acid (11-HPODE) is rarely seen except in cases where a good hydrogen donor is present. This was demonstrated in the presence of  $\alpha$ -tocopherol, a good hydrogen donor, where a mixture of 1:1:1, 9-:11-:13-HPODE was generated by autoxidation<sup>109</sup>.

Isomerization of the double bond allylic to the peroxy radical also occurs in the 9- and 13- positional isomers. In the presence of a good hydrogen donor, the peroxy radical will be trapped generating the *Z,E*-9-HPODE or *Z,E*-13-HPODE in equal amounts. As mentioned above, oxygen addition is reversible. After regeneration of the peroxy radical, oxygen can add at either position potentially resulting in a second allylic bond isomerization, generating *E,E*-9-HPODE and *E,E*-13-HPODE. When no good hydrogen donor is present, the *E,E*:*Z,E*-HPODE ratio will be 4:1, designating *Z,E*-HPODE as the kinetic product, and *E,E*-HPODE as the thermodynamic product (Figure 5)<sup>110, 111</sup>.

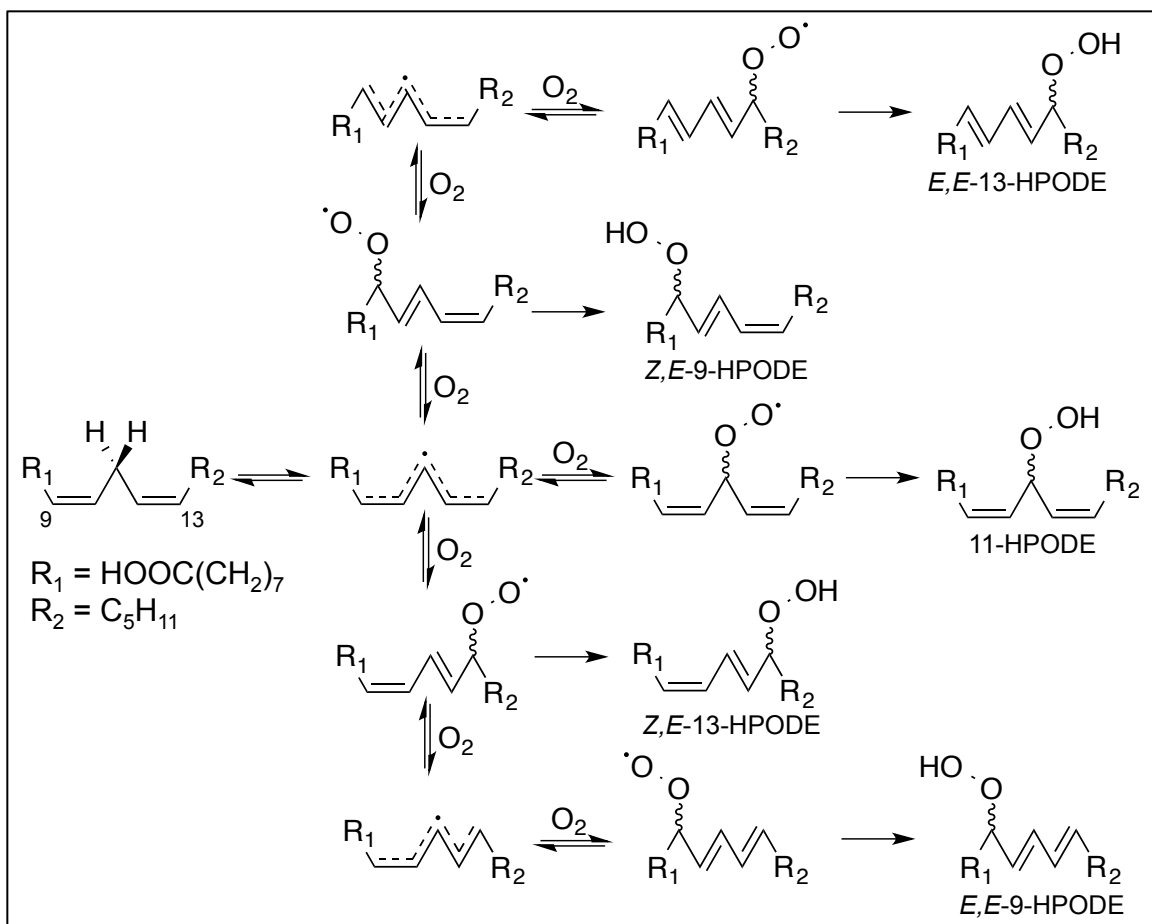


**Figure 5.** Autoxidation products of LA. After *bis*-allylic hydrogen abstraction, the pentadienyl radical of LA can react at three different positions, generating three distinct peroxy radicals. The peroxy radicals can be quenched generating HPODE, or they can revert to the pentadienyl radical. The pentadienyl radical can then react with molecular oxygen at any of the three original positions, reforming a peroxy radical. With each reversal of the peroxy radical, double bond isomerization from *cis* to *trans* will occur. If allowed to reverse a sufficient amount of times, *trans* double bonds will form preferentially as they are a lower energy state.

In addition to the various positional and geometric isomers generated, HPODE is also a chiral molecule. During autoxidation, oxygen can add from either side of the molecule generating both the *R* and *S* enantiomers. Analysis of *R/S* ratios is one of the most accurate methods to determine *in vivo* if lipid peroxidation is occurring by an enzymatic or non-enzymatic process because microenvironment factors like hydrogen donor ability do not play a role in the

stereochemistry observed. Therefore an *R/S* ratio of 1 indicates an autoxidation process, whereas a ratio greatly skewed to one enantiomer over the other suggests an enzymatic process<sup>112-114</sup>.

AA oxidation generates a much more complex autoxidation profile than LA due to it having 3 *bis*-allylic positions at the 7-, 10-, and 13-carbons. A single oxygen addition generates six positional isomers: *E,Z,Z,Z*-5-hydroperoxy eicosatetraenoic acid (*E,Z,Z,Z*-5-HPETE), *Z,E,Z,Z*-8-HPETE, *Z,E,Z,Z*-9-HPETE, *Z,Z,E,Z*-11-HPETE, *Z,Z,E,Z*-12-HPETE, and *Z,Z,Z,E*-15-HPETE<sup>103</sup>. As with LA, *bis*-allylic peroxides are rarely observed and a mixture of *R* and *S* enantiomers are formed from autoxidation<sup>115</sup>. Additionally, little HPETE is observed with more than one *trans* double bond because the rate of cyclization is estimated to be greater than the rate of reversal of the peroxy radical<sup>116</sup>. The additional reactive positions of AA also allow for endoperoxide formation by cyclization, resulting in  $F_2\alpha$ -isoprostanes ( $F_2\alpha$ -isoP), products structurally similar to prostaglandin  $F_2\alpha$  ( $PGF_2\alpha$ ), and a host of other cyclized products<sup>117-119</sup>.  $F_2\alpha$ -isoPs have been used as an *in vivo* biomarker for the identification of increased oxidative stress and lipid peroxidation<sup>120, 121</sup>. The mixture of isoprostanes generated is extremely complex, with four hydroxyl positional isomers possible: 5-, 8-, 12-, and 15- $F_2\alpha$ -isoP, with the 5- and 15-positional isomers the most abundant (Figure 6)<sup>119</sup>. Each series of isoprostane has five chiral centers, resulting in eight unique enantiomers for each<sup>120</sup>.

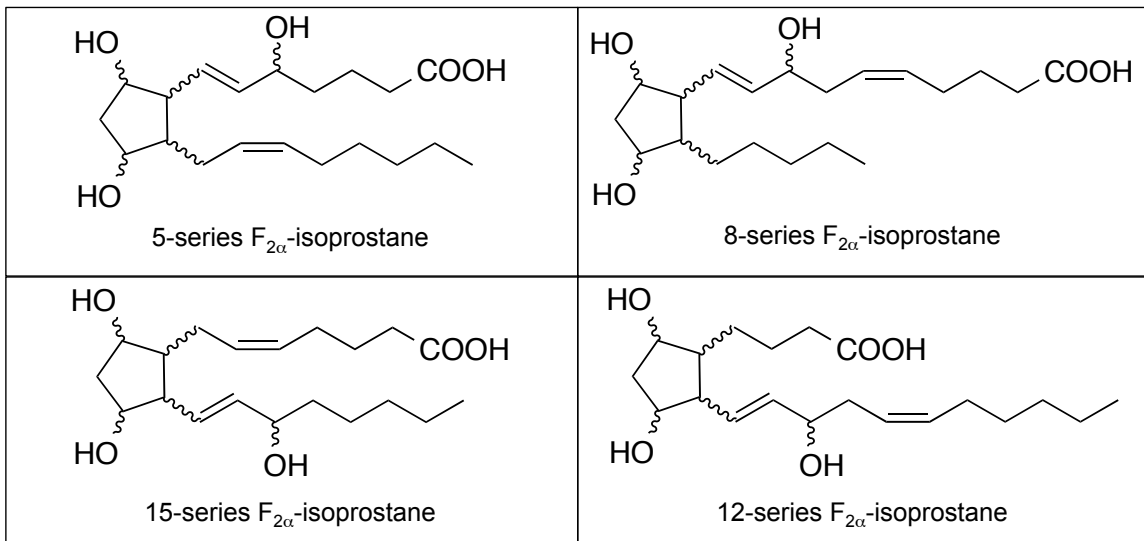


**Figure 6.** Autoxidation of AA generates  $F_{2\alpha}$ -isoprostanes. The  $F_{2\alpha}$ -isoprostanes are a series of autoxidation AA metabolites that are structurally similar to prostaglandins. The mechanism of formation of isoprostanes is similar to that of prostaglandins, but because they are formed non-enzymatically, they have a mixture of positional isomers and enantiomers.

### Cyclooxygenases

PUFAs can also be oxygenated in a much more controlled fashion by enzymes that direct hydrogen abstraction as well as oxygen addition to get a specific product profile with defined isomers and stereochemistry. One such set of enzymes are the COXs, which use a heme-bound iron to catalyze hydrogen abstraction<sup>122</sup>. Two enzymes comprise this class: COX-1<sup>123</sup>, which is the constitutively expressed species, and COX-2<sup>124</sup>, which is the species induced in response to an inflammatory stimulus. Both enzymes are capable of oxygenating LA<sup>125</sup>, AA<sup>125</sup>, as well as other PUFAs of both the  $\omega$ -6 and  $\omega$ -3 families<sup>126</sup>. COX-2 also exclusively oxygenates neutral ester and amide derivatives of AA, including 2-arachidonoylglycerol and arachidonylethanolamine<sup>127</sup>. The result of these oxygenation events are potent and diverse signaling molecules involved in a host

of cellular functions including vascular dilation and constriction, platelet aggregation, and mucosal regeneration<sup>128</sup>.

Due to the potent signaling capabilities of COX metabolites, the enzymes were the focus of pharmacology long before their existence and products were known. Historically, extract of willow bark was given to patients to treat pain and inflammation. The active ingredient in willow bark is salicylic acid, which when acetylated by Felix Hoffman in 1897, created aspirin, a pharmaceutical agent still used today<sup>129</sup>. Inhibition of the COX enzymes is the basis of a multibillion-dollar set of drugs including the nonsteroidal anti-inflammatory drugs (NSAIDs) ibuprofen, naproxen, celecoxib, and indomethacin<sup>130-132</sup>. With the prominent role of COXs in generating cell signaling molecules, it is no wonder that COX expression has been linked to a host of disease including cancer<sup>133</sup>, cardiovascular disease<sup>134</sup>, rheumatoid arthritis<sup>135</sup>, and neurodegenerative diseases<sup>136</sup>.

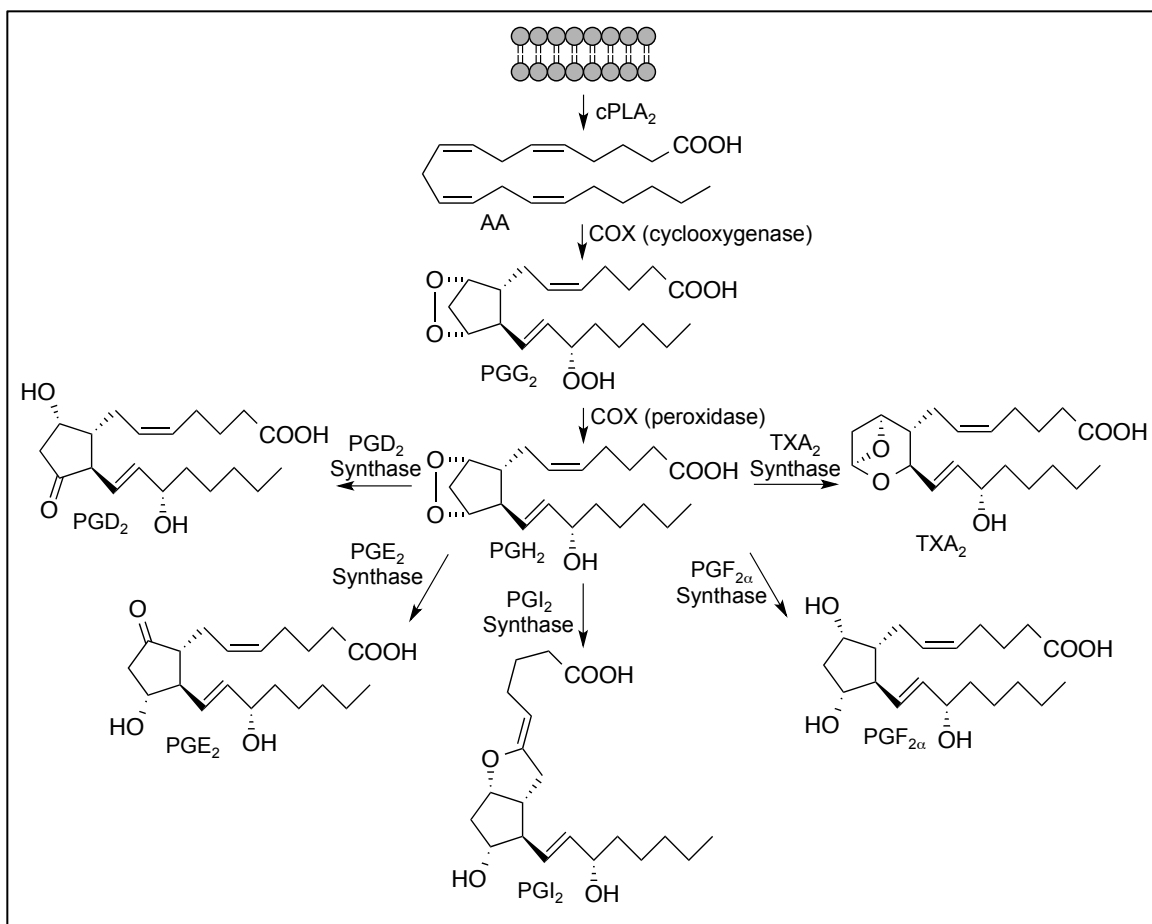


**Figure 7.** COX metabolism of AA. The COX enzymes consist of two active sites that act on free AA released from the lipid bilayer by cPLA<sub>2</sub>. The cyclooxygenase active site bis-dioxygenates and cyclizes AA to form PGG<sub>2</sub>. PGG<sub>2</sub> is then reduced at the peroxidase active site to PGH<sub>2</sub>. PGH<sub>2</sub> is the precursor to other eicosanoids including PGD<sub>2</sub>, PGE<sub>2</sub>, PGI<sub>2</sub>, PGF<sub>2α</sub>, and TXA<sub>2</sub>, which are generated by their respective synthases.

The COX enzymes are structural homodimers that act as functional heterodimers to *bis*-dioxygenate and cyclize AA, released from the lipid bilayer by cytosolic phospholipase A<sub>2</sub> (cPLA<sub>2</sub>)<sup>137, 138</sup>. Oxygenation and cyclization occur in the cyclooxygenase active site forming PGG<sub>2</sub> (Figure 7). The peroxide of PGG<sub>2</sub> is then reduced in the peroxidase active site to give PGH<sub>2</sub>. PGH<sub>2</sub> is the precursor to the signaling molecules PGE<sub>2</sub>, PGD<sub>2</sub>, PGF<sub>2α</sub>, PGI<sub>2</sub>, and thromboxane A<sub>2</sub> (TXA<sub>2</sub>), which are generated by their respective synthases<sup>122</sup>.

The prostaglandins have a panoply of signaling roles, including both vasodilation and constriction, muscle contraction, as well as the pain and fever associated with inflammation<sup>128</sup>. Additionally, COXs can generate several monooxygenated arachidonic acid species including 11(*R*)-HETE and 15(*S*)-HETE<sup>139</sup>. Aspirin, a COX inhibitor that acetylates Ser530, does not abolish the activity of COXs, but shifts the product profile from one generating PGH<sub>2</sub> to one generating 15(*R*)-HETE<sup>140</sup>. Many studies have used COX variants to determine the residues responsible for the cyclooxygenase and peroxidase activity as well as inhibitor binding to the COX enzymes<sup>139, 141-143</sup>. LA is also a substrate for the COX enzymes. Since LA only has one *bis*-allylic carbon, cyclized LA products are not generated. The major products generated by COX metabolism of LA are the monooxygenated products at the 9- and 13-carbons, 9-HPODE and 13-HPODE respectively<sup>125</sup>.

### ***Lipoxygenases***

Like the COXs, LOXs represent a controlled mechanism of lipid oxidation, with both LA and AA being potential substrates. LOXs can act on both free<sup>144</sup> and esterified<sup>145</sup> fatty acids. Despite having an active role in inflammatory signaling, LOXs have not been successful drug targets like the COXs. In fact there is only one approved drug targeting 5-LOX, Zileuton<sup>146</sup>, which has a limited patient population because of its generation of a cytotoxic compound, 5-oxo eicosatetraenoic acid (5-KETE)<sup>147</sup>. Even though they have not been

pharmacological targets, 5-LOX<sup>148</sup>, 12-LOX<sup>149</sup>, and 15-LOX<sup>150</sup> inhibitors as well as pan-LOX inhibitors<sup>151</sup> have been generated for research purposes.

There are many LOX enzymes that are named differently depending on the organism and the oxygenation position of the fatty acid substrate, but all of them use a non-heme iron for their chemistry. LOXs first discovered to oxygenate LA were named 9-LOX and 13-LOX indicating that they add oxygen to the 9- or 13-carbon generating 9-HPODE or 13-HPODE respectively<sup>152</sup>. Conversely, LOXs first discovered to oxygenate AA are named 5-LOX, 8-LOX, 12-LOX, or 15-LOX indicating oxygenation of AA at the 5-, 8-, 12-, or 15-carbon, generating 5-HPETE, 8-HPETE, 12-HPETE, or 15-HPETE respectively<sup>153</sup>. Much substrate overlap can be seen between these groups of LOX enzymes. For example soybean 15-LOX-1 functions as a 15-LOX when AA is the substrate, but a 13-LOX when LA is the substrate<sup>154, 155</sup>. Another example is potato 5-LOX, which functions as a 5-LOX when AA is the substrate, but a 9-LOX when LA is the substrate<sup>156</sup>.

While not quite as vast as COX metabolism, LOXs generate a host of biologically active metabolites. 15-HPETE and 15-hydroxy eicosatetraenoic acid (15-HETE) generated by 15-LOX, have been shown to be angiostatic and angiogenic respectively<sup>157</sup>. Increased levels of LOX-derived 13-hydroxy octadecadienoic acid (13-HODE) results in increased growth in hepatocellular carcinoma<sup>158</sup>. However, the most studied class of metabolites resulting from LOX metabolism are the leukotrienes<sup>159</sup> (Figure 8), which result from 5-LOX metabolism of AA<sup>160</sup>. The first step in leukotriene biosynthesis is the release of



AA from the lipid bilayer by cPLA<sub>2</sub><sup>161</sup>. 5-LOX is an interesting PUFA metabolizing enzyme because it requires a second protein, 5-LOX activating protein (FLAP), to metabolize AA<sup>162</sup>. The mechanism by which FLAP confers activity to 5-LOX is not fully understood, but it is known that FLAP does not have enzymatic activity of its own, and it is hypothesized that FLAP delivers AA to 5-LOX<sup>163</sup>. During leukotriene biosynthesis, AA is oxygenated by 5-LOX to 15(S)-HPETE, reduced in the cell medium to 15(S)-HETE, then oxidized again by 5-LOX to leukotriene A<sub>4</sub> (LTA<sub>4</sub>)<sup>164, 165</sup>. LTA<sub>4</sub> is then further oxidized by LTA<sub>4</sub> hydrolase to leukotriene B<sub>4</sub> (LTB<sub>4</sub>)<sup>166</sup> or conjugated to GSH by LTC<sub>4</sub> synthase (LTC<sub>4</sub>S) generating leukotriene C<sub>4</sub> (LTC<sub>4</sub>)<sup>167</sup>. The GSH of LTC<sub>4</sub> can be further degraded sequentially losing glutamate to form leukotriene D<sub>4</sub> (LTD<sub>4</sub>), and then glycine to form leukotriene E<sub>4</sub> (LTE<sub>4</sub>)<sup>168</sup>. Leukotrienes are pro-inflammatory in their signaling, and have been implicated in many diseases associated with inflammation<sup>169</sup> including rheumatoid arthritis<sup>170</sup>, irritable bowel syndrome<sup>171</sup>, and asthma<sup>172</sup>. The only drug targeting LOXs, Zileuton, inhibits 5-LOX and thus leukotriene biosynthesis, and has been implemented as a treatment for many of the diseases associated with leukotriene biosynthesis<sup>171, 173</sup>.

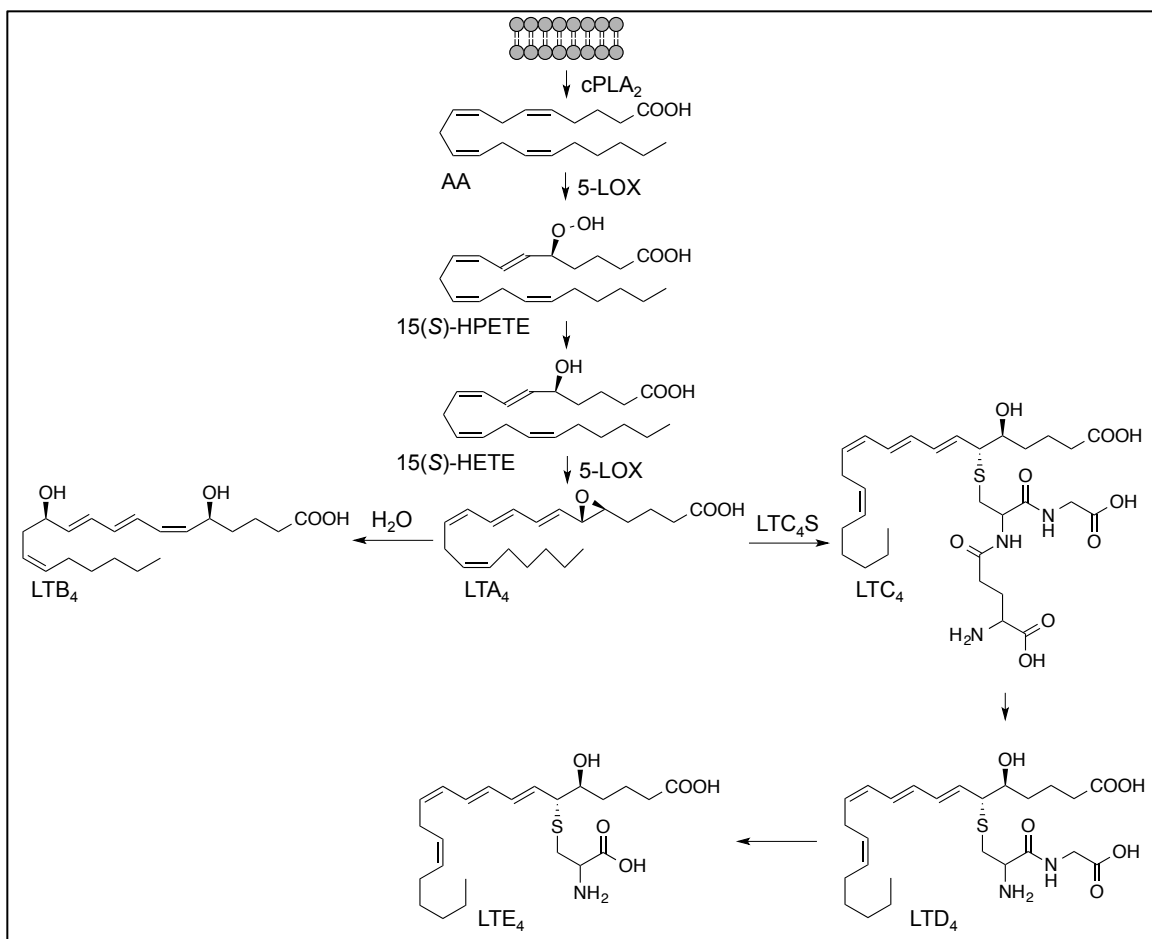


**Figure 8.** 5-LOX metabolism of AA. 5-LOX catalyzes the addition of molecular oxygen to AA released from the lipid bilayer by cPLA<sub>2</sub> to generate 15(S)-HPETE. 15(S)-HPETE is quickly reduced to 15(S)-HETE in the cellular milieu. 5-LOX also oxidizes 15(S)-HETE to LTA<sub>4</sub>. LTA<sub>4</sub> can be converted to LTB<sub>4</sub> by LTA<sub>4</sub> hydrolase or conjugated to GSH to form LTC<sub>4</sub> by LTC<sub>4</sub> synthase. The GSH of LTC<sub>4</sub> can be degraded to LTD<sub>4</sub> then LTE<sub>4</sub> by losing glutamate and glycine sequentially.

## Lipid Electrophiles

### *Generation of lipid electrophiles*

Further oxidation and degradation of the oxidized lipid species mentioned above results in the generation of various chain length  $\alpha,\beta$ -unsaturated carbonyls and free aldehydes. These lipid species are electrophilic, reacting with

nucleophilic groups of cellular macromolecules forming adducts, and potentially altering function. I will focus on adducts formed on nucleophilic amino acid residues in proteins. By no means has the entire electrophile pool been discovered, and thus we don't know exactly how they are formed. However, the chemistry of formation has been identified for several of the more highly studied lipid electrophiles.

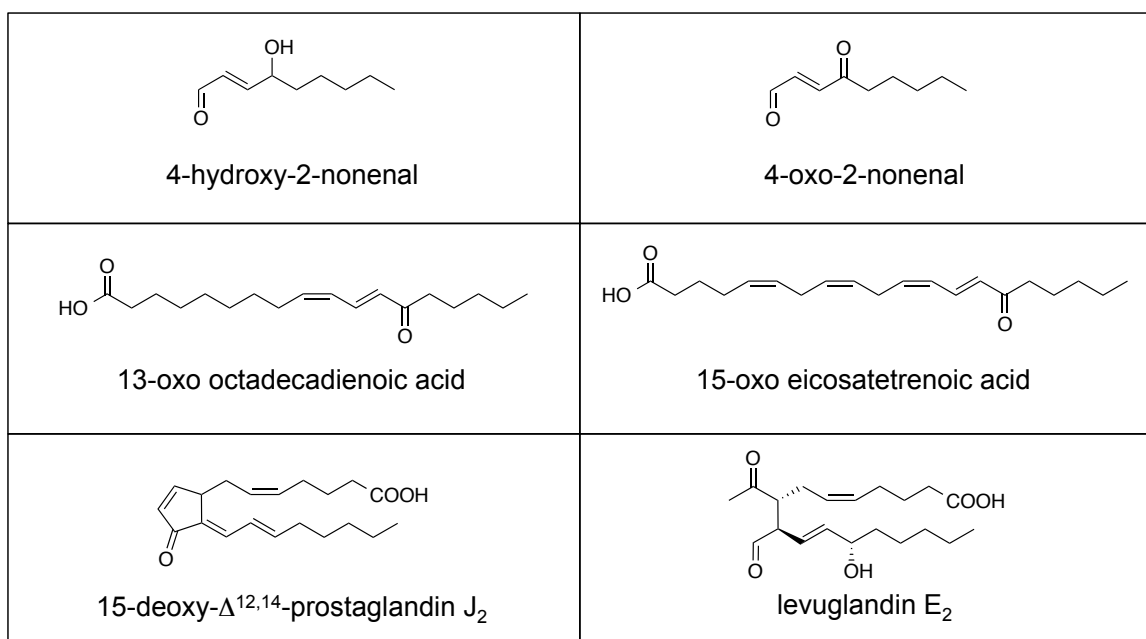


**Figure 9.** Structures of some commonly studied lipid electrophiles.

Several mechanisms have been proposed to explain the formation of these reactive lipid species. Both 4-hydroxy-2-nonenal (HNE) and 4-oxo-2-nonenal (ONE) can be generated from both LA and AA metabolism<sup>174</sup>. LOX<sup>175, 176</sup> and COX-2<sup>177</sup> derived 15-HPETE can be converted to ONE. Additionally, COX-2 metabolism of 5-HETE generated by 5-LOX can result in HNE formation<sup>178</sup>. LA can be converted to both HNE<sup>179, 180</sup> and ONE<sup>180, 181</sup> by autoxidation *in vitro*.

$\text{Fe}^{2+}$ <sup>182</sup> and vitamin C<sup>183</sup> have been shown to cause the degradation of lipid hydroperoxides to electrophiles. HNE and ONE formation has also been proposed to occur in cardiolipin pools, where PUFAs are in close proximity to each other allowing for intermolecular peroxidation<sup>184</sup>. This mechanism was further supported with *bis*-allylically deuterated linoleic acid. These experiments use the kinetic isotope effect of linoleic acid to stop radical propagation through phospholipid pools resulting in less lipid oxidation, and presumably less lipid electrophile generation<sup>185, 186</sup>. Cardiolipin can also be enzymatically oxidized by cytochrome c, which is inhibited with acetaminophen<sup>187</sup>.

Oxo fatty acids comprise a large class of lipid electrophiles. They are all generated from single molecule addition of oxygen to a fatty acid, followed by oxidation to a conjugated ketone. The enzymatic and non-enzymatic mechanisms discussed above are responsible for the initial lipid oxidation product. After that, there are several dehydrogenases that have been reported to oxidize the lipid to the ketone including 15-hydroxyprostaglandin dehydrogenase<sup>188</sup> and 13-HODE dehydrogenase<sup>189</sup>. Oxo fatty acids have also been measured esterified in the lipid bilayer, indicating that they can be formed from esterified fatty acids, or reinserted into the lipid bilayer after generation<sup>190</sup>. Oxo PUFAs are formed in the mitochondrion by cytochrome c peroxidation of PUFAs in cardiolipin pools. This study also showed that these oxidized fatty acids are enzymatically released from cardiolipin, diffusing out of the mitochondrion to exert signaling effects<sup>191</sup>.

Prostanoid-derived lipid electrophiles have structural similarities to prostaglandins, but can be formed by both COX oxidation and autoxidation mechanisms. The final product of COX metabolism is PGH<sub>2</sub>, which has a defined stereochemistry at the five chiral carbons generated<sup>122</sup>. An isobaric and structurally similar family of metabolites, H<sub>2</sub>-isoprostanes, are generated by autoxidation, and have multiple stereochemistries<sup>192</sup>. Both of these metabolites can rearrange to highly reactive  $\gamma$ -ketoaldehydes, with PGH<sub>2</sub> rearrangement resulting in levuglandins<sup>193, 194</sup>, and H<sub>2</sub>-isoprostane rearrangement resulting in isoketals<sup>195</sup>.

Additionally, PGH<sub>2</sub> can be converted to PGE<sub>2</sub> and PGD<sub>2</sub> by their respective synthases or hydrolysis in solution. These prostaglandins can dehydrate to form PGA<sub>2</sub> and PGJ<sub>2</sub> respectively, both a part of the cyclopentenone series of lipid electrophiles. PGJ<sub>2</sub> readily undergoes further dehydrations to form the electrophile, 15-deoxy- $\Delta^{12,14}$ -prostaglandin J<sub>2</sub> (15d-PGJ<sub>2</sub>)<sup>196, 197</sup>. A similar set of electrophiles without defined stereochemistry is generated by autoxidation from H<sub>2</sub>-isoprostanes<sup>198</sup>. These cyclopentenone lipid electrophiles have been extensively studied, and even detected *in vivo*<sup>197</sup>.

### **Reactivity of lipid electrophiles**

Lipid electrophiles react with nucleophilic amino acids of proteins to form a variety of protein adducts. Generally, cysteine<sup>199</sup> is the most reactive amino acid followed by lysine<sup>200</sup>, histidine<sup>201</sup>, and arginine<sup>202</sup>, but there are some caveats to this rule<sup>200</sup>. Hard-soft acid base theory, which states that soft electrophiles will

react with soft nucleophiles and *vice versa*, has been employed to better explain the reactivity between nucleophilic amino acids and lipid electrophiles. Cysteine, a soft nucleophile, is extremely reactive with  $\alpha,\beta$ -unsaturated carbonyls, soft electrophiles, forming Michael adducts, which can also be formed on lysine and histidine, harder nucleophiles (Figure 10A)<sup>203</sup>. Michael adducts are reversible to varying degrees, however, reduction of the carbonyl to hydroxyl prevents the retro-Michael reaction, and thus facilitates the study of proteins with Michael adducts without worry of adduct loss<sup>204</sup>.

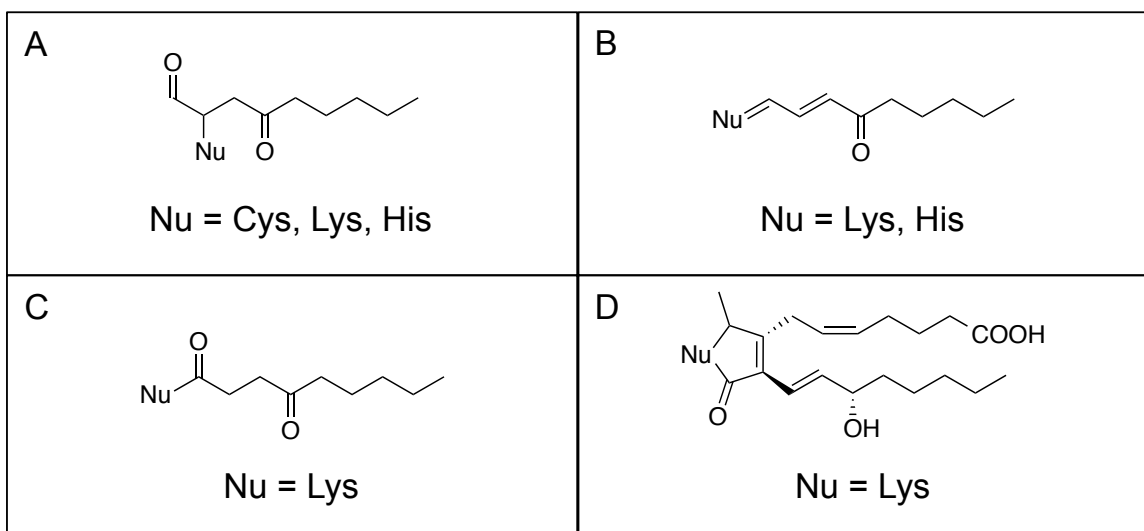


**Figure 10.** Adducts formed on amino acids by lipid electrophiles. A) ONE Michael adduct formed with cysteine, lysine and histidine. B) ONE Schiff base adduct formed with lysine and histidine. C) ONE ketoamide adduct formed with lysine. D) Levuglandin lactam adduct formed with lysine.

Several electrophiles contain aldehydes as reactive groups, which are considered hard electrophiles. These electrophiles do not generate stable products when reacted with cysteine, but do with the harder nucleophiles, lysine and histidine to form a Schiff base (Figure 10B)<sup>205</sup>. Schiff bases are generally

reversible, but some adducts, such as HNE can cyclize to form a much more stable pyrrole adduct<sup>205</sup>.  $\gamma$ -ketoaldehydes also form Schiff base adducts then cyclize to pyrroles. The pyrrole is not easily isolated because it is heavily alkylated, and thus oxidizes further to a highly stable lactam (Figure 10D) or hydroxylactam<sup>195, 206</sup>. The  $\gamma$ -ketoaldehydes are much more reactive than the commonly studied HNE,<sup>195</sup> which has allowed for the development of  $\gamma$ -ketoaldehyde-preferential scavengers<sup>207</sup>. Another interesting adduct formed by Schiff base chemistry is the ketoamide (Figure 10C). The first step in ketoamide adduction is hemiaminal formation, but not dehydration to the Schiff base. Then, three tautomerizations generate a stable amide adduct that is irreversible<sup>208</sup>. Many of the *bis*-electrophiles can also result in protein-protein crosslinks<sup>205, 209</sup>.

### ***Cellular consequences of lipid electrophile adduction***

The impact of lipid electrophile adduction on cellular signaling is vast. Many transcriptional changes occur just from treatment with a single electrophile at sub lethal doses<sup>210, 211</sup>. As already discussed electrophiles can react with the Keap1/Nrf2 complex to induce transcription of antioxidant genes associated with the transcription factor Nrf2<sup>67</sup>. HNE induces Hmox1 expression at sub lethal doses through Nrf2 signaling<sup>211</sup>. Additionally, several reports have shown that lipid electrophiles have anti-inflammatory signaling capabilities<sup>212</sup>. One report shows that HNE reduces the production of proinflammatory cytokines IL-1 $\beta$ , IL-6, and TNF $\alpha$  in lipopolysaccharide-activated macrophages. The authors propose that the reduction in proinflammatory cytokines is the results of altered NF- $\kappa$ B

signaling<sup>24</sup>. Electrophiles have been shown to react with many proteins in the NF- $\kappa$ B family. Both HNE<sup>213, 214</sup> and 15d-PGJ<sub>2</sub><sup>215</sup> adduct IKK- $\alpha$ , and 15d-PGJ<sub>2</sub><sup>216</sup> and neuroprostane A<sub>4</sub><sup>217</sup> adduct IKK- $\beta$ , all preventing NF- $\kappa$ B translocation to the nucleus and reducing pro-inflammatory signaling of the pathway. NF- $\kappa$ B signaling is also inhibited by 15d-PGJ<sub>2</sub> binding to NF- $\kappa$ B itself preventing DNA binding<sup>218</sup>.

Lipid electrophiles have also been reported to participate in a host of negative cellular consequences.  $\gamma$ -ketoaldehydes induce apoptosis by modifying cytochrome c<sup>219</sup>. Additionally, both HNE and ONE induce apoptosis in a p53 dependent mechanism<sup>211, 220, 221</sup>. 15d-PGJ<sub>2</sub> also can induce apoptosis, in neuronal cells, by adducting p53 responsive genes. This adduct is measured in high amounts by antibodies in spinal cord motor neurons of ALS patients<sup>222</sup>. Protein adduction by lipid electrophiles, and the resulting apoptosis is thought to be a contributing factor to neuronal death associated with ALS.

In addition to initiating apoptotic signaling, 15d-PGJ<sub>2</sub><sup>223</sup> and HNE<sup>224</sup> inhibit proteasomal turnover by binding proteins of the 26S proteasome. Exogenous addition of 15d-PGJ<sub>2</sub> to purified 26S proteasomes identifies S6 ATPase as a target of adduction *in vitro*<sup>225</sup>. Lupus patients show an increase in HNE-modified proteins. These adducted proteins induce the generation of anti-DNA antibodies, which may be a contributing factor to the etiology of lupus<sup>226</sup>. Pyrroles formed from  $\gamma$ -ketoaldehydes have also been shown to generate an autoimmune response<sup>227</sup>, and  $\gamma$ -ketoaldehydes bind and inhibit the 20S proteasome<sup>228</sup>. Inhibition of proteasomal degradation results in an accumulation of non-functional proteins. Attempted clearance of these excess non-functional proteins results in



the generation of autoimmune antibodies, providing a mechanistic link between autoimmunity and oxidative stress. This accumulation of non-functional proteins is also associated with AD, PD, and HD disease progression, further linking oxidative stress and neurological disorders.

Lipid electrophiles can also induce pro-inflammatory signaling. The ketoamide adduct has been detected at high levels in atherosclerotic lesions. LDL proteins modified by ketoamides have similar signaling effects as acetylated LDLs, inducing inflammatory responses in macrophages<sup>229</sup>. HNE adducts have also been detected in atherosclerotic lesions, in close proximity to COX-2. From this, it was found that HNE also induces COX-2 protein expression independent of NF- $\kappa$ B, presumably by stabilization of COX-2 mRNA<sup>230, 231</sup>.

Due to the negative impact that increased lipid electrophile generation can have, cells have evolved several detoxification methods to relieve lipid electrophile stress. All of these methods take advantage of the chemical reactivity of lipid electrophiles. GSH is a ubiquitous tripeptide that plays a major role in scavenging reactive cellular metabolites, including lipid electrophiles. The lipid electrophiles 15d-PGJ<sub>2</sub><sup>232</sup>, 15-KETE<sup>177</sup>, HNE<sup>204</sup>, and ONE<sup>176</sup> are all detoxified by GSH conjugation. Additionally, HNE is an order of magnitude more reactive with Cys34 on human serum albumin (HSA), an extremely abundant plasma protein, than GSH indicating a protective role of HSA against diffusible lipid electrophile damage<sup>233</sup>.

Lipid electrophiles have been chemically targeted to the mitochondrion. Mitochondrially targeted electrophiles do not induce Nrf2 signaling indicating that

they are in fact targeted to the mitochondrion, and spend little time in the cytosol making them unable to adduct Keap1 efficiently. These targeted electrophiles reduce oxygen consumption rates more effectively than untargeted electrophiles, showing that the proteins of the electron transport chain are highly sensitive to lipid electrophiles. However, exogenously added electrophiles do not normally target electron transport chain proteins, presumably because the detoxification methods mentioned above do not allow electrophiles to reach the mitochondrion under normal cellular conditions<sup>234</sup>.

### ***Studying lipid electrophiles in disease models***

With the diverse array of adduct species that can be formed, identifying proteins that are susceptible to adduction as well as its cellular consequences is a daunting task. Several methods have been undertaken in attempts to solve this problem. Many of these techniques can be used in both a qualitative and quantitative way to identify changes in lipid electrophile adduction of proteins. These methods include reactive probe pull downs, antibody pull downs, targeted analyses for anticipated electrophiles, electrophiles prepared for future affinity purification, and *in vitro* treatment of purified protein with electrophiles. Two distinct methods of lipid electrophile generation are used to study the cellular targets of lipid electrophile adduction. Exogenously generated lipid electrophiles are those generated outside of the system under investigation. These species are already electrophilic when added to the model system under investigation. On the contrary, endogenously generated lipid electrophiles are generated from

a non-electrophilic precursor, in our case PUFAs, *in situ* by the existing biological machinery of cell or animal under investigation.

### ***Exogenously generated lipid electrophiles***

Most lipid electrophile studies have been performed with exogenously added electrophiles added to purified proteins, and sites of adduction as well as activity changes monitored. This is the most reductionist way to study lipid electrophile adduction of proteins. HNE reacted with purified human serum albumin (HSA) *in vitro* revealed ten sites of modification identified as His and Lys Michael adducts<sup>235</sup>. HNE incubated with purified glyceraldehyde-3-phosphate dehydrogenase (GAPDH) resulted in adduction (His, Cys, and Lys) and inactivation<sup>236</sup>. Inactivation of GAPDH was previously reported in kidney cells treated with exogenous HNE<sup>237</sup>. HNE was added to purified heat shock protein 90 (HSP90), and several histidine residues were identified as adducted<sup>238</sup>. Cytochrome C was adducted by HNE, and based on modeling, the residues adducted may affect tertiary structure and thus its electron transport function<sup>239</sup>. HNE and ONE binding to purified myoglobin<sup>84</sup> and myoglobin in human plasma *in vitro*<sup>83</sup> resulted in adducts on both histidine and lysine residues, which induced structural instability, facilitating oxidation of normally unexposed amino acids. 78 kDa glucose regulated protein (GRP78) was treated with ONE and HNE, and sites of modification were identified in its ATP binding region. This modification inhibited ATPase activity, dose dependently<sup>240</sup>. HNE added to SIRT3 *in vitro* dose dependently increased adduction and decreased activity<sup>241</sup>. The catalytic

cysteine in peptidyl-prolyl *cis/trans* isomerase A1 (PIN1) was identified as adducted by HNE exogenously added to both cells and purified protein. Activity changes were implied by the fact that knockdown of PIN1 reduced growth changes induced by HNE treatment<sup>242</sup>.

Electrophiles attached to affinity tags or dyes have been added to cells for visualization of adduction and affinity purification of adducted proteins. 15d-PGJ<sub>2</sub> covalently linked to a boron-dipyrromethene (BODIPY) dye, was added to cells, and immunocytochemistry analysis showed the cellular localization of adduction, which was confirmed by subcellular fractionation and SDS-PAGE<sup>243</sup>. Biotinylated 15d-PGJ<sub>2</sub> adducts thioredoxin in cells and *in vitro* targeting one redox active cysteine, and one structural cysteine. Over expression of thioredoxin reduces the proinflammatory activity of 15d-PGJ<sub>2</sub><sup>244</sup>.

An alternative approach to this is to use reactive biotin probes that will react with lipid electrophile protein adducts<sup>245</sup>. Exogenous addition of 15d-PGJ<sub>2</sub>, then biotin hydrazide capture and 2-dimensional gel electrophoresis identifies 26S proteasomal proteins, specifically S6 ATPase as adducted. This was confirmed on purified 26S proteasomes *in vitro*<sup>225</sup>. HNE was added to cells, and then biotin conjugated geldanamycin probe was used to purify HSP90 to identify sites of modification. Modification of multiple histidines were identified and correlated to decreased client protein binding<sup>238</sup>. Targets of exogenously added HNE across multiple concentrations were analyzed. Proteins were isolated by biotin-hydrazide capture. Adducted protein levels will change with HNE concentration, while proteins nonspecific bound to the affinity purification beads

will be constant across all HNE concentrations, allowing for the bioinformatic removal of these nonadducted proteins<sup>224</sup>.

One study has used activity-based protein profiling, comparing the reactivity of HNE with an iodoacetylated probe. The rank-order of reactivities of cysteines were determined by this method. They identified proteins that assemble iron-sulfur cluster complexes as particularly susceptible to adduction of cysteines by HNE<sup>246</sup>. It should be noted that these experiments were done on cellular lysates, and are thus only able to suggest rank-order of reactivity based on cysteine alone. Cellular localization, microenvironment factors, and cellular defenses against exogenous electrophile attack will most likely change the order of reactivities seen in a physiological setting.

The generation of azido and alkynyl electrophiles has greatly simplified and expedited the global profiling of lipid electrophile protein targets by allowing for a more selective isolation of adducted proteins by using click chemistry<sup>247</sup> to attach affinity tags, in this case biotin. This technique has been used to profile protein targets of adduction by aHNE<sup>248</sup>. The selectivity of the release of adducted proteins was much improved with the invention of a UV-cleavable biotin linker<sup>249</sup> (Figure 11). This made it possible to globally profile targets of adduction by lipid electrophiles without worry of releasing nonspecifically bound proteins, as is the case with harsh mechanisms of release like boiling or pH extremes. These tools were used to profile and compare the targets of aHNE and aONE adduction in two distinct cell types. This study determined that different classes of proteins have different reactivities to the electrophiles. We were also able to correlate

protein adduction levels to the electrophile defense levels [GSH] of the cells. Additionally, we were able to compile a list of the least reactive or most protected proteins, which were identified as never being adducted across cell types, electrophile identity, and electrophile concentration<sup>204</sup>.

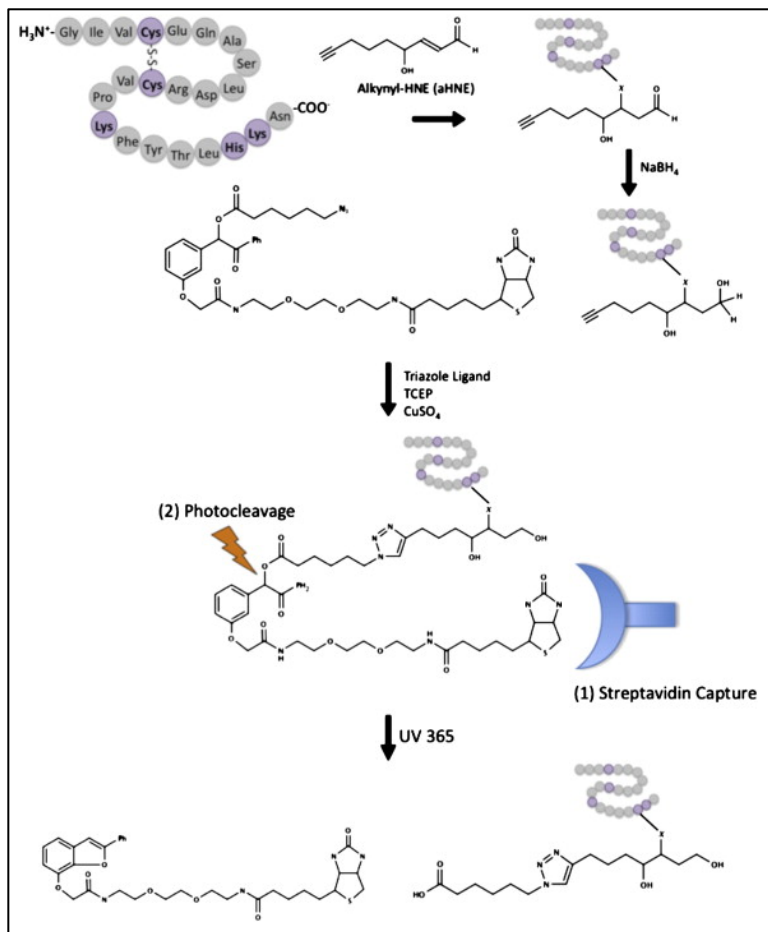


**Figure 11.** Analysis of lipid electrophile adducted proteins using click chemistry, affinity purification, and UV-cleavable biotin. Workflow for attachment of UV-cleavable biotin by click chemistry, affinity purification of lipid electrophile adducted proteins, and selective release by UV-irradiation for proteomic identification of adducted proteins. Reprinted from *Biochimica et Biophysica Acta*, 1818, Ullery, J.C. and Marnett, L.J., Protein modification by oxidized phospholipids and hydrolytically released lipid electrophiles: Investigating cellular responses, 2424-2435, Copyright (2012)<sup>3</sup>, with permission from Elsevier.

### ***Endogenously generated lipid electrophiles***

Analysis of proteins adducted by endogenously generated lipid electrophiles gives the most physiologically relevant identification of what electrophiles are generated and what proteins are important targets for lipid electrophile adduction. The possible pool of lipid electrophiles generated is massive, making identification and analysis a technological challenge. So, many techniques were developed to help enrich for adducted proteins, simplifying the analysis. Antibodies to lipid electrophile adducts have been generated that are highly specific, but constrain analyses to looking at anticipated lipid electrophiles. Reactive tags are currently the most promising method available for the study of endogenously generated lipid electrophiles. However, the promiscuity of their chemistry makes analysis of large data sets difficult because most tags rely on hydrazide groups, which react nonspecifically with carbonyls, a common biological functional group. From a bioinformatics angle, labs have developed software algorithms to better search proteomic data sets to identify both adducted proteins and lipid electrophile adducting species<sup>250</sup>. Finally, bio-orthogonal chemistry has the potential to be the future of protein tagging, allowing for truly global profiling seen with reactive affinity tags, but using reactive groups not present in biology to avoid promiscuity of the reactive affinity tags.

Several labs have attempted a semi-endogeneous approach to lipid electrophile generation. This analysis has endogenous characteristics because a PUFA covalently modified with a dye or affinity tag is metabolized by cellular machinery to lipid electrophiles, and protein adduction is studied. However, this

method also has exogenous characteristics in that the covalent modifier prevents incorporation into and distribution throughout native phospholipid pools, and thus does not truly mimic PUFA incorporation by cells. BODIPY modified AA was added to cells, and PUFA oxidation was initiated with H<sub>2</sub>O<sub>2</sub>. The BODIPY allowed for the qualitative assessment of increased adduction with H<sub>2</sub>O<sub>2</sub> treatment across the proteome by SDS-PAGE separation and visualization<sup>251</sup>. A biotinylated-LA containing phospholipid-like molecule was added to human plasma, and lipid oxidation was induced. Adducted proteins were recovered by streptavidin capture, and apolipoprotein A1 was identified as the major adducted species<sup>252</sup>.

Antibodies have been raised to many of the common electrophiles as well as some of their unique adduct structures. While antibodies have been used in pull-down experiments, much of the work has been focused on qualitative changes in adduction between different disease states. It was determined that HNE adducted proteins are higher in perinatal brains of patients with pontosubicular neuronal necrosis resulting in cellular developmental differences<sup>253</sup>. 13-HODE associated with oxidized LDLs *in vivo* indicates that oxidative stress is higher in atherosclerotic lesions<sup>254</sup>. Additionally, 15d-PGJ<sub>2</sub> protein adducts have been measured at higher levels in atherosclerotic lesions versus in healthy vasculature<sup>197</sup>. Increased levels of both HNE and ONE were measured in liver samples taken from mice with alcoholic liver disease<sup>255</sup>. Endogenously generated isoketal adducts are increased in dendritic cells of angiotensin II treated mice over untreated mice and those treated with isoketal



scavengers<sup>256</sup>, as determined by a single chain antibody to the isoketal adduct<sup>257</sup>.

Reactive probes can also be used for endogenously generated electrophiles, most notable biotin hydrazide<sup>245</sup>, to tag adducted proteins. Streptavidin affinity purification is used to isolate adducted proteins for identification by targeted western blotting or untargeted proteomic analysis. This technique was used to identify GRP78<sup>240</sup>, HSP90<sup>258</sup>, and SIRT3<sup>241</sup> as adducted by HNE in alcoholic liver disease. These studies were also able to measure decreased ATP binding to adducted GRP78<sup>240</sup>, decreased client protein binding to adducted HSP90<sup>258</sup>, and increased protein acetylation in SIRT3 adducted samples<sup>241</sup>, indicating that endogenous lipid electrophile modification is modulating protein activity in these samples. This technique has also been used to assess endogenous HNE modification of proteins in adipose tissue<sup>259</sup>.

Lipid electrophile adduction of charged amino acid residues on proteins will result in pI changes for that protein and differential mobility in 2-dimensional gel electrophoresis. Once a gel spot is identified as differentially adducted, it can be excised and identified by proteomic methods. This phenomenon has been exploited to identify proteins adducted by lipid electrophiles in mouse brain<sup>260</sup> and liver<sup>255</sup>. This method has also been used to identify mitochondrial proteins as heavily adducted by HNE during doxorubicin induced oxidative stress. Changes in mitochondrial function were measured that directly correlate with the proteins identified as adducted losing function<sup>261</sup>. Additionally, mitochondrial proteins were identified as adducted by HNE in a *C. elegans* model for PD<sup>262</sup>, the brains of

human down-syndrome patients<sup>263</sup>, and the brains of human patients with mild cognitive impairment, a precursor to AD<sup>264</sup>. These studies all appear to correlate mitochondrial dysfunction, endogenous oxidative protein modification, and neurodegeneration.

Oxidized PUFAs play an important role in both physiological and pathophysiological cellular processes. These roles are through both non-covalent and covalent signaling actions. Covalent signaling actions have the potential to be longer lived as they have been shown to affect protein turnover. Therefore, it is important to further investigate how lipid electrophiles are generated, what proteins are the cellular targets of endogenously generated lipid electrophiles, and what are the cellular consequences of lipid electrophile adduction.

### **Dissertation Aims**

The major aim at the outset of this dissertation was to develop and apply methodology that would allow for the global analysis of protein adduction by endogenously generated lipid electrophiles. Much work has been done previously to understand the targets of both endogenously generated or exogenously added lipid electrophiles. However, all of these studies failed to address one or more of the following aspects: 1.) Lipid electrophiles are not generated at a discrete time point. 2.) Lipid electrophiles are not generated at a discrete concentration. 3.) Lipid electrophiles are generated inside of the cell and in distinct cellular components, not outside of it. 4.) A diverse array of electrophiles are generated. We designed a series of  $\omega$ -alkynyl fatty acids to use

as surrogates for native fatty acids, which would allow us to generate lipid electrophiles endogenously based on all of the criteria mentioned above, use click chemistry and affinity purification to retrieve lipids, lipid electrophiles generated, as well as electrophile adducted proteins for further analysis.

In Chapter II we evaluated the chemistry of oxidation of  $\omega$ -alkynyl linoleic acid (*a*LA) and  $\omega$ -alkynyl arachidonic acid (*a*AA). We were able to determine that the chemistries of autoxidation were indistinguishable, that there were slight differences in LOX mediated oxidation, and large differences in COX mediated oxidation. In Chapter III, we perform further validation of the model by showing that *a*LA is incorporated into phospholipids, and is biosynthesized to *a*AA as would be expected with LA-incorporation. Additionally, we incorporated *a*LA into macrophages and used click chemistry and affinity purification to isolate lipid electrophile adducted proteins generated during RAW264.7 macrophage activation. Stable isotope labeling of amino acids in cell culture was used to quantify expression and adduction differences before and after activation. We were able to identify membrane and mitochondrial proteins as heavily induced and heavily adducted, and show that mitochondrial superoxide is necessary for the formation of lipid electrophiles. The pathways most affected are those responsible for ATP synthesis and oxidant defense, and we were able to measure activity changes of proteins in these pathways that correlate to lipid electrophile adduction. Chapter IV investigates the origin and mechanism by which PUFAs are oxidized and electrophiles are formed. In Chapter III we learned that adduction was occurring primarily in the mitochondrion and

dependent upon mitochondrial superoxide, which led us hypothesize that the lipid electrophiles measured are being formed by an autoxidation mechanism. We were able to show that much of the PUFA oxidation in activated RAW264.7 macrophages is generated by autoxidation, and that various inhibitors are able to reduce PUFA oxidation and protein adduction by lipid electrophiles correlating the two. These data resulted in the observation that both mitochondrial superoxide and COX-2 activity are necessary for the formation of lipid electrophiles during macrophage activation. Finally, Chapter V has a brief discussion of the implications of our findings. Additionally, some ideas for future experiments will be discussed including new disease models where *a*PUFAs can be applied, and incorporating *a*LA into mouse models of disease.

## Chapter II

### **$\omega$ -ALKYNYL LIPID SURROGATES FOR POLYUNSATURATED FATTY ACIDS: FREE RADICAL AND ENZYMATIC OXIDATIONS**

#### **Introduction**

The lipidome is a complex mixture of fatty acid and sterol molecular species, which include the fatty acid esters of sterols, triglycerides, glycerophospholipids, such as the ethanolamines, cholines and inositols, and many more species<sup>265</sup>. Polyunsaturated fatty acids (PUFAs) such as linoleic acid (LA) (18:2) and arachidonic acid (AA) (20:4) and their esters are particularly important components of the lipidome. These essential fatty acids are involved in a number of consequential metabolic transformations via their oxidation by lipoxygenase (LOX) and cyclooxygenase (COX) enzymes<sup>122, 266-268</sup>. Oxidized lipids play a significant role in a number of physiological and pathophysiological events, including cardiovascular disease, cancer, and neurodegenerative diseases<sup>44</sup>. As discussed in Chapter I, the nonenzymatic peroxidation of both LA and AA by molecular oxygen generates intermediate peroxy free radicals<sup>105, 110, 269-271</sup>. Products that result from this lipid peroxidation include peroxides and hydroperoxides, as well as secondary electrophilic products capable of covalently modifying biomolecules, potentially altering their function<sup>248, 272-274</sup>.

Tracking lipids, lipid metabolites, and lipid decomposition products in cells is a formidable task as the complexity of the mixture challenges the most powerful analytical tools<sup>275-278</sup>. Stable isotope derivatives of lipids have been

used with some success to track the distribution of molecular species into different lipid classes in organelles, but detecting a minor metabolic byproduct from thousands of different lipid species is particularly difficult since stable isotope labeled compounds are often isobaric with endogenous species<sup>279</sup>. Radiolabels have also been used successfully in many applications, but associating a particular radioactive chromatography fraction with the structure of a molecular species in a complex mixture is a challenge. Recently, an affinity labeling technique that makes use of terminal alkynyl lipid analogs was reported<sup>280</sup>. In this approach, stable, but reversible alkyne-cobalt complexes are formed on a phosphine-modified silica to isolate alkynyl lipids. This strategy has been used to monitor the distribution of alkynyl fatty acids into various cellular phospholipid classes along with the subsequent lipase-catalyzed metabolism of those lipids<sup>281</sup>. In recent studies, terminal alkynyl analogs of 4-hydroxy-2-nonenal (HNE) and 4-oxo-2-nonenal (ONE), lipid-derived electrophiles known to modify proteins and nucleic acids, were used to globally profile electrophile adduction of proteins. UV-cleavable biotin azide was used to isolate, identify, and quantify cellular protein-electrophile adducts<sup>204, 248, 249</sup>. This affinity chemistry allows protein-lipid adducts to be concentrated and identified by standard proteomic protocols. One shortcoming of adding electrophiles exogenously to cells is that it does not mimic endogenous lipid electrophile diversity, concentration, time course of generation, and location of formation. To address these issues, we have developed a series of  $\omega$ -alkynyl PUFAs to investigate endogenous lipid oxidation and its cellular consequences.

Tracking lipid incorporation and metabolism in cellular systems has long been a goal for chemists, biochemists, and biologists alike. Alkynyl analogs of lipid and cholesterol species have been utilized to facilitate the tracking and retrieval of these species in cells<sup>248, 280, 282</sup>. During these studies, it is assumed that the  $\omega$ -alkyne confers only a minimal structural change to its lipid analog, resulting in nearly identical chemical, biochemical and biological properties. Here, we report the oxidation chemistry for the alkynyl lipid analogs,  $\omega$ -alkynyl arachidonic acid (*aAA*) and  $\omega$ -alkynyl linoleic acid (*aLA*), revealing that alkyne substitution has no effect on fatty acid free radical autoxidation, and minimal effect on enzymatic oxidation. This establishes that alkynyl PUFAs provide a method to selectively study lipid distribution, chemistry, and lipid metabolite interactions with cellular macromolecules.

## Materials and Methods

*Materials.* All reagents are from Sigma, St. Louis, MO unless otherwise noted. All native fatty acids and deuterated lipid metabolites are from Cayman Chemical, Ann Arbor, MI unless otherwise noted. The alkynyl fatty acids, *aLA* and *aAA*, were synthesized as previously described<sup>280, 282</sup>. N-methyl benzohydroxamic acid (NMBHA) has been prepared as previously described<sup>283</sup>. Benzene (HPLC grade) was passed through a column of neutral alumina and stored over molecular sieves (benzene is a carcinogen and mutagen, and should be used with extreme care). Commercial  $\alpha$ -tocopherol was chromatographed before use. Diazomethane was prepared by portion-wise addition of

nitrosomethylurea into heterogeneous mixture of 40% aqueous KOH and ethanol at 0 °C. The deep yellow organic layer was decanted and dried over NaOH. The dried ethereal MeN<sub>2</sub> was used immediately.

*Formation and analysis of alkynyl hydroxy octadecadienoic acid (aHODE) by autoxidation.* To a solution of aLA in benzene was added 2,2'-azobis(4-methoxy-2,4-dimethylvaleronitrile) (MeOAMVN) in benzene, and the mixture was incubated at 37 °C. After 45 min, a solution of butylated hydroxytoluene (BHT) and triphenyl phosphine (PPh<sub>3</sub>) in benzene was added, and the mixture was vortexed for 1 min. Benzene was evaporated under a stream of argon, and the residual material was reconstituted in of 1.2% isopropanol in hexanes with 0.1% acetic acid for HPLC-UV analysis. For direct infusion MS studies of aHODE, eluted peaks from HPLC-UV analysis were collected, and solvents were evaporated under a stream of argon, then the residues were reconstituted in methanol. For NMR studies of aHODE, corresponding peaks collected from HPLC-UV analysis were combined, solvents were evaporated and the residues were dried under high vacuum for 2 h. These dried materials were reconstituted in benzene-d<sub>6</sub> and placed into 1.7 mm outside diameter sample tubes for NMR analysis.

*Formation and analysis of alkynyl hydroxy eicosatetraenoic acid (aHETE) by autoxidation.* To a mixture of aAA and NMBHA in acetonitrile was added MeOAMVN in acetonitrile. After 35 h of incubation at 37 °C, BHT/PPh<sub>3</sub> in acetonitrile was added, and the mixture was vortexed for 2 min. Acetonitrile was removed under a stream of argon and the remaining material was reconstituted



in of 1.2% isopropanol in hexanes with 0.1% acetic acid for HPLC-UV analysis. MS studies of *a*HETE, and NMR studies of *a*HETE were performed as described above for *a*HODE.

*HPLC-UV/MS analysis of (a)HODEs and (a)HETEs.* All HPLC Analyses of (*a*)HETE and (*a*)HODE were carried out on a single Beckman 5  $\mu$ m ultrasphere silica column (250 x 4.6 mm) using isocratic normal phase conditions (1.2% 2-propanol in hexanes containing 0.1% acetic acid)<sup>284</sup>. Chiral HPLC analyses of HETE and HODE methyl esters were performed on a Chiralpak AD column (250 x 4.6 mm) produced by Chiral Technologies Inc., Exton, PA. *a*HETE products have been eluted with 2% ethanol in hexanes, whereas *a*HODE were eluted with 5% methanol in hexanes. Direct infusion MS experiments were performed on ThermoFinnigan TSQ Quantum triple quadrupole mass spectrometer, whereas all HPLC-MS analyses were conducted on the same instrument coupled with a Surveyor MS Pump and Surveyor Autosampler (for RP-HPLC) or with Waters Alliance 2690 Separation Module (NP-HPLC). Detailed information about solvent gradients and MS settings applied during these analyses is given in the appropriate protocols presented below. Unless stated otherwise, all the HPLC separations were conducted with a solvent flow rate of 1 mL/min.

*Formation and analysis of alkynyl F<sub>2 $\alpha$</sub> -Isoprostane (aF<sub>2 $\alpha$</sub> -IsoP).* MeOAMVN was added to a 165 mM solution of *a*AA in benzene and the mixture was incubated at 37 °C for 24 h. Solvent was then evaporated, and the residue was treated with mixture of 1mmol BHT and 10 mmol P(OMe)<sub>3</sub> in 3:1, acetonitrile:water and vortexed for 5 min. The following solvent gradient was

applied: 10% (95:5, acetonitrile:methanol) in 2 mM ammonium acetate was held for 10 min, then ramped to 25% (95:5, acetonitrile:methanol) in 2 mM ammonium acetate over 45 min. LC-MS/MS with negative ion mode electrospray ionization (ESI) was used, and the important mass spectrometer parameters were optimized for commercially available PGF<sub>2α</sub>. The *m/z* transitions monitored were for a5-F<sub>2α</sub>-IsoP (349 > 115), a8-F<sub>2α</sub>-IsoP (349 > 127), a12-F<sub>2α</sub>-IsoP (349 > 151), and a15-F<sub>2α</sub>-IsoP (349 > 193). Control oxidations of AA were performed using analogous reaction conditions, however slightly different analytical conditions were applied to analyze the AA oxidation products. The following solvent gradient was applied for AA oxidation products: 20% (95:5, acetonitrile:methanol) in 2 mM ammonium acetate was held for 10 min, then ramped to 40% (95:5, acetonitrile:methanol) in 2 mM ammonium acetate over 40 min. The *m/z* transitions monitored were for 5-F<sub>2α</sub>-IsoP (353 > 115), 8-F<sub>2α</sub>-IsoP (353 > 127), 12-F<sub>2α</sub>-IsoP (353 > 151), and 15-F<sub>2α</sub>-IsoP (353 > 193).

*Cyclooxygenase O<sub>2</sub> Uptake Kinetics.* Quantification of cyclooxygenase activity was performed in a thermostatted cuvette at 37 °C with stirring and monitored using a polarographic electrode with an Instech System 203 oxygen monitor (Instech Laboratories Inc., Plymouth Meeting, PA). Substrates were solubilized in dimethyl sulfoxide (DMSO). Activity assays were performed in 100 mM Tris buffer containing 500 μM phenol, with hematin-reconstituted cyclooxygenase protein. Substrate concentration was varied (1-50 μM), and maximal reaction velocity data were obtained from the linear portion of the

oxygen uptake curves. The data were analyzed by nonlinear regression with GraphPad Prism (GraphPad, San Diego, CA).

*Crude lipoxygenase kinetic parameters.* LOX activity was detected by monitoring the absorbance of the conjugated diene product, HPETE, at 235 nm. UV assays were monitored using a Hewlett Packard 8453 diode array spectrophotometer equipped with a thermostatted cuvette at 25 °C, with stirring at 180 rpm. The enzyme reactions included reaction buffer 50 mM Tris pH 7.4 with 0.03% Tween-20 and substrate, and were initiated by the addition of enzyme. Compounds were dissolved in acetonitrile containing 10% acetic acid before addition to the reaction buffer; acetonitrile was kept below 1% of the total reaction volume. Substrate concentration was varied (1-50  $\mu\text{M}$ ), and maximal reaction velocity data were obtained from the linear portion of the absorbance curves. Rates were converted from absorbance units/s to  $\mu\text{M aHPETE/s}$  using the molar absorptivity constant of  $0.027 \mu\text{M}^{-1}\text{cm}^{-1}$ . The data were analyzed by nonlinear regression with GraphPad Prism.

*Kinetic Measurements of aLA, LA, aAA, and AA by s15-LOX-1.* Soybean 15-Lipoxygenase-1 (s15-LOX-1) (Cayman Chemical, Ann Arbor, MI), LA, AA, aLA, and aAA were all diluted to 2X final concentration in 100 mM borate pH 9 at 25 °C. 1 mL fatty acid was added to a 1 cm cuvette in a Beckman-Coulter DU-800 spectrophotometer as a blank control. 1 mL enzyme was added, and the reaction was monitored at 235 nm sampling every 1.5 s in triplicate. The slope was averaged over ten points in the linear portion of the curve to get the  $\Delta\text{absorbance per second}$ , which was converted to  $V_o$  using the molar extinction

coefficients of  $0.023 \mu\text{M}^{-1}\text{cm}^{-1}$  for HPODE and  $0.027 \mu\text{M}^{-1}\text{cm}^{-1}$  for HPETE. Kinetic parameters were determined in GraphPad Prism using Michaelis-Menten fitting.

*Enzymatic oxidation of aLA and LA for LC-MS/MS analysis.* s15-LOX-1 was diluted to have a final concentration ratio of 100:1, fatty acid:enzyme in 100 mM borate pH 9. Potato 5 lipoxygenase (5-LOX) (Cayman Chemical) was diluted to have a final concentration ratio of 100:1, fatty acid:enzyme in 100 mM phosphate pH 6.3. LA and aLA were added from 100X stocks in DMSO, and incubated 15 min at 25 °C. The reactions were quenched, and fatty acid metabolites extracted with ethyl acetate containing 0.5% acetic acid, PPh<sub>3</sub>, +/- 9-HODE-d<sub>4</sub>, and +/- 13-HODE-d<sub>4</sub>. Organic layer was dried under inert gas and dissolved in methanol for LC-MS/MS analysis. Metabolites were analyzed on a Thermo Finnigan TSQ Quantum with ESI source interfaced to Surveyor MS Pumps and Surveyor Autosampler in both full scan and SRM modes. Metabolites were separated by reverse-phase gradient HPLC on a C<sub>18</sub> (50 x 2.1 mm, 3 μm) column (Supelco, St. Louis, MO) using 0.1% formic acid in water and 0.1% formic acid in acetonitrile as the A and B mobile phases respectively. Full scan samples were separated by holding 20% B for 2 min, then ramping to 98% B over 6 min, holding 98% B for 3 min, then equilibrating to 20% B for 3 min. Q1 was scanned in negative ion mode from 250 *m/z* to 380 *m/z* in 1 sec. SRM samples were separated by holding 40% B for 0.5 min, then ramping to 98% B over 2 min, holding at 98% B for 2 min, then equilibrating to 40%B for 2.5 min. Metabolites were detected by SRM in negative ion mode observing the *m/z* transitions for a9-HODE (291.2 > 171.2), a13-HODE (291.2 > 195.2), 9-HODE

(295.2 > 171.2), 13-HODE (295.2 > 195.2), 9-HODE-d<sub>4</sub> (299.2 > 172.2), and 13-HODE-d<sub>4</sub> (299.2 > 198.2) for 100 msec each.

Mouse COX2 (COX-2) was diluted to have a final concentration ratio of 100:1, fatty acid:enzyme in 100 mM Tris, 500 μM phenol, 2X [COX-2] Hematin pH 8. The COX-2 was incubated 5 min at 37 °C. LA and aLA were added from 100X stocks in DMSO, and incubated 15 min at 37 °C. The reactions were quenched, and fatty acid metabolites extracted and analyzed as detailed for the lipoxygenase enzymes.

*Enzymatic oxidation of aAA and AA for LC-MS/MS analysis.* s15-LOX-1 was diluted to a final concentration ratio of 100:1, fatty acid:enzyme in 100 mM borate pH 9. AA and aAA were diluted to 100X stocks in DMSO. Fatty acids were separately added to enzyme solutions, and incubated 15 min at 25 °C. The reactions were quenched, and fatty acid metabolites extracted with ethyl acetate containing 0.5% acetic acid, PPh<sub>3</sub>, and +/- 15-HETE-d<sub>8</sub>. The organic layer was dried under inert gas and dissolved in methanol for LC-MS/MS analysis. Metabolites were analyzed on a Thermo Finnigan TSQ Quantum with ESI source interfaced to Surveyor MS Pumps and Surveyor Autosampler in both full scan and SRM modes. Metabolites were separated by gradient HPLC on a C<sub>18</sub> (50 x 2.1 mm, 3 μm) column using 0.1% formic acid in water and 0.1% formic acid in acetonitrile as the A and B mobile phases respectively. Full scan samples were separated by holding 20% B for 2 min, then ramping to 98% B over 6 min, holding 98% B for 3 min, then equilibrating to 20% B for 3 min. Q1 was scanned in negative ion mode from 250 *m/z* to 380 *m/z* in 1 sec. SRM samples were

separated by holding 40% B for 0.5 min, then ramping to 98% B over 2 min, holding at 98% B for 2 min, then equilibrating to 40%B for 2.5 min. Metabolites were detected by SRM in negative ion mode observing the  $m/z$  transitions for *a*15-HETE (315.2 > 253.2), 15-HETE (319.2 > 257.2), and 15-HETE- $d_8$  (327.2 > 264.2) for 100 msec each.

COX-2 was diluted to a final concentration ratio of 100:1, fatty acid:enzyme in 100 mM Tris, 500  $\mu$ M phenol, 2X [COX-2] Hematin pH 8. The COX-2 was incubated 5 min at 37 °C. AA and *a*AA were added from 100X stocks in DMSO, and incubated 15 min at 37 °C. The reactions were quenched, and fatty acid metabolites extracted and analyzed as detailed for the lipoxygenase enzyme full scan mode experiment.

*Monitoring the oxidation of LA, AA, aLA, and aAA to completion.* s15-LOX-1, LA, AA, *a*LA, and *a*AA were diluted to 2X final concentration in 100 mM borate pH 9 at 25 °C. 1 mL fatty acid was added to a 1 cm cuvette in a Beckman-Coulter DU-800 spectrophotometer and blanked. 1 mL enzyme was added, and the reaction was monitored at 235 nm sampling every 1.5 s, until the  $\Delta$ absorbance reached 0. The data was fit to a one-phase exponential association in GraphPad Prism to get  $R^2$  values and maximum absorbances.

*NMR of aAA metabolites.* COX-2 was incubated 5 min in 100 mM Tris, 500  $\mu$ M phenol, and 2X [COX-2] hematin pH 8 at 37 °C. *a*AA was added, and the reaction was allowed to proceed for 15 h at 37 °C. The reaction was extracted with two volumes ethyl acetate, organic layer removed, and evaporated under inert gas. The residue was dissolved in ethanol and separated by reverse-phase

HPLC on a SUPELCOSIL C<sub>18</sub> (150 x 3.0 mm, 5 μm) column, eluted with a linear gradient with A and B buffers consisting of 0.1% acetic acid in water and 0.1% acetic acid in acetonitrile. The gradient was held at 10% B for 10 min, then ramped to 100% B over the next 20 min, then held at 100% B for 5 min, all at the flow rate of 1.0 mL/min. The elution profile was monitored by absorbance at 235 nm. Peaks were collected, dried under inert gas and dissolved in CDCl<sub>3</sub> for NMR analysis. <sup>1</sup>H and <sup>1</sup>H-<sup>1</sup>H COSY spectra were recorded on Bruker AV-II 600 MHz spectrometer equipped with a cryoprobe. Chemical shifts are reported in parts per million relative to the signal of residual nondeuterated solvent.

*LC-MS/MS based kinetics for COX-2.* Metabolites of COX-2 do not have an absorbance that can be used to perform kinetic measurements. Therefore, LC-MS/MS was used to measure kinetic parameters based on specific metabolites. COX-2 was diluted to 25 nM in 100 mM Tris, 500 μM phenol, 50 nM Hematin pH 8, and incubated at 37 °C. AA and aAA were added from 100X stocks in DMSO, and incubated at 37 °C. The length of incubation was optimized to give less than 20% substrate turnover. The reactions were quenched, and fatty acid metabolites extracted with ethyl acetate containing 0.5% acetic acid, PGE<sub>2</sub>-d<sub>4</sub>, and 13-HODE-d<sub>4</sub>. Metabolites were separated by reverse-phase gradient HPLC on a C<sub>18</sub> (50 x 2.1 mm, 3 μm) column using 0.1% formic acid in water and 0.1% formic acid in acetonitrile as the A and B mobile phases respectively. Metabolites were separated by holding 25% B for 0.5 min, then ramping to 99% B over 2.5 min, holding at 99% B for 3 min, then equilibrating to 25% B for 3 min. Metabolites were analyzed in negative ion mode by SRM, monitoring the

transitions for *a*11-HETE (315.2 > 167.2), *a*PG (347.2 > 267.2), PG (351.2 > 271.2), 13-HODE-*d*<sub>4</sub> (299.2 > 198.2), PGE<sub>2</sub>-*d*<sub>4</sub> (355.2 > 275.2) on an ABI/Sciex 3200 QTrap interfaced to a Shimadzu LC system. No deuterated standard exists for 11-HETE. The signal intensity ratio between *a*11-HETE and 13-HODE-*d*<sub>4</sub> was observed to be similar in both full scan MS and SRM modes, indicating that 13-HODE-*d*<sub>4</sub> can be used to quantify *a*11-HETE. The amount of each product formed was converted into a concentration, and then into initial reaction rates (*V*<sub>0</sub>) using the incubation time. Kinetic parameters were determined in GraphPad Prism using Michaelis-Menten fitting.

*RAW264.7 macrophage enrichment, activation, and measurement of aAA metabolites.* RAW264.7 macrophages (ATCC, Manassas, VA) were plated at 10% confluence in Dulbecco's Modified Eagle Medium + Glutamax (DMEM) (Life Technologies, Grand Island, NY) supplemented with 10% fetal bovine serum (Atlas Biologicals, Fort Collins, CO). 6:1 fatty acid free BSA:*a*AA was prepared as previously described<sup>285</sup>. After 24 h, media was replaced with serum free DMEM+Glutamax containing *a*AA/BSA added to 15 μM final concentration of *a*AA. After 24 h, the cells were washed with one volume DMEM to remove any unincorporated *a*AA, and treated with DMEM +/- 100 ng/mL Kdo<sub>2</sub>-lipid A (KLA) (Avanti Polar Lipids, Alabaster, AL), prepared as previously described<sup>286</sup>. After 24 h, cells were scraped into media, and extracted with two volumes ethyl acetate containing 0.5% acetic acid, PGE<sub>2</sub>-*d*<sub>4</sub>, and 13-HODE-*d*<sub>4</sub>. The organic layer was dried under inert gas stream and dissolved in methanol for LC-MS/MS analysis. Metabolites were separated by reverse-phase gradient HPLC on a C<sub>18</sub> (50 x 2.1



mm, 3  $\mu$ m) column using 0.1% formic acid in water and 0.1% formic acid in acetonitrile as the A and B mobile phases respectively. Metabolites were separated by holding 25% B for 0.5 min, then ramping to 99% B over 2.5 min, holding at 99% B for 3 min, then equilibrating to 25%B for 3 min. Metabolites were analyzed in negative ion mode by SRM, monitoring the transitions for *a*11-HETE (315.2 > 167.2), *a*11-8,9-HEET (331.2 > 165.2), *a*PG (347.2 > 267.2), PG (351.2 > 271.2), 13-HODE-*d*<sub>4</sub> (299.2 > 198.2), and PGE<sub>2</sub>-*d*<sub>4</sub> (355.2 > 275.2) on an ABI/Sciex 3200 QTrap interfaced to a Shimadzu controller, autosampler, and HPLC pumps.

## Results

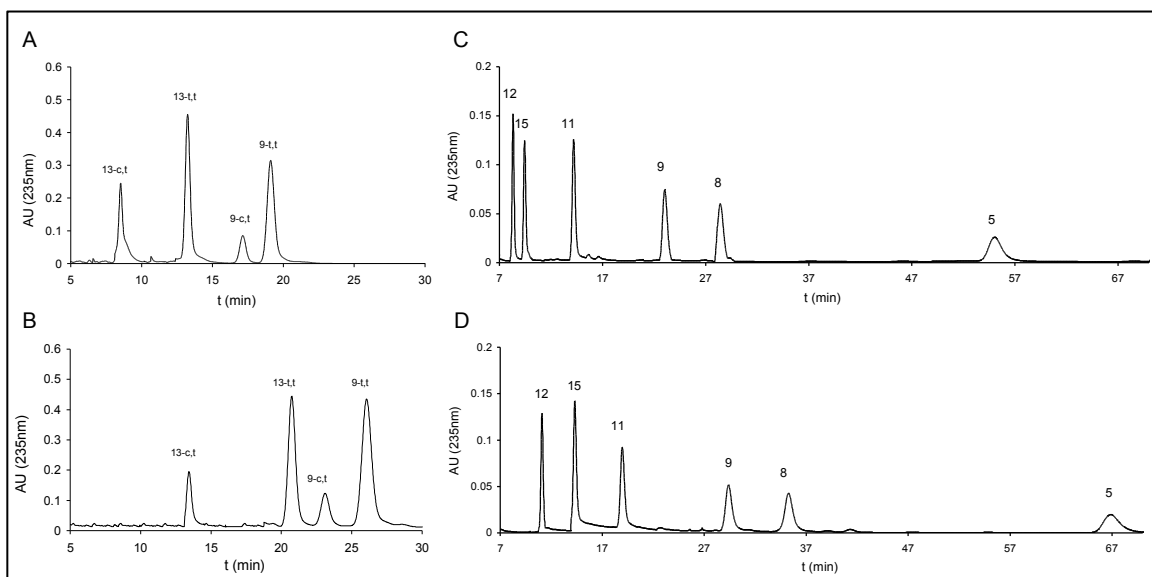


**Figure 1.** Autoxidation products of LA A), aLA B), AA C), aAA D). LA/aLA peaks are labeled with the hydroxyl position on either the 9 or 13 carbon, and the double bond configuration which resulted in either *cis/trans* (*c,t*) or *trans/trans* (*t,t*). AA/aAA peaks are labeled with the position of the oxygen on either the 5-, 8-, 9-, 11-, 12-, or 15-carbon. Both fatty acid pairs oxidize to similar product profiles with similar elution orders. Reprinted with permission from Beavers, W. N., Serwa, R., Shimozu, Y., Tallman, K. A., Vaught, M., Dalvie, E. D., Marnett, L. J., and Porter, N. A. (2014) omega-Alkynyl Lipid Surrogates for Polyunsaturated Fatty Acids: Free Radical and Enzymatic Oxidations. *J Am Chem Soc*, 136, 11529-11539.

LA and aLA were oxidized under conditions that would allow us to compare autoxidation rates and products. As shown in Figure 1, four  $\omega$ -alkynyl conjugated diene hydroperoxides ( $\omega$ -alkynyl hydroperoxyoctadecadienoic acids, aHPODEs) were produced as primary products from aLA autoxidation, a result directly analogous to the chemistry observed with LA<sup>270</sup>. Reduction of the hydroperoxides to the corresponding alcohols, aHODEs, was carried out immediately after peroxidation since the HODEs are more stable and better suited for HPLC analysis than HPODEs. HPLC-UV analysis revealed that

oxidation of an equimolar amounts of *a*LA and LA in parallel generated equivalent amounts of *a*HODEs and HODEs, with identical elution orders to that of the natural compounds.<sup>270</sup> The isolated products were then analyzed by ESI-MS and NMR to confirm hydroxyl position and conjugated diene geometry. Utilizing chiral chromatography, it was determined that the autoxidation of *a*LA produces a mixture of *R* and *S* HODE enantiomers, similar to that of LA (Figure 2).

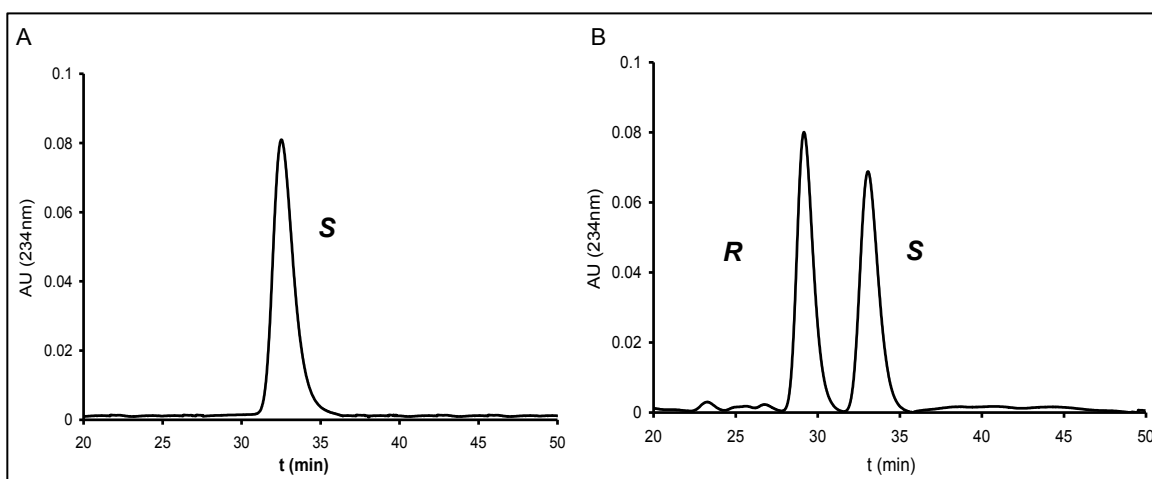


**Figure 2.** Chiral analysis of alkynyl 13-*c,t*-HODE. The methyl ester of 13-*c,t*-HODE produced enzymatically by the reaction with s15-LOX-1 giving an optically pure product A), and non-enzymatically giving mixture of optical enantiomers B). Reprinted with permission from Beavers, W. N., Serwa, R., Shimozu, Y., Tallman, K. A., Vaught, M., Dalvie, E. D., Marnett, L. J., and Porter, N. A. (2014) omega-Alkynyl Lipid Surrogates for Polyunsaturated Fatty Acids: Free Radical and Enzymatic Oxidations. *J Am Chem Soc*, 136, 11529-11539.

Contrary to the simplicity of products generated from LA autoxidation, peroxidation of AA yielded a much more complex mixture of products. In addition to acyclic hydroxy and hydroperoxy products (HETEs and HPETEs) analogous to HODEs and HPODEs, a mixture of diastereomeric isoprostanes (IsoPs) was produced from AA peroxidation<sup>287-290</sup>. Oxidation of *a*AA under conditions that

gave HPETEs as major products was promoted by NMBHA<sup>283</sup>. As shown in Figure 1, characterization of peroxidation products was performed on the *a*HETEs after reduction of the corresponding hydroperoxides. The HPLC-UV elution profile for *a*HETEs was similar to the profile obtained for their natural analogs. MS analyses established the position of oxygen substitution on the carbon chain, and NMR analysis provided information about stereoisomeric geometry. The major HETE stereoisomers have *Z,E*-conjugated diene geometry, analogous to the structure of AA-derived HETEs. These experiments show that the elution order of *a*HETEs is identical to the elution order observed for HETEs. Additionally, oxidation of equimolar mixtures of AA and *a*AA generated nearly equimolar mixtures of HETE and *a*HETE.

HETEs are not the only autoxidation products formed from AA, so *a*AA was exposed to the radical initiator MeOAMVN in the absence of NMBHA under conditions of oxidation and workup that were expected to yield significant quantities of the *a*F<sub>2 $\alpha$</sub> -IsoPs. LC-MS/MS analysis of the major (*a*)F<sub>2 $\alpha$</sub> -IsoPs formed in this sequence determined that 5- and 15- series (*a*)F<sub>2 $\alpha$</sub> -IsoPs are formed in a large excess compared to the 8- and 12- regioisomers. The preference for formation of the 5- and 15- regioisomers and the elution profiles observed for both the natural and  $\omega$ -alkynyl analogues are consistent with a previous report<sup>291</sup>.

**Table 1.** Kinetic values comparing *aAA* and AA with COX and LOX enzymes. Kinetic values were determined for the enzymes ovine cyclooxygenase 1 (oCOX-1), human cyclooxygenase 2 (hCOX-2), human platelet-type 12-lipoxygenase (plt12-LOX), porcine leukocyte-type 12-lipoxygenase (lk12-LOX), rabbit reticulocyte 15-lipoxygenase 1 (r15-LOX-1), and soybean 15-lipoxygenase 1 (s15-LOX-1). All COX enzymes except were assayed using oxygen electrode. LOX enzymes were assayed using absorbance at 235 nm. AA kinetic values taken from the literature are in parentheses<sup>2</sup>.  $V_{max}/K_m$  values are reported for crude enzyme preparations, while  $k_{cat}/K_m$  values are reported for purified enzymes. Reprinted with permission from Beavers, W. N., Serwa, R., Shimozu, Y., Tallman, K. A., Vaught, M., Dalvie, E. D., Marnett, L. J., and Porter, N. A. (2014) omega-Alkynyl Lipid Surrogates for Polyunsaturated Fatty Acids: Free Radical and Enzymatic Oxidations. *J Am Chem Soc*, 136, 11529-11539.

Enzyme	Substrate	Product	$K_m$ ( $\mu\text{M}$ )	$V_{max}$ ( $\mu\text{Ms}^{-1}$ )	$k_{cat}$ ( $\text{s}^{-1}$ )	$k_{cat}/K_m$ ( $\mu\text{M}^{-1}\text{s}^{-1}$ )	$V_{max}/K_m$ ( $\text{s}^{-1}$ )
oCOX-1	<i>aAA</i>	$\text{O}_2$ cons.	6.2±0.8	n/a	57±6	9±6	n/a
	AA		(3.4±0.6)		(51±3)	(15±3)	
hCOX-2	<i>aAA</i>	$\text{O}_2$ cons.	4.5±0.7	n/a	11±1	2±1	n/a
	AA		(6.1±0.6)		(14.7±0.5)	(2.4)	
plt12-LOX	<i>aAA</i>	Abs	7.0±0.3	4.53±0.08	n/a	n/a	0.6±0.3
	AA	235nm	(9.5±0.7)	(13.3±0.3)			(1.4±0.7)
lk12-LOX	<i>aAA</i>	Abs	4±1	1.37±0.09	n/a	n/a	0.3±1
	AA	235nm	(7.8±1.3)	(13.1±0.7)			(2±1)
r15-LOX-1	<i>aAA</i>	Abs	7±2	0.61±0.05	n/a	n/a	0.09±2
	AA	235nm	(20±3)	(8.6±0.4)			(0.4±3)
s15-LOX-1	<i>aAA</i>	Abs	3.1±0.9	0.025±0.002	2.5±0.2	0.8±0.2	n/a
	AA	235nm	6±1	0.12±0.01	24±2	4.3±0.2	

Using alkynyl fatty acids to further probe the biochemistry of cellular systems requires detailed knowledge of the chemistry of enzymatic oxidation. Kinetic parameters were determined for the transformations of *aAA* in the presence of several LOX and COX enzymes by measuring alkene formation or  $\text{O}_2$  consumption respectively. Data presented in Table 1 demonstrate small differences in  $k_{cat}/K_M$  for the alkynyl and natural fatty acids, suggesting that *aAA* is an efficient substrate for both COX-1 and COX-2. The catalytic efficiency of human platelet-type 12-LOX in the presence of *aAA* was also found to be similar to the efficiency observed for AA as a substrate. On the other hand, porcine

leukocyte-type 12-LOX, rabbit reticulocyte 15-LOX1, and s15-LOX-1 did not oxidize *a*AA as efficiently as AA, illustrated by the relatively large differences in  $V_{\max}/K_m$  and  $k_{\text{cat}}/K_m$  values between these substrates. Despite these differences in kinetic parameters, *a*AA is completely reacted when incubated with s15-LOX-1 for long enough times (Figure 3).

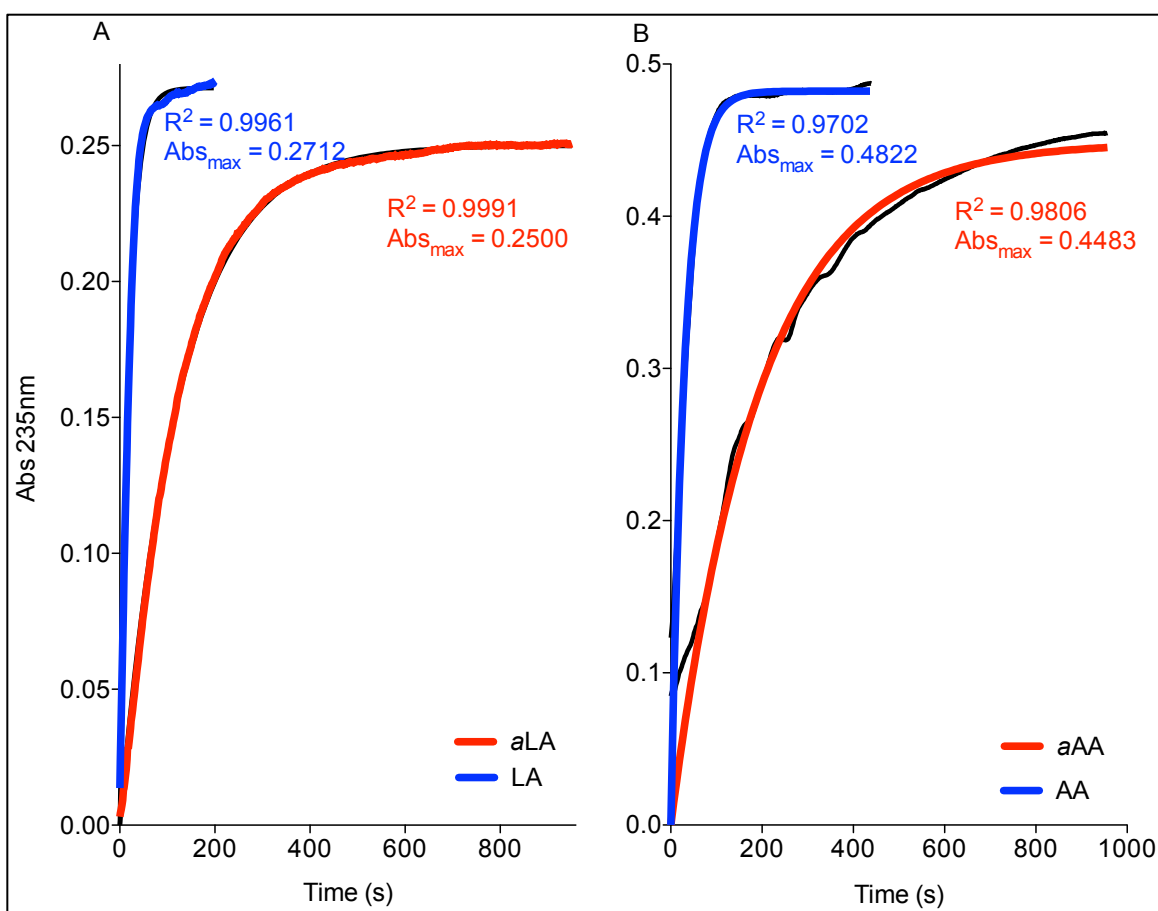


**Figure 3.** s15-LOX-1 metabolism of LA, aLA, AA, and aAA. LA, aLA, AA, and aAA were all incubated with s15-LOX-1 and observed at 235nm until  $\Delta\text{Abs} = 0$ . Despite having different kinetic parameters, fatty acid pairs *a*LA/LA A) and *a*AA/AA B), are eventually oxidized completely. Reprinted with permission from Beavers, W. N., Serwa, R., Shimozu, Y., Tallman, K. A., Vaught, M., Dalvie, E. D., Marnett, L. J., and Porter, N. A. (2014) omega-Alkynyl Lipid Surrogates for Polyunsaturated Fatty Acids: Free Radical and Enzymatic Oxidations. *J Am Chem Soc*, 136, 11529-11539.

The kinetic parameters for the transformations of *a*LA and LA by s15-LOX-1 were also measured, and  $k_{cat}/K_m$  values were determined to be  $0.51 \pm 0.07 \mu\text{M}^{-1}\text{s}^{-1}$  and  $5.2 \pm 0.6 \mu\text{M}^{-1}\text{s}^{-1}$ , respectively. These values are similar to those observed for *a*AA and AA (Table 1), and like *a*AA, *a*LA is also eventually completely reacted (Figure 3). *a*LA and LA give a similar product profile of primarily (*a*)9-HODE or (*a*)13-HODE for the enzymatic transformation by 5-LOX or s15-LOX-1 respectively (Figure 4 and 5). *a*13-HODE produced from s15-LOX-1 was assessed for optical purity, and determined to be entirely the *S* isomer, as anticipated from the stereochemistry of LA oxidation (Figure 2). Ovine COX-1 generated a similar product profile to COX-2 when reacted with LA, and neither enzyme oxygenated *a*LA (Figure 5).

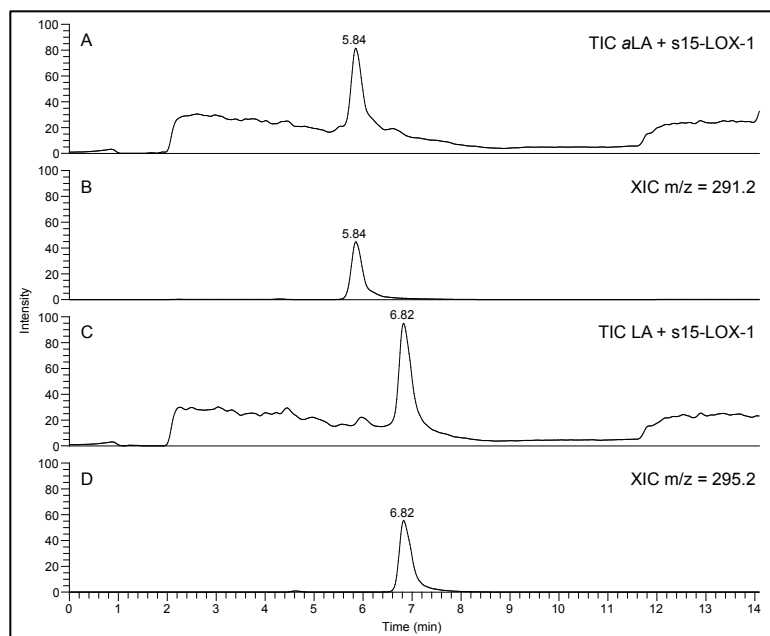


**Figure 4.** Comparison of the metabolite profiles of aLA A) and LA C) with s15-LOX-1. The metabolism of aLA by s15-LOX-1 shows a single product showing the addition of oxygen. The metabolism of LA by s15-LOX-1 also shows a single product showing the addition of oxygen. Reprinted with permission from Beavers, W. N., Serwa, R., Shimozu, Y., Tallman, K. A., Vaught, M., Dalvie, E. D., Marnett, L. J., and Porter, N. A. (2014) omega-Alkynyl Lipid Surrogates for Polyunsaturated Fatty Acids: Free Radical and Enzymatic Oxidations. *J Am Chem Soc*, 136, 11529-11539.



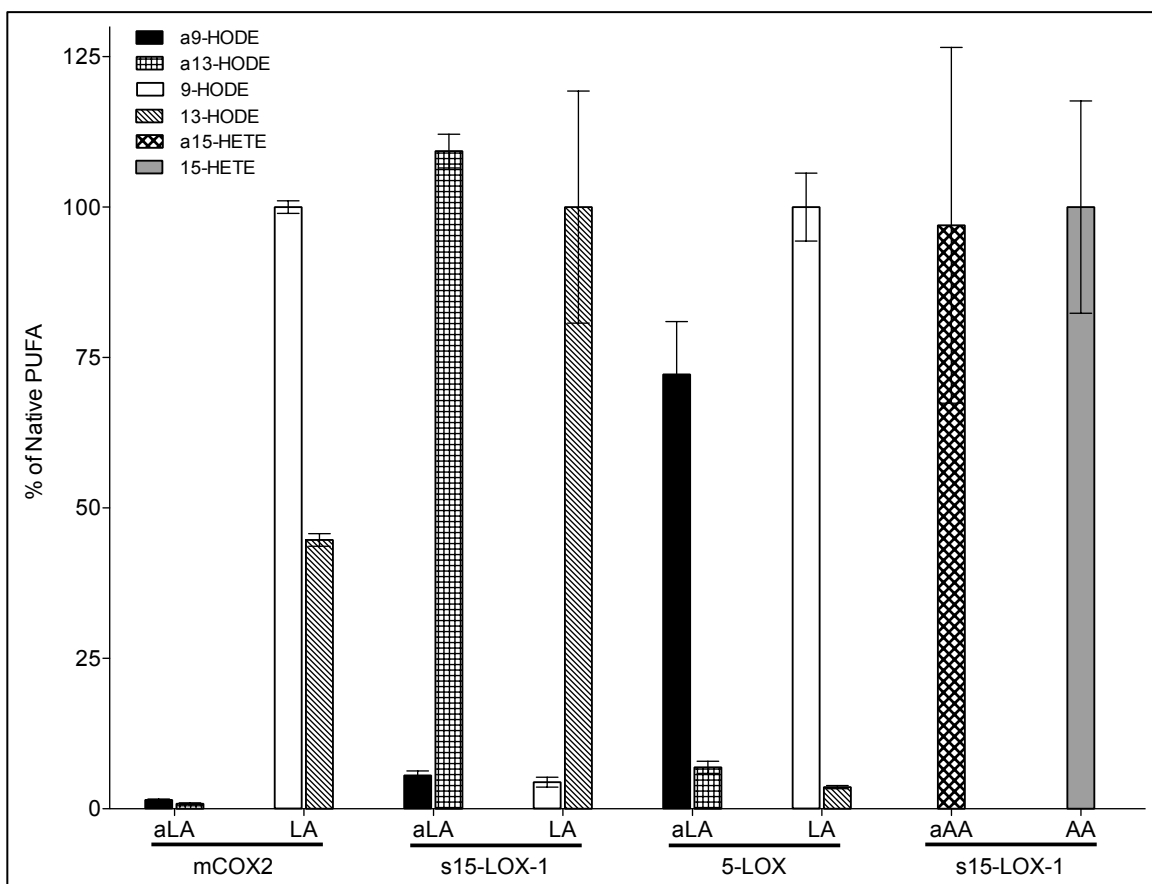


**Figure 5.** COX and LOX *in vitro* metabolism of LA, aLA, AA, and aLA. Quantification of single oxygenation metabolites for the reaction between the PUFA pairs aLA/LA and aAA/AA with murine COX2 (mCOX2), s15-LOX-1, and 5-LOX. Fatty acid pairs are normalized to the most abundant native (LA or AA) metabolite for each enzyme. Reprinted with permission from Beavers, W. N., Serwa, R., Shimozu, Y., Tallman, K. A., Vaught, M., Dalvie, E. D., Marnett, L. J., and Porter, N. A. (2014) omega-Alkynyl Lipid Surrogates for Polyunsaturated Fatty Acids: Free Radical and Enzymatic Oxidations. *J Am Chem Soc*, 136, 11529-11539.

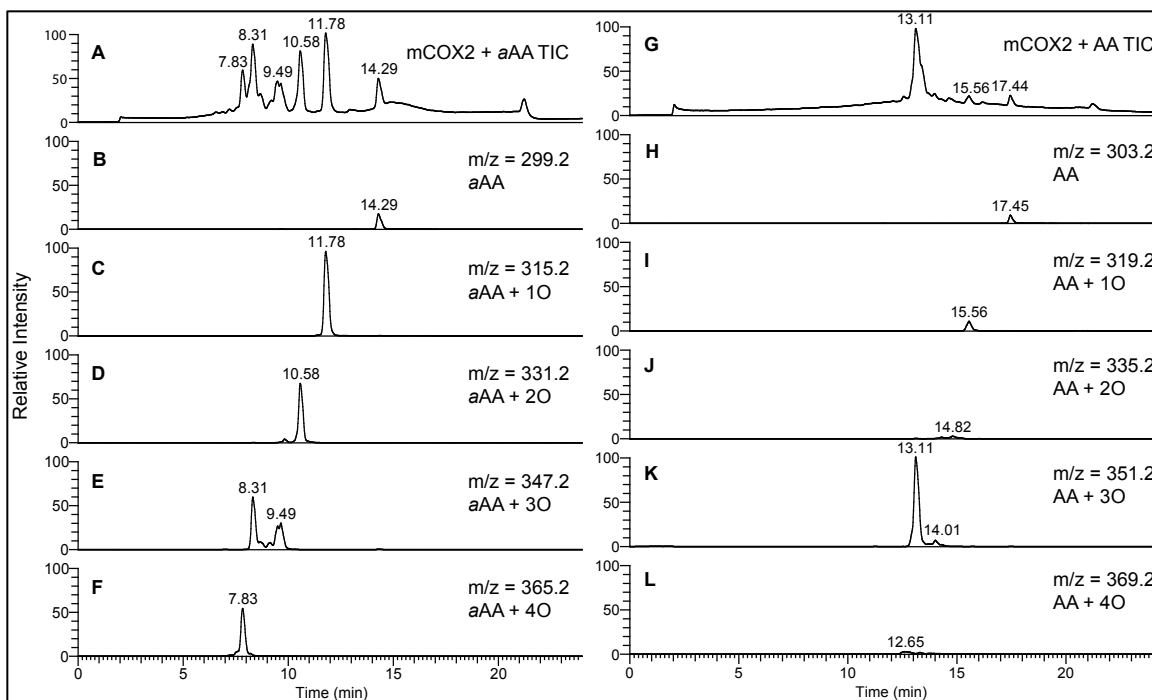


**Figure 6.** COX-2 in vitro metabolite profiles of *aAA* and AA. XIC analysis of the metabolite profiles of *aAA* A) and AA G) catalyzed by COX-2 show very different products. The metabolism of *aAA* by COX-2 shows some *aAA* remaining B) and four products corresponding to the addition of one C), two D), three E), and four F) atoms of oxygen. The profiles in B-F are all to the same scale. The metabolism of AA by COX-2 shows a single major product showing the addition of three atoms of oxygen and having the same  $m/z$  as  $\text{PGE}_2/\text{PGD}_2$  K). In addition to the major metabolite and remaining AA H), metabolism of AA by COX-2 shows three other products corresponding to the addition of one I), two J), and four L) oxygen. These AA products correspond to the non-alkynylated versions of the products seen when *aAA* is metabolized by COX-2. The profiles in H-L are to the same scale. Reprinted with permission from Beavers, W. N., Serwa, R., Shimozu, Y., Tallman, K. A., Vaught, M., Dalvie, E. D., Marnett, L. J., and Porter, N. A. (2014) omega-Alkynyl Lipid Surrogates for Polyunsaturated Fatty Acids: Free Radical and Enzymatic Oxidations. *J Am Chem Soc*, 136, 11529-11539.

We compared the kinetics of COX-2 oxidation of *aAA* determined by  $\text{O}_2$  uptake (Table 1) to values determined by LC-MS/MS and noticed that the product profile from *aAA* was different from that of AA. As demonstrated in Figure 6, four *aAA*-derived oxygenation products were identified by MS, which correspond to the addition of one ( $m/z = 315.2$ ), two ( $m/z = 331.2$ ), three ( $m/z = 347.2$ ), and four atoms of oxygen ( $m/z = 365.2$ ). The product at  $m/z = 315.2$  corresponds to *a11*-HETE and the product at  $m/z = 347.2$  corresponds to

*a*PGE<sub>2</sub>/PGD<sub>2</sub>. One possibility for the identity of the product at  $m/z = 331.2$  is *a*HPETE; however, attempted reduction of the hydroperoxide with either TCEP or PPh<sub>3</sub> did not alter the peak elution time (data not shown), indicating a chemically distinct species from the hydroperoxide. Although the metabolite profile of AA by COX-2 resulted in peaks with  $m/z$  values corresponding to the addition of one, two, three, and four atoms of oxygen, similar to what was seen with *a*AA, the intensity of the peaks displayed major differences. AA oxygenation by COX-2 results in a major peak at  $m/z = 351.2$ , corresponding to PGE<sub>2</sub>/PGD<sub>2</sub>, and a minor peak at  $m/z = 319.2$ , corresponding to a single oxygen atom incorporation. The remaining oxygen addition peaks were very minor by comparison, but have similar retention time and molecular weight shifts relative to PG as was seen with *a*AA. Ovine COX-1 generated a similar product profile to COX-2 for *a*AA and AA (data not shown).

To identify the metabolites depicted in Figure 6, product peaks at  $m/z = 315.2$  and  $331.2$  were isolated and analyzed via 1D and 2D NMR. The compound present at  $m/z = 365.2$  was not stable through the isolation process and thus was not analyzed. Figure 7 shows the structure and <sup>1</sup>H-<sup>1</sup>H COSY for the peak at  $m/z = 315.2$ . It was determined that the identity of this peak is (5Z, 8Z, 12E, 14Z)-11-Hydroxyicosa-5,8,12,14-tetraen-19-ynoic acid or ω-alkynyl 11-hydroxy eicosatetraenoic acid (*a*11-HETE). Table 2 shows the chemical shifts and coupling constants as determined from the <sup>1</sup>H-NMR. The coupling constants for the alkene between C12 and C13,  $J_{12,13} = 15.2$  Hz and 15.1 Hz respectively, identify the bond as *trans*. Figure 8 shows the structure and <sup>1</sup>H-<sup>1</sup>H COSY for the

peak at  $m/z = 331.2$ . It was determined that the identity of this peak is (Z)-7-(3-((3E, 5Z)-2-Hydroxyundeca-3,5-dien-10-yn-1-yl)oxiran-2-yl)hept-5-enoic acid or  $\omega$ -alkynyl 11-hydroxy-8,9-epoxy-eicosatrienoic acid (a11-8,9-HEET). Table 3 shows the chemical shifts and coupling constants as determined from the  $^1\text{H-NMR}$ . The coupling constants  $J_{12,13} = 15.2$  Hz and 15.1 Hz, assign the alkene between C12 and C13 as *trans*. The coupling constants for the epoxide were measured as  $J_{8,9} = 4.2$  Hz and 4.3 Hz, identifying the epoxide as *cis*.

**Table 2.**  $^1\text{H-NMR}$  chemical shifts and coupling constants of the COX-2 aAA metabolite with  $m/z = 315.2$ . The metabolite was identified to be a11-HETE. Reprinted with permission from Beavers, W. N., Serwa, R., Shimozu, Y., Tallman, K. A., Vaught, M., Dalvie, E. D., Marnett, L. J., and Porter, N. A. (2014) omega-Alkynyl Lipid Surrogates for Polyunsaturated Fatty Acids: Free Radical and Enzymatic Oxidations. *J Am Chem Soc*, 136, 11529-11539.

Chemical shift	Multiplicity	Proton(s)	Coupling Constant
<i>ppm</i>		<i>carbon no.</i>	<i>Hz</i>
6.54	<i>dd</i>	H13	$J_{12,13} = 15.1$
6.01	<i>t</i>	H14	$J_{14,15} = 11.0$
5.70	<i>dd</i>	H12	$J_{12,13} = 15.2$
5.51	<i>m</i>	H6	
5.39	<i>m</i>	H5, 8, 9, 15	
4.23	<i>q</i>	H11	
2.78	<i>m</i>	H7	
2.34	<i>m</i>	H2a, 10, 16	
2.19	<i>m</i>	H18	
2.12	<i>quint</i>	H4	
1.70	<i>m</i>	H3	
1.61	<i>quint</i>	H17	

**Table 3.**  $^1\text{H-NMR}$  chemical shifts and coupling constants of the COX-2 aAA metabolite with  $m/z = 331.2$ . The metabolite was identified to be a11-8,9-HEET. Reprinted with permission from Beavers, W. N., Serwa, R., Shimozu, Y., Tallman, K. A., Vaught, M., Dalvie, E. D., Marnett, L. J., and Porter, N. A. (2014) omega-Alkynyl Lipid Surrogates for Polyunsaturated Fatty Acids: Free Radical and Enzymatic Oxidations. *J Am Chem Soc*, 136, 11529-11539.

Chemical shift	Multiplicity	Proton(s)	Coupling Constant
<i>ppm</i>		<i>carbon no.</i>	<i>Hz</i>
6.59	<i>dd</i>	H13	$J_{12,13} = 15.1$
6.02	<i>t</i>	H14	$J_{14,15} = 11.0$
5.72	<i>dd</i>	H12	$J_{12,13} = 15.2$
5.51	<i>m</i>	H5,6	
5.45	<i>dt</i>	H15	$J_{14,15} = 10.6$
4.48	<i>q</i>	H11	
3.08	<i>quint</i>	H9	$J_{8,9} = 4.2$
2.95	<i>dt</i>	H8	$J_{8,9} = 4.3$
2.24	<i>m</i>	H2,4,7,16,18	
1.90	<i>m</i>	H10a	
1.72	<i>m</i>	H10b	
1.61	<i>quint</i>	H17	

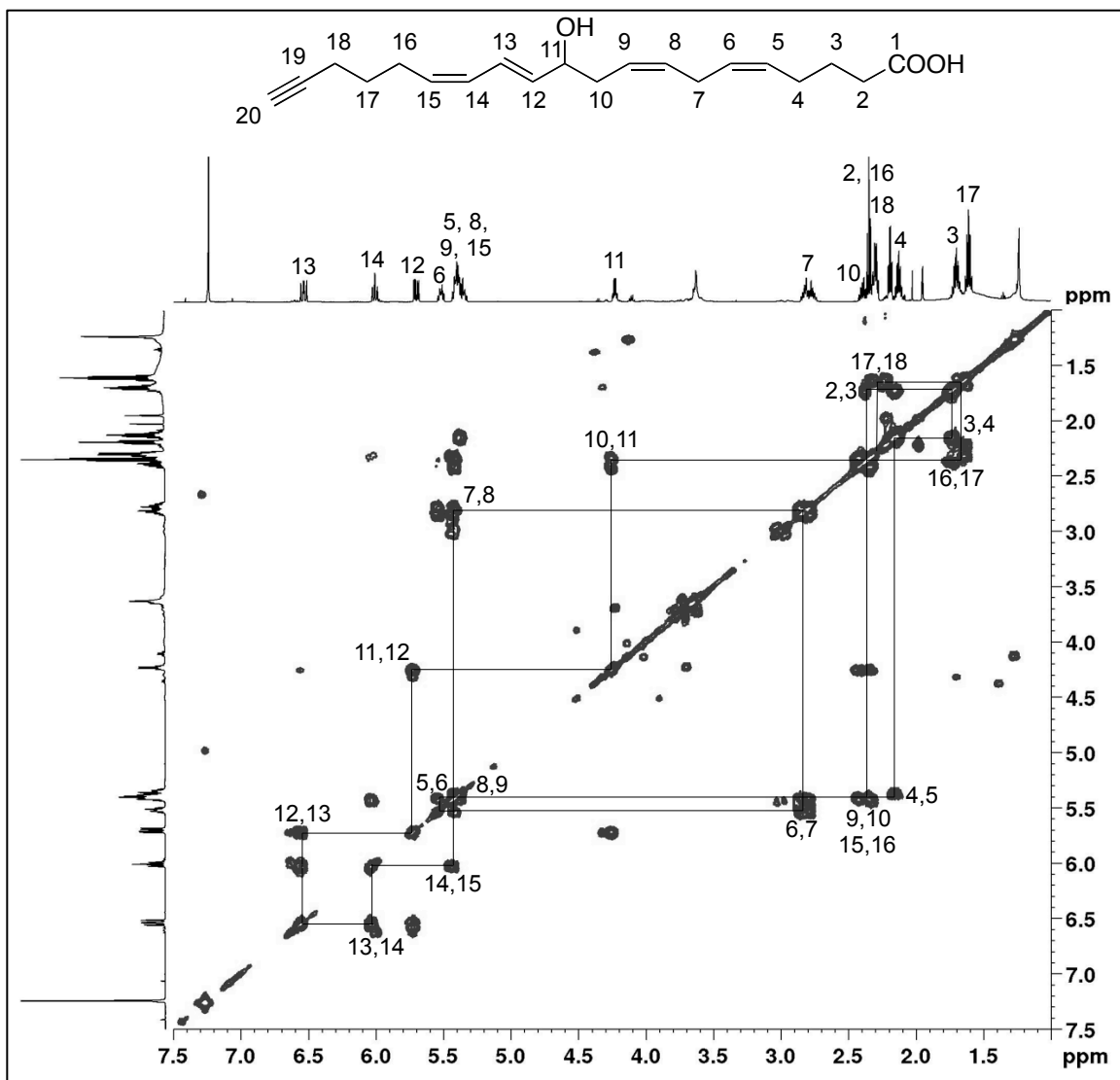


**Figure 7.**  $^1\text{H}$ - $^1\text{H}$  COSY spectrum of the COX-2 aAA metabolite with  $m/z = 315.2$ . The metabolite was identified to be a11-HETE. Reprinted with permission from Beavers, W. N., Serwa, R., Shimozu, Y., Tallman, K. A., Vaught, M., Dalvie, E. D., Marnett, L. J., and Porter, N. A. (2014) omega-Alkynyl Lipid Surrogates for Polyunsaturated Fatty Acids: Free Radical and Enzymatic Oxidations. *J Am Chem Soc*, 136, 11529-11539.

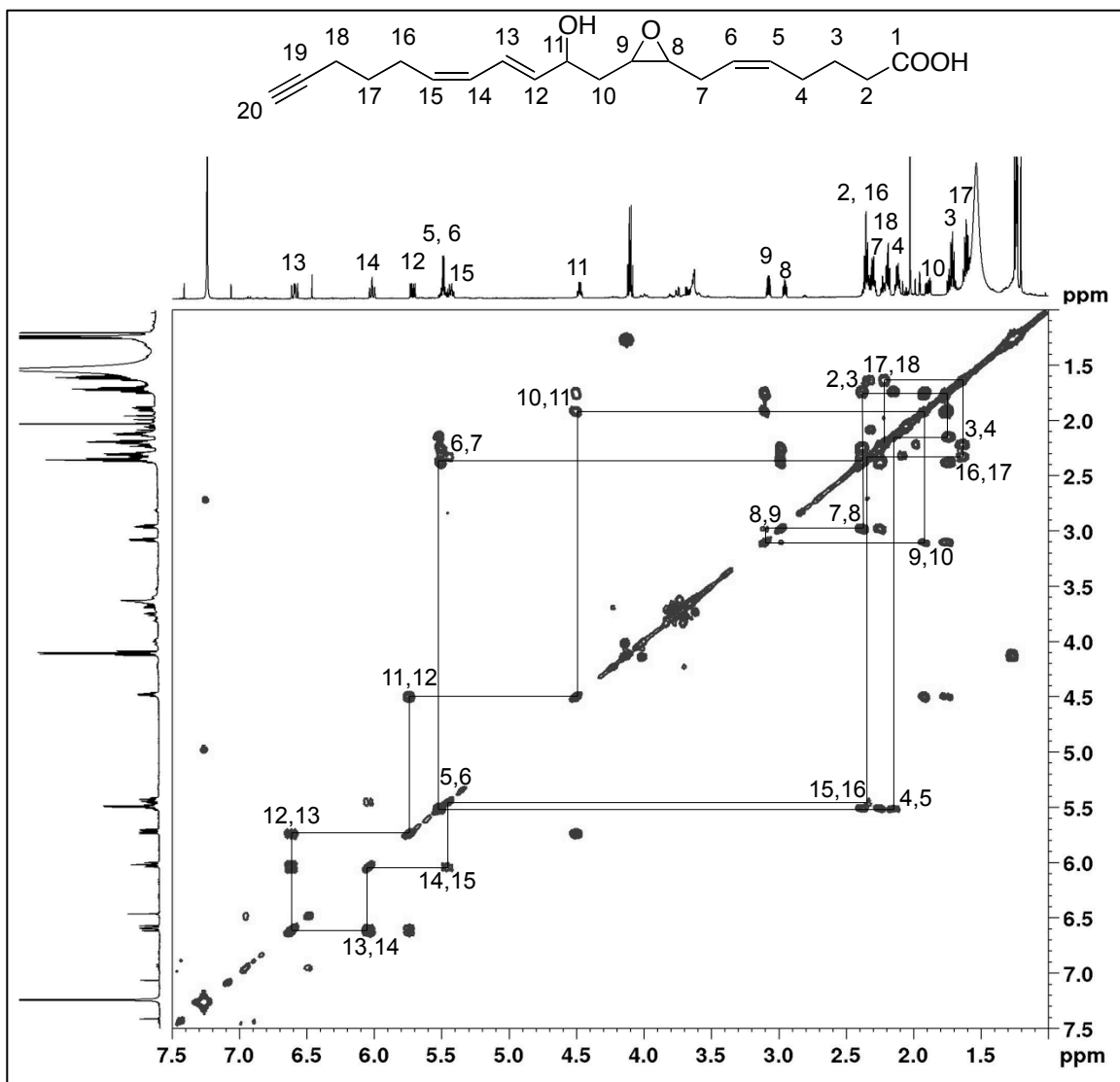


**Figure 8.**  $^1\text{H}$ - $^1\text{H}$  COSY spectrum of the COX-2 aAA metabolite with  $m/z = 331.2$ . The metabolite was identified to be a11-8,9-HEET. Reprinted with permission from Beavers, W. N., Serwa, R., Shimozu, Y., Tallman, K. A., Vaught, M., Dalvie, E. D., Marnett, L. J., and Porter, N. A. (2014) omega-Alkynyl Lipid Surrogates for Polyunsaturated Fatty Acids: Free Radical and Enzymatic Oxidations. *J Am Chem Soc*, 136, 11529-11539.

Due to the distinct product profile of *aAA* metabolism, the kinetic parameters for *aAA* were reevaluated by LC-MS/MS. AA kinetic parameters were determined using the product PGE<sub>2</sub>, whereas the kinetic parameters for *aAA* were determined using *a*PGE<sub>2</sub> and *a*11-HETE. Michaelis-Menten plots for these three kinetic experiments are found in Figure 9. The catalytic efficiency for the formation of PGE<sub>2</sub> by COX-2,  $1.6 \pm 0.2 \mu\text{M}^{-1}\text{s}^{-1}$ , was similar to the oxygen uptake value for hCOX2 seen in Table 1. The small difference between the two can be explained by the formation of the nonenzymatic PG degradation product, 12-hydroxy heptadecatrienoic acid (HHT), which accounts for approximately 20% of the total PG signal (data not shown). The catalytic efficiencies for *aAA* products were very different, however, at  $0.019 \pm 0.005 \mu\text{M}^{-1}\text{s}^{-1}$  for *a*PG formation and  $0.4 \pm 0.1 \mu\text{M}^{-1}\text{s}^{-1}$  for *a*11-HETE formation. When these values are compared to the hCOX2 oxygen uptake during *aAA* metabolism value,  $2 \pm 1 \mu\text{M}^{-1}\text{s}^{-1}$ , it can be seen that most of the oxygen consumption is due to the formation of *a*11-HETE.

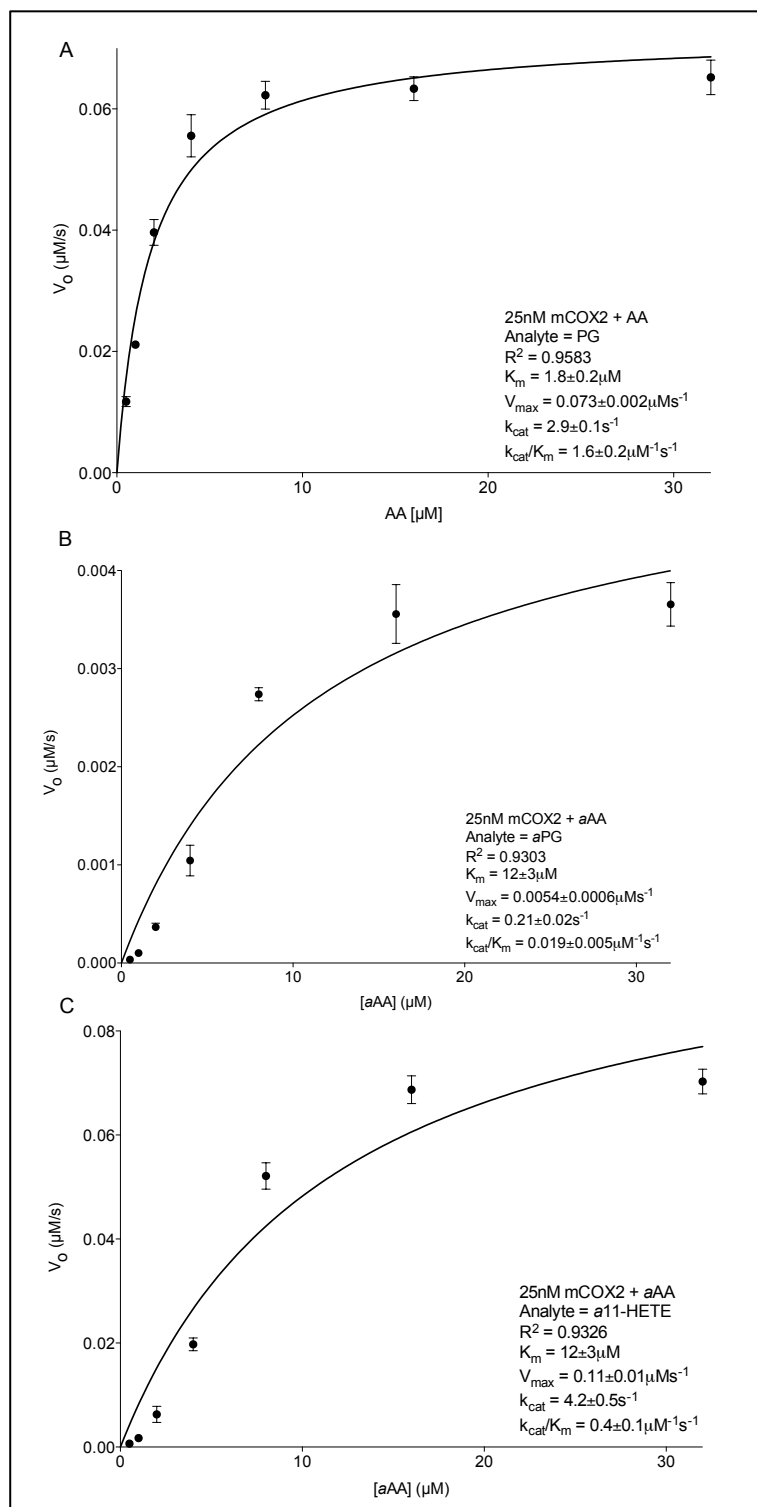


**Figure 9.** Michaelis-Menten plots and relevant kinetic parameters for COX-2 metabolism of AA and aAA. Kinetics were determined by measuring the formation of PG A), aPG B), and a11-HETE C). Reprinted with permission from Beavers, W. N., Serwa, R., Shimozu, Y., Tallman, K. A., Vaught, M., Dalvie, E. D., Marnett, L. J., and Porter, N. A. (2014) omega-Alkynyl Lipid Surrogates for Polyunsaturated Fatty Acids: Free Radical and Enzymatic Oxidations. *J Am Chem Soc*, 136, 11529-11539.



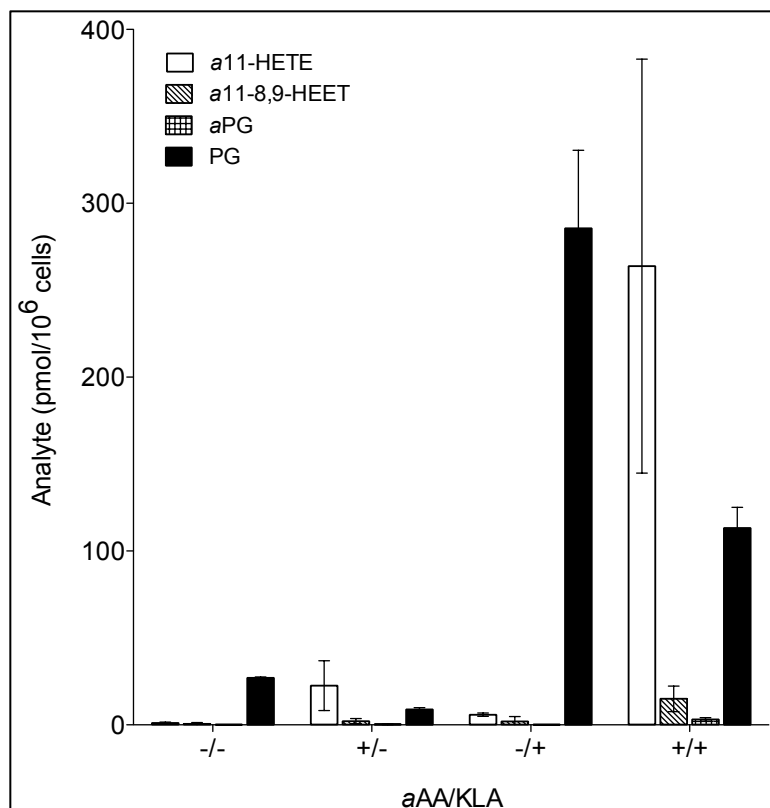


**Figure 10.** Activated macrophages generate *aAA* metabolites. RAW264.7 macrophages were incorporated +/-*aAA*, then activated with +/-100 ng/mL KLA for 24 h. Metabolite levels were measured by LC-MS/MS for the media and cells combined. Reprinted with permission from Beavers, W. N., Serwa, R., Shimozu, Y., Tallman, K. A., Vaught, M., Dalvie, E. D., Marnett, L. J., and Porter, N. A. (2014) omega-Alkynyl Lipid Surrogates for Polyunsaturated Fatty Acids: Free Radical and Enzymatic Oxidations. *J Am Chem Soc*, 136, 11529-11539.

To evaluate the potential of *aAA* as a tool in cellular settings, its incorporation, release, and metabolism was tested in RAW264.7 macrophages. BSA/*aAA* complexes were formed as previously described, and then added to serum-free DMEM for 24 h<sup>285</sup>. Macrophages were then washed with serum-free DMEM to remove any unincorporated *aAA*, and activated with 100 ng/mL KLA for 24 h. Fatty acid metabolites were extracted from the combined media and cells. Figure 10 shows the quantification of *a11*-HETE, *a11*-8,9-HEET, *aPG*, and PG in macrophages incorporated with *aAA* and activated with KLA. The alkynylated

products were only seen at high levels in the *a*AA-enriched and KLA-activated macrophages, which corresponds to the conditions where levels of fatty acid release and COX-2 expression are highest. Further correlating to the kinetic and *in vitro* experiments, *a*11-HETE was more abundant than *a*PG and *a*11-8,9-HEET in activated macrophages. The ratio of *a*11-HETE to *a*PG and *a*11-8,9-HEET is increased from the purified protein analyses indicating that cellular and purified enzyme metabolite profiles may have slight differences.

## Discussion

Understanding both the enzymatic and non-enzymatic metabolism of alkynyl fatty acids is important because lipid oxygenation products and lipid electrophile formation has been reported to result from both enzymatic and non-enzymatic mechanisms<sup>126, 184, 292</sup>. Our data indicate that *a*LA and LA are kinetically equivalent substrates for free radical chain oxidation; (*a*)HODEs are formed as two positional isomers with oxidation at the 9- and 13-carbons. Additionally, the conjugated dienes are in two different conformations, the *Z,E* kinetic product, and the *E,E* thermodynamic product. Analyzing the *Z,E/E,E* product ratios can be used as a “peroxyl radical clock” to measure peroxidation propagation rate constants<sup>293</sup>, further confirming that these two substrates are equivalently oxidized.

Similarly, *a*AA and AA are also equivalent substrates for autoxidation. The mechanism of HPETE and IsoP formation has been studied in great detail and it has been established that six major *Z,E*-HPETE products form with

hydroperoxide substitution at carbons 5-, 8-, 9-, 11-, 12- and 15- of the twenty carbon eicosanoate chain<sup>294</sup>. The IsoPs are formed as a mixture of stereoisomers, the four sets of regioisomers identified by the position of the allylic alcohol in the chain, 5-, 8-, 12-, and 15-<sup>295</sup>. Each regioisomeric set of IsoPs contains eight diastereomers. Quantification of the IsoP isomeric mixture has been used in recent years as a measure of oxidative stress *in vivo*<sup>118, 119, 269</sup>. Both *aAA* and AA form the respective HPETEs and IsoPs at similar levels. This is an important finding for setting up future lipid oxidation studies since many disease states, including models for cardiovascular disease and neurodegenerative diseases, are characterized by a high level of oxidative stress<sup>44</sup>.

The kinetic values measured here indicate that with some notable exceptions, *aAA* is a reasonable enzymatic substrate for both COX and LOX classes of enzymes. Enzymatically, both alkynyl PUFAs are metabolized by various LOX enzymes to similar product profiles as the native PUFAs. Despite the observed differences in catalytic efficiency, *aAA*, AA, *aLA*, and LA are completely oxygenated by s15-LOX-1 when allowed to react to completion (Figure 3). We hypothesize that the reduced efficiency observed is the result of the alkyne altering the conformation of the lipid within the LOX active site. Model systems designed to study cellular processes all have limitations, and the reduced enzymatic efficiency seen here may restrict the use of this model to understand short-term enzymatic lipid metabolism. However, in many biological settings, this reduced enzymatic efficiency remains negligible in understanding

and tracking lipid metabolism because many studies will be looking at changes over long time periods.

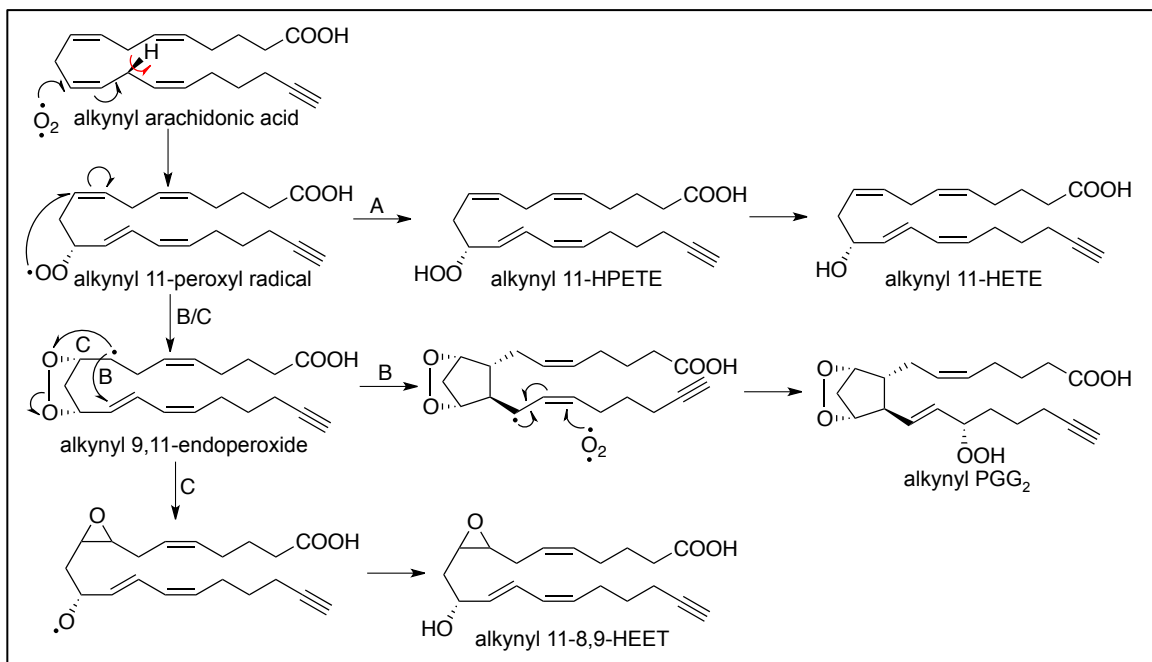


**Figure 11.** Proposed mechanism of COX-2 oxygenation of aAA. All products result from the same first steps, abstraction of the 13-(S)-hydrogen and addition of molecular oxygen to the 11-carbon. Pathway A shows the formation of a11-HETE when the reaction is terminated before 9,11-endoperoxide is formation. After endoperoxide formation, closure of the 5-membered prostaglandin ring results in pathway B and the formation of aPGG<sub>2</sub>, the precursor for all aPGs. However, if ring closure does not occur (pathway C), the endoperoxide can cleave resulting in an epoxide and an 11-alkoxyl radical. The alkoxyl radical can be terminated to form a11-8,9-HEET. Reprinted with permission from Beavers, W. N., Serwa, R., Shimozu, Y., Tallman, K. A., Vaught, M., Dalvie, E. D., Marnett, L. J., and Porter, N. A. (2014) omega-Alkynyl Lipid Surrogates for Polyunsaturated Fatty Acids: Free Radical and Enzymatic Oxidations. *J Am Chem Soc*, 136, 11529-11539.

These data demonstrate the potential usefulness of aPUFAs for the study of lipids in a biological setting; however, one major finding is the differential metabolism of AA and aAA by COX-2 and oCOX1. All of the products in our proposed mechanism (Figure 11) result from the same first two steps, 13-(S)-hydrogen abstraction and oxygen addition to C11 forming the alkylnyl 11-

hydroperoxyl radical. The remaining reactions proceed through two critical junctions, endoperoxide formation and prostaglandin ring closure. The  $\alpha$ 11-hydroperoxyl radical can be reduced by H-atom transfer to form  $\alpha$ 11-HETE (Figure 11A), which was identified as one of the major products by LC-MS/MS and 2D-NMR (Figure 7). When endoperoxide formation is followed by prostaglandin ring closure, and a final oxygenation at C15,  $\alpha$ PGG<sub>2</sub>, the precursor to all prostaglandins is formed (Figure 11B). However, when endoperoxide formation is not followed by prostaglandin ring closure, endoperoxide homolytic cleavage results in 8,9-epoxide and 11-alkoxyl radical formation. The alkoxyl radical can then be terminated to give  $\alpha$ 11-8,9-HEET (Figure 11C), which was identified by 2D-NMR (Figure 8). The epoxide was identified as *cis* due to the coupling constants for H8 and H9, which were measured at 4.2 Hz and 4.3 Hz respectively. This is an interesting observation indicating that the epoxide is formed in the enzyme active site, before the bond between C7 and C8 can rotate. Non-enzymatic epoxidation from endoperoxide scission would be expected to give a 3:1 *trans:cis* geometry due to the free rotation of the C7-C8 bond<sup>296</sup>. 11-8,9-HEET was first identified when 8,9 epoxy-eicosatrienoic acid was incubated with cyclooxygenase enzymes, adding oxygen to C11<sup>297, 298</sup>. The major COX-2 products of  $\alpha$ AA oxygenation we have identified are structurally similar to previously reported COX-2 variant AA metabolites<sup>139</sup>. Schneider *et al.* demonstrated that mutations at Gly526 and Leu384 to larger amino acids restrict endoperoxide formation and prostaglandin ring closure, resulting in the generation of multiple products including 11-HPETE and PGs. Their proposed

mechanism proceeds through several intermediates that when terminated will give the AA-derived products similar to those we have identified.

While we have been unable to solve a crystal structure of *aAA* in a productive conformation in the COX-2 active site, we can look at other substrates to corroborate the idea that *aAA* may not be binding properly in the active site, resulting in an altered product profile. One substrate that can be investigated is the endocannabinoid 2-arachidonoylglycerol (2-AG). The crystal structure of its isomer, 1-AG, has been solved for COX-2, and it was revealed that it sits in the active site in two different conformations. The structural difference in these conformations is a slight change in the position of the  $\omega$ -tail in the active site. Oxygenation may occur in both conformations because abstractable hydrogen atoms on C13 are in line with the catalytic Tyr385, but different distances in each conformation<sup>299</sup>. 2-AG has two major products, PG-glycerol and 11-HETE-glycerol,<sup>300</sup> which further corroborates that there are multiple modes of binding. These data are potentially relevant to *aAA* binding in the COX-2 active site, because they indicate that small changes in the binding of the  $\omega$ -tail has an impact on the oxygenation and cyclization events at the center of the fatty acid. Additionally,  $K_m$  has been used as an estimate of  $K_D$  for COX-2. When we compare these numbers,  $1.8 \pm 0.2 \mu\text{M}$  for AA and  $12 \pm 3 \mu\text{M}$  for *aAA*, we see that there is a distinct difference in binding between AA and *aAA*. Therefore, we hypothesize that the alkynyl tail changes the way *aAA* sits in the COX-2 active site, resulting in similar  $\text{O}_2$  consumption despite its altered product profile, as defined in these studies.

Based on all of the *in vitro* oxidation, we investigated the viability of alkynyl probes for the analysis of lipid metabolite detection and tracking in a biological setting. RAW264.7 macrophages are the prototypical cell line used to study lipid metabolism because their lipid chemistry has been extensively cataloged by the Lipid MAPS Consortium ([www.lipidmaps.org](http://www.lipidmaps.org)). Therefore we investigated if the *in vitro* COX-2 metabolites of *aAA* could be measured in cultured cells, and observed *a11*-HETE as the major *aAA* metabolite in cells, with *aPG* and *a11*-8,9-HEET also detected, but at a much lower level. This product ratio matches the kinetic efficiencies measured *in vitro* for *a11*-HETE and *aPG* formation. Many molecules have been reported to potentiate COX-2 activity *in vitro*, including free fatty acids<sup>137</sup>. It is not unreasonable to think that many of these species are present in cells, and could potentiate the formation of *a11*-HETE as was seen in our data. 11-HETE has been reported in many animal and cell models as a COX-2 derived metabolite<sup>301-304</sup>. Additionally, it has been reported that hydroxy fatty acid metabolites of COX-2, including 11-HETE<sup>305, 306</sup>, can be further oxidized by cellular dehydrogenases to oxo fatty acids<sup>126</sup>. These oxo fatty acids are electrophilic, reacting with nucleophilic amino acids of proteins potentially changing cellular functions. Prostaglandins are not readily converted to electrophilic species; so hydroxy fatty acids are the most viable method to study this chemistry in cells. 11-Oxoeicosatetraenoic acid, the oxidized product of 11-HETE, has been detected in cells, and shown to be antiproliferative<sup>305, 306</sup>. This avenue of exploration is potentially viable using *aAA* as a part of a COX-2 mediated metabolite study, in the appropriate context.

Collectively, these studies demonstrate that *a*PUFAs are metabolized similarly to native PUFAs and represent a viable tool for studying lipid distribution, metabolism, and reactions between lipid metabolites and cellular macromolecules in many physiological and pathophysiological models. While there are some caveats regarding the enzymatic metabolism of *a*AA, specifically the metabolism of these surrogates by the cyclooxygenase enzymes, the non-enzymatic metabolism is indistinguishable from the native lipid species. Therefore, *a*PUFAs can be used as analogs for PUFAs, especially in cellular disease models involving high amounts of oxidative stress resulting in high levels of lipid oxidation.



## Chapter III

### ENDOGENOUSLY GENERATED LIPID ELECTROPHILES TARGET MITOCHONDRIAL PROTEINS IN ACTIVATED RAW264.7 MACROPHAGES

#### Introduction

Oxidative stress is associated with numerous pathologies, including cardiovascular disease, neurodegenerative diseases, and cancer<sup>44</sup>. Reactive oxygen species (ROS) generated during oxidative stress can result from either an acute stimulus such as traumatic injury<sup>20</sup> or through low-level, prolonged stimulation (e.g. atherosclerosis)<sup>38, 93</sup>. ROS formation induces in the oxidation of polyunsaturated fatty acids (PUFAs), leading to the increased generation of electrophilic lipid species. These lipid electrophiles can form adducts on nucleophilic groups of cellular macromolecules, including proteins<sup>307</sup>. Increased levels of lipid electrophile-adducted proteins have been observed in many disease states<sup>222, 226, 229</sup>, and adduction can impact protein function, altering cellular signaling<sup>210, 211, 238</sup>. However, the role of lipid electrophiles in disease initiation and progression is not fully understood partially due to the inability to globally identify and quantify protein targets of adduction.

Lipid electrophiles are in a constant state of flux during both normal cellular function and episodes of oxidative stress. Currently there are three general approaches to study protein adduction. Antibodies<sup>253</sup> and probes<sup>224</sup> targeting known lipid electrophiles have been used to identify gross changes in

adduction. These techniques have also been used to enrich for proteins adducted by a specific lipid electrophile to identify individual targets of adduction<sup>255</sup>. Protein targets of known electrophiles have been identified and quantified using targeted proteomic approaches *in vivo*<sup>255</sup> and in cells<sup>308</sup>. In this approach, a mass shift associated with a known electrophile adduct can be bioinformatically searched as an amino acid posttranslational modification. While these studies measure lipid electrophiles formed in physiologically relevant settings, the methods are constrained to studying anticipated electrophile adducts or using nonspecific chemistries that label unintended biological molecules. Other analyses have relied on bolus-dosing of exogenously formed electrophiles to cell culture systems<sup>204, 238, 242, 309</sup>. This method enables the accurate identification of proteins that are susceptible to adduction by exogenous electrophiles, and the assignment of relative reactivities to nucleophilic amino acid residues. However, electrophiles are not generated at discrete concentrations, at distinct time points, or extracellularly, so these experiments miss potential cellular microenvironment factors that modulate electrophile formation and reactivity. Collectively, each method currently used to study lipid electrophile adduction of proteins fails to address at least one aspect of electrophile formation, including physiologically relevant time scales of formation, concentrations of electrophiles, cellular locations of formation, or the diverse array of electrophiles generated.

Recently we expanded the study of lipid electrophile adduction of proteins by introducing alkynyl electrophiles. The alkynyl group of these electrophiles

allows for the selective recovery of adducted proteins by attaching an affinity tag via click chemistry<sup>204, 248, 310</sup>. This method gives a distinct advantage over previous methods of affinity tagging electrophiles because the functional groups used in click chemistry do not exist in biological systems, making the reaction bioorthogonal, and alleviating concerns of side reactions. However, an exogenously formed electrophile was still added at a set concentration and time point, and thus the previously mentioned criticisms of this method still apply. To study lipid electrophiles in a physiological setting, we have developed a series of  $\omega$ -alkynyl PUFAs that can be incorporated into cells for the endogenous generation of lipid electrophiles and the resulting protein adducts.

In Chapter II, we report that the susceptibility to and products of *in vitro* autoxidation of  $\omega$ -alkynyl linoleic acid (aLA) and  $\omega$ -alkynyl arachidonic acid (aAA) are similar to those of native linoleic acid (LA) and arachidonic acid (AA) oxidation, respectively. Based on this precedent, we expect equivalent electrophilic products of native and alkynyl fatty acids to be generated when the latter are oxidized in physiological settings<sup>311</sup>. In the present study, we demonstrate that aLA is incorporated into the phospholipids of RAW264.7 macrophages and transformed into aAA. Oxidation of incorporated alkynyl fatty acid upon activation of the cells with Kdo<sub>2</sub>-lipid A (KLA)<sup>286</sup> leads to increased electrophile formation and protein adduction.

A challenge in assessing endogenous lipid electrophile adduction of proteins is quantifying differences in adduction between cell phenotypes. Therefore, we chose to apply stable isotope labeling of amino acids in cell culture

(SILAC), which uses metabolically labeled heavy ( $[^{13}\text{C}_6, ^{15}\text{N}_2]$ -lysine,  $[^{13}\text{C}_6, ^{15}\text{N}_4]$ -arginine) and light ( $[^{12}\text{C}_6, ^{14}\text{N}_2]$ -lysine,  $[^{12}\text{C}_6, ^{14}\text{N}_4]$ -arginine) proteomes to globally quantify protein level changes in physiologically relevant settings<sup>312-317</sup>. Affinity purification of posttranslationally modified proteins has previously been used in a SILAC proteome to quantify differences in protein modification<sup>318</sup>. We combined SILAC, click chemistry, and previously described affinity enrichment techniques<sup>204, 248, 310</sup> to quantify both protein expression changes and targets of adduction from endogenously generated lipid electrophiles during macrophage activation. These studies identify over 1,000 protein adduction targets, including important enzymes involved in energy generation and oxidant defense, representing a comprehensive and biologically relevant assessment of lipid electrophile-mediated protein damage.

## **Materials and Methods**

*Materials.* All chemicals were purchased from Sigma-Aldrich, St. Louis, MO, unless otherwise stated. aLA was synthesized as previously described<sup>282</sup>.

*KLA Preparation.* KLA (Avanti Polar Lipids, Alabaster, AL) was stored at -20 °C in aliquots dissolved in sterile Dulbecco's Phosphate Buffered Saline (DPBS) at 1 mg/mL. Aliquots were diluted 1:10 in sterile DPBS and sonicated 15 min before being diluted to 100 ng/mL in culture medium<sup>286</sup>.

*Cell Culture.* RAW264.7 macrophages (ATCC, Manassas, VA) were passaged in Dulbecco's Modified Eagle Medium + Glutamax (DMEM) (Invitrogen, Grand Island, NY) containing 10% FBS (Atlas Biologicals, Fort Collins, CO).

Cells were plated in the passaging medium to keep them near 50% confluence at the time of harvesting. After 24 h at 37 °C, the medium was replaced with serum-free DMEM with or without 15 µM aLA. After 24 h at 37 °C, the cells were washed with serum-free DMEM to remove any aLA not incorporated into the cell membranes. The cells were then treated with serum-free DMEM with or without 100 ng/mL KLA for 24 h at 37 °C.

*aLA Incorporation Analysis of Phospholipid Pools.* RAW264.7 macrophages were enriched with aLA and activated with KLA as described above. Phospholipids were isolated and quantified as previously described<sup>279</sup>.

*aLA Elongation to aAA.* RAW264.7 macrophages were incorporated with aLA as described above. Cells were scraped into DPBS containing 1 mM butylated hydroxytoluene (BHT) and 1 mM tris(2-carboxyethyl)phosphine (TCEP), and counted on BioRad TC10 automated cell counter. Heptadecanoic acid was added to each cell pellet as an internal standard, and the pellets were taken up in 5% HCl. A 2:1 mixture of chloroform:methanol containing 50 mg/L BHT was added to each sample. Samples were vortexed, then centrifuged for 10 min at 15,000 rpm. The organic layer was removed and blown dry under stream of N<sub>2</sub>, and dissolved in MeOH with 1.0 M KOH. Samples were vortexed, then incubated for 1 h at 37 °C. After incubation, samples were immediately placed on ice and acidified with 1.0 M HCl. BHT/PPh<sub>3</sub> in ethanol was added to each sample, then extracted with 4:1 chloroform:ethyl acetate mixture. Organic layer was dried under a stream of N<sub>2</sub>, dissolved in methanol, and stored at -80 °C until analysis.

Reverse-phase high-performance liquid chromatography mass spectrometry analysis was performed on a Supelco Analytical Discovery C<sub>18</sub> column (150 x 2.1 mm, 5 μm), which was eluted at 0.2 mL/min with methanol and 0.1% acetic acid. The effluent of the column was introduced by atmospheric-pressure chemical ionization (APCI) into a triple quadrupole mass spectrometer (TSQ, Thermo). The transfer capillary was heated to 300 °C, discharge current was set to 22.0 V, and the ion isolation width was set to 1. The collision energy was set at 10 V. Scans were recorded at 0.25 s intervals and utilized the Gaussian algorithm for peak smoothing (Xcalibur software).

*Generation of Samples for Click-blots.* RAW264.7 macrophages were incorporated with aLA and activated with KLA as described above. TEMPOL or MitoTEMPO were both added to 10 μM, when present, at the same time as KLA. Cells were scraped, pelleted, and lysed in 1% IGEPAL (MP Biomedicals), 150 mM NaCl, 50 mM HEPES, and 0.5% mammalian protease inhibitor cocktail. Electrophile adducts were stabilized to the proteome with 5 mM NaBH<sub>4</sub> for 1 h, and the reduction was quenched with acetone. Samples were diluted to 2 mg/mL total protein and precleared overnight at 4 °C with streptavidin sepharose beads (GE Healthcare). After preclearing, samples were diluted to 1 mg/mL, click reagents were added to the concentrations, 1 mM CuSO<sub>4</sub>, 1 mM TCEP, 0.1 mM tris[(1-benzyl-1H-1,2,3-triazole-4-yl)methyl]amine (TBTA), and 0.2 mM N<sub>3</sub>-biotin, and the samples were turned end over end for 2 h<sup>204</sup>. Proteomes were separated by SDS-PAGE (Bio-Rad), transferred to 0.45 μm nitrocellulose (Bio-Rad), and probed with Actin anti-goat (Santa Cruz) primary and Streptavidin IRDye 800CW

(LI-COR) overnight at 4 °C. Secondary anti-goat IGG IRDye 680LT antibody was from LI-COR and incubated with the blots for 1 h at 25 °C. Blots were visualized on a LI-COR Odyssey system scanning at 800 nm emission for streptavidin and 700 nm emission for actin.

*SILAC RAW264.7 Macrophages Line.* All SILAC reagents were from Pierce, Rockford, IL. RAW264.7 macrophages were passaged in SILAC DMEM containing 10% SILAC FBS. Heavy medium contained 0.1 mg/mL  $^{13}\text{C}_6^{15}\text{N}_2$ -lysine and  $^{13}\text{C}_6^{15}\text{N}_4$ -arginine, while the light medium contained 0.1 mg/mL  $^{12}\text{C}_6^{14}\text{N}_2$ -lysine and  $^{12}\text{C}_6^{14}\text{N}_4$ -arginine. After four passages, the cell lines were harvested, lysed, proteins separated by SDS-PAGE, and stained with SimplyBlue (Invitrogen). Similar molecular weight areas of the stained gel were excised for both the light and heavy lines, digested with trypsin, and analyzed by LC-MS/MS. The resulting comparison of heavy/light peptide ratios for each sample individually confirmed that the heavy and light samples have greater than 99% incorporation of the respectively labeled lysine and arginine.<sup>319</sup>

*SILAC Sample Preparation.* Incorporation of SILAC samples with aLA was performed as above on both the heavy and light lines individually. Light cells were treated with vehicle, and represent the unactivated state, while heavy cells were treated with KLA, and represent the activated state. After harvesting, the cells were lysed, and proteins quantified by BCA assay (Pierce). The heavy and light lines were combined in equal weights of protein, and adducts were stabilized with  $\text{NaBH}_4$  and attached to 0.2 mM UV-biotin<sup>249</sup> via click chemistry instead of  $\text{N}_3$ -biotin as described above.

*Streptavidin Affinity Purification.* After attaching UV-biotin, the sample was dialyzed against PBS to remove any excess click reagents using 2,000 Da molecular weight cutoff dialysis cassettes (Pierce). After dialysis, the sample was added to streptavidin beads (GE Healthcare), and turned end over end overnight at 4 °C in the dark. The beads were washed twice each with 1% SDS, 4 M urea, 1 M NaCl in PBS, PBS, and water. Adducted proteins were eluted into water by stirring the beads under 365 nm light for 2 h.<sup>204</sup>

*SILAC Proteomic Analysis.* Proteome (input) and adductome (eluate) samples were precipitated with 25% trichloroacetic acid on ice for 1 h. Following incubation, samples were centrifuged at 18,000 x *g* at 4 °C, and precipitates were washed with cold acetone, dried, and reconstituted in 50 mM Tris, pH 8.0, containing 50% 2,2,2-trifluoroethanol (TFE). Samples were reduced with TCEP, carbamidomethylated with iodoacetamide, diluted 5-fold with 100 mM Tris, pH 8, (to obtain a final solution containing 10% TFE), and digested with sequencing-grade trypsin overnight (Promega).

Digests were acidified to 0.1% formic acid, and peptides were loaded onto a self-packed biphasic C<sub>18</sub>/strong cation exchange (SCX) MudPIT column using a helium-pressurized cell (pressure bomb). The MudPIT column consisted of 360 x 150 µm fused silica, which was fritted with a filter-end fitting (IDEX Health & Science) and packed with 6 cm of Luna SCX material (5 µm, 100 Å) followed by 4 cm of Jupiter C<sub>18</sub> material (5 µm, 300 Å, Phenomenex). Once the sample was loaded, the MudPIT column was connected using an M-520 microfilter union (IDEX Health & Science) to an analytical column (360 x 100 µm), equipped with a



laser-pulled emitter tip and packed with 20 cm of C<sub>18</sub> reverse phase material (Jupiter, 3 μm beads, 300 Å, Phenomenex). Using an Eksigent NanoLC Ultra HPLC and Autosampler, MudPIT analysis was performed with an 11-step salt pulse gradient (25, 50, 75, 100, 150, 200, 250, 300, 500, 750, and 1000 mM ammonium acetate). Following each salt pulse, peptides were gradient-eluted from the reverse analytical column at a flow rate of 500 nL/min, and the mobile phase solvents consisted of 0.1% formic acid, 99.9% water (solvent A) and 0.1% formic acid, 99.9% acetonitrile (solvent B). For the peptides from the first 10 SCX fractions, the reverse phase gradient consisted of 2–40% B in 90 min, followed by a 15 min equilibration at 2% B. For the last SCX-eluted peptide fraction, the peptides were eluted from the reverse phase analytical column using a gradient of 2-98% B in 100 min, followed by a 10 min equilibration at 2% B. Peptides were introduced via nano-electrospray into an LTQ-Orbitrap Velos mass spectrometer (Thermo Scientific), and the data were collected using a 17-scan event data-dependent method. Full scan (*m/z* 350-2000) spectra were acquired with the Orbitrap as the mass analyzer (resolution 60,000), and the sixteen most abundant ions in each MS scan were selected for collision-induced dissociation in the LTQ. An isolation width of 2 *m/z*, activation time of 10 ms, and 35% normalized collision energy were used to generate MS/MS spectra. The MS<sup>n</sup> automatic gain control target value was set to 1 x 10<sup>4</sup>, and the maximum injection time was set to 100 ms. Dynamic exclusion was enabled, using a repeat count of 1 within 10 s and exclusion duration of 15 s.

For peptide and protein identification, data were analyzed using the MaxQuant software package, version 1.3.0.5.<sup>320, 321</sup> MS/MS spectra were searched against a mouse subset database created from the UniprotKB protein database (2012\_05). Precursor mass tolerance was set to 20 ppm for the first search, and for the main search, an 8 ppm precursor mass tolerance was used. The maximum precursor charge state was set to 6. Variable modifications included carbamidomethylation of cysteines (+57.0214), oxidation of methionines (+15.9949), and acetylation of N-termini (+42.0106). Enzyme specificity was set to Trypsin/P, and a maximum of 3 missed cleavages was allowed. The target-decoy false discovery rate (FDR) for peptide and protein identification was set to 1% for peptides and proteins. A multiplicity of 2 was used, and Arg10 and Lys8 heavy labels were selected. For SILAC protein ratios, a minimum of 1 unique peptide and a minimum ratio count of 2 were required, and the requantify option was enabled. Protein groups identified as reverse hits, or contaminants were removed from the datasets. All reported protein groups were identified with two or more distinct peptides and were quantified with two or more ratio counts.

*Normal distribution and selection of common proteins.* All MaxQuant normalized activated:unactivated were converted to  $\log_2(\text{activated}/\text{unactivated})$  and put into a frequency distribution with a bin size of 0.1 using GraphPad Prism. Using Gaussian fitting, the normal distribution parameters, mean, standard deviation, and  $R^2$  were determined for each proteome and adductome sample. Pairwise Spearman correlations were calculated comparing each proteome and adductome to every other proteome and adductome. Only proteins that were

common across all six samples were included in this analysis. We applied *limma* to estimate the significance of the heavy/light ratio across three replicates of both the proteome and adductome. This method is similar to single-sample t-test except it uses empirical Bayes method to adjust for variable dependence.

*WebGestalt pathway analysis.* Analysis of adductome target location and pathway enrichment was performed in WebGestalt (<http://bioinfo.vanderbilt.edu/webgestalt/>).<sup>322</sup> Adductome protein lists with adjusted  $P < 0.05$  and heavy/light  $> 1.5$  were analyzed for cellular compartment enrichment. Additionally, the adductome and proteome proteins were analyzed for pathway enrichment using the WikiPathway function in WebGestalt. Uniprot accession numbers of the three proteome samples were analyzed in VENNY (<http://bioinfogp.cnb.csic.es/tools/venny/index.html>), an interactive tool for comparing lists with Venn Diagrams, and used as the reference proteome. Settings in WebGestalt were as follows, Statistical Method: Hypergeometric, Multiple Test Adjustment: Benjamini Hochberg (BH), Significance Level (adjusted P value): 0.05, Minimum Number of Genes for a Category: 3.

*MitoTEMPO modulation of adduction.* RAW264.7 macrophages were incorporated with aLA and activated with KLA as described above. MitoTEMPO was added to both vehicle and KLA-activated samples at the same time as KLA, when present, as describe above. Cells were isolated, lipid electrophile adducts stabilized, and attached to UV-biotin by click chemistry as described. Adducted proteins were affinity purified with streptavidin beads and UV-elutes as described above. Total recovered protein was assessed by SDS-PAGE separation of the

recovered adductome followed by Simply Blue staining. Levels of individual adducted proteins were assessed by western blot as described above using anti-Sod2 (Cayman Chemical) or anti-COX-2 (Cayman Chemical) primary antibodies both from rabbit hosts. Anti-rabbit IGG IRDye 800CW antibody from LI-COR was used as the secondary antibody.

*Time course of adduction.* RAW264.7 macrophages were incorporated with aLA and activated with KLA as described above. At 0, 3, 6, 9, 12, and 24 h post activation, adducted proteins were isolated using UV-biotin as described for the affinity enrichment for the SILAC experiments. Levels of individual adducted proteins were assessed by western blot as described above using anti-Sod2 or anti-COX-2 primary antibodies both from rabbit hosts.

*Mitochondria and Cytosol Separation.* Cells were lysed in 250 mM sucrose + 1 mM EDTA + 20 mM HEPES + 0.2% protease inhibitor cocktail on ice, and passed through a 26 gauge needle ten times. Nuclei and debris were pelleted at 500 x *g* and 4 °C for 5 min. Supernatant containing mitochondria was transferred, and mitochondria were pelleted at 10,000 x *g* and 4 °C for 10 min. Mitochondria were washed twice more in the sucrose buffer and pelleted. Mitochondria were lysed in 150 mM sucrose containing 10 mM HEPES, 1.5 mM MgCl<sub>2</sub>, 10 mM KCl, 1% IGEPAL, and 0.2% mammalian protease inhibitor cocktail on ice.

*Superoxide Dismutase Activity.* Mitochondrial and cytosolic lysates (2 µg protein) were assessed for activity as described in the Superoxide Dismutase Activity Kit (Cayman Chemical). Absorbance was measured at 450 nm after 30 min of incubation at 25 °C to determine activity. Activity was normalized to Sod1

or Sod2 expression in the cytosol and mitochondria respectively, as determined by western blot. Statistical significance was determined by an unpaired t-test in GraphPad Prism. Expression levels were determined by densitometry using ImageJ<sup>323</sup> and normalized to actin expression. Statistical significance of expression levels were determined by Two-Way ANOVA with Tukey *post hoc* analysis in GraphPad Prism.

## Results

*aLA is incorporated into native phospholipids in RAW264.7 macrophages.*

When added to the culture medium, *aLA* (Figure 1A), was incorporated into the phospholipid pool (Figure 2). The content of *aLA* in the phospholipid pool was determined by quantifying the amount of 36:2 or *a*36:2, which consists of LA or *a*LA, respectively, at the *sn*-2 position and stearic acid at the *sn*-1 position, across the five major phospholipid species (Figure 2A). Figure 3A shows that during *aLA* incorporation, the amount of LA decreases, but the total LA + *a*LA pool does not change (Figure 3B). These data demonstrate that *aLA* is incorporated into the same phospholipid pools as LA and, in fact, that *aLA* displaces LA.

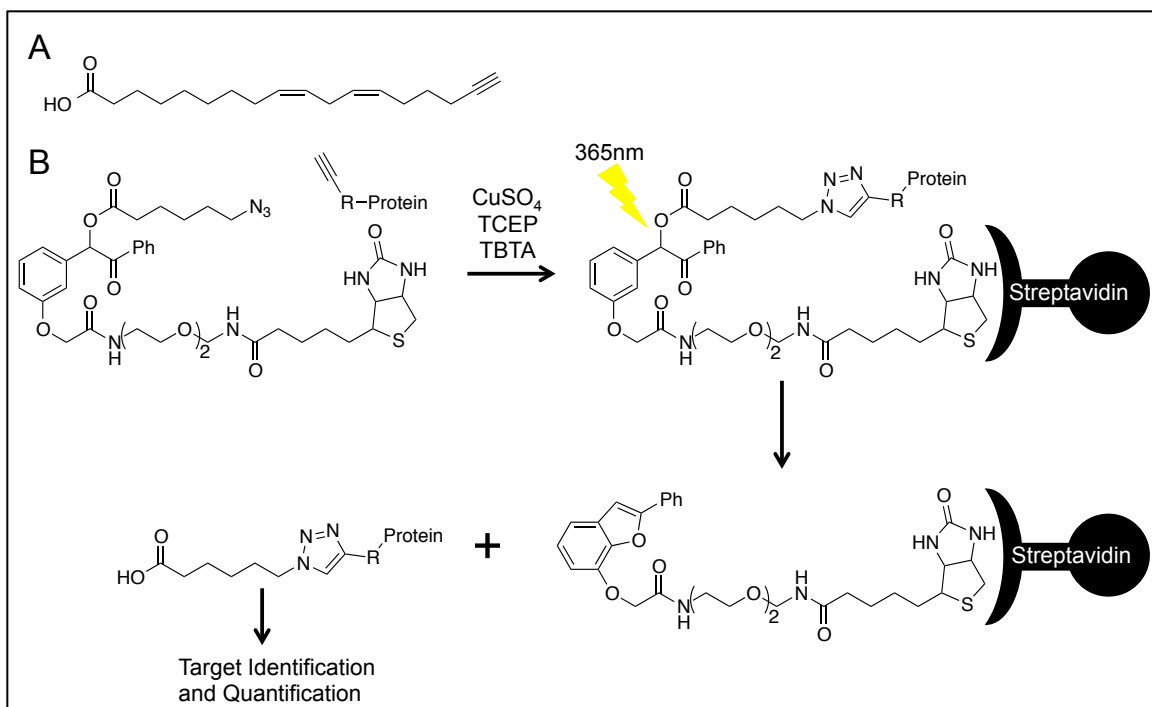


**Figure 1.** Click chemistry scheme for protein adduction. A) The structure of  $\omega$ -alkynyl linoleic acid. B) Copper-mediated click chemistry was used to attach a previously reported UV-cleavable biotin linker to  $\omega$ -alkynyl electrophile- (R-) adducted proteins. Streptavidin bead affinity-captured biotinylated proteins, and UV-irradiation selectively released proteins adducted by alkyne electrophiles for identification of the protein targets. Azido-biotin linkers ( $N_3$ -biotin) that are not UV-cleavable and streptavidin-based fluorophores can be used in place of the beads to measure the extent of adduction across the entire proteome qualitatively.

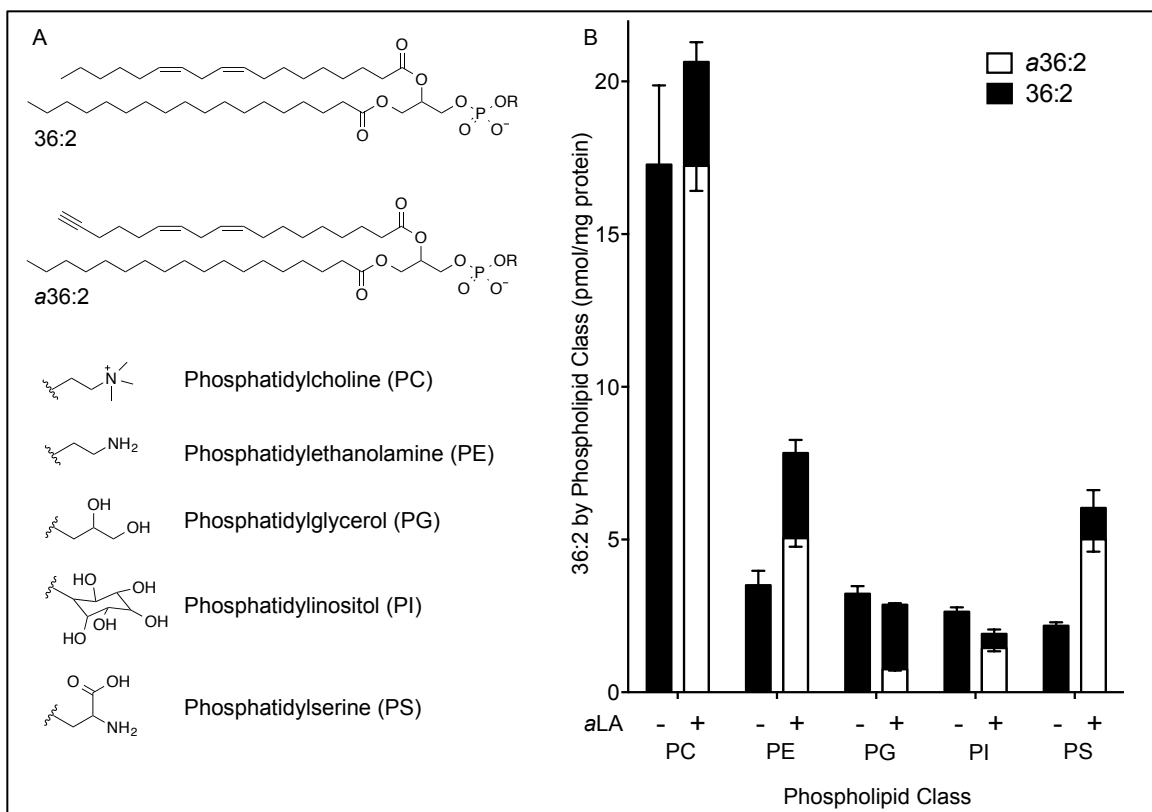


**Figure 2.** Extent of aLA incorporation into phospholipid pools. aLA was incorporated into the lipid bilayer of RAW264.7 macrophages. Lipidomic quantified A) 36:2 and a36:2 in the phospholipid bilayer in the five major phospholipid classes, PC: phosphatidylcholine, PE: phosphatidylethanolamine, PG: phosphatidylglycerol, PI: phosphatidylinositol, PS: phosphatidylserine. B) Incorporation of aLA, which is compared between macrophages untreated (-) and those treated with aLA (+), where white bars are native LA and black bars are aLA showed incorporation into all 36:2 phospholipid classes. As expected, aLA was not measured in the unincorporated cells, but was measured in aLA-incorporated macrophages. In PC, PG, and PI phospholipid classes, aLA displaces LA, and adds to it in PE and PS. Data are mean  $\pm$  standard deviation of triplicate determinations.

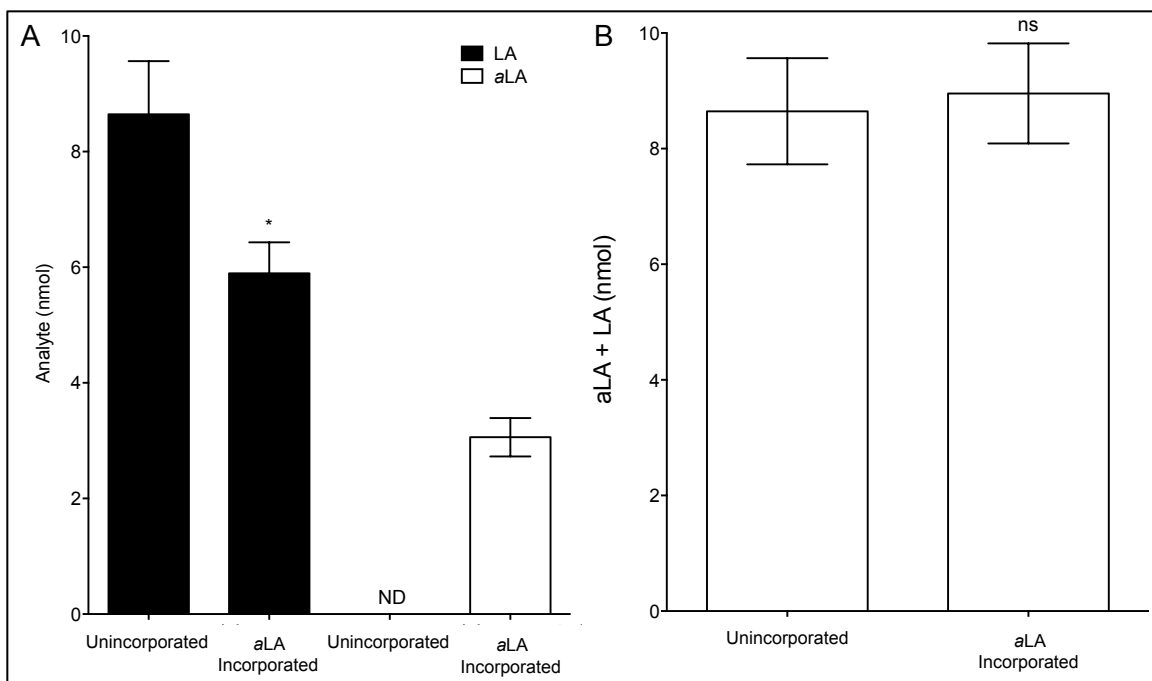


**Figure 3.** Total amounts of aLA and LA in RAW264.7 macrophages before and after aLA incorporation. A) The total amount of LA decreases between unincorporated and aLA-incorporated macrophages. aLA is not detected in unincorporated macrophages, but is present in the aLA-incorporated macrophages in quantities approximately equal to the decrease in LA in those cells. B) This results in no change in the total LA + aLA pool, indicating that aLA is displacing LA. Data are mean  $\pm$  standard deviation of triplicate determinations. Statistical significance determined by an unpaired t-test where \* =  $P < 0.05$  and ns =  $P > 0.05$ .

*aLA is elongated to aAA in RAW264.7 macrophages.* Linoleic acid is an essential fatty acid and serves as the precursor for synthesis of arachidonic acid (AA) as well as other signaling PUFAs<sup>122, 160, 324, 325</sup>. Figure 4 demonstrates that aLA is converted to aAA when incubated with RAW264.7 macrophages. Expected intermediates along the pathway from aLA to aAA,  $\omega$ -alkynyl  $\gamma$ -linolenic acid (aGLA) and  $\omega$ -alkynyl dihomo- $\gamma$ -linolenic acid (aDGLA), were also observed. Approximately 80% of the aLA taken up by the macrophages was converted to one of the elongation products, with aAA comprising nearly 60% of the detected alkynyl fatty acids. Unlike aLA, aAA does not displace its native fatty acid, AA, but instead increases the pool size of arachidonate-containing species (Figure



5A and 5B). These data are in agreement with previous studies demonstrating that RAW264.7 macrophages are AA-deficient, and readily able to increase AA levels in phospholipid pools<sup>278</sup>. The present experiment shows that when *a*LA is the most abundant fatty acid available, it will be converted to *a*AA, further confirming the findings in Chapter II that *a*LA is treated in a similar manner to LA by cellular enzymes of lipid metabolism. The findings also support the hypothesis that, under conditions of oxidative stress, alkynyl lipid electrophiles can be generated from both *a*LA and *a*AA.

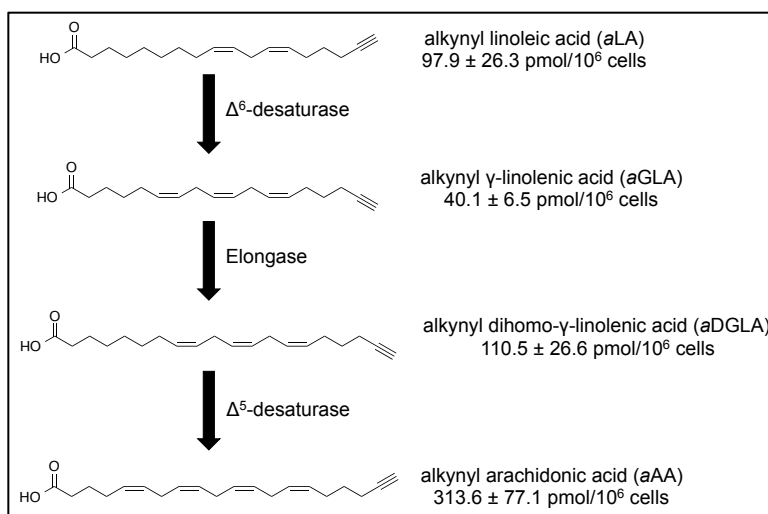


**Figure 4.** *a*AA is biosynthesized from *a*LA. Elongation products of *a*LA to *a*AA were measured in *a*LA incorporated RAW264.7 macrophages. During *a*AA biosynthesis, *a*LA is desaturated to form  $\omega$ -alkynyl  $\gamma$ -linolenic acid (*a*GLA), which is elongated to  $\omega$ -alkynyl dihomo- $\gamma$ -linolenic acid (*a*DGLA), and then desaturated again to reach the final product of *a*AA. These findings further confirm that *a*LA is recognized similarly as native LA in RAW264.7 macrophages.

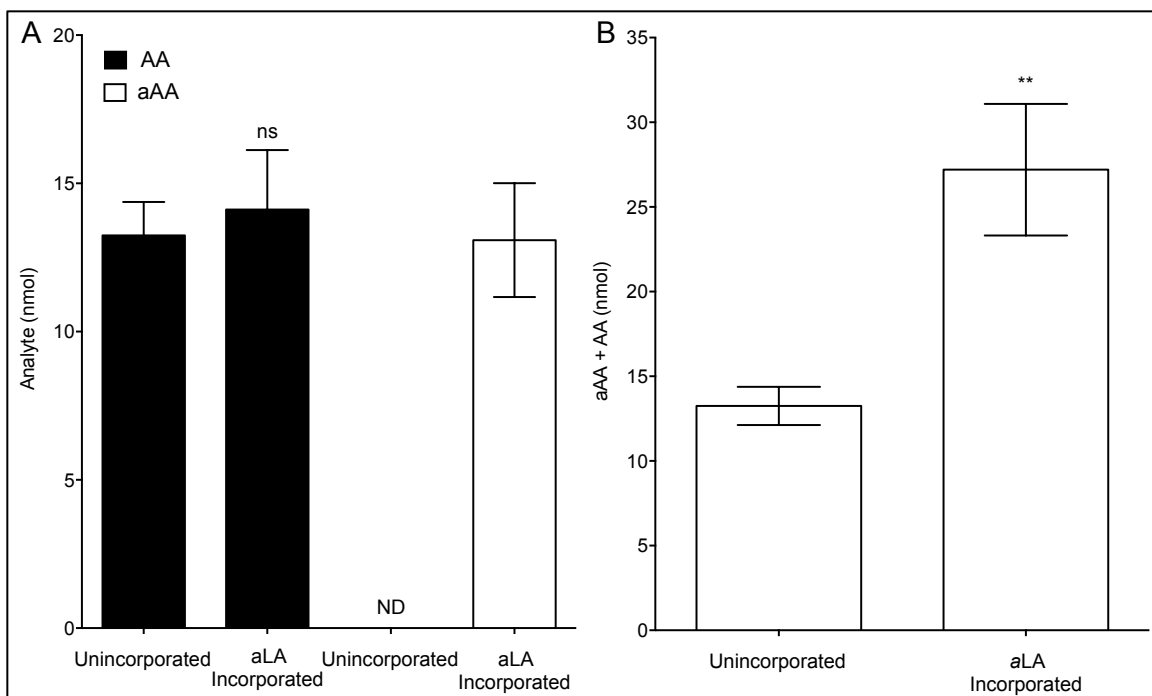


**Figure 5.** Total amounts of aAA and AA in RAW264.7 macrophages before and after aLA incorporation. A) The total amount of AA does not change between unincorporated and aLA-incorporated macrophages. aAA is not detected in unincorporated macrophages, but is present in the aLA-incorporated macrophages in quantities approximately equal to the amount of AA in those cells. B) This results in a significant increase in the total AA + aAA pool, indicating that aAA is not displacing AA. Data are mean  $\pm$  standard deviation of triplicate determinations. Statistical significance determined by an unpaired t-test where \*\* =  $P < 0.01$  and ns =  $P > 0.05$ .

*Activation of RAW264.7 macrophages induces lipid electrophile-protein adducts.* To evaluate protein targets susceptible to adduction by lipid-derived electrophilic species, macrophages were preincubated in the presence or absence of aLA then treated with or without KLA or a vehicle control. KLA is a chemically defined lipopolysaccharide known to stimulate the production of ROS<sup>286</sup>. Following activation by KLA, the cells were lysed and a protein extract prepared and treated with NaBH<sub>4</sub> to stabilize protein-electrophile conjugates. Each adducted protein containing an alkyne tag was conjugated to a biotin derivative using click chemistry. Proteins were separated by SDS-PAGE, and

biotin-containing bands were visualized using a streptavidin-based fluorophore. As shown in Figure 6, activation with KLA resulted in a substantial increase in measurable protein adduction in *a*LA-incorporated macrophages when compared to unactivated controls or macrophages with no *a*LA incorporation. Low levels of protein adduction can be seen in unactivated, *a*LA-incorporated macrophages as lipid oxidation and electrophile generation occurs during normal cellular functions.

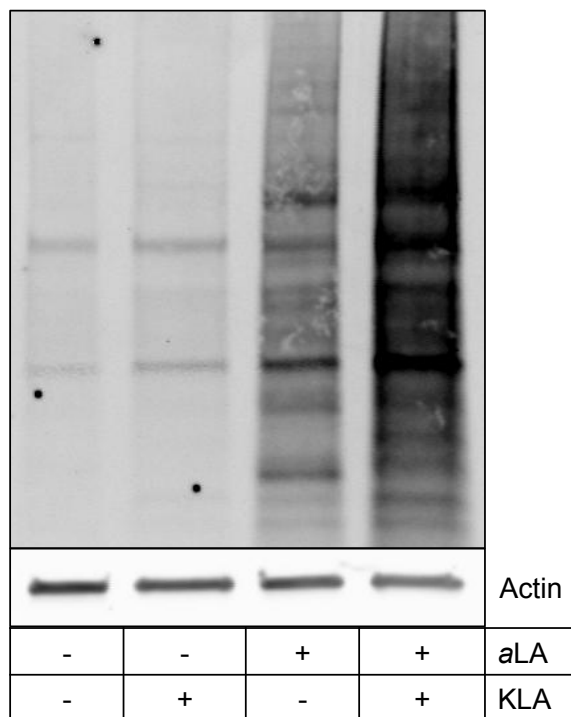


**Figure 6.** KLA activation induces lipid electrophile protein adduction. RAW264.7 macrophages incorporated with *a*LA then activated with KLA show increased adduction over unactivated macrophages. Click chemistry was used to attach a biotin linker to alkynyl lipid electrophile adducted proteins. The extent of proteomic adduction was visualized by probing with a streptavidin-based fluorophore, which shows differential adduction between activated and unactivated macrophages. The first and second lanes are unincorporated for *a*LA, and the visualized biotin signal is from endogenously biotinylated proteins. The third and fourth lanes show macrophages incorporated with *a*LA and unactivated or activated with KLA respectively. These lanes show that lipid electrophiles are generated during normal physiological processes of the cell (+*a*LA/-KLA), and that there is increased adduction across the entire proteome by endogenously formed lipid electrophiles in activated macrophages (+*a*LA/+KLA).

*SILAC quantification of lipid electrophile-adducted proteins reveals nearly half of the detectable proteome is adducted.* KLA activation of RAW264.7 macrophages results in marked changes in both protein expression and lipid electrophile adduction of proteins. To quantify changes in protein adduction, we employed a well-characterized SILAC model<sup>319</sup>. As shown in Figure 7A, a heavy cell line was created by enriching for  $^{13}\text{C}_6^{15}\text{N}_2$ -lysine and  $^{13}\text{C}_6^{15}\text{N}_4$ -arginine, while a light cell line was enriched with  $^{12}\text{C}_6^{14}\text{N}_2$ -lysine and  $^{12}\text{C}_6^{14}\text{N}_4$ -arginine. Both cell lines were preincubated with aLA, and the heavy cells were activated with KLA, whereas the light cells were treated as the unactivated control. The cells were harvested, homogenized, and aliquots of the resultant heavy and light samples containing equal amounts of total protein were then combined. Three biological replicates of the input (proteome) samples were analyzed via multidimensional protein identification technology tandem mass spectrometry (MudPIT-MS/MS). A total of 2,406 input proteins were identified as common across the three replicates (Figure 8A), constituting the reference proteome. The reference proteome is a list of all proteins detectable before affinity enrichment for electrophile-adducted proteins, and the ratio of heavy peptides/light peptides for each protein provides a relative quantification of expression changes resulting from KLA activation of the macrophages.

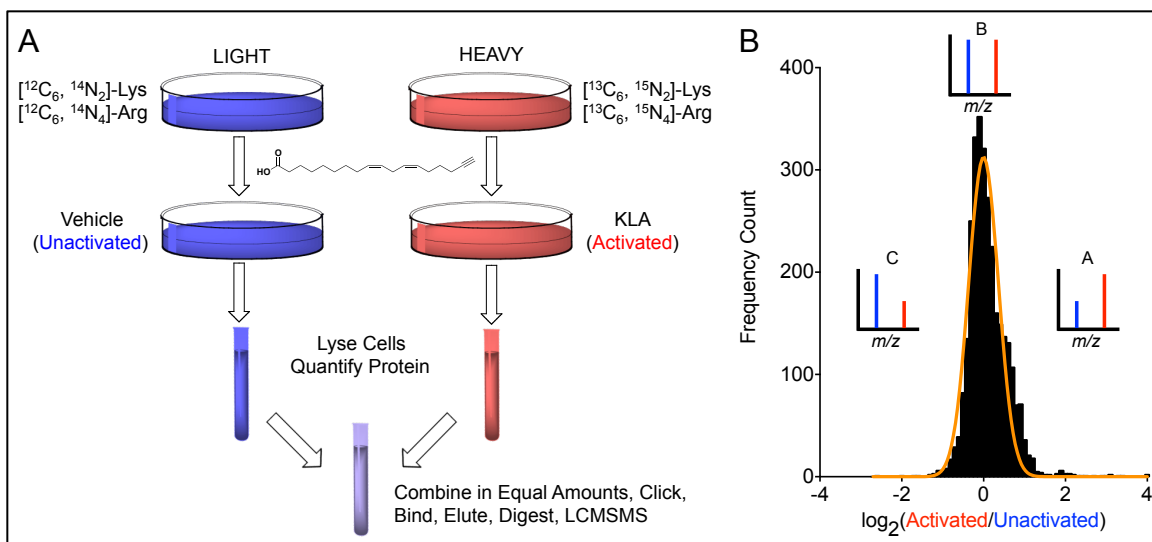


**Figure 7.** A) SILAC workflow. Both heavy and light cell lines were incorporated with aLA. The light cell line was unactivated (treated with vehicle) while the heavy cell line was activated with KLA. After activation, the heavy and light cells were harvested and lysed. Protein was quantified, and the two samples were then combined in equal amounts. Adducts were stabilized by reduction with NaBH<sub>4</sub> and then attached to UV-biotin by click chemistry for enrichment of adducted proteins (Figure 1B). Adducted proteins were analyzed by proteomic methods. B) A series of heavy/light (activated/unactivated) ratios was generated from the adductome data set. After log<sub>2</sub> transformation, the frequency count of these ratios was shown to fit a Gaussian distribution with R<sup>2</sup> > 0.94 for all replicates. Three distinct regions can be observed that are described by different activated/unactivated ratios. Theoretical spectra for the three potential activated/unactivated ratios are seen for protein A where activated/unactivated > 1; protein B where activated/unactivated = 1; and protein C where activated/unactivated < 1. These represent the scenarios where protein A is more adducted in the activated sample; protein B is equally adducted in the activated and unactivated sample; and protein C is more adducted in the unactivated sample.

Protein targets of adduction were adsorbed to streptavidin-coated beads after attachment of a biotin linker by click chemistry, and eluted by UV-irradiation, which cleaved the photo-activated linker between the biotin moiety and the protein conjugation site (Figure 1B). Three biological replicates of the eluted samples (adductome) were also analyzed via MudPIT-MS/MS. A total of 1,043 unique targets common to all three replicates were detected after affinity enrichment for electrophile-adducted proteins, and their heavy/light ratios were determined (Figure 8C). These proteins constitute the adductome.

*One hundred ninety-two proteins show the largest increase in expression during macrophage activation.* To identify protein targets with the greatest change in expression, we transformed each proteome data set to  $\log_2(\text{Activated/Unactivated})$ . These data are represented as a frequency distribution, with all three of the replicates fitting a Gaussian distribution well ( $R^2 > 0.92$ ) (Figure 9A, 9B, and 9C). We generated a P value for each expression heavy/light ratio to determine if it significantly changed (heavy/light  $\neq 1$ ). In total, we observed 192 proteins with heavy/light  $> 1.5$ . Our data provided an experimental power of 0.9 to predict a 1.5-fold change, and  $P < 0.05$ . We focused on these proteins because they are likely involved in signaling changes associated with oxidative stress during inflammation. Many of the expression changes we observed are for proteins known to show large expression changes during macrophage activation, including cyclooxygenase 2 (COX-2) (heavy/light = 18.9)<sup>27</sup>, tumor necrosis factor-alpha (TNF $\alpha$ ) (heavy/light = 5.6)<sup>27</sup>, and immune-responsive gene 1 (Irg1) (heavy/light = 16.4)<sup>326</sup>.

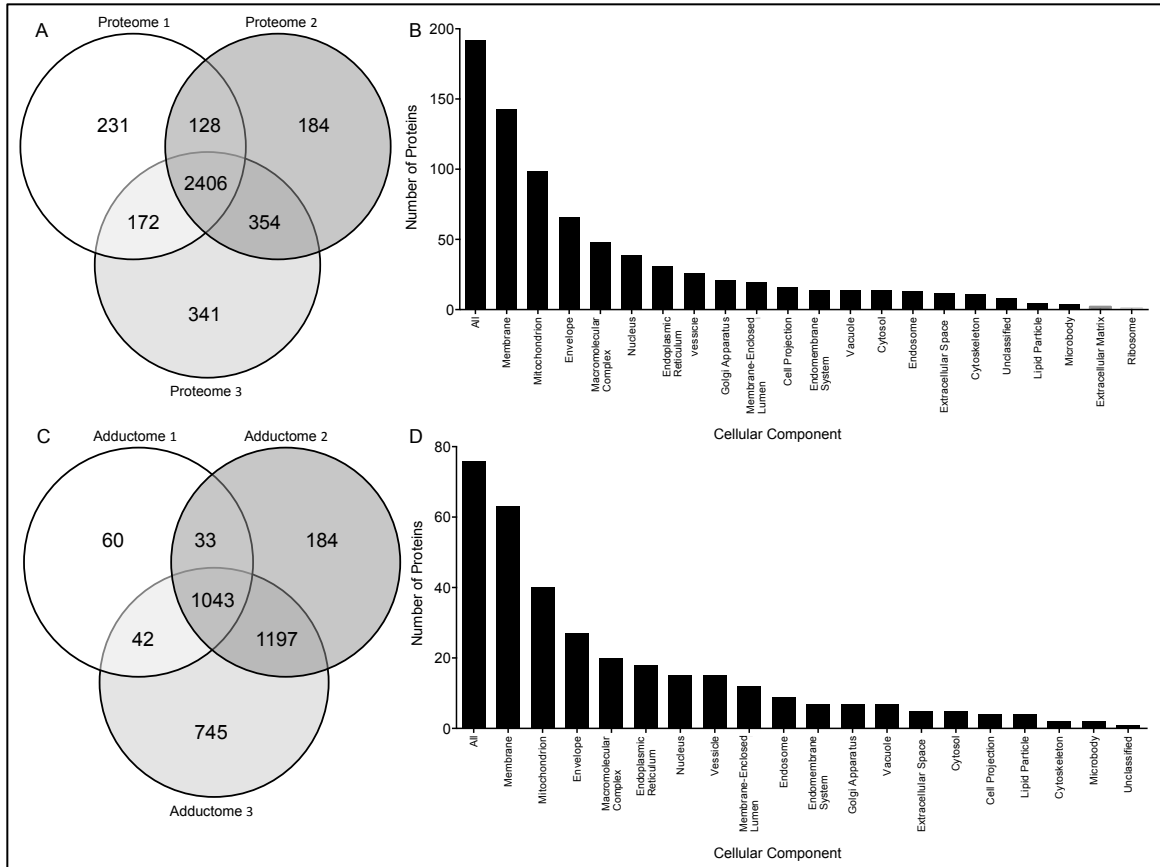


**Figure 8.** Analysis of expression and adduction changes during KLA-activation of macrophages. A) Venn diagram depicting common proteins based on Uniprot accession numbers across three proteome replicates. In total 3,816 proteins were detected, with 2,406 proteins in common across all three proteome replicates. B) Cellular compartment enrichment of the 192 most differentially expressed proteins during macrophage activation ( $P < 0.05$ , heavy/light  $> 1.5$ ). Membrane and mitochondrial proteins are the most heavily enriched cellular locations as increased for protein expression. C) Venn diagram depicting common proteins based on Uniprot accession numbers across three adductome replicates. In total, 3,304 proteins were detected as adducted, with 1,043 proteins commonly adducted across all three adductome replicates. D) Cellular compartment enrichment of the 76 most differentially adducted proteins by lipid electrophiles in activated macrophages ( $P < 0.05$ , heavy/light  $> 1.5$ ). Membrane and mitochondrial proteins are the most heavily enriched cellular locations as proteins targets for lipid electrophiles.

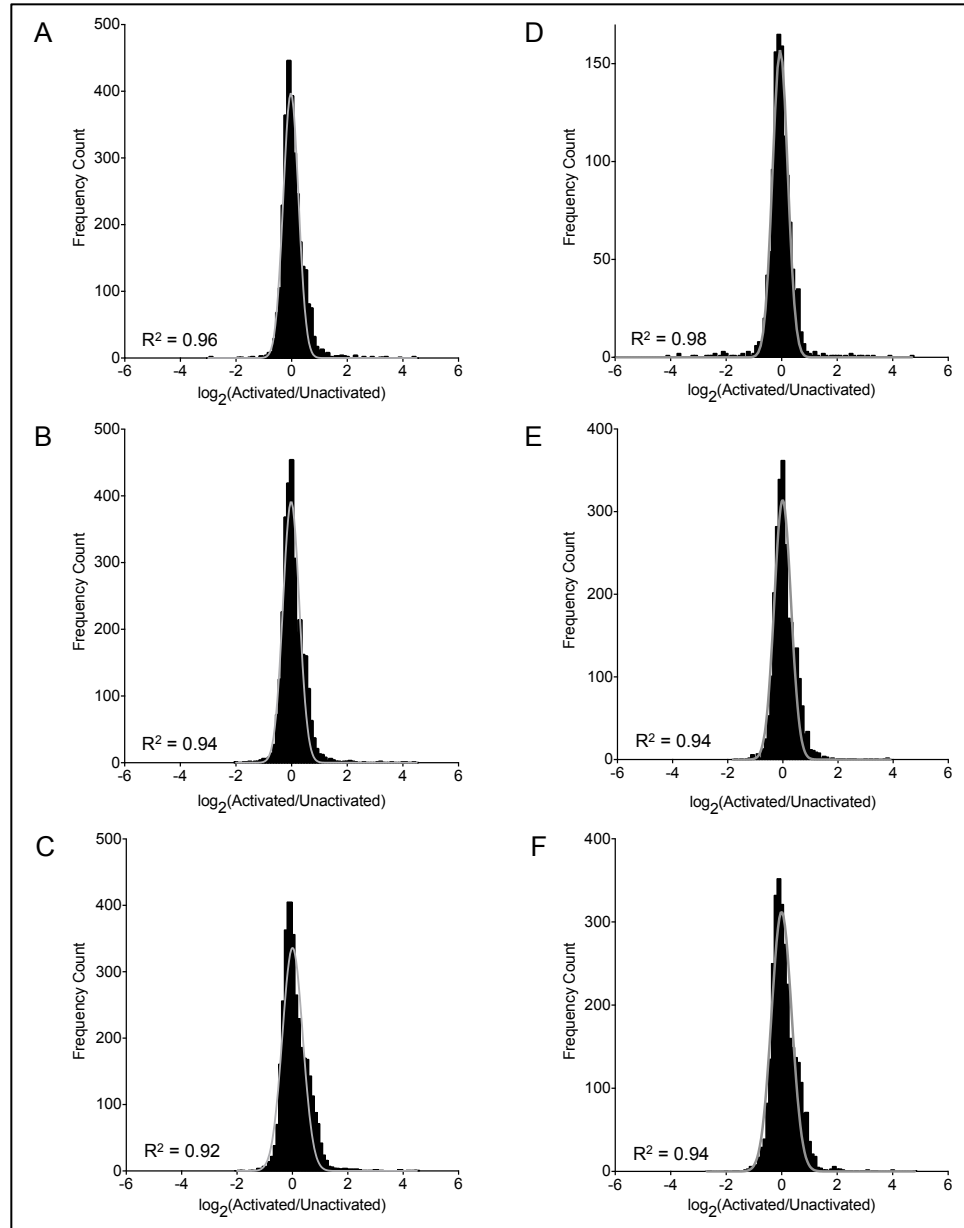


**Figure 9.** Frequency counts for each proteome replicate, A) replicate 1, B) replicate 2, and C) replicate 3. Proteome Activated/Unactivated ratios were converted to  $\log_2$  and plotted versus frequency count. All data fit a Gaussian distribution with  $R^2 > 0.92$ . Frequency counts for each adductome replicate, D) replicate 1, E) replicate 2, and F) replicate 3. Adductome Activated/Unactivated ratios were converted to  $\log_2$  and plotted versus frequency count. All data fit a Gaussian distribution with  $R^2 > 0.94$ .

*Seventy-six proteins show the largest increase in adduction during macrophage activation.* Similarly to the proteome data sets above, we transformed each adductome data set to  $\log_2(\text{Activated/Unactivated})$ . These data



are represented as a frequency distribution (Figure 7B), with all three of the replicates fitting a Gaussian distribution well ( $R^2 > 0.94$ ) (Figure 9D, 9E, and 9F). We generated a P value for each adduction heavy/light ratio to determine if the level of adduction changed significantly (heavy/light  $\neq 1$ ) during macrophage activation. Individual proteins fall into three distinct classes (Figure 7B) based on their heavy/light ratio. These classes have been defined as A: the protein is more adducted in the activated sample; B: the protein is equally adducted in the activated and unactivated samples; and C: the protein is less adducted in the activated sample. In total, we observed 151 proteins in class A (heavy/light  $> 1$ ,  $P < 0.05$ ), and will focus on these because they appear most potentially involved in functional changes associated with inflammation. To identify adductome protein targets with the largest fold-enrichment for adduction in activated macrophages, a heavy/light  $> 1.5$  was applied, as our data provide an experimental power of 0.9 to predict a 1.5-fold change. These filters resulted in a list of 76 unique proteins, which represents the most differentially adducted class of proteins during macrophage activation. The most adducted class of proteins contains many proteins involved in inflammatory signaling as well as oxidant defense, including cyclooxygenase 2 (COX-2) (heavy/light = 18.6), tumor necrosis factor-alpha (TNF $\alpha$ ) (heavy/light = 9.5), and superoxide dismutase 2 (Sod2) (heavy/light = 4.6).

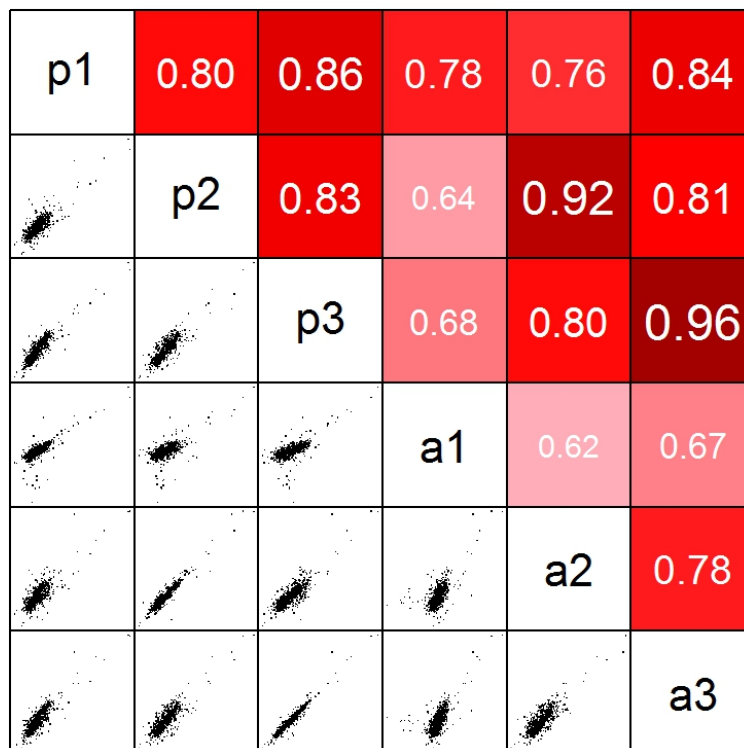


**Figure 10.** Spearman correlation coefficients relating the proteome and adductome replicates to each other. The heavy/light ratios were plotted for proteins common across all three proteome (p1, p2, and p3) and adductome (a1, a2, and a3) replicates. Each replicate is labeled in the diagonal. The x-axis is the heavy/light ratio for the column replicate, and the y-axis is the heavy/light ratio for the row replicate. Each point represents a protein detected, and shows the intersection of its column and row heavy/light ratios. The Spearman correlation coefficients between replicates are given in the red squares. A ratio of 1 indicates a perfect correlation between the respective column and row. High Spearman coefficients ( $> 0.75$ ) between the each proteome and adductome replicate indicate that adduction and induction are closely related for many proteins detected. However, this relationship does not indicate cause and effect for the two.

*Adduction and expression are correlated for many proteins.* The reference proteome and adductome were compared for each replicate individually to better understand the relationship between protein expression and lipid electrophile adduction. Figure 10 shows that many proteins in the proteome and adductome exhibit similar heavy/light ratios, as evidenced by their high Spearman coefficients. This may indicate that proteins are more adducted because of an

increase in abundance, or that proteins are adducted and then their expression induced to compensate for a loss of function.

*Membrane and mitochondrial proteins show the highest increase in expression during macrophage activation.* We evaluated the cellular location of the 192 proteins that show the greatest increase in expression using Webgestalt<sup>322</sup>, a web-based proteomic enrichment analysis tool (Figure 8B). The most increased classes were membrane proteins and mitochondrial proteins. These classes of proteins represented 74.5% and 51.6% of the 192 induced proteins, respectively. It should be noted that a protein may reside in more than one cellular component category. The reference proteome reveals that membrane and mitochondrial proteins represent 42.7% and 19.1% of the quantifiable proteins, respectively. Therefore, we observe a 1.7-fold enrichment for membrane protein expression and 2.7-fold enrichment for mitochondrial protein expression above what would be expected if protein expression changes were randomly distributed across the detectable proteome.

*Membrane and mitochondrial proteins also show the highest increase in adduction by lipid electrophiles during macrophage activation.* The cellular components affected by protein adduction were also identified using Webgestalt. Figure 3D shows the cellular localization for all 76 proteins that are significantly enriched for adduction in activated macrophages. The most enriched classes were membrane proteins and mitochondrial proteins. These classes of proteins represented 82.9% and 52.6% of the 76 targets of adduction, respectively. The reference proteome revealed that membrane and mitochondrial proteins

represent 42.7% and 19.1% of the measurable proteins, respectively, giving a 1.9-fold enrichment for membrane proteins and a 2.8-fold enrichment for mitochondrial proteins. Not all cellular locations were identified as enriched for adduction; nuclear proteins represented 19.7% of the most differentially adducted proteins, but 38.7% of the reference proteome, indicating that nuclear proteins are not heavily adducted by the alkynyl lipid electrophiles generated here.

**Table 1.** Wikipathway enrichment for the 192 proteins in the most differentially expressed class as determined by Webgestalt. Proteins: number of proteins identified in each pathway, which was limited to pathways with greater than three proteins; Enrichment: -fold enrichment as compared to the reference proteome; adjusted P, which was limited to pathways with adjP < 0.05; and Protein Identification: Entrez gene names for each protein identified.

Pathway	Proteins	Enrichment	adjP value	Protein Identifications
Electron Transport Chain	25	6.4	1.7x10 <sup>-14</sup>	Atp5a1, Atp5b, Atp5c1, Atp5d, Atp5f1, Atp5h, Atp5j, Atp5j2, Atp5k, Atp5l, Atp5o, Atp8, Cox17, Uqcrc1, Uqcrc2, Uqcr10, Uqcrcs1, Uqcrcq, Ndufab1, Ndufb10, Sdha, Sdhb, Sdhc, Slc25a4, Slc25a5
TCA Cycle	8	4.3	0.0030	Cs, Dld, Dlst, Mdh2, Ogdh, Sdha, Sdhb, Sdhc
Amino Acid Metabolism	11	2.4	0.032	Arg2, Cs, Dld, Dlst, Glud1, Got2, Hibadh, Mdh2, Oat, Ogdh, Sdha
Oxidative Damage	3	7.1	0.032	Cyca, Tnf, Tnfrsf1b

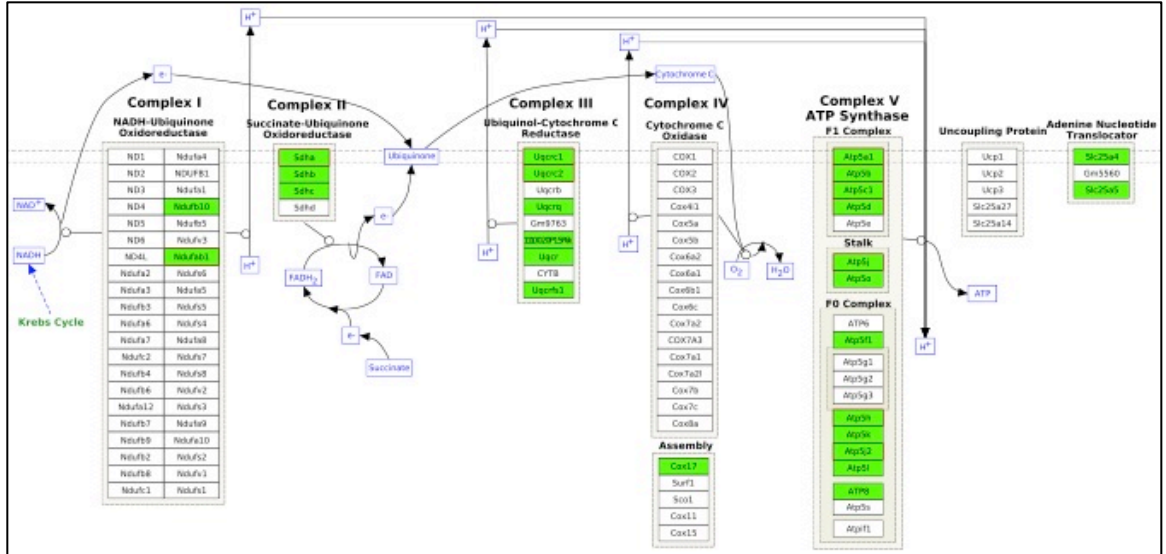


**Figure 11.** Complex V of the electron transport chain is the most differentially expressed pathway in activated macrophages. Electron transport chain proteins in the most differentially expressed class of protein targets are shaded in green. Expression can be seen in all of the subunits, with complex II, III, and V being the most heavily expressed. Figure modified from <http://wikipathways.org/index.php/Pathway:WP295>.

*The electron transport chain is the major mitochondrial pathway both induced and targeted by lipid electrophiles during macrophage activation. A pathway enrichment analysis of the 192 most differentially expressed and 76 most differentially adducted proteins during macrophage activation described above was also performed in Webgestalt using the Wikipathway functionality. As expected from the cellular component analyses described above, mitochondrial pathways were heavily represented in the pathway enrichment analyses. Table 1 shows pathways that contained three or more proteins and an adjusted P value less than 0.05 with increased expression during activation. The electron transport chain (ETC) is the most significantly increased for expression, exhibiting 6.4-fold enrichment when compared to the reference proteome. Expression changes of the ETC occur mainly in complexes II, III, and V (Figure 11). In addition to the*

ETC, the TCA cycle, amino acid metabolism, and oxidative damage pathways all show increased protein expression during macrophage activation. Table 2 shows that the ETC is also the most significantly enriched pathway for adduction, exhibiting a 7.1-fold enrichment in the adductome as compared to the reference proteome. Adduction in the ETC occurs predominately in complex V (ATP synthase) as can be seen by the pathway enrichment for oxidative phosphorylation (Figure 12). Within ATP synthase, a majority of the adduction occurred in the F<sub>1</sub> subunit (4 out of 5 proteins), which is the catalytic subunit of ATP synthase responsible for the conversion of ADP to ATP. Enzymes involved in central carbon metabolism were also heavily adducted, with the TCA cycle, amino acid metabolism, glycolysis, and gluconeogenesis represented in the most heavily adducted pathways. In addition, many enzymes that play important roles in ROS detoxification were in the most heavily adducted class, including superoxide dismutase 2 (Sod2), heme oxygenase 1 (Hmox1), and peroxiredoxin 5 (Prdx5).

**Table 2.** Wikipathway enrichment for the 76 proteins in the most differentially adducted class as determined by Webgestalt. Proteins: number of proteins identified in each pathway, which was limited to pathways with greater than three proteins; Enrichment: -fold enrichment as compared to the reference proteome; adjusted P, which was limited to pathways with adjP < 0.05; and Protein Identification: Entrez gene names for each protein identified.

Pathway	Proteins	Enrichment	adjP value	Protein Identifications
Electron Transport Chain	11	7.1	$2.7 \times 10^{-6}$	Atp5a1, Atp5b, Atp5c1, Atp5d, Atp5h, Atp5j, Atp5j2, Uqcrc1, Uqcrc2, Ndufab1, Sdha
Amino Acid Metabolism	6	5.0	$5.0 \times 10^{-4}$	Cs, Mdh2, Got2, Dlst, Hibadh, Glud1, Oat, Dld, Sdha
TCA Cycle	5	6.8	$2.6 \times 10^{-3}$	Cs, Mdh2, Dlst, Dld, Sdha
Glycolysis and Gluconeogenesis	4	4.8	0.02	Slc2a1, Mdh2, Got2, Dld

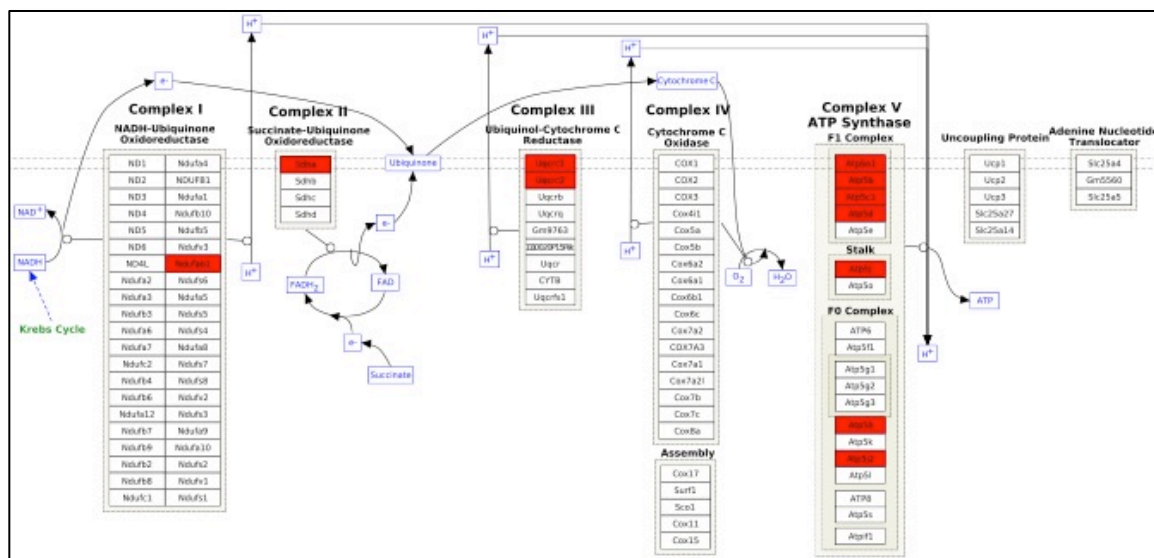


**Figure 12.** Complex V of the electron transport chain is the most differentially adducted pathway in activated macrophages. Electron transport chain proteins in the most differentially adducted class of protein targets are shaded in red. Adduction can be seen in all of the subunits except complex IV, with complex V or ATP synthase being the most heavily adducted. Figure modified from <http://wikipathways.org/index.php/Pathway:WP295>.

*MitoTEMPO modulates lipid electrophile adduction in activated macrophages.* Superoxide is generated in the mitochondrion as an oxidative phosphorylation byproduct. Our adductome SILAC data showed significant enrichment for mitochondrial proteins, leading to the hypothesis that mitochondrial superoxide is a major source of ROS that leads to electrophile generation and protein adduction. To test this hypothesis, we employed two superoxide-scavenging agents to evaluate the effects of quenching mitochondrial superoxide on protein adduction: MitoTEMPO, which localizes to the mitochondrion, and TEMPOL, which is ubiquitously dispersed throughout the cell<sup>327</sup>. MitoTEMPO or TEMPOL was added at the same time as KLA to RAW264.7 macrophages that had been incorporated with aLA, and adduction across the proteome was assessed via click chemistry and streptavidin blotting. Figure 13 demonstrates that MitoTEMPO reduced measurable lipid electrophile adduction to nearly basal levels in KLA-activated samples. Additionally, MitoTEMPO reduced the basal electrophile adduction in unactivated macrophages. TEMPOL did not modulate protein adduction in either activated or unactivated macrophages. The differential effects of MitoTEMPO and TEMPOL indicate that mitochondrial superoxide plays a major role in both physiological and pathophysiological lipid electrophile generation. These data are in agreement with our SILAC adductome, which shows that mitochondrial proteins are adducted during activation.



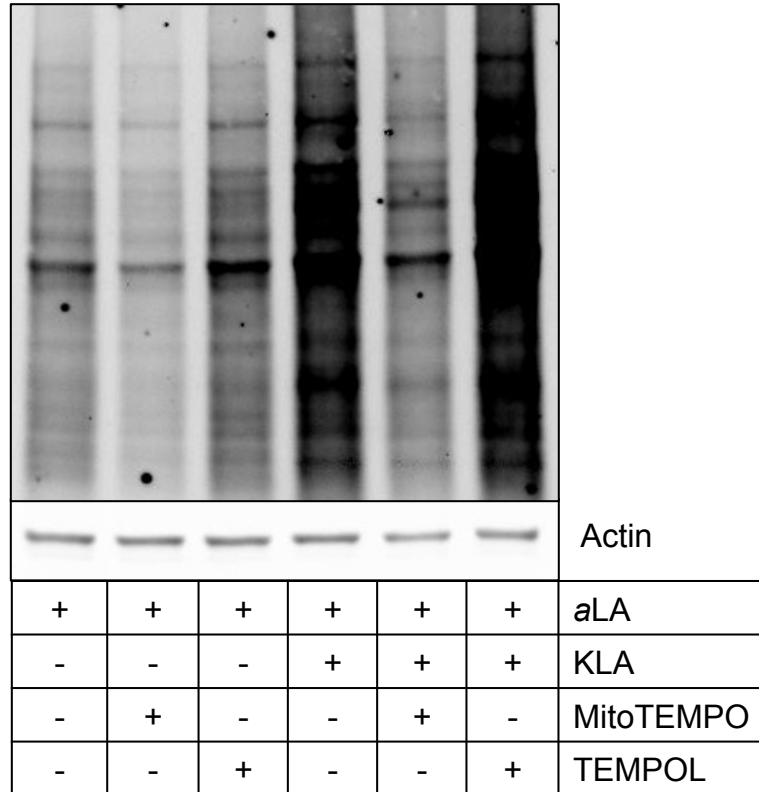


**Figure 13.** MitoTEMPO modulates KLA-induced protein adduction, while TEMPOL does not. MitoTEMPO, a mitochondrially targeted superoxide scavenger was able to reduce both physiological (second lane) and pathophysiological (fifth lane) protein adduction by lipid electrophiles, identifying mitochondrial superoxide as a precursor to lipid electrophile formation. TEMPOL, a ubiquitously dispersed superoxide scavenger, did not modulate electrophile formation, further implicating mitochondrial superoxide in the formation of lipid electrophiles.

We used click chemistry, affinity purification, and western blotting to test the effect of MitoTEMPO on the extent of protein adduction on specific targets of adduction. Figure 14A shows an increase in recovered protein in the KLA-activated samples indicating increased adduction during macrophage activation, which is consistent with what we have seen using a streptavidin based fluorophore to assess the extent of lipid electrophile adduction. Also consistent with what we have seen above, MitoTEMPO reduces the amount of adducted protein in both the vehicle and KLA-activated sample, further demonstrating a

role for mitochondrial superoxide in lipid electrophile generation. Figure 14B shows that MitoTEMPO does not affect the KLA-induced expression of Sod2, but drastically reduces the amount of lipid electrophile adducted Sod2. Figure 14C shows that MitoTEMPO has similar effects on COX-2; it does not affect COX-2 induction, but decreases COX-2 adduction. These data indicate that the expression changes observed during macrophage activation are dependent upon signaling during activation, and that lipid electrophile adduction is related to mitochondrial superoxide.

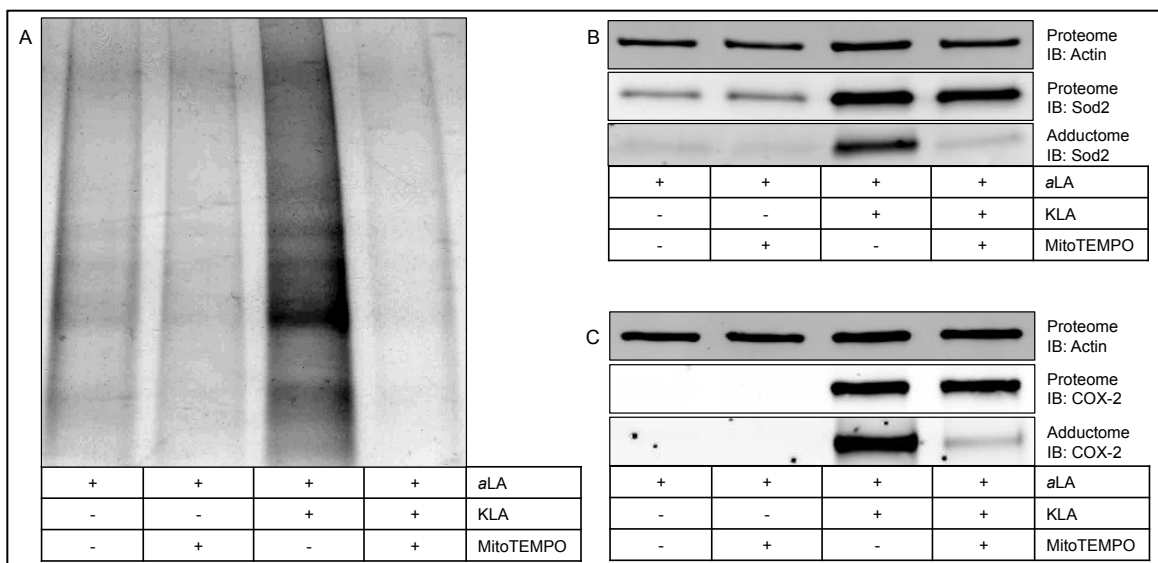


**Figure 14.** MitoTEMPO modulates the amount of adducted protein affinity purified in aLA-incorporated macrophages. A) Consistent with previous results, affinity-purified adducted protein is greatest in the KLA-activated macrophages (third lane). MitoTEMPO reduces total adducted protein in both the vehicle treated (second lane) and KLA-activated (fourth lane) macrophages. B) MitoTEMPO does not change the KLA-induced expression (Proteome) of Sod2, but does decrease the amount of Sod2 adduction (Adductome). C) MitoTEMPO also does not change the expression (Proteome) of COX-2 induced during activation, and also decreases the amount of COX-2 adduction (Adductome). These data indicate that both mitochondrial and non-mitochondrial targets of adduction are adducted by lipid electrophiles generated through a process that involves mitochondrial superoxide.

*Immunoblotting confirms targets of adduction.* Adducted proteins enriched by adsorption to streptavidin beads were probed with antibodies against individual adducted proteins at 0, 3, 6, 9, 12, and 24 h post-activation to validate their status as targets of adduction. Figure 15A reveals that there is minimal adduction of Sod2 at 0, 3, and 6 h post KLA activation. Adduction of Sod2 appears first at the 9 h time point, with the majority occurring between the 9 and 12 h time points and then further increasing between the 12 and 24 h time points. COX-2 adduction was also confirmed by immunoblotting, with adduction first appearing at the 9 h time point and the majority occurring between the 12, and 24 h time points (Figure 15B). Both Sod2 and COX-2 show changes in expression levels, with Sod2 having a basal expression level, but COX-2 being nearly undetectable at the 0 h time point. Additionally, the adduction levels tend to follow the expression levels for both proteins.

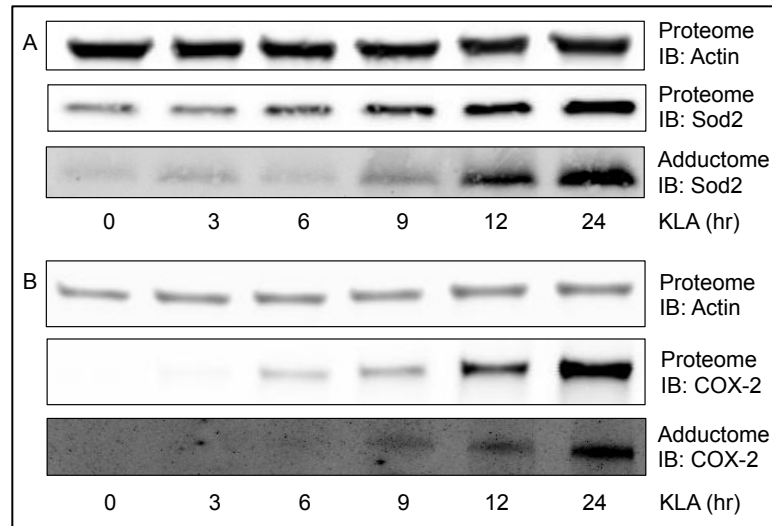


**Figure 15.** Western blot confirmation of protein targets of lipid electrophile adduction. A) Affinity purification and western blotting were used to confirm Sod2 as adducted by lipid electrophiles during macrophage activation. Adduction can be seen to first appear between the 6 h and 9 h time points, and further increases out to the 24 h time point. An input blot shows expression increases for Sod2 that mimic increases in adduction. B) COX-2 is increasingly adducted by lipid electrophiles during macrophage activation. Adduction first appears between the 6 h and 9 h time points, and increases most dramatically by the 24 h time point. An input blot shows COX-2 expression is first detected at the 6 h time point, and increases until the 24 h time point.

*Sod2 adduction inversely correlates to Sod2 activity, and is rescued by MitoTEMPO.* Sod activity was determined in both cytosolic and mitochondrial fractions, representing Sod1 and Sod2 activity, respectively. The activities presented in Figure 16 are normalized to protein expression levels of Sod1 in the cytosol or Sod2 in the mitochondrion as determined in Figure 17. Sod1 has a heavy/light average adduction ratio of 1.1 in the SILAC adductome experiments, indicating no change in adduction following activation. Sod1 activity exhibited an increase in the KLA-activated macrophages (Figure 16A). This increase could be explained by contamination with Sod2 in the KLA-activated cytosolic isolates (Figure 17A). In contrast, a significant decrease in Sod activity normalized to Sod2 expression was observed in the mitochondrial fractions, even though the

absolute activity of Sod2 was increased in the KLA-activated mitochondria (Figure 18). Sod2 showed a heavy/light adduction ratio of 4.6, indicating that it is heavily adducted post-activation. This increase in adduction is inversely correlated to Sod2 activity in the mitochondrial fraction (Figure 16B). The mitochondrial fractions showed no contamination with Sod1 (Figure 17B). When macrophages were co-treated with KLA and MitoTEMPO (Figure 16C), Sod2 activity normalized to expression was restored to levels observed in unactivated macrophages. MitoTEMPO did not prevent the induction of Sod2 during KLA activation (Figure 17C) indicating that Sod2 induction is a result of KLA signaling. These data suggest a potential deleterious impact of lipid electrophile adduction on Sod2 activity, which is rescued by quenching mitochondrial superoxide.

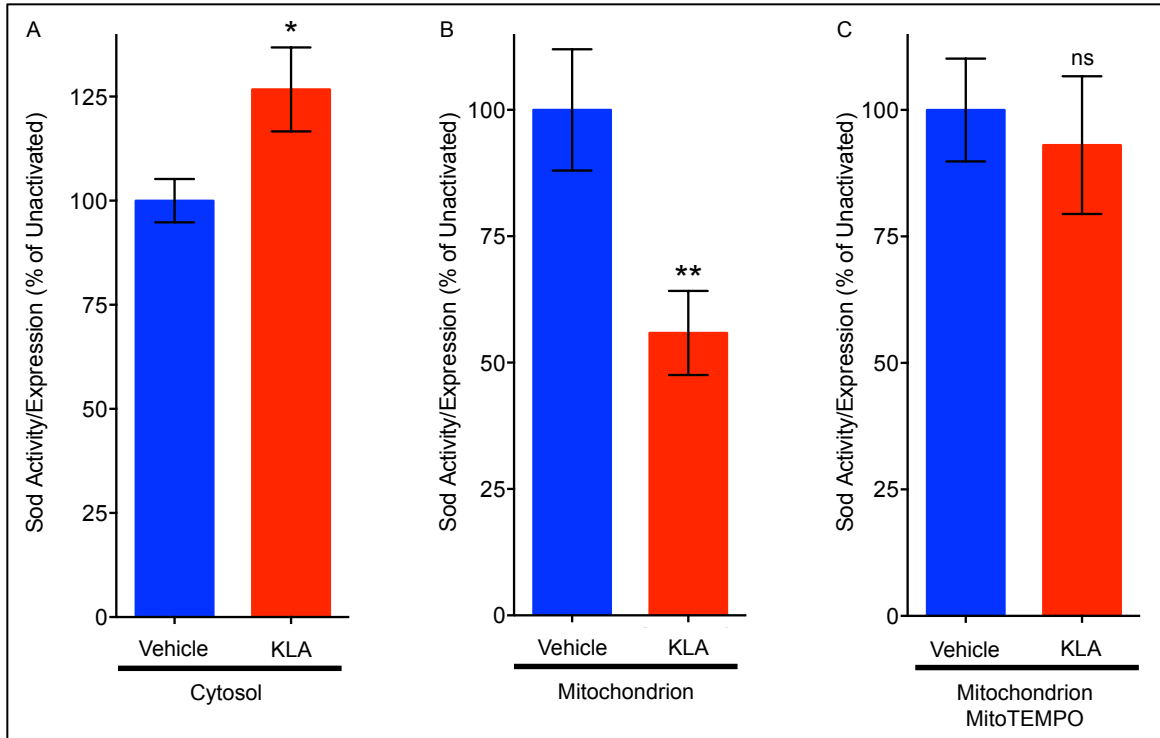


**Figure 16.** Activity changes associated with lipid electrophile adduction of superoxide dismutase 2. A) KLA induces no decrease in Sod1 activity, but B) causes a reduction in Sod2 activity, which is consistent with no adduction changes measured for Sod1, but increased adduction for Sod2 after KLA activation. C) MitoTEMPO, rescues the activity of Sod2 by reducing lipid electrophile adduction of Sod2. Each data point is the average of three technical replicates. Data are normalized to Sod1 or Sod2 expression for the cytosolic and mitochondrial fractions respectively, and are mean  $\pm$  standard deviation of a triplicate experiment. Statistical significance determined by an unpaired t-test where \* =  $P < 0.05$ , \*\* =  $P < 0.01$ , and ns =  $P > 0.05$ .

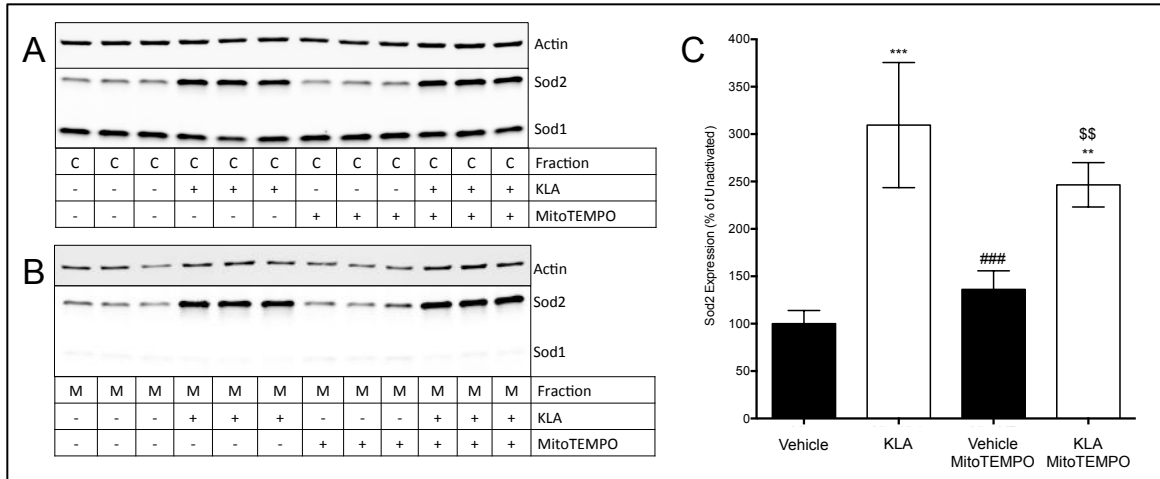


**Figure 17.** Superoxide dismutase 1 and 2 (Sod1 and Sod2) expression in mitochondrial and cytosolic isolates. A) Cytosolic (C) isolates show some contamination for Sod2, with much more contamination present in the KLA activated macrophages. B) Mitochondrial (M) isolates show very little Sod1 contamination. C) The densitometry plot for B) shows that MitoTEMPO does not induce Sod2 expression in Vehicle MitoTEMPO relative to Vehicle. MitoTEMPO also does significantly reduce Sod2 expression in KLA-activated macrophages indicating that Sod2 expression is a function of macrophage activation. Data are mean  $\pm$  standard deviation of a triplicate experiment. Statistical significance compared to Vehicle (\*), KLA (#), or Vehicle MitoTEMPO (\$) was determined by Two-Way ANOVA with Tukey *post hoc* analysis, where \*\* =  $P < 0.01$ . Absence of a symbol indicates  $P > 0.05$ .

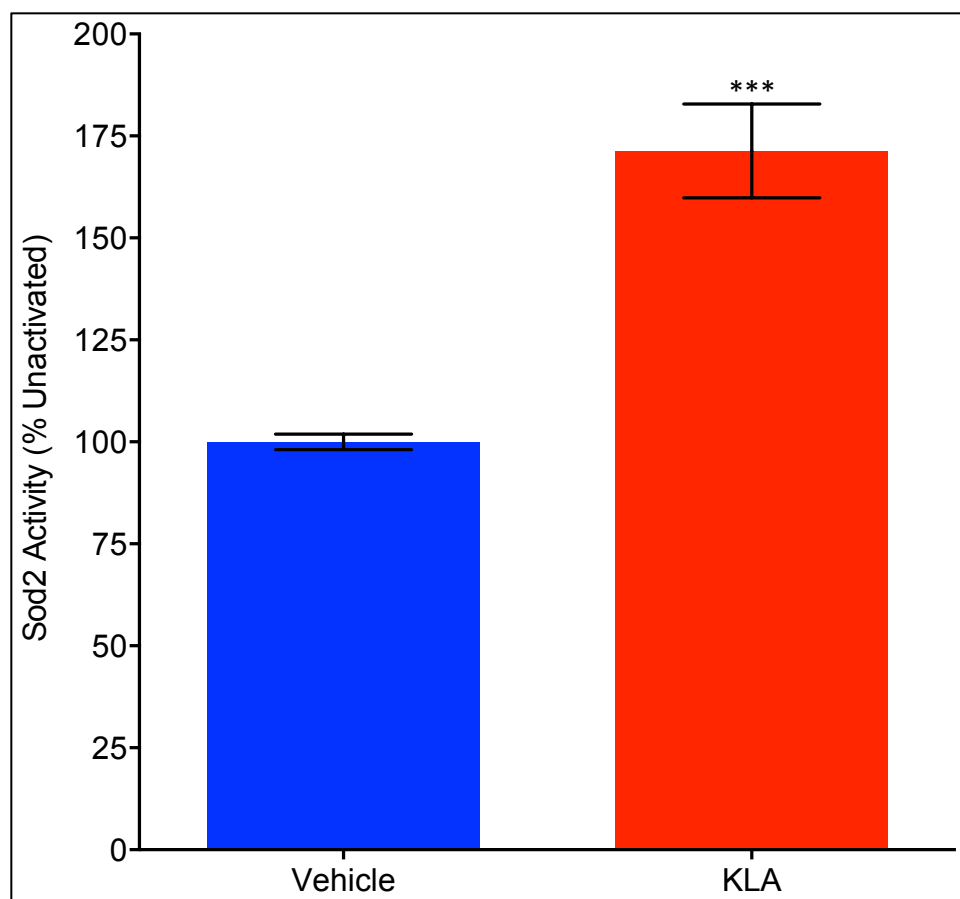


**Figure 18.** Absolute Sod2 activity in unactivated and activated RAW264.7 macrophage mitochondria. Total Sod2 activity is increased in KLA-activated RAW264.7 macrophages. We hypothesize that this increase in activity is related to the increases in expression seen in KLA-activated macrophages and represents a mechanism to defend the macrophages from increased oxidative stress during activation. Each data point is the average of three technical replicates. Data represented are mean  $\pm$  standard deviation of a triplicate experiment. Statistical significance determined by an unpaired t-test where \*\*\* =  $P < 0.001$ .

## Discussion

The global identification and quantification of proteins adducted by endogenous lipid electrophiles has previously been hindered by the inability to comprehensively enrich for electrophile-adducted proteins, mainly due to the complexity of the electrophile pool generated. Here we use *a*LA incorporation and KLA activation of RAW264.7 macrophages to generate alkynyl lipid



electrophiles in a physiologically relevant setting. We have previously shown that alkynyl fatty acids have similar autoxidation chemistry as their native counterparts<sup>311</sup>. Here we determined that *a*LA is incorporated into the phospholipid bilayer, and metabolized by the desaturases and elongases involved in AA biosynthesis. We detected all of the alkynyl intermediates in the biosynthesis of *a*AA from *a*LA. These data support our assertions in Chapter II that *a*LA is a viable surrogate to use in place of LA to study cellular lipid chemistry. In addition to further validating our model system, the biosynthesis of *a*AA from *a*LA increases the number of *a*PUFA precursors from which alkynyl electrophiles can be generated. This increase in lipid precursor complexity more closely mimics what is observed in physiological conditions where there are multiple PUFA sources for electrophiles. This discovery gives us the ability to more comprehensively profile the lipid electrophile adductome during macrophage activation by increasing the diversity of electrophile species generated.

Click chemistry makes possible the selective qualitative assessment of protein adduction as well as the selective recovery of proteins adducted by alkynyl electrophiles for quantitative measurements. SILAC paired with affinity purification and MudPIT-MS/MS proteomic analysis allows for the global identification and relative quantification of adducted proteins without knowing the identity of the electrophile species generated, accounting for the complex diversity of the electrophile pool. Basal lipid oxidation and electrophile formation is a physiological process yielding electrophiles that serve as signaling molecules

in normal cellular functions<sup>328</sup>. Thus, lipid electrophile generation is expected to occur under normal growth conditions as well as during episodes of increased oxidative stress. Consistent with this notion, we show qualitatively that protein adduction by lipid electrophiles can be measured in both activated and unactivated aLA-incorporated macrophages, and that activation results in an increase in protein adduction by lipid electrophiles.

In addition to profiling proteins that are adducted by lipid electrophiles, MudPIT-MS/MS proteomic analysis of our SILAC samples before affinity purification yields an inventory of protein expression changes that occur during KLA activation. KLA activation induces ROS production as well as expression of many proteins associated with the inflammatory response including COX-2<sup>27</sup>, TNF $\alpha$ <sup>27</sup>, and Irg1<sup>326</sup>, as well as the anti-inflammatory response including Sod2<sup>329</sup> and Hmox1<sup>330</sup>. We also show that mitochondrial proteins are heavily induced during the first 24 h of macrophage activation. ROS production and lipid electrophile generation have been associated with mitochondrial dysfunction<sup>331</sup> and changes in protein expression<sup>210, 211</sup>. COX-2 can be induced by lipid electrophiles independent of the COX-2 induction during initial inflammatory signaling<sup>230</sup>. Hmox1 is induced by lipid electrophiles through Keap1/Nrf2 signaling, producing CO, which has been shown to be both anti-inflammatory and to stimulate mitochondrial biogenesis<sup>330</sup>. Hmox1 induction of mitochondrial biogenesis is hypothesized to be a mechanism by which macrophages restore degraded mitochondrial function, helping the cells recover from the deleterious effects of inflammatory signaling<sup>332</sup>. The established link between Hmox1

expression and mitochondrial biogenesis further supports the increase in mitochondrial proteins we see during macrophage activation.

Here we also identify the mitochondrion as the cellular compartment that is most highly targeted for endogenous electrophile-mediated protein adduction. We see proteins associated with ATP generation, central carbon metabolism, as well as oxidant defense heavily adducted. Adduction of these proteins important for cellular function corroborates a previous study showing mitochondrial dysfunction during macrophage activation<sup>331</sup>. One of the major functions of the mitochondrion is to consume glucose and oxygen, generating the ATP used for cellular energy<sup>327</sup>. A byproduct of this process, superoxide anion, is produced when an electron leaks out of the electron transport chain and reacts with molecular oxygen. Superoxide is a precursor to many oxidants generated during inflammatory signaling<sup>333</sup>, and superoxide dismutases exist to convert superoxide to hydrogen peroxide, the first step in superoxide detoxification<sup>334, 335</sup>. Superoxide also reacts rapidly with nitric oxide to generate peroxynitrite, a potent oxidant that degrades to various other cellular oxidants<sup>336</sup>. Therefore, we hypothesized that mitochondrial superoxide is potentially a precursor to the cellular oxidant(s) responsible for lipid peroxidation. We used the superoxide scavengers MitoTEMPO and TEMPOL to test this hypothesis. MitoTEMPO, which has been reported to concentrate 1,000-fold in the mitochondrion relative to other cellular components<sup>327</sup>, reduces measurable protein adduction in both unactivated and activated macrophages. TEMPOL, which is evenly dispersed throughout the cell, was unable to modulate adduction in either activated or unactivated

macrophages at the concentrations tested. These data indicate that physiological and pathophysiological lipid electrophiles share a common mechanism of formation involving mitochondrial superoxide, further implicating mitochondrial superoxide as a precursor to lipid electrophiles.

With the highest expression and adduction changes measured in similar cellular locations, similar signaling pathways, and involving similar proteins in those pathways, we wanted to see how the induction and adduction ratios compared. We determined that there is a high correlation between increased protein expression and increased protein adduction. Three possible explanations exist for this correlation, and all may exist concurrently in a cell depending on the protein being investigated: 1) protein expression increases, and thus adduction increases because there is more protein to be adducted; 2) proteins are adducted, lose function, and that activity loss is compensated for by increased expression; or 3) the macrophages have evolved to induce proteins upon KLA-activation that assist in oxidant defense in anticipation of increased levels of oxidative stress.

MitoTEMPO qualitatively reduces proteome-wide lipid electrophile adduction when detected with a streptavidin fluorophore, but we also wanted to see if MitoTEMPO reduces adduction levels of individual proteins. We generated alkynyl lipid electrophile-adducted proteomes, attached UV-biotin, streptavidin affinity purified, and UV-eluted as in the SILAC experiments. The total amount of protein eluted was greatest in the KLA activated samples, which is consistent with macrophage activation generating lipid electrophiles. Additionally,

MitoTEMPO reduced both physiological and pathophysiological total protein adduction amounts. We probed for a mitochondrial protein, Sod2, and a non-mitochondrial, but membrane-associated protein, COX-2, to determine the effects of MitoTEMPO on protein adduction. MitoTEMPO reduced adduction of both proteins investigated, but did not change expression increases associated with macrophage activation. This further indicates that mitochondrial superoxide is a precursor to lipid electrophiles generated during macrophage activation. These data also show that expression increases, at least for these two proteins, are not driven by a compensatory mechanism initiated by lipid electrophile adduction.

Previous studies validated adduction targets by changing the electrophile concentration to demonstrate dose-dependence<sup>204</sup>. Our model system does not allow for direct alteration of electrophile dose because the electrophiles are generated endogenously. However, a detailed knowledge of inflammatory signaling in response to KLA activation can predict when electrophile generation and protein adduction is expected. Based on prostaglandin synthesis and TNF $\alpha$  expression, two well-studied markers of inflammatory response, inflammatory signaling in activated RAW264.7 macrophages reaches a maximum during 3-6 h post activation<sup>27</sup>. We expect that much of the superoxide generation occurs during this time period, and that lipid oxidation, electrophile generation, and protein adduction will follow. We determined by western blot that two targets of adduction, Sod2 and COX-2, begin to be adducted between 6 and 9 h post-activation, and adduction increases dramatically between the 9 and 12 h time

points. These data indicate that protein adduction follows inflammatory signaling, but not closely enough to be explained exclusively by superoxide generated during the initial inflammatory response. Other studies have shown that lipid electrophile adduction of electron transport chain proteins, which we observed as well, disrupts oxidative phosphorylation<sup>234, 261</sup>. We hypothesize that the damage incurred during the inflammatory response to mitochondrial proteins results in increased electron leakage and superoxide formation, leading to the larger increases in adduction seen later in the time course.

RAW264.7 macrophages have two superoxide dismutase enzymes, Sod1 and Sod2, which are localized in the cytosol and mitochondrion, respectively. The heavy/light adduction ratios measured for Sod1 and Sod2 were 1.1 and 4.6, respectively, indicating that adduction of Sod2 is increased during activation and that Sod1 adduction does not change. These data match well with our other observations that much of the adduction occurs in the mitochondrion. There was no decrease in cytosolic superoxide dismutase activity in activated macrophages compared to unactivated macrophages, which correlates with the heavy/light ratio for Sod1 of 1.1. Conversely, an increase in adduction of Sod2 in the activated sample correlates to a decrease in activity normalized to Sod2 expression. MitoTEMPO, which we have shown decreases Sod2 adduction by lipid electrophiles, restores Sod2 activity in KLA-activated macrophages to that of unactivated macrophages. These data further suggest that lipid electrophile adduction of Sod2 plays a role in modulating Sod2 activity. It has been previously shown that acetylation of Sod2 results in altered electrostatics in the channel that

draws superoxide into the Sod2 active site, decreasing activity<sup>337-339</sup>. These studies indicate that alkylation of certain nucleophilic amino acids of Sod2 decreases activity.

Increased expression of Sod2 (expression heavy/light = 4.3) in the activated cells is observed, and is consistent with what has been previously reported in activated macrophages<sup>329</sup>. This increase in expression gives an absolute Sod2 activity higher than what is seen in the unactivated mitochondria. MitoTEMPO treatment does not change Sod2 expression levels, therefore, we hypothesize that induction of Sod2 is a mechanism to compensate for increased ROS, lipid electrophile generation, and Sod2 inactivation that occurs during macrophage activation. This hypothesis is in agreement with previous studies noting that Sod2 is the only superoxide dismutase necessary for organism survival<sup>340, 341</sup>. Neither expression (heavy/light = 1.0) nor adduction (heavy/light = 1.1) of Sod1 changes upon macrophage activation, which further implicates protein damage playing a role in Sod2 induction. The expression changes we observed are consistent with a previous study looking at LPS-treated pulmonary cells. This study noted a large increase in Sod2 expression, but no changes in Sod1 expression 24 h after LPS treatment<sup>342</sup>.

This model system allows us to identify and quantify any protein adducted by an electrophile that retains the alkyne. We show that *a*LA is elongated to *a*AA, which indicates that our surrogate PUFAs are recognized as physiological fatty acids, but also complicates identifying electrophilic species by expanding the diversity of the electrophile pool generated. Potential electrophilic species include

4-oxo-2-nonenal, derived from both LA and AA oxidation, which we have previously shown to adduct histones in these macrophages using the same activation conditions<sup>308</sup>. The electrophilic species could also be one of many cyclopentenone<sup>197</sup> or isoketal/levuglandin<sup>195, 343</sup> species generated exclusively from AA. Additionally, the incorporation of a single oxygen atom at multiple potential positions of the PUFA can create a,b-unsaturated carbonyls of both LA and AA, oxo-octadecadienoic acid or oxo-eicosatetraenoic acid respectively<sup>203</sup>. These oxo-fatty acids have been observed esterified in the phospholipid bilayer, further diversifying the pool electrophiles by introducing multiple combinations of phospholipid head groups and *sn*-1 esterified fatty acids<sup>190</sup>. Nitration of LA and AA also produce a class of lipid electrophiles that have protein-adducting capabilities<sup>344</sup>. The plethora of possible electrophiles makes it extremely challenging to comprehensively search for and identify endogenously generated adducting species in an unbiased manner.

Global profiling of proteins adducted during KLA activation by endogenously formed lipid electrophiles is an important step in understanding the potential pathological mechanisms of inflammatory signaling. Here we present a model system for the identification of protein targets of endogenously generated lipid electrophiles. Using *a*LA as a surrogate fatty acid, we have identified the targets of adduction resulting from alkynyl fatty acid peroxidation to be mitochondrial proteins important for cellular metabolism and the removal of ROS. These same proteins are also the most induced during macrophage activation. Adduction levels of Sod2, an important enzyme involved in oxidant defense, are



inversely correlated with Sod2 activity. This activity loss is restored when electrophile generation is inhibited, thereby connecting cellular ROS defenses and lipid electrophile adduction. Increased protein adduction has been measured in patients with inflammation-related diseases, including the brains of patients with Alzheimer's disease<sup>345</sup>, the spinal cord motor neurons of patients with amyotrophic lateral sclerosis<sup>222</sup>, and the arteries of patients with atherosclerosis<sup>230</sup>. Our current study combined with these previous observations suggest that uncontrolled ROS generation and the resulting mitochondrial protein damage by lipid electrophiles may be an initiating and propagating factor in disease pathogenesis.

## Chapter IV

### PATHWAYS OF PEROXIDATION: STUDIES TO DETERMINE ROUTES OF LIPID OXIDATION AND ELECTROPHILE FORMATION

#### Introduction

In Chapter III, we globally profiled protein targets of endogenously generated lipid electrophiles in macrophages activated with Kdo<sub>2</sub>-lipid A (KLA)<sup>286</sup>, a chemically defined lipopolysaccharide. Our method allowed us to quantify differences in adducted proteins between unactivated and activated macrophages without knowing the identity of the adducting species. We showed that KLA-induced adduction is heavily enriched for membrane-associated and mitochondrial proteins. Therefore, we used MitoTEMPO<sup>327</sup>, a mitochondrially targeted superoxide scavenger, to parse the role of mitochondrial reactive oxygen species (ROS) in lipid electrophile formation. The results of these experiments showed that mitochondrial superoxide is necessary for lipid electrophile protein adduction. Due to the fact that the major polyunsaturated fatty acid (PUFA) oxidizing enzymes are not located in the mitochondrion and that the process is dependent upon mitochondrial superoxide, we hypothesized that lipid electrophile generation during macrophage activation is primarily the result of non-enzymatic PUFA oxidation.

PUFAs are easily oxidized lipids because of the presence of *bis*-allylic hydrogens that are abstracted to form highly stabilized pentadienyl radicals. The pentadienyl radicals then readily react with molecular oxygen to form peroxy

radicals that, in turn, generate a plethora of products with different positional isomers, geometric isomers, and enantiomers. Enzyme-catalyzed oxidation yields products with defined regiochemistry and stereochemistry, whereas autoxidation generates a mixture of regioisomers and stereoisomers (Figure 1). Thus, determination of the regiochemistry and stereochemistry of fatty acid oxidation can provide insight into the identity of the pathway (enzymatic or non-enzymatic) responsible for oxidation<sup>103, 104, 346</sup>.

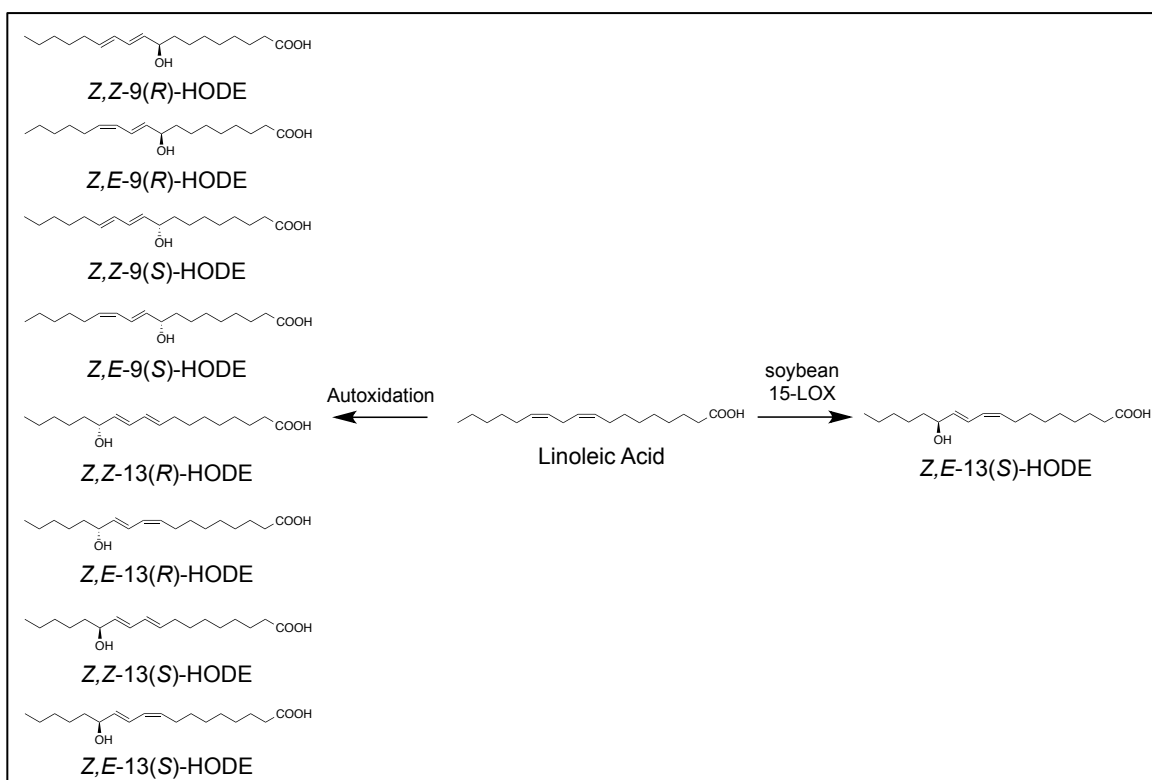


**Figure 1.** Enzymatic and autoxidation products of LA. Enzymatic oxidation of linoleic acid results in a much smaller pool of oxidized products than autoxidation because enzymatic oxidation gives a defined stereochemistry and regiochemistry, while autoxidation will give a mixture of all possible isomers. Soybean 15-LOX generates exclusively Z,E-13(S)-HODE. Autoxidation generates a mixture of 9- and 13-positional isomers, R and S enantiomers, and Z,E and Z,Z geometric isomers.

As discussed in Chapter I, Linoleic acid (LA) has one of the simplest profiles of oxidation, as it possesses only one pair of abstractable hydrogen atoms between its two *cis* double bonds. Two positional isomers are observed in biological settings, representing oxygen addition at the 9- or 13-carbon<sup>106</sup>. The initial oxygenation results in isomerization of the adjacent double bond, shifting the geometry from *Z,Z* to *Z,E*<sup>108</sup>. Addition of a hydrogen atom at this point yields the kinetically favored *Z,E* product. Alternatively, reversal of oxygenation<sup>107</sup> reforms the pentadienyl radical, which can then react with molecular oxygen at the opposite position with a second isomerization resulting in the thermodynamically favored *E,E* product<sup>110, 111</sup>. The presence of a hydrogen donor favors rapid trapping of the *Z,E* product, leading to an equal mixture of *E,E/Z,E*; in the absence of a donor, *E,E* is four-fold more abundant than *Z,E* (Figure 2)<sup>109</sup>. Oxygen addition also creates a chiral center that can be either the *R* or *S* enantiomer. Autoxidation of LA results in an equal mixture of 9- and 13-positional isomers as well as *R* and *S* enantiomers (Figure 1)<sup>112</sup>. Enzymatic oxidation, however, yields a defined positional and geometric isomer as well as a single enantiomer. For example, soybean 15-lipoxygenase-1 oxidizes LA exclusively to *Z,E*-13(*S*)-hydroperoxy octadecadienoic acid (*Z,E*-13(*S*)-HPODE) at physiological pH (Figure 1)<sup>154, 155</sup>. In biological settings HPODEs, are quickly reduced to the corresponding hydroxy octadecadienoic acids (HODEs), which are the products typically measured to assess LA oxidation levels.

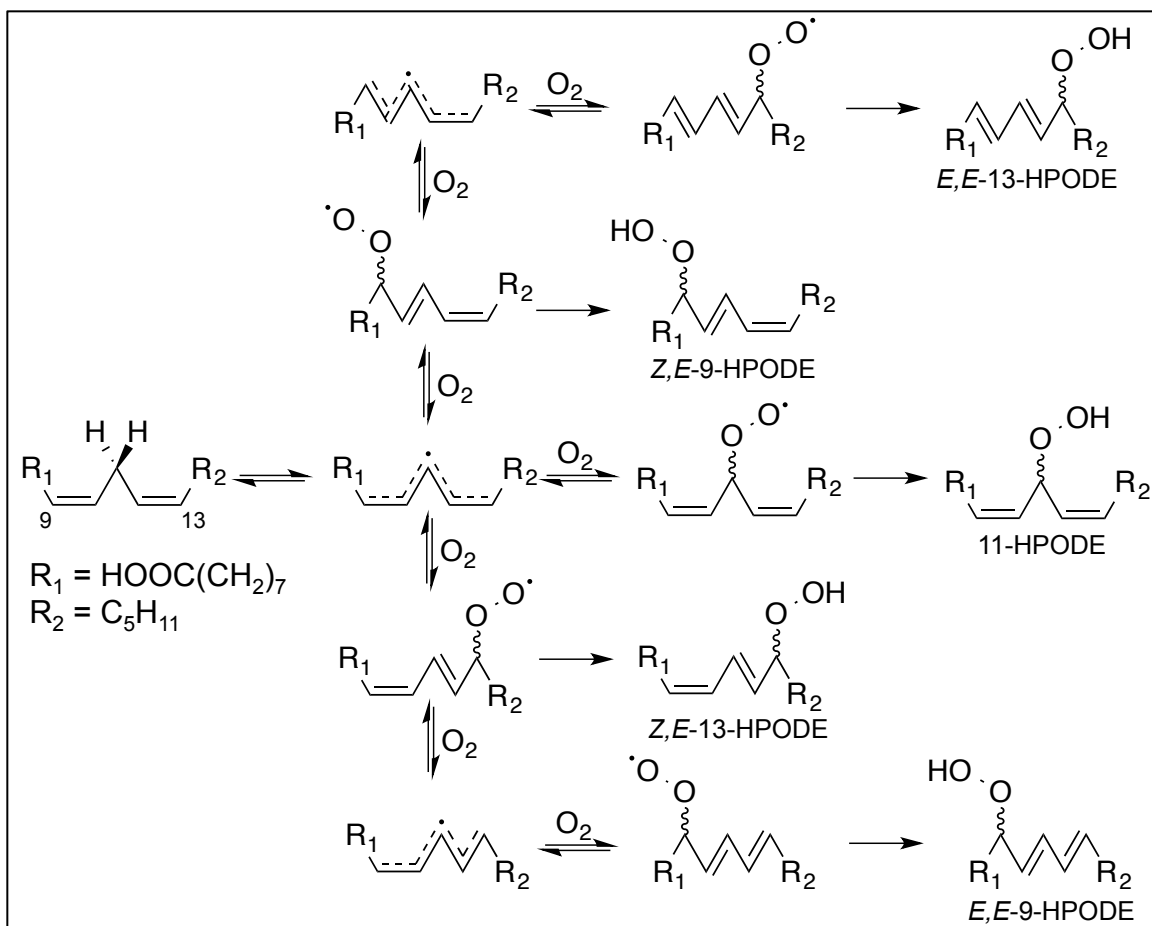


**Figure 2.** Kinetic and thermodynamic autoxidation products of LA. After *bis*-allylic hydrogen abstraction, the pentadienyl radical of LA can react at three different positions, generating three distinct peroxy radicals. The peroxy radicals can be quenched generating HPODE, or they can revert to the pentadienyl radical. The pentadienyl radical can then react with molecular oxygen at any of the three original positions, reforming a peroxy radical. With each reversal of the peroxy radical, double bond isomerization from *cis* to *trans* will occur. If allowed to reverse a sufficient amount of times, *trans* double bonds will form preferentially as they are a lower energy state.

Arachidonic acid (AA), with three *bis*-allylic positions between four *cis* double bonds, yields a much more complex oxidation profile. This includes the hydroperoxy eicosatetraenoic acids (HPETEs), which are structurally similar to HPODEs, as well as many cyclized products, such as the isoprostanes<sup>104</sup>, which are structurally similar to prostaglandins (PGs). As with all PUFAs, hydrogen

abstraction is the initial oxidation event, with oxygen addition possible at the 5-, 8-, 9-, 11-, 12-, and 15-positions<sup>103</sup>. Similar to LA, the addition of oxygen results in geometric isomerization to give one *trans* double bond. However, the rate of cyclization is faster than the rate of reversal, so three *cis* and one *trans* double bond is the abundant geometry of HPETEs<sup>116</sup>. Autoxidation produces a mixture of both positional isomers and enantiomers, while enzymatic oxidation of AA results in a defined product. For example, soybean 15-lipoxygenase-1 oxidizes AA exclusively to *Z,Z,Z,E*-15(*S*)-HPETE<sup>154</sup>. Similar to HPODEs, HPETEs are quickly reduced to the single oxygen product, HETEs, in biological settings.

Further oxidation and/or degradation of PUFA oxidation products can result in a series of electrophilic  $\alpha,\beta$ -unsaturated carbonyls and aldehydes<sup>174, 181, 182</sup>. As discussed in greater detail in Chapter I, these lipid electrophiles can react with nucleophilic groups on biological macromolecules, including DNA<sup>347</sup> and proteins<sup>204</sup>. Many of the adducts formed on DNA have been shown to be highly mutagenic<sup>348</sup>. Protein adducts result in functional alterations that lead to cellular consequences<sup>238, 306</sup>. The exact source and mechanism of lipid electrophile generation is not fully understood. However, it has been shown that lipid electrophiles can be produced non-enzymatically by autoxidation<sup>184</sup> and enzymatically by the cyclooxygenases (COXs)<sup>177</sup> and the lipoxygenases (LOXs)<sup>178</sup>. Inhibition of COX<sup>126</sup> or quenching of mitochondrial superoxide (Chapter III) reduces lipid electrophile formation, providing further evidence that lipid electrophiles are generated by both enzymatic and non-enzymatic processes.

Here we seek to determine the chemistry of LA and AA oxidation during macrophage activation. We characterize the distribution of positional isomers, enantiomers, and geometric isomers for many of the common oxidized products and determine that autoxidation is the major mechanism for esterified PUFA oxidation. Additionally, we use *a*LA and inhibition of COX-1 and COX-2 (via indomethacin and celecoxib), cytosolic phospholipase A<sub>2</sub> (cPLA<sub>2</sub>) (via giripladib), and mitochondrial superoxide (via MitoTEMPO) to determine that both COX-2 activity and mitochondrial superoxide are necessary for lipid electrophile generation.

## **Materials and Methods**

*Materials.* All reagents are from Sigma, St. Louis, MO unless otherwise noted. All native fatty acids and deuterated lipid metabolites are from Cayman Chemical, Ann Arbor, MI unless otherwise noted. Alkynyl linoleic acid (*a*LA) was synthesized as previously described<sup>280</sup>.

*Cell culture conditions.* RAW264.7 macrophages (ATCC, Manassas, VA) were maintained in Dulbecco's Modified Eagle Medium + Glutamax (DMEM) (Life Technologies, Grand Island, NY) supplemented with 10% fetal bovine serum (Atlas Biologicals, Fort Collins, CO) at 37 °C and 5% CO<sub>2</sub>. Macrophages were plated at a density so as to be 50% confluent at the time of harvesting and incubated 24 h at 37 °C. Alkynyl fatty acid incorporation was achieved by adding 15 μM *a*LA to the medium and incubating for 24 h at 37 °C. After incorporation, the medium was aspirated, and the macrophages were washed with serum-free

DMEM to remove any unincorporated aLA. To activate the macrophages, serum-free DMEM with 100 ng/mL KLA (Avanti Polar Lipids, Alabaster, AL) was added to the cells, and the cultures were incubated 24 h at 37 °C. Dulbecco's phosphate buffered saline (DPBS) was added to the vehicle samples. When used, inhibitors (or dimethylsulfoxide vehicle) were added at the same time as KLA. Final inhibitor concentrations were 10 µM MitoTEMPO, 1 µM or 100 nM indomethacin, 5 µM or 500 nM celecoxib , and 10 nM girdipladib.

*Base hydrolysis of fatty acids from phospholipids.* Macrophages were plated, aLA-incorporated, and activated as described above. After activation, the medium was removed, cells scraped into DPBS with 1 mM tris(2-carboxyethyl)phosphine (TCEP) and 1 mM butylated hydroxytoluene (BHT), and counted on a BioRad TC10 automated cell counter. Heptadecanoic acid and 13(S)-HODE-d<sub>4</sub> were added as internal standards. Samples were taken up in 5% HCl and added to a 2:1 mixture of chloroform:methanol containing 50 mg/L BHT. Vials were vortexed, then centrifuged for 10 min at 15,000 rpm. The organic layer was blown dry under a stream of N<sub>2</sub> and dissolved in methanol and 1.0 M KOH. Samples were vortexed and incubated for 1 h at 37 °C. After incubation, samples were immediately cooled on ice. Following acidification with 1.0 M HCl, 50 µL of a mixture of BHT/PPh<sub>3</sub> in ethanol (10 mg/25 mg in 10 mL) was added to each sample. The samples were then extracted with 4:1 chloroform:ethyl acetate. The organic layer was evaporated to dryness under a stream of N<sub>2</sub> and stored at -80 °C until analysis.



*Measurement of esterified, oxidized lipids.* Normal-phase high performance liquid chromatography tandem mass spectrometry (NP-HPLC-MS/MS) analysis was performed using a Waters 2695 autosampler and HPLC pump in conjunction with a Phenomenex Luna Silica column (150 x 4.6 mm, 3  $\mu$ m) eluted at 1.0 mL/min with 98.5:1.4:0.1 hexanes:isopropanol:acetic acid. The effluent of the column was introduced by atmospheric-pressure chemical ionization into a triple quadrupole mass spectrometer (TSQ Quantum, Thermo Finnigan). Metabolites were analyzed in negative ion mode by selected reaction monitoring (SRM) for the following transitions: 13-HODE (295.2 > 195.1), 13(S)-HODE-d<sub>4</sub> (299.2 > 198.1), 9-HODE (295.2 > 171.1), 15-HETE (319.2 > 219.1), 11-HETE (319.2 > 167.1), and 5-HETE (319.2 > 115.1). 13(S)-HODE-d<sub>4</sub> was used as an internal standard for all HODEs and HETEs as previously described (Chapter II)<sup>311</sup>. The transfer capillary was heated to 300 °C, discharge current was set to 22.0 V, and the ion isolation width was set to 1. The collision energy was set at 21 V. Scans were recorded at 0.25 s intervals.

*Chiral analysis of esterified, oxidized lipids.* Macrophages were plated, aLA-incorporated, activated, harvested, and hydrolyzed as described above. Chiral LC-MS/MS was performed by using a Waters 2695 autosampler and HPLC pump in conjunction with a Daicel Chemical Industries Chiralpak AD-H column (250 x 4.6 mm) eluted at 1.0 mL/min with 97:3:0.1 hexanes:ethanol:acetic acid. Source and mass spectrum settings, along with metabolite fragments, were identical to those described above. Standard chiral metabolites were obtained and injected independently to authenticate the cell

sample analysis. These metabolites include: 15(S)-HETE-d<sub>8</sub> (327.2 > 226.1), 11(S)-HETE (319.2 > 167.1), and 5(S)-HETE-d<sub>8</sub> (327.2 > 116.1). Furthermore, the order of elution for *R* and *S* enantiomers of all metabolites was determined by analysis of racemic mixtures of the particular compound. These mixtures were obtained by HPLC purification of solution autoxidations of LA, aLA, AA, and ω-alkynyl-AA (aAA) as previously described (Chapter II)<sup>311</sup>.

*PG analysis of the medium.* Macrophages were plated, aLA-incorporated, and activated as described above. After activation, medium was extracted with two volumes of ethyl acetate containing 0.5% acetic acid and the deuterated internal standard, PGE<sub>2</sub>-d<sub>4</sub>. The organic layer was dried to completion under inert gas and dissolved in methanol for LC-MS/MS analysis. PGs were separated by reversed-phase gradient HPLC on a C<sub>18</sub> (50 x 2.1 mm, 3 μm) column using 0.1% formic acid in water and 0.1% formic acid in acetonitrile as the A and B mobile phases respectively. Metabolites were separated by holding 25% B for 0.5 min, then ramping to 99% B over 2.5 min, holding at 99% B for 3 min, then equilibrating to 25% B for 3 min. PGs were analyzed in negative ion mode by SRM, for the following *m/z* transitions, PGE<sub>2</sub> and PGD<sub>2</sub> (351.2 > 271.2) and PGE<sub>2</sub>-d<sub>4</sub> (355.2 > 275.2) on an ABI/Sciex 3200 QTrap interfaced to a Shimadzu controller, autosampler, and HPLC pumps. PGs were quantified by comparing the analyte area under the curve (AUC) to the deuterated standard AUC, and multiplying by the amount of deuterated internal standard.

*Analysis of protein adduction by alkynyl electrophiles.* After the medium was removed for PG analysis, the cells were scraped and pelleted. Cells were

lysed in 1% IGEPAL (MP Biomedicals), 150 mM NaCl, 50 mM HEPES, and 0.5% mammalian protease inhibitor cocktail. Electrophile adducts were stabilized with 5 mM NaBH<sub>4</sub> for 1 h, and the reduction was quenched with acetone. Samples were diluted to 2 mg/mL total protein and precleared overnight at 4 °C with streptavidin sepharose beads (GE Healthcare) to remove endogenously biotinylated proteins. After preclearing, samples were diluted to 1 mg/mL, and click reagents were added to the following concentrations, 1 mM CuSO<sub>4</sub>, 1 mM TCEP, 0.1 mM tris[(1-benzyl-1H-1,2,3-triazole-4-yl)methyl]amine (TBTA), and 0.2 mM N<sub>3</sub>-biotin. The samples were then turned end over end for 2 h. Proteomes were separated by SDS-PAGE (Bio-Rad), transferred to 0.45 mm nitrocellulose (Bio-Rad), and probed with a goat anti-actin (Santa Cruz) primary antibody and Streptavidin IRDye 800CW (LI-COR) overnight at 4°C. Secondary anti-goat IgG IRDye 680LT antibodies was from LI-COR and incubated with the blots for 1 h at 25 °C. Blots were visualized on a LI-COR Odyssey system scanning at 800 nm emission for streptavidin and 700 nm emission for actin.

*Exogenous PG addition.* RAW264.7 macrophages were plated, aLA-incorporated, and activated with KLA with and without celecoxib or indomethacin as described above. PGs were added 6 h post KLA activation at a 5:1 PGD<sub>2</sub>:PGE<sub>2</sub> ratio, to provide a total of 200 pmol/10<sup>6</sup> macrophages plated, concentrations reflecting those produced by KLA-activated RAW264.7 macrophages<sup>27</sup>. After PG addition, the cells were incubated 18 h longer at 37°C to expose them to KLA-containing medium for 24 h total. PGs in the medium

were analyzed as described above. Protein adduction by alkynyl lipid electrophiles was also analyzed as described above.

*Measurement of esterified, oxidized lipids after inhibitor treatment.*

Macrophages were plated, aLA-incorporated, KLA-activated with and without indomethacin or giripladib, harvested, and phospholipids were base-hydrolyzed as described above. Free fatty acids were separated by reversed-phase gradient HPLC on a C<sub>18</sub> (50 x 2.1 mm, 3 μm) column using 0.1% formic acid in water and 0.1% formic acid in acetonitrile as the A and B mobile phases respectively at a flow rate of 400 μL/min. Metabolites were separated by holding 40% B for 0.5 min, then ramping to 80% B over 9.5 min, then immediately ramping to 99% B, which was held for 5 min. The column was equilibrated to 40% B for 5 min. Metabolites were analyzed in negative ion mode by SRM, for the following *m/z* transitions, 9-HODE (295.2 > 171.1), 9-HODE-d<sub>4</sub> (299.2 > 172.1), 13-HODE (295.2 > 195.1), 13-HODE-d<sub>4</sub> (299.2 > 198.1), 5-HETE (319.2 > 115.1), 5-HETE-d<sub>8</sub> (327.2 > 116.1), 11-HETE (319.2 > 167.1), 15-HETE (319.2 > 219.1), and 15-HETE-d<sub>8</sub> (327.2 > 226.1) on an ABI/Sciex 3200 QTrap interfaced to a Shimadzu controller, autosampler, and HPLC pump. Metabolites were quantified by comparing the analyte AUC to the deuterated standard AUC and multiplying by the amount of deuterated standard. Due to the lack of available deuterated standard, 11-HETE was quantified using 13-HODE-d<sub>4</sub> as previously described (Chapter II)<sup>311</sup>. Metabolite amounts were normalized to the number of cells counted at the time of harvesting.

## Results

*Esterified oxidized products of LA, aLA, AA, and aAA are generated in KLA-activated RAW264.7 macrophages.* Oxidative stress was induced in aLA-incorporated RAW264.7 macrophages by activation with KLA. Lipids were extracted and treated with base to hydrolyze phospholipid-bound fatty acids, and oxidation products were quantified by LC-MS/MS. Figure 3A reveals that both LA and aLA oxidized products were present in the lipid extracts. Oxidation of aLA yielded equal amounts of *Z,E-a13-HODE*, *E,E-a13-HODE*, *Z,E-a9-HODE*, and *E,E-a9-HODE*. Similarly LA oxidation produced an equal mixture of *Z,E-13-HODE*, *E,E-13-HODE*, *Z,E-9-HODE*, and *E,E-9-HODE*. LA oxidized products were approximately 20-fold more abundant, which can be partially, but not completely, explained by a greater abundance of LA relative to aLA in the macrophages (Chapter III).

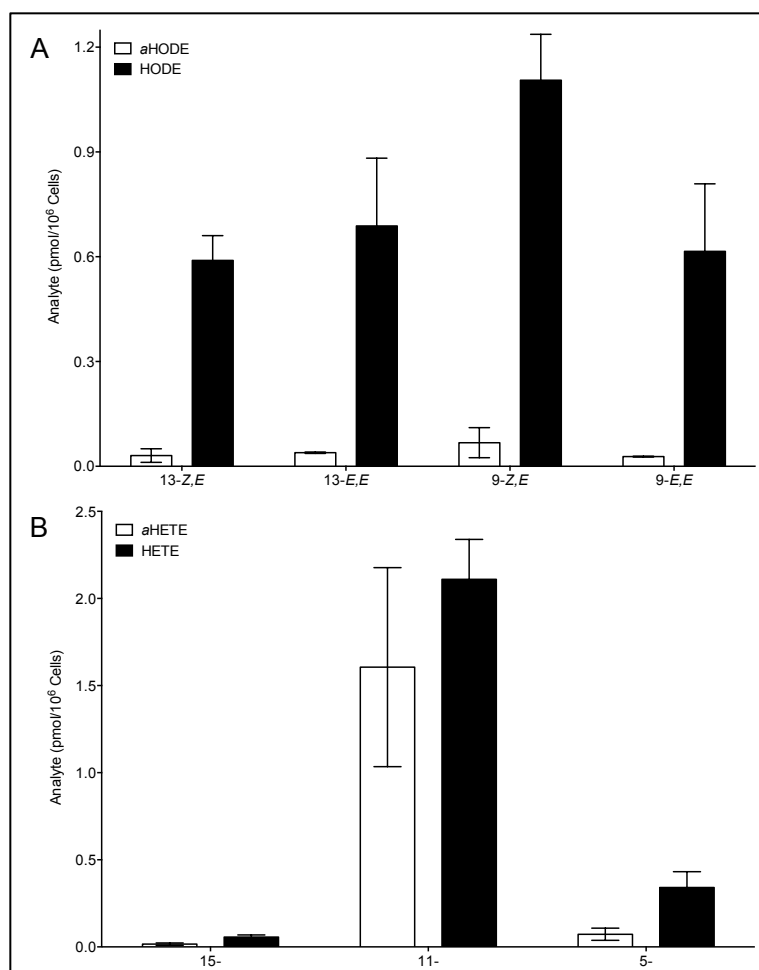


**Figure 3.** Quantification of positional and geometric isomers of esterified hydroxy polyunsaturated fatty acids. A) Alkynyl and native HODEs were quantified after base hydrolysis in *a*LA-incorporated and KLA-activated RAW264.7 macrophages, separating the 9- and 13-positional isomers as well as the *Z,E* and *E,E* geometric isomers for each species. B) Alkynyl and native HETEs were quantified after base hydrolysis in *a*LA-incorporated and KLA-activated RAW264.7 macrophages, separating the 5-, 11-, and 15-positional isomers. Experiment was performed in triplicate, and data represented are mean  $\pm$  standard deviation.

We have previously shown that *a*AA is biosynthesized from *a*LA through desaturation and elongation (Chapter III). Consequently, we also quantified the levels of oxidized *a*AA and AA products in *a*LA-incorporated RAW264.7 macrophages. Unlike with LA and *a*LA, the AA and *a*AA oxidized products were of a similar quantity (Figure 3B), which correlates with a similar level of incorporation between AA and *a*AA (Chapter III). The most abundant products

were 11-HETE and *a*11-HETE, respectively. Additionally, 15-HETE, *a*15-HETE, 5-HETE, and *a*5-HETE were detected.

**Table 1.** *R/S* ratios for esterified hydroxy polyunsaturated fatty acids. Chiral chromatography was used to determine the *R/S* ratio for each hydroxy fatty acid that was abundant enough to be detected. It was determined that 9-HODE, 13-HODE, 15-HETE, *a*5-HETE, and 5-HETE are all formed by autoxidation because they have *R/S* ratios approaching 1. 11-HETE and *a*11-HETE were both formed by an enzymatic process because they are exclusively the *R* enantiomer, which is the COX-2 metabolism product.

Analyte	<i>R/S</i>
9-HODE	1.7
13-HODE	0.9
15-HETE	0.3
11-HETE	<i>R</i> only
<i>a</i> 11-HETE	<i>R</i> only
<i>a</i> 5-HETE	0.8
5-HETE	1.4

*11-HETE and a11-HETE are the sole enzymatically generated esterified oxidized lipid products.* The enantiomeric composition of the oxidized lipid products was determined to evaluate if they were formed from an enzymatic or non-enzymatic process. The *a*HODEs and *a*15-HETE were not abundant enough to determine enantiomeric purity. Table 1 shows the *R/S* ratios for the products measured. The LA-derived products 9-HODE and 13-HODE both had *R/S* ratios near 1, indicating their origin as autoxidation products. Representative profiles of 9-HODE and 13-HODE enantiomeric standards as well as cell extracts can be seen in Figure 4. Similarly, the AA-derived products 15-HETE and 5-HETE, as well as the *a*AA-derived product *a*5-HETE exhibited *R/S* ratios near 1, indicating an autoxidation-dependent origin. Figures 5 and 6 show representative profiles of

chiral standards and cell extracts of AA and *a*AA oxidized products. The only products that appear to be enzymatically formed are 11-HETE and *a*11-HETE, both present exclusively as the *R* enantiomer. Notably, 11(*R*)-HETE is a known product of the COX-2-dependent oxidation of AA (Chapter II)<sup>311</sup>.

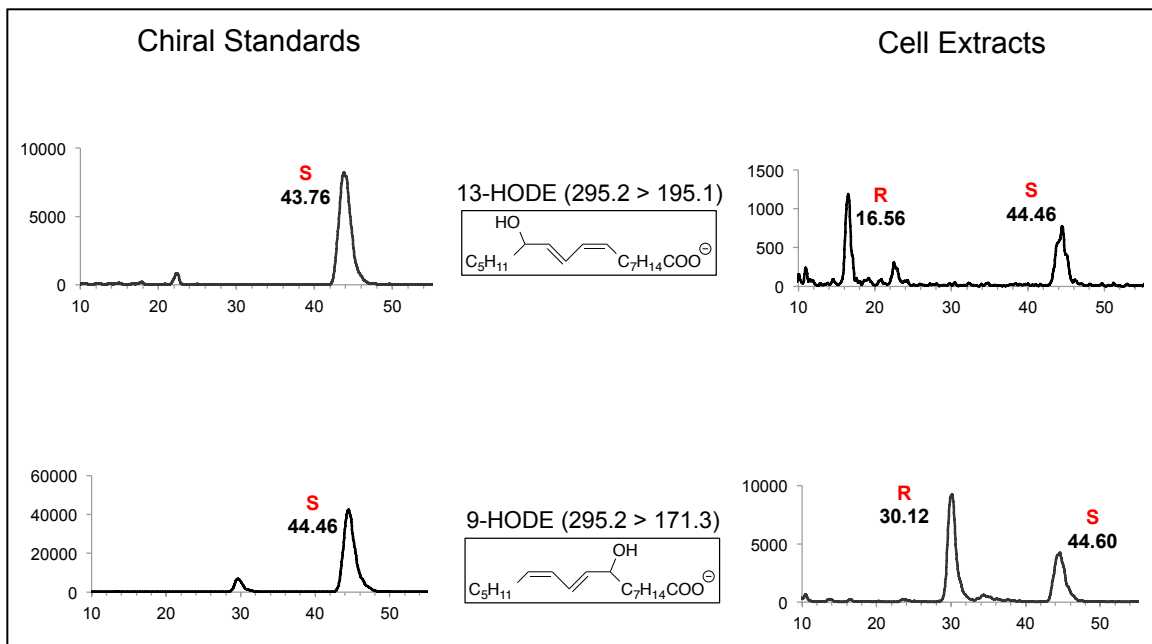


**Figure 4.** Chiral standards and cell extracts of LA oxidation products. Both 9-HODE and 13-HODE were determined to have *R/S* ratios near 1, indicating an autoxidation mechanism of formation.



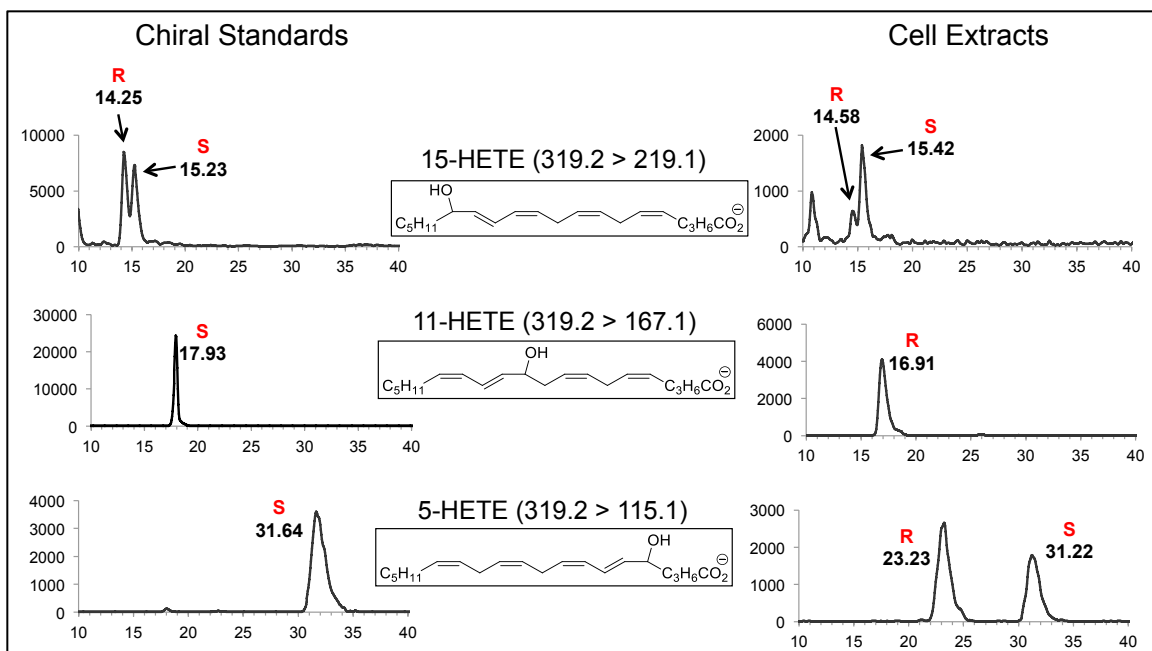


**Figure 5.** Chiral standards and cell extracts of AA oxidation products. Both 15-HETE and 5-HETE were determined to have *R/S* ratios near 1, indicating an autoxidation mechanism of formation. 11-HETE was exclusively detected as the *R* enantiomer, the COX-2 product, indicating an enzymatic mechanism of formation.

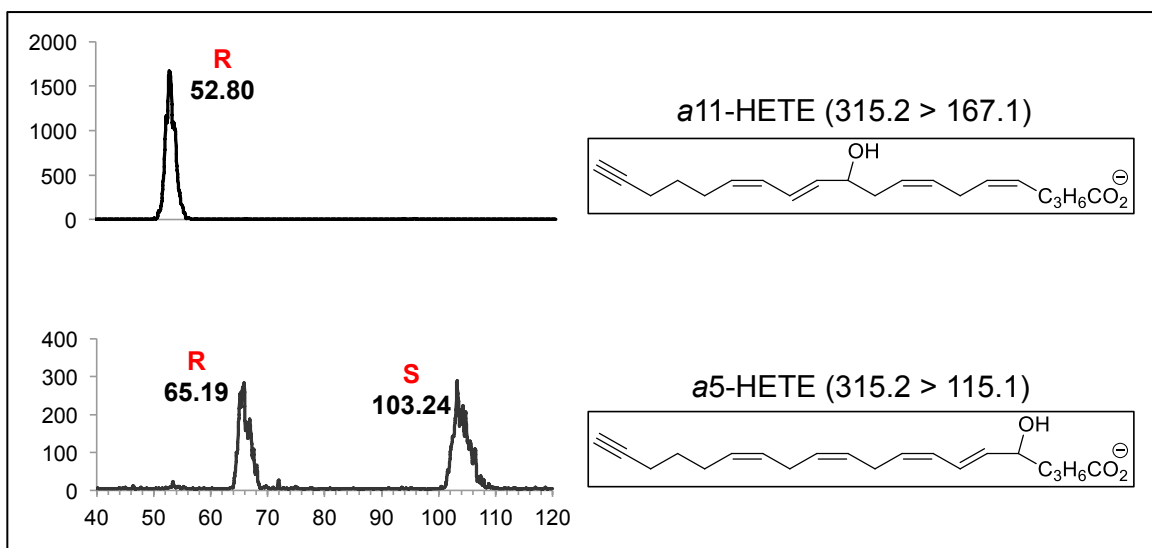


**Figure 6.** Chiral analysis of abundant  $\omega$ -alkynyl fatty acid metabolites. Only a11-HETE and a5-HETE were abundant enough to determine optical purity. a11-HETE was exclusively of the *R* enantiomer, while a5-HETE was a mixture of *R* and *S* enantiomers, indicating enzymatic and autoxidation mechanisms of formation.

*MitoTEMPO modulates lipid electrophile protein adduction, but not PG biosynthesis.* Previous reports have implicated COX-2-mediated AA metabolism in the formation of lipid electrophiles<sup>126, 177, 178</sup>. Data presented in Chapter III and Figure 7A show that MitoTEMPO, a scavenger of mitochondrial superoxide, reduces lipid electrophile adduction of proteins in both unactivated and activated RAW264.7 macrophages. However, as shown in in Figure 7B, MitoTEMPO does not modulate PG synthesis in KLA-activated macrophages. These results suggest that the MitoTEMPO-inhibitable lipid electrophile protein adduction is not COX-2-dependent.

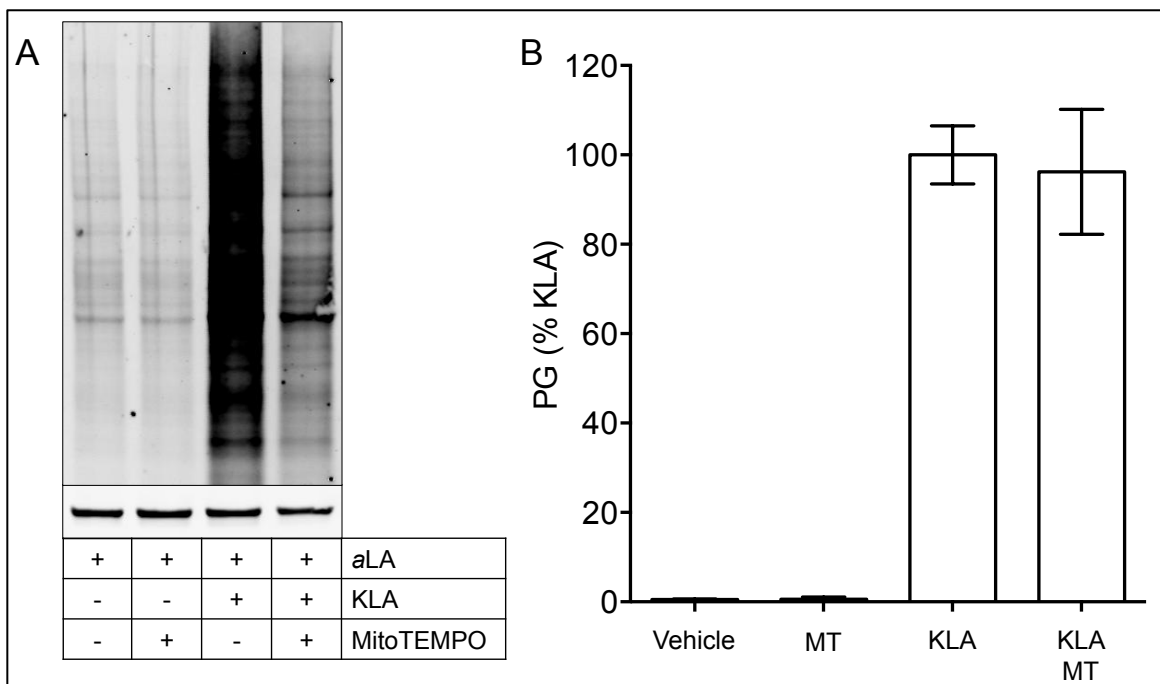


**Figure 7.** Click blot and PG analysis for MitoTEMPO treated macrophages. RAW264.7 macrophages were preincubated in the presence of KLA and/or MitoTEMPO as indicated and described in Materials and Methods. Following the treatment, macrophages were harvested and A) analyzed for protein adduction by click blot and B) the medium was analyzed for PGs by LC-MS/MS. MitoTEMPO treatment reduces protein adduction in activated macrophages, but does not affect PG levels. PG experiment was performed in triplicate, and data represented are mean  $\pm$  standard deviation.

*Indomethacin inhibits PG formation and lipid electrophile protein adduction.* To further explore the role of COX-2 in lipid electrophile generation, we examined protein adduction levels in KLA-activated macrophages treated with or without the COX-1 and COX-2 inhibitor, indomethacin. Figure 8A shows that indomethacin inhibits lipid electrophile adduction to basal levels at a concentration that also completely inhibits PG production (Figure 8B). These data are consistent with a previous report that indomethacin-mediated inhibition of COX-2 eliminated lipid electrophile generation<sup>126</sup> and suggest that COX-2-dependent oxygenation of AA is a direct source of lipid electrophiles that form protein adducts in KLA-activated RAW264.7 macrophages.

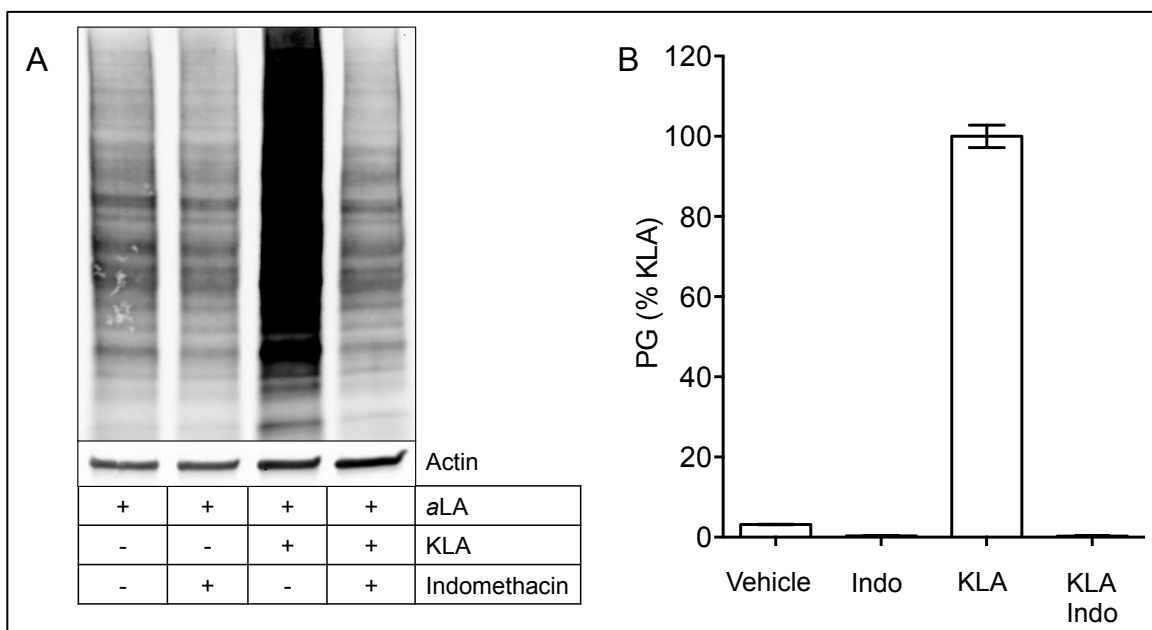


**Figure 8.** Click blot and PG analysis for indomethacin treated macrophages. RAW264.7 macrophages were preincubated in the presence of KLA and/or indomethacin as indicated and described in Materials and Methods. Following the treatment, macrophages were harvested and A) analyzed for protein adduction by click blot and B) the medium was analyzed for PGs by LC-MS/MS. Indomethacin treatment reduces both protein adduction and PG levels in activated macrophages. PG experiment was performed in triplicate, and data represented are mean  $\pm$  standard deviation.

*Celecoxib inhibits PG and lipid electrophile adduction similarly to indomethacin.* An alternative explanation of the effects of indomethacin on protein adduction is that indomethacin inhibits lipid electrophile formation secondarily by reducing inflammatory signaling or through off-target effects such as the modulation of peroxisome proliferator-activated receptor gamma signaling<sup>349</sup>. To test this hypothesis, protein adduction was determined in the presence of a lower concentration of indomethacin, and also in the presence of two concentrations of celecoxib, a COX-2 inhibitor that is structurally distinct from indomethacin. Figure 9 shows that both indomethacin and celecoxib inhibited PG formation (Figure 9B) at all concentrations tested, and both of the inhibitors completely suppressed lipid electrophile adduction of proteins (Figure 9A). These data, in combination with the MitoTEMPO data, suggest that although COX-2-dependent metabolism of AA is not the direct source of lipid electrophiles, inflammatory signaling molecules generated by COX-2 play a role in stimulating mitochondrial ROS production and thus, lipid electrophile generation.

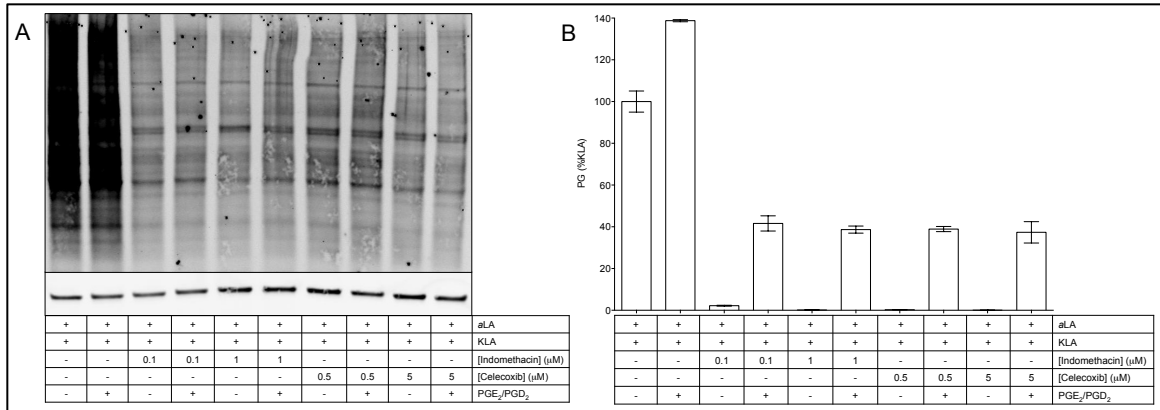


**Figure 9.** Click blot and PG analysis for COX-inhibited macrophages with and without PG supplementation. RAW264.7 macrophages were preincubated in the presence of KLA and/or two concentrations of indomethacin or celecoxib as indicated and described in Materials and Methods. PGs were and were not supplemented into the medium. Following the treatment, macrophages were harvested and A) analyzed for protein adduction by click blot and B) the medium was analyzed for PGs by LC-MS/MS. Both COX inhibitors at both concentrations inhibited protein adduction by lipid electrophiles. PG supplementation had not effect on protein adduction by lipid electrophiles. Both COX inhibitors at both concentrations inhibited PG formation. PG supplementation was measured as increased PG levels in the medium. PG experiment was performed in triplicate, and data represented are mean  $\pm$  standard deviation.

*Exogenously added PGs do not induce lipid electrophile adduction of proteins.* PGs are known to be potent signaling molecules, able to contribute to proinflammatory processes<sup>350, 351</sup>. To test if PG signaling is required for the generation of lipid electrophiles, we treated indomethacin- and celecoxib-inhibited, KLA-activated macrophages with exogenous PGE<sub>2</sub>/PGD<sub>2</sub> at ratios and amounts similar to what is generated in activated macrophages<sup>27</sup>. The presence of the exogenously added PGs was confirmed by LC-MS/MS analysis of the culture medium of the treated cells (Figure 9B); however, exogenous PG addition did not return lipid electrophile-mediated protein adduction in indomethacin- or celecoxib-treated cells to levels observed in cells not treated with indomethacin or celecoxib (Figure 9A), indicating that prostaglandin signaling is not triggering mitochondrial ROS formation.

*Giripladib inhibits PG formation, but not lipid electrophile protein adduction.* To further parse the role of COX-2-dependent metabolism in lipid electrophile generation, we used a cPLA<sub>2</sub> inhibitor, giripladib. Giripladib inhibits the release of AA from membrane phospholipids and subsequent PG formation, but does not directly inhibit COX-2 activity (Mitchener manuscript in review). Figure 10A shows that giripladib does not inhibit lipid electrophile protein adduction in KLA-activated RAW264.7 macrophages. However, giripladib does inhibit PG production (Figure 10B). These data further support the conclusion that COX-2-dependent metabolism of AA is not the source for lipid electrophile generation in activated macrophages.

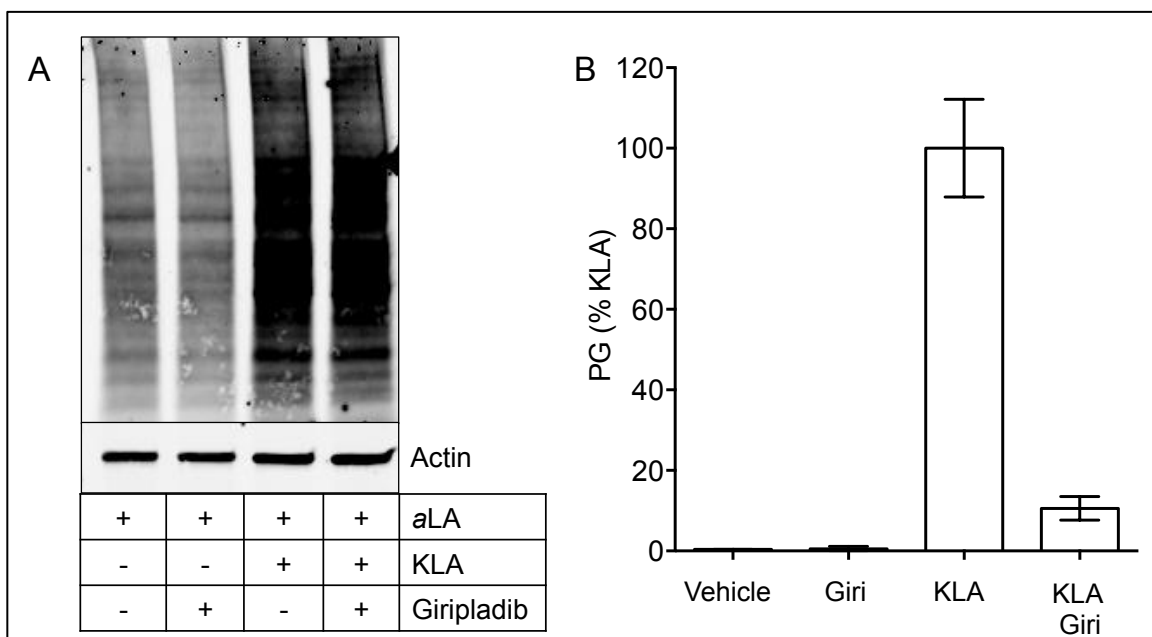


**Figure 10.** Click blot and PG analysis for giripladib treated macrophages. RAW264.7 macrophages were preincubated in the presence of KLA and/or giripladib as indicated and described in Materials and Methods. Following the treatment, cells were harvested and A) analyzed for protein adduction by click blot and B) the medium was analyzed for PGs by LC-MS/MS. Giripladib does not affect protein adduction levels in activated macrophages, but reduces PG levels. PG experiment was performed in triplicate, and data represented are mean  $\pm$  standard deviation.

*Indomethacin inhibits formation of esterified oxidized fatty acid products.*

Since the data did not support a relationship between free PG levels and lipid electrophile adduction of proteins, we investigated the effects of the inhibitors of enzymatic AA metabolism on the levels of esterified oxidized lipids. Indomethacin completely inhibited KLA-induced formation of 9-HODE and 13-HODE from LA (Figure 11A and 11B) as well as 15-HETE and 11-HETE from AA (Figure 12A and 12B), but it had no effect on 5-HETE formation (Figure 12C). This inhibition of esterified lipid oxidation correlates with the decreases in lipid electrophile adduction seen with indomethacin treatment. These data indicate that COX-2 inhibition results in a more general reduction of lipid oxidation, leading to a reduction in formation of products, such as the HODEs, that are not direct products of COX-2. Therefore, the reduction of lipid electrophile adduction that results from COX-2 inhibition appears to result from a general suppression of inflammatory signaling rather than a direct effect on COX-2-mediated PUFA oxidation.

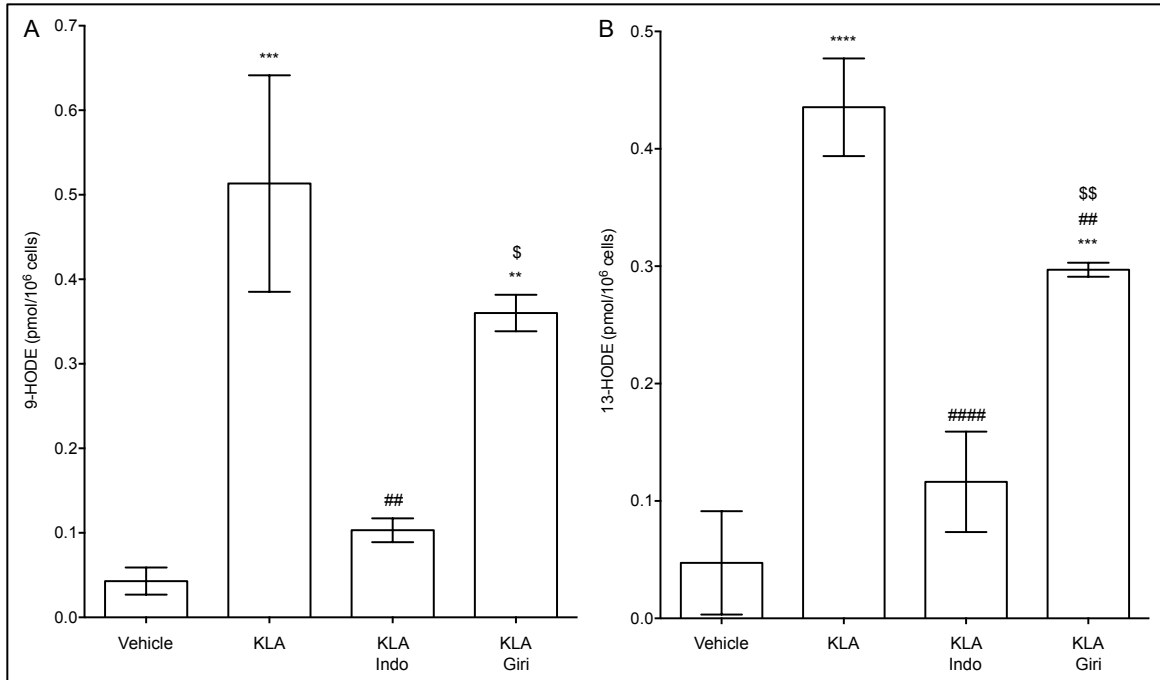


**Figure 11.** Quantification of esterified HODEs in indomethacin and giripladib treated macrophages. Esterified A) 9-HODE and B) 13-HODE was quantified after base hydrolysis by LC-MS/MS in activated and unactivated RAW264.7 macrophages treated with or without indomethacin or giripladib. Indomethacin treatment reduced both HODEs to basal levels, while giripladib saw a small reduction, but not a return to basal levels. Experiment was performed in triplicate, and data represented are mean  $\pm$  standard deviation. Statistical significance compared to Vehicle (\*), compared to KLA (#), or compared to KLA Indo (\$) was determined by Two-way ANOVA with Tukey *post hoc* analysis where \* =  $P < 0.05$ , \*\* =  $P < 0.01$ , \*\*\* =  $P < 0.001$ , and \*\*\*\* =  $P < 0.0001$ . Absence of a symbol indicates  $P > 0.05$ .



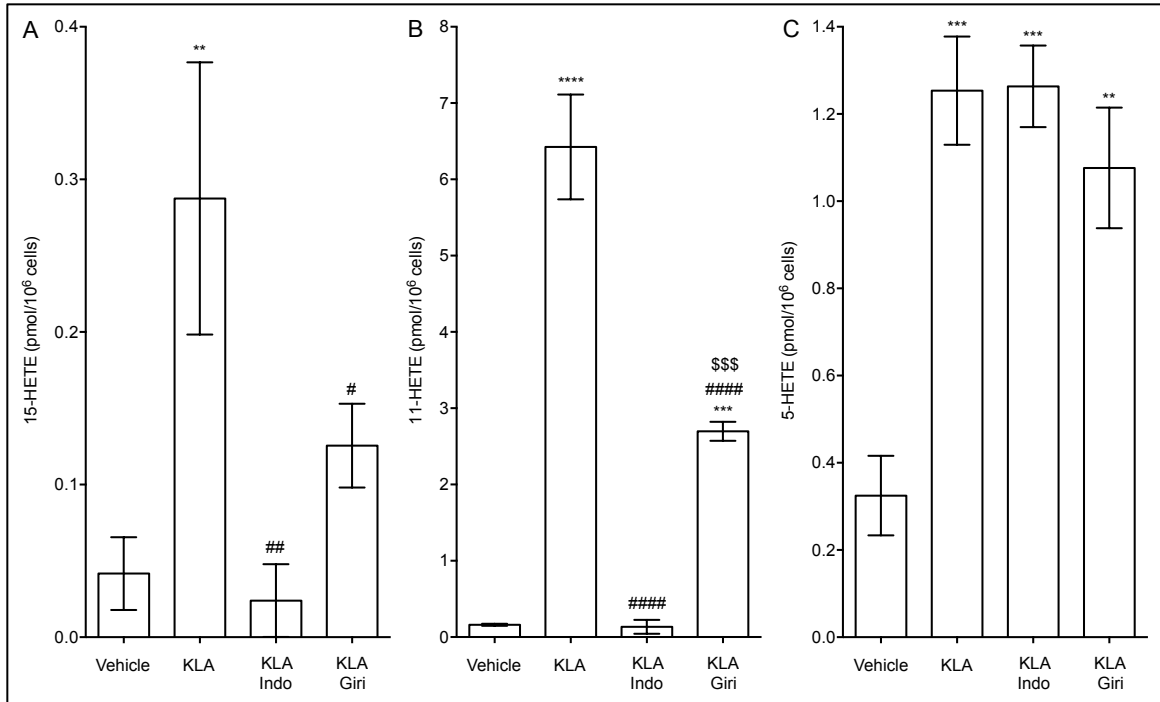


**Figure 12.** Quantification of esterified HETEs in indomethacin and girepladib treated macrophages. Esterified (A) 15-HETE, (B) 11-HETE, and (C) 5-HETE was quantified after base hydrolysis in activated and unactivated RAW264.7 macrophages treated with and without indomethacin or girepladib. Indomethacin treatment reduced both 15-HETE and 11-HETE to basal levels, but did not change 5-HETE levels. Girepladib reduced 15-HETE levels, reduced 11-HETE, but not to basal levels, and did not change 5-HETE levels. Experiment was performed in triplicate, and data represented are mean  $\pm$  standard deviation. Statistical significance compared to Vehicle (\*), compared to KLA (#), or compared to KLA Indo (\$) was determined by Two-way ANOVA with Tukey *post hoc* analysis where \* =  $P < 0.05$ , \*\* =  $P < 0.01$ , \*\*\* =  $P < 0.001$ , and \*\*\*\* =  $P < 0.0001$ . Absence of a symbol indicates  $P > 0.05$ .

*Girepladib does not inhibit esterified oxidized fatty acid products formation.*

Exposure to girepladib reduced oxidized LA products in the lipid bilayer of KLA-activated RAW264.7 macrophages (Figures 11A and 11B), but the levels were significantly higher than those measured in cells not exposed to KLA or cells exposed to KLA in the presence of indomethacin. The effects of girepladib on 11-HETE and 15-HETE formation were similar to its effects on HODE formation (Figure 12A and 12B), although in the case of 15-HETE, the data did not reach

statistical significance. Alternatively, as in the case of indomethacin, giripladib had no effect on 5-HETE generation (Figure 12C).

## Discussion

PUFA oxidation results in a plethora of oxidized lipid products. This mixture, while complex, can also tell much about the chemistry of oxidation. Therefore, we set out to define the chemistry of oxidation of esterified LA and AA during KLA-mediated activation of macrophages and to relate this chemistry to protein adduction by lipid electrophiles. We measured equal amounts of the LA oxidation products *Z,E*-13-HODE, *E,E*-13-HODE, *Z,E*-9-HODE, and *E,E*-9-HODE, as well as the aLA oxidation products *Z,E-a*13-HODE, *E,E-a*13-HODE, *Z,E-a*9-HODE, and *E,E-a*9-HODE in the phospholipids of KLA-activated macrophages. Equal formation of these isomers indicates that the HODEs and aHODEs were generated by autoxidation in a microenvironment with good hydrogen donating capacity<sup>109</sup>. Enantiomeric purity assessment for both 9-HODE and 13-HODE indicated equal mixtures of the *R* and *S* enantiomers, further confirming that they are generated by an autoxidation mechanism. A previous study has shown that lipid electrophiles can be produced non-enzymatically from LA by intermolecular peroxidation reactions in phospholipid pools<sup>184</sup>. Our data showing autoxidation products of esterified LA implicates this fatty acid as a potential source of lipid electrophiles.

The major esterified AA products measured were 5-HETE, 11-HETE, and 15-HETE. Since the formation of HETEs is not accompanied by the generation of

multiple double bond configurations, enantiomeric purity is the only way to assess if their origin is by enzymatic oxidation or autoxidation. Both 5- and 15-HETE were generated by autoxidation, as determined by the presence of equal amounts of the *R* and *S* enantiomers in KLA-activated macrophage phospholipids. In contrast, 11-HETE was present solely as the *R* enantiomer, indicating an enzymatic pathway of generation, and consistent with reports showing that 11(*R*)-HETE is a byproduct of COX-2-dependent AA oxygenation (Chapter II)<sup>311</sup>. Lipid electrophiles generated from 5-HETE have been detected esterified in the lipid bilayer<sup>190</sup>. Additionally, 15-HETE has been shown to be a source of lipid electrophiles, although these studies have focused on enzymatically generated 15-HETE<sup>175, 177</sup>. 11-HETE has also been extensively studied as a source of endogenously generated lipid electrophiles<sup>305, 306</sup>.

The profound effect of MitoTEMPO treatment on lipid electrophile adduction of proteins seen in Chapter III suggests that the electrophiles are produced via non-enzymatic lipid peroxidation involving mitochondrial superoxide. Here we confirmed those earlier results and also showed that MitoTEMPO does not inhibit COX-2 activity. This was an important finding, as previous studies have implicated COX-2-dependent AA oxygenation as a major source of lipid electrophiles in activated macrophages<sup>126, 177, 178</sup>. The suppression of lipid electrophile-mediated protein adduction in the absence of an effect on PG formation suggests that the relevant lipid electrophiles are not derived from the COX-2 pathway in KLA-activated RAW264.7 macrophages.

Having demonstrated MitoTEMPO's ability to completely suppress lipid electrophile protein adduction in the presence of normal PG synthesis, the finding that the COX-2 inhibitors indomethacin and celecoxib eliminated protein adduction appears contradictory, although as noted above, it is consistent with previous reports<sup>126, 177, 178</sup>. Adding to the complexity of these results was our finding that the cPLA<sub>2</sub> inhibitor girdipladib could completely eliminate PG biosynthesis while having no effect at all on lipid electrophile protein adduction. Together, the results suggest that COX-2 activity is required for lipid electrophile generation, but the PG products of the COX-2 pathway are not. This hypothesis was further tested in KLA-activated macrophages that had been treated with either indomethacin or celecoxib, and then supplemented with exogenous PGs to induce signaling. The presence of the exogenously added PGs was confirmed by LC-MS/MS, but PG supplementation was unable to reverse the suppressive effects of COX-2 inhibition on lipid electrophile adduction of proteins, thereby confirming that PG-dependent signaling is not required to stimulate mitochondrial superoxide production or lipid electrophile generation.

The suppression of lipid electrophile protein adduction by COX-2 inhibition led to the hypothesis that COX-2 activity is required for non-enzymatic lipid peroxidation to occur. We tested this hypothesis by exploring the effects of COX-2 and cPLA<sub>2</sub> inhibitors on the levels of oxidized lipids in the membrane phospholipids of KLA-activated macrophages. Indomethacin treatment eliminated the formation of esterified HODEs, 11-HETE, and 15-HETE, which is consistent with its complete elimination of protein adduction by lipid electrophiles. In

contrast, giropladib treatment only partially suppressed the generation, of these products, in agreement with its inability to block protein adduction by lipid electrophiles. Based on these findings, we hypothesize that COX-2 inhibition reduces lipid electrophile formation by reducing inflammatory signaling and thus reducing autoxidation products. Additionally, these findings indicate that esterified HODEs, 11-HETE, and 15-HETE are potential sources of lipid electrophiles because their generation levels correlate with the trends seen for protein adduction by lipid electrophiles (Table 2). In contrast, esterified 5-HETE levels were not affected by any of the inhibitors tested. This would suggest that 5-HETE is likely not a precursor of the relevant lipid electrophiles because its esterified levels do not correlate to the measured adduction levels (Table 2). An alternative explanation is that reactive intermediates to lipid electrophile generation may not be present in sufficient quantity to be measured 24 h post KLA-activation as we have previously seen that the majority of protein adduction by lipid electrophiles is occurring by 12 h post KLA-activation (Chapter III). Therefore, these oxidized lipid species that persist to 24 h post KLA-activation may be stable and not sources of lipid electrophiles. If this proves to be the case, quantifying esterified oxidized lipids is still a useful diagnostic indicator of whether autoxidation or enzymatic oxidation is the dominant mechanism of lipid oxidation.

**Table 2.** Comparison of protein adduction and esterified HODEs and HETEs in macrophages with indomethacin and giripladib treatment. Indomethacin inhibited protein adduction, 9-HODE, 13-HODE, 11-HETE, and 15-HETE formation, but not 5-HETE formation. Giripladib did not inhibit the formation of any oxidized PUFAs.

	Protein Adduction	9-HODE	13-HODE	5-HETE	11-HETE	15-HETE
Indomethacin	X	X	X	✓	X	X
Giripladib	✓	✓	✓	✓	✓	✓

The effects of indomethacin and giripladib on phospholipid-bound 11-HETE and 15-HETE generation are similar to their effects on the phospholipid-bound HODEs. This is particularly interesting in the case of 11-HETE, because unlike 15-HETE or the HODEs, our data indicate that 11-HETE is enzymatically derived. The origin of the phospholipid-bound 11(*R*)-HETE is of some interest. The generation of 11(*R*)-HETE by COX-2 from free AA is known, but if this is the relevant pathway, one must assume that AA is first released by cPLA<sub>2</sub>, then metabolized by COX-2 to 11(*R*)-HETE, which must subsequently be reincorporated into the membrane phospholipid. Consistent with this proposed pathway, indomethacin treatment completely inhibited 11(*R*)-HETE formation, but inconsistently, giripladib treatment did not. Our laboratory has previously reported that AA release is reduced by 94% with giripladib treatment of KLA-activated RAW264.7 macrophages (Mitchener manuscript under review). Here, we see that PG levels are reduced to a similar extent (90%), but that esterified 11-HETE is only reduced by 50%. These data suggest an alternative mechanism by which 11-HETE is generated since the amount of 11-HETE formed as a byproduct of

PG synthesis from free AA should change to a similar degree as AA release and PG synthesis. It has been shown that COX-1 does not metabolize phospholipid-bound AA<sup>352</sup>, but similar data have not been reported for COX-2. Our laboratory has demonstrated that COX-1 and COX-2 have very different affinities for esterified AA as a substrate<sup>353</sup>. Therefore, it is not impossible that COX-2 is generating 11(*R*)-HETE by metabolizing phospholipid-bound AA, which would circumvent the effects of giripladib on AA release. If COX-2-dependent oxygenation of phospholipid-bound AA occurs, we hypothesize that the efficiency of the cyclization events required for PG formation would be reduced due to the bulky group esterified to AA. This change in efficiency has been seen to skew the metabolite profile toward 11-HETE generation in the case of other bulky AA analogs (Chapter II)<sup>300, 311, 353</sup>. An alternative pathway to phospholipid-bound 11(*R*)-HETE, is through COX-2-dependent metabolism of 2-arachidonoylglycerol (2-AG), which generates an equal mixture of PG glyceryl ester and 11(*R*)-HETE glyceryl ester (11(*R*)-HETE-G)<sup>353</sup> and is increased in giripladib-treated RAW264.7 macrophages (Mitchener manuscript under review). Subsequent hydrolysis of the 11(*R*)-HETE-G by lysophospholipase A<sub>2</sub><sup>354</sup> followed by esterification into phospholipid or direct incorporation of 11(*R*)-HETE-G into phospholipid would complete the pathway.

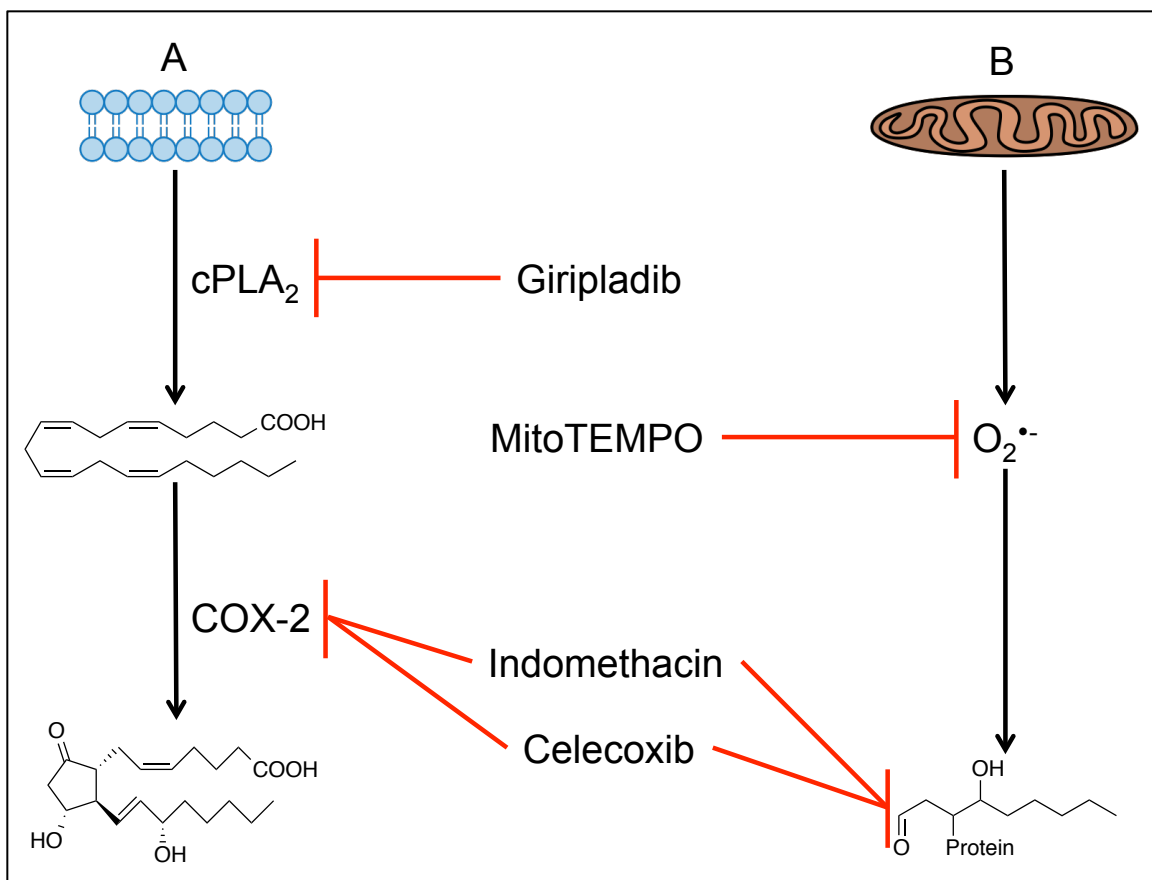


**Figure 13.** Inhibitor effects on PG synthesis and protein adduction by lipid electrophiles in macrophages. A) Arachidonic acid is released from the lipid bilayer by cPLA<sub>2</sub>, and then converted to PGs by COX-2. Giripladib, indomethacin, and celecoxib all inhibited PG synthesis by inhibiting a step in this pathway. Giripladib inhibits cPLA<sub>2</sub>, depriving COX-2 of its preferred substrate; AA, while indomethacin and celecoxib both inhibit COX-2 directly. MitoTEMPO did not inhibit PG synthesis. B) Mitochondrial superoxide is necessary for the generation of protein adducts by lipid electrophiles. MitoTEMPO, indomethacin, and celecoxib all inhibited the formation of lipid electrophiles. MitoTEMPO scavenges mitochondrial superoxide, while the mechanism of lipid electrophile inhibition by indomethacin and celecoxib is currently unknown. Giripladib did not affect protein adduction by lipid electrophiles. These findings lead to the conclusion that both COX-2 activity, but not PG synthesis, and mitochondrial superoxide are necessary to generate lipid electrophiles.

The data in these inhibitor studies have inspired some interesting conclusions, which are illustrated in Figure 13. First, scavenging of mitochondrial superoxide greatly reduces lipid electrophile formation, indicating that mitochondrial superoxide is necessary for the generation of lipid electrophiles in KLA-activated RAW264.7 macrophages. The phospholipid bilayer of KLA-



activated RAW264.7 macrophages contains many oxidized PUFAs, which are generated both non-enzymatically by autoxidation and enzymatically, based on the identity and enantiomeric purity of the products. Second, inhibition of COX-2 activity abolishes generation of most of these oxidized lipid species as well as protein adduction. However, the PG products of the COX-2 pathway do not appear to be directly or indirectly involved in lipid electrophile generation. Although AA is its major substrate, COX-2, is also capable of metabolizing many other fatty acid analogs. For example, the COX-2-dependent oxygenation of the endocannabinoids 2-AG and arachidonylethanolamine yields PG-like molecules with as yet undiscovered roles in cell signaling<sup>127</sup>. Further work will be required to determine if products such as these play a role in the induction of mitochondrial superoxide that leads to lipid electrophile generation and ultimately, protein adduction.

### **Future Directions**

This project is not complete, and a few experiments are still necessary. First, the effect of MitoTEMPO on esterified HETE and HODE levels must be determined. We also plan to look for esterified electrophiles, specifically, the products of additional oxidation of HODEs and HETEs to ketones, since it has been reported that these oxo fatty acids can be esterified. After that we will try a few more targeted add back experiments. The target substances that we would be most likely to try are PG-glycerol esters, 11-HETE, and 11-HETE-G.

## Chapter V

### SUMMARY/FUTURE VISIONS

#### Summary

As discussed in detail in Chapter I, inflammatory signaling generates many potent signaling molecules. One particularly abundant class of molecules generated during inflammation are oxidized polyunsaturated fatty acids (PUFAs)<sup>104</sup>. PUFA oxidation can occur through both autoxidation<sup>104</sup> and enzymatic oxidation mechanisms, for example by the cyclooxygenases (COX)<sup>122</sup> and lipoxygenases (LOX)<sup>160</sup>. The products formed are very diverse and can range from single oxygen insertions to multiple molecules of oxygen inserted. Cyclization events can also occur through both endoperoxide formation as well as carbon-carbon bond formation. These reactions create multiple chiral centers generating numerous enantiomers. These isobaric species, while virtually indistinguishable by most analytical techniques, can have vastly different signaling capabilities<sup>104</sup>.

Further oxidation and degradation of these oxidized PUFAs has been shown to generate a series of  $\alpha,\beta$ -unsaturated carbonyls and aldehydes<sup>203</sup>. These lipid metabolites are electrophilic, and react with nucleophilic groups on biological macromolecules. Of particular interest to us are the reactions between these lipid electrophiles and the nucleophilic amino acid side chains in cellular proteins, cysteine, histidine, lysine, and arginine<sup>205</sup>. Much work has been done to

study the generation of lipid electrophiles, the protein targets of lipid electrophiles, and the cellular consequences resulting from protein adduction by lipid electrophiles. Most of the studies profiling proteins adducted by lipid electrophiles have not been able to account for all key aspects of lipid electrophile generation: 1.) Lipid electrophiles are not generated at a discrete time points or 2.) at a single concentration because lipid electrophiles are in a constant state of flux during cellular metabolism and signaling. 3.) Lipid electrophiles are generated inside of the cell, not outside of it, and in distinct cellular locations as a result of organelle microenvironment factors. 4.) A diverse array of electrophiles are generated.

To address many of these shortcomings, we generated a series of  $\omega$ -alkynyl PUFAs, including  $\omega$ -alkynyl linoleic acid (*a*LA) and  $\omega$ -alkynyl arachidonic acid (*a*AA). We tested the chemistry of oxidation of both *a*LA and *a*AA, and determined that their chemistry of oxidation is indistinguishable from the native counterparts when autoxidation is the method of oxidation (Chapter II)<sup>311</sup>. The similarity in autoxidation chemistry is important for future studies with *a*PUFAs because we have evidence that lipid electrophile generation is generated by an autoxidation mechanism.

Enzymatic metabolism displayed some differences between the *a*PUFAs and native PUFAs. When LOXs are the oxidizing enzyme, the *a*PUFAs have slightly decreased kinetic parameters of oxidation when compared to the native PUFAs, but result in the same metabolic profile, and are oxidized to completion. COXs did not oxidize *a*LA, and oxidized *a*AA to a metabolic profile different from

AA. We identified the major COX-2 *a*AA metabolites and proposed a mechanism that they result from incomplete prostaglandin synthesis, a pathway previously discovered by COX-2 mutagenesis<sup>139</sup>. Interestingly this resulted in a large decrease discrepancy in kinetic values when prostaglandins (PG) were compared to *a*PG. However, when kinetic parameters were determined by O<sub>2</sub> consumption, *a*AA and AA appeared to be metabolized with similar efficiencies. We hypothesized that the alkyne is introducing just enough structural instability to reduce the kinetic parameters for LOXs and change the metabolite profile for COXs. Showing that *a*PUFA metabolism is not an *in vitro* phenomenon, we were able to detect and quantify *a*AA COX-2 metabolites in activated macrophages incorporated with *a*AA (Chapter II)<sup>311</sup>.

We further tested these *a*PUFAs as replacements for their native fatty acids by showing that *a*LA is incorporated into phospholipid pools. Additionally, we saw that *a*LA is biosynthesized to *a*AA in cells. We believe that this is through the same pathway that biosynthesizes AA from LA because we were able to measure all of the *a*PUFA intermediates. These experiments further validated that PUFA processing machinery of cells recognizes and metabolizes *a*PUFAs as well.

Using previously established techniques to attach biotin to  $\omega$ -alkynyl electrophiles by click chemistry, we were able to qualitatively visualize protein adduction changes resulting from the inflammatory signaling generated during macrophage activation. We further used affinity purification and selective UV-elution to isolate proteins adducted by endogenously generated  $\omega$ -alkynyl lipid

electrophiles. A set of stable isotope-labeled amino acid in cell culture (SILAC) cell lines were used to quantify relative changes in both protein expression and lipid electrophile adduction between activated and unactivated macrophages. These experiments allowed us to quantify protein adduction between these two states from lipid electrophiles generated in physiologically relevant settings. Additionally, we can quantify adducted proteins without knowledge of the adducting species, allowing us to sample a diverse array of known and unknown physiologically generated electrophiles.

These data show that mitochondrial proteins are both heavily induced and heavily adducted during macrophage activation. Many of the proteins induced, which are important for inflammatory signaling: COX-2, energy generation: complex V of the electron transport chain, and oxidant defense: superoxide dismutase 2 (Sod2), are also heavily adducted. We are unable to determine if there is a cause and effect relationship between induction and adduction. Further confirming the mitochondrion as the location of lipid electrophile generation, MitoTEMPO, a mitochondrially targeted superoxide scavenger<sup>327</sup> reduces protein adduction by lipid electrophiles in both activated and unactivated macrophages. TEMPOL, which is a ubiquitously dispersed superoxide scavenger<sup>327</sup>, did not reduce lipid electrophile formation. These data indicate that lipid electrophiles are generated during both physiological and pathophysiological cellular metabolism, and that electrophile formation is dependent on mitochondrial superoxide levels.

Increased adduction was measured in the catalytic subunit of complex V of the electron transport chain; so cellular adenosine triphosphate (ATP) levels

were measured in activated macrophages and correlated back to adduction. Activation reduces ATP levels in macrophages compared to vehicle controls, but MitoTEMPO does not show any rescue of ATP levels. This data appears to indicate that lipid electrophiles are not playing a role in modulating ATP levels in macrophages, however, several alternative explanations are possible. Cellular ATP levels are not solely a measure of ATP production, so the decrease in ATP that persists through MitoTEMPO treatment may reflect an increase in ATP consumption in that state that is unchanged with MitoTEMPO treatment. Also, we have qualitatively shown that MitoTEMPO reduces protein adduction by lipid electrophiles, but have not identified the targets of adduction during MitoTEMPO treatment. Therefore, MitoTEMPO may reduce electrophile adduction overall, but also shift the adduction profile, leaving complex V as still adducted during activation with MitoTEMPO treatment.

Another potentially interesting protein target of adduction tested for activity is Sod2. These macrophages have two superoxide dismutases: Sod1 located in the cytosol and Sod2 located in the mitochondrion. Consistent with our SILAC data that mitochondrial proteins are more adducted, Sod1 did not show any changes in adduction during activation, and Sod2 adduction increased nearly 5-fold. This increase in adduction resulted in a decrease in activity, which was rescued with MitoTEMPO treatment. These data indicate that lipid electrophile adduction of Sod2 modulates the activity of Sod2, which was supported by previous studies showing alkylation of nucleophilic amino acid residues played a role in modulating Sod2 activity<sup>337, 338</sup>.

MitoTEMPO modulation of lipid electrophiles indicates that electrophiles are generated by an autoxidation mechanism. We wanted to further test this by measuring esterified oxidized lipids as well as changes in both adduction and lipid oxidation with various inhibitors. We measured many of the expected esterified oxidized lipid products including 9-*E,E*-HODE, 9-*E,Z*-HODE, 13-*E,E*-HODE, 13-*E,Z*-HODE, 5-HETE, 11-HETE, and 15-HETE. Chiral chromatography allowed us to generate an *R/S* enantiomeric ratio determining if oxidation was the result of enzymatic oxidation or autoxidation. The only measured species that was produced by an enzymatic process was 11-HETE, exclusively the *R* enantiomer, which is the COX-2 product. All of the other esterified oxidized lipids had *R/S* ratios near one, indicating an autoxidation mechanism of formation.

As described before, MitoTEMPO reduces lipid electrophile adduction of proteins in activated macrophages, but we also were able to determine that MitoTEMPO does not inhibit COX-2 activity. Indomethacin and celecoxib, structurally distinct COX-2 inhibitors, were both shown to inhibit COX-2 activity and protein adduction by lipid electrophiles. These experiments led us to hypothesize that prostaglandin signaling increases mitochondrial superoxide and thus increase lipid electrophile generation. To test this hypothesis, we inhibited prostaglandin production with both indomethacin and celecoxib, and supplemented back prostaglandins. This supplementation did not result in increased lipid electrophile formation. Further evaluating the role of COX-2 signaling in lipid electrophile generation, we inhibited the release of AA with giripladib. As expected, depriving COX-2 of its preferred substrate reduced

prostaglandins to near basal levels. However, it did not result in any changes in protein adduction by lipid electrophiles. These studies led us to conclude that both COX-2 activity and mitochondrial superoxide are necessary for lipid electrophile generation.

Esterified oxidized lipid levels were quantified again using indomethacin and girepladib as inhibitors to see if the trends of oxidized lipids correlate to the trends of protein adduction by lipid electrophiles. The trends correlate for LA oxidation products with both 9- and 13-HODE being eliminated by indomethacin treatment, but not by girepladib treatment. A similar trend was seen with 11-HETE. Both inhibitors eliminated 15-HETE, and neither inhibited 5-HETE. These data indicate that the source of the electrophiles is potentially 9-HODE, 13-HODE, or 11-HETE, but not likely to be 5-HETE or 15-HETE. Further experiments will be performed to test this hypothesis.

We present here a novel method to study endogenous lipid electrophile generation and the resulting protein adduction. Using *n*-PUFAs, we are able to generate lipid electrophiles under physiologically relevant conditions. This method allows us to globally profile lipid electrophile protein adduction without needing to know the identities of the lipid electrophile species. The method of lipid electrophile generation appears to be an autoxidation mechanism, taking place in the mitochondrion, and involving mitochondrial superoxide. Finally, we were able to correlate changes in Sod2 activity to adduction by lipid electrophiles. In total, this work, will allow for the unbiased profiling of protein targets of lipid



electrophiles in any model system that can be incorporated with  $\omega$ -alkynyl polyunsaturated fatty acids.

## **Future Visions**

### ***Rotenone generation of lipid electrophile protein adducts***

The optimization of these methods allows us to expand to other model systems to study lipid electrophile adduction of proteins. We first wanted to try a system that would allow us to see if generation of lipid electrophiles and the resulting protein adduction were exclusively an activated macrophage phenomenon. A recent study showed that rotenone, an electron transport chain complex I inhibitor, increases mitochondrial superoxide generation<sup>355</sup>. Rotenone has also been linked to Parkinson's-like symptoms in mice<sup>356-358</sup>, and mitochondrial dysfunction has long been linked to Parkinson's disease<sup>359, 360</sup>.

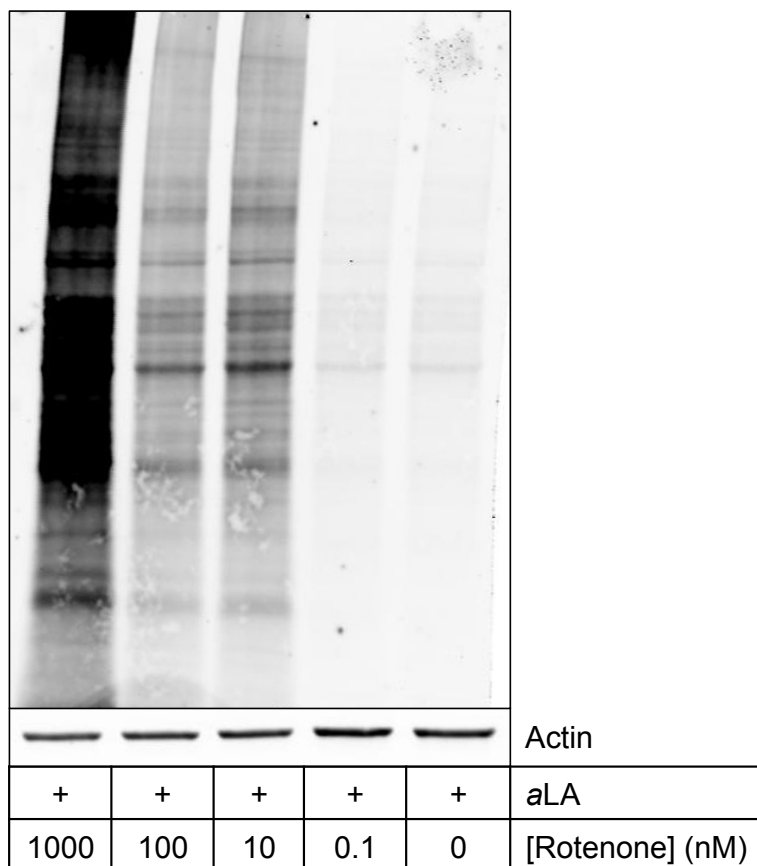


**Figure 1.** Rotenone induced protein adduction in RAW264.7 macrophages. Rotenone dose dependently generates lipid electrophile protein adducts in aLA-incorporated RAW264.7 macrophages.

We treated aLA-incorporated RAW264.7 macrophages with a range of rotenone concentrations. Click chemistry was utilized to attach biotin, the proteome was separated by SDS-PAGE, and adducted proteins visualized with a streptavidin fluorophore as described in Chapter III<sup>248</sup>. Rotenone dose dependently generates protein adduction (Figure 1). Rotenone also generates lipid electrophiles independent of macrophage activation as determined by measuring COX-2 expression (Figure 2). Kdo<sub>2</sub>-lipid A (KLA)<sup>286</sup> treatment showed an increase in COX-2 expression, indicating that the macrophages were

activated. Rotenone did not induce COX-2 expression at any of the concentrations tested. These data indicate that lipid electrophile adduction of proteins is not specific to macrophage activation by endotoxins, but that other processes also induce lipid electrophile generation.

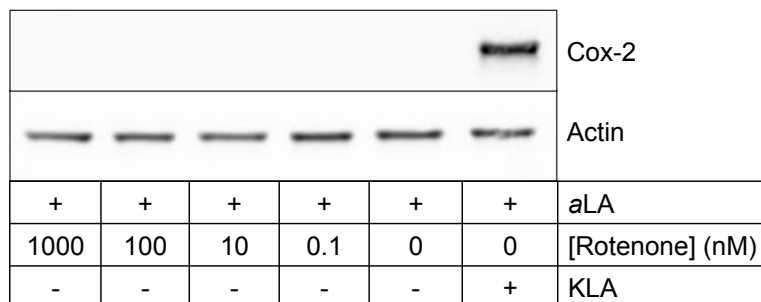


**Figure 2.** Rotenone does not activate RAW264.7 macrophages. COX-2 expression was used as a marker for macrophage activation. Macrophages treated with KLA showed a large increase in COX-2 expression indicating that they are activated. None of the concentrations of rotenone activated the macrophages.

We also wanted to test if rotenone is inducing lipid electrophile generation through the increase in mitochondrial superoxide as was previously reported<sup>355</sup>. We treated aLA-incorporated macrophages with rotenone and either MitoTEMPO, a mitochondrially enriched superoxide scavenger, or TEMPOL, a ubiquitously dispersed superoxide scavenger as described in Chapter III<sup>327, 361</sup>. Figure 3 shows that both 10  $\mu$ M and 1  $\mu$ M MitoTEMPO reduces rotenone induced protein adduction by lipid electrophiles. This reduction in adduction is dose dependent as 10  $\mu$ M MitoTEMPO reduces adduction to a greater extent than 1  $\mu$ M MitoTEMPO. TEMPOL does not reduce adduction by lipid electrophiles at either concentration tested. These results indicate that

mitochondrial superoxide is a precursor to lipid electrophile generation as was seen in KLA-activated macrophages (Chapter III).

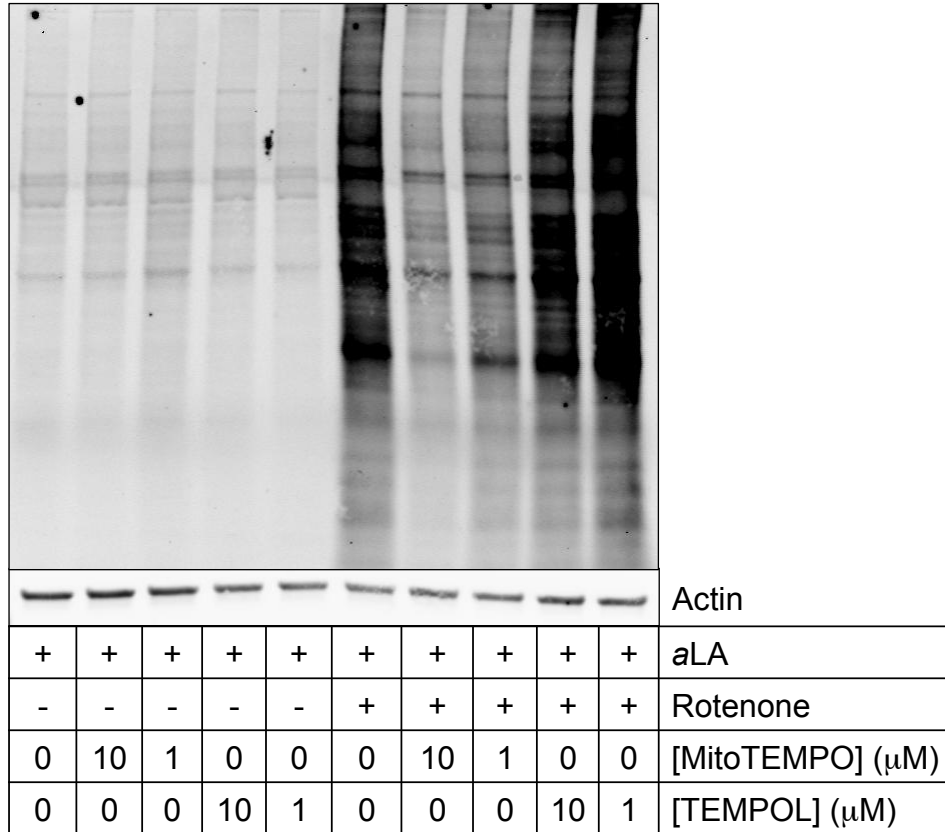


**Figure 3.** MitoTEMPO reduces lipid electrophile adduction induced by rotenone. MitoTEMPO, a mitochondrially targeted superoxide scavenger showed reduction of lipid electrophile adduction at both concentrations testes. TEMPOL, a ubiquitously dispersed superoxide scavenger did not. These data indicate that rotenone induces lipid electrophile generation in a process that involves mitochondrial superoxide, similarly to lipid electrophile generation during KLA activation.

These initial rotenone experiments gave us several important insights into the generation of lipid electrophiles and the resulting protein adduction. First, lipid electrophile generation in our system is not activation specific. Without activating the macrophages, rotenone is able to induce lipid electrophile generation. Second, rotenone generates lipid electrophiles through a mechanism that

involves mitochondrial superoxide. Finally, rotenone toxicity is known to induce mitochondrial dysfunction<sup>359, 360</sup>. The data generated here indicate that lipid electrophile adduction of proteins may be a mechanism of rotenone induced mitochondrial dysfunction, and thus is a good model system in which to study lipid electrophile generation and protein adduction.

### ***Identification of the site of modification of Sod2***

Human Embryonic Kidney 293 cells (HEK-293) were chosen for further testing of rotenone induced protein adduction by lipid electrophiles because despite being kidney in origin have been reported to be more neuronal-like than kidney-like<sup>362</sup>. The cells were incorporated with and without aLA, and then treated with various concentrations of rotenone. Protein adduction was measured by SDS-PAGE separation, and click chemistry methods discussed in Chapter III<sup>248</sup>. Figure 4 shows that rotenone induces measurable lipid electrophile protein adduction at higher concentrations, and only in aLA-incorporated cells.

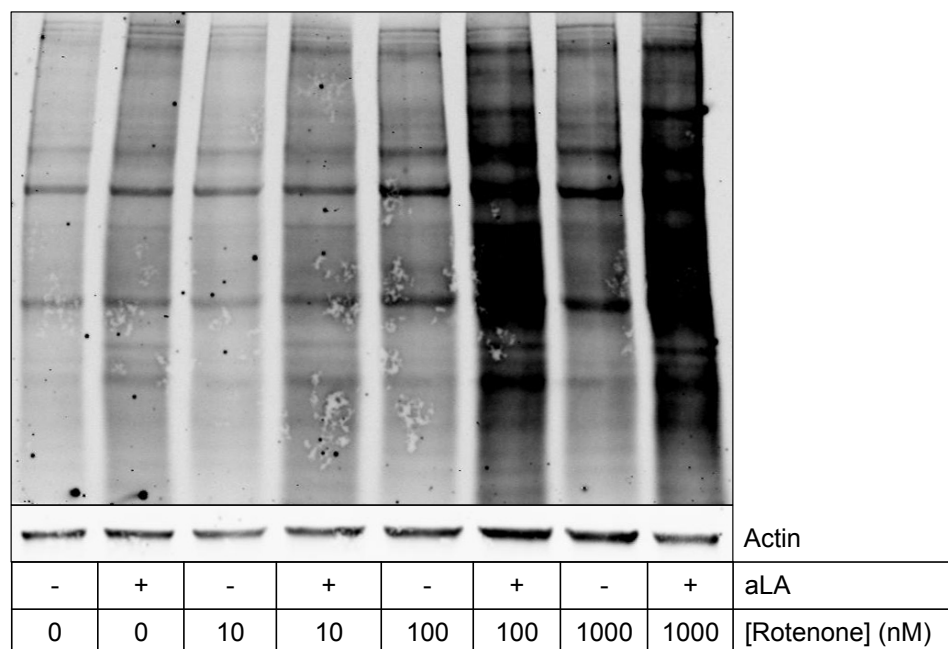


**Figure 4.** Rotenone induces lipid electrophile protein adducts in HEK-293 cells. Rotenone dose dependently generates lipid electrophile protein adducts in aLA-incorporated HEK-293 cells.

HEK-293 cells were also chosen because they are much more easily transfectable than RAW264.7 macrophages. We plan to use them for the targeted analysis of proteins that are adducted by lipid electrophiles to determine sites of modification. Sod2 is the first target protein we have chosen. As discussed in Chapter III, Sod2 is heavily adducted by lipid electrophiles, and also shows a decrease in activity that correlates with electrophile adduction. To see if Sod2 is adducted in the HEK-293 and rotenone system, aLA-incorporated and unincorporated HEK-293 cells were treated with rotenone. Click chemistry was utilized to attach UV-cleavable biotin<sup>249</sup> for affinity purification and selective release by UV-irradiation<sup>204</sup>. After UV-elution, adducted proteins were separated by SDS-PAGE, and targeted analysis of adduction was performed by western blotting as described in Chapter III. Figure 5 shows that Sod2 is more adducted

in the aLA-incorporated HEK-293 cells, indicating that Sod2 is a target for lipid electrophile adduction in this system.

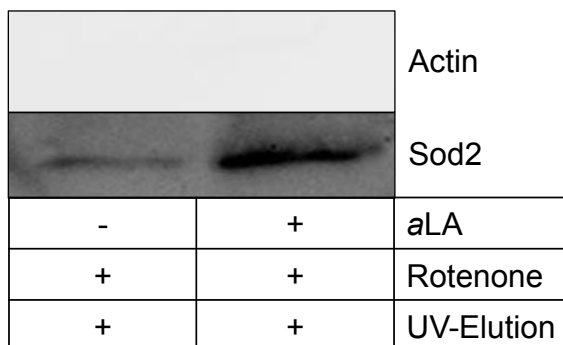


**Figure 5.** Sod2 is adducted by lipid electrophiles in rotenone treated HEK-293 cells. HEK-293 cells were incorporated with and without aLA then treated with rotenone. Proteins were isolated using previously described (Chapter III) affinity purification methods. Western blotting shows a stronger Sod2 signal in the aLA incorporated versus unincorporated sample indicating greater adduction of Sod2 in that sample.

We will transfect a C-terminal 6X histidine tagged Sod2 (Sod2-His<sub>6</sub>) into HEK-293 cells, and then induce lipid electrophile formation with rotenone. The His<sub>6</sub> tag will allow us to retrieve Sod2-His<sub>6</sub> for identification of the sites of modification as well as well as identification of the adducting species. Figure 6 shows that we are able to successfully transfect in, and purify Sod2-His<sub>6</sub> as determined by western blotting. The His<sub>6</sub> tag was placed C-terminally to leave the N-terminal mitochondrial targeting sequence intact. Figure 7 shows that Sod2-His<sub>6</sub> is successfully shuttled into the mitochondrion, similarly to the native Sod2 protein, when previously described subcellular fractionation and western blotting techniques are applied (Chapter III). Currently we are attempting to identify the sites of adduction as well as the adducting species on Sod2-His<sub>6</sub>.

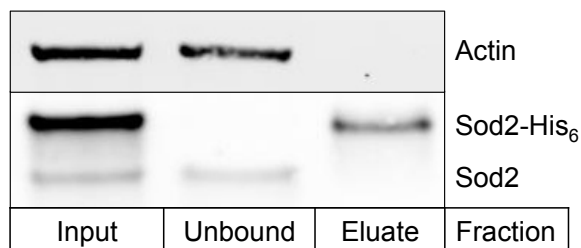


**Figure 6.** Expression and purification of Sod2-His<sub>6</sub>. Sod2-His<sub>6</sub> was successfully expressed in HEK-293 cells and purified by metal affinity chromatography.

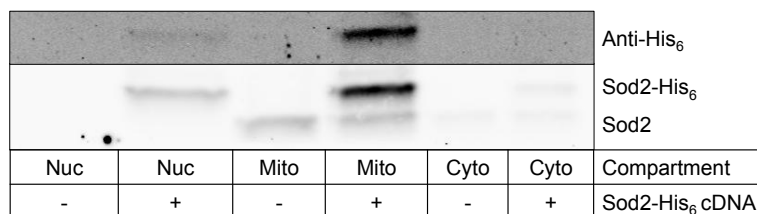


**Figure 7.** Subcellular fractionation of Sod2-His<sub>6</sub>. Organelles were separated into nucleus (Nuc), mitochondrion (Mito), and cytosol (Cyto). Sod2-His<sub>6</sub>, similarly to native Sod2 is mitochondrially localized.

### ***aLA in vivo***

The ultimate goal of this project was to eventually be able to move out of cultured cells, and study lipid electrophile generation and protein adduction in animal models for disease using *a*PUFAs. One factor that has hindered our move *in vivo* studies has been the amount of material necessary to incorporate a whole animal with *a*PUFA. Most studies looking at fatty acid incorporation into whole animals supplement the fatty acid into the chow in large quantities<sup>363-365</sup>. Limited quantities and difficult synthetic schemes have made generating *a*PUFA-incorporated chow prohibitive. However, fatty acids have been injected into mice previously, and incorporation measured in the lipid bilayer<sup>366</sup>.



David Harrison's group at Vanderbilt has a mouse model for hypertension in which angiotensin II (AngII) is infused into mice<sup>367</sup>. They have discovered that this infusion leads to activation of dendritic cells of the spleen and increased oxidative stress resulting in hypertension. The increased oxidative stress results in increased protein adduction by lipid electrophiles, specifically isoketals, in the aorta, heart, and dendritic cells of the spleen<sup>256</sup>. We injected mice with aLA, and then infused AngII to see if we could measure  $\omega$ -alkynyl lipid electrophiles in these animals. The animals were sacrificed and the spleen (S), lung (Lu), brain (B), heart (H), liver (Li), and kidney (K) were harvested. Proteins were isolated, clicked to biotin, separated, and visualized as described above<sup>248</sup>. Figure 8 shows that there were different adduction patterns for each of the organs isolated. Additionally, the differences between AngII treated and untreated mice were most distinct in the liver and heart. The adduction differences in the heart are consistent with the study previously mentioned<sup>256</sup>.

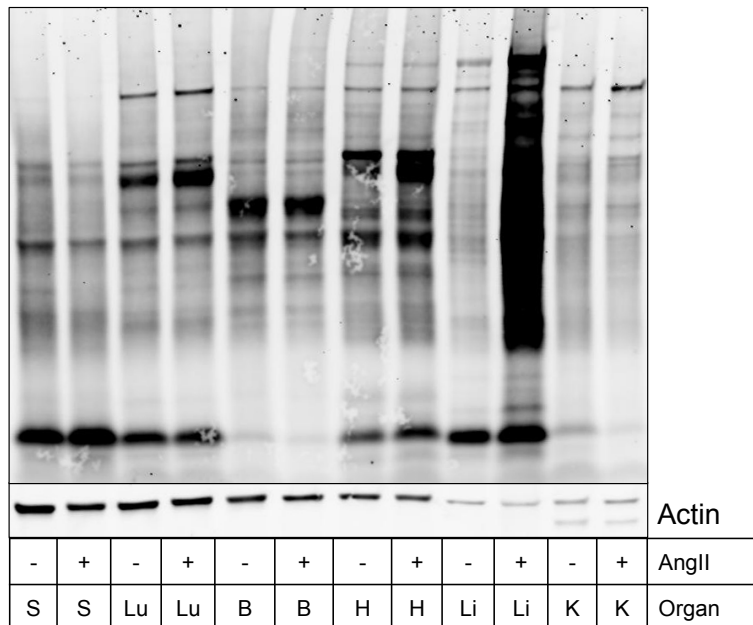


**Figure 8.** Lipid electrophile protein adduction in *aLA*-incorporated mice treated with AngII. Lipid electrophile adduction of the proteome was measured in spleen (S), lung (Lu), brain (B), heart (H), liver (Li), and kidney (K).

Here we present some future visions for this project. We show that lipid electrophile adduction of proteins is not a macrophage-activation specific phenomenon. We have also developed a system where we can perform targeted studies of mitochondrial proteins adducted by lipid electrophiles to identify the sites of adduction as well as the adducting species. Finally, we performed some promising pilot experiments to move *aPUFAs in vivo*. These preliminary studies show that the future of using *aPUFAs* to study endogenously generated lipid electrophiles and the resulting protein adduction is limitless, with many opportunities and model systems to explore.

## REFERENCES

- (1) Taghizadeh, K., McFaline, J. L., Pang, B., Sullivan, M., Dong, M., Plummer, E., and Dedon, P. C. (2008) Quantification of DNA damage products resulting from deamination, oxidation and reaction with products of lipid peroxidation by liquid chromatography isotope dilution tandem mass spectrometry. *Nat Protoc*, 3, 1287-1298.
- (2) Prusakiewicz, J., Turman, M., Vila, A., Ball, H., Al-Mestarihi, A., Marzo, V., and Marnett, L. (2007) Oxidative metabolism of lipoamino acids and vanilloids by lipoxygenases and cyclooxygenases. *Arch Biochem Biophys*, 464, 260-268.
- (3) Ullery, J. C., and Marnett, L. J. (2012) Protein modification by oxidized phospholipids and hydrolytically released lipid electrophiles: Investigating cellular responses. *Biochim Biophys Acta*, 1818, 2424-2435.
- (4) Metchnikoff, E., and Binnie, F. G. (1905) *Immunity in infective diseases*. University Press, Cambridge.
- (5) Kaufmann, S. H. (2008) Immunology's foundation: the 100-year anniversary of the Nobel Prize to Paul Ehrlich and Elie Metchnikoff. *Nature immunology*, 9, 705-712.
- (6) Naito, M., Hasegawa, G., and Takahashi, K. (1997) Development, differentiation, and maturation of Kupffer cells. *Microsc Res Tech*, 39, 350-364.
- (7) Gehrmann, J., Matsumoto, Y., and Kreutzberg, G. W. (1995) Microglia: intrinsic immune effector cell of the brain. *Brain Res Brain Res Rev*, 20, 269-287.
- (8) Nijweide, P. J., Burger, E. H., and Feyen, J. H. (1986) Cells of bone: proliferation, differentiation, and hormonal regulation. *Physiol Rev*, 66, 855-886.
- (9) Ginhoux, F., Tacke, F., Angeli, V., Bogunovic, M., Loubreau, M., Dai, X. M., Stanley, E. R., Randolph, G. J., and Merad, M. (2006) Langerhans cells arise from monocytes in vivo. *Nature immunology*, 7, 265-273.
- (10) Twigg, H. L., 3rd. (2004) Macrophages in innate and acquired immunity. *Semin Respir Crit Care Med*, 25, 21-31.
- (11) Ziegler-Heitbrock, L., Ancuta, P., Crowe, S., Dalod, M., Grau, V., Hart, D. N., Leenen, P. J., Liu, Y. J., MacPherson, G., Randolph, G. J., Scherberich, J., Schmitz, J., Shortman, K., Sozzani, S., Strobl, H.,

- Zembala, M., Austyn, J. M., and Lutz, M. B. (2010) Nomenclature of monocytes and dendritic cells in blood. *Blood*, 116, e74-80.
- (12) Cline, M. J. (1994) Histiocytes and histiocytosis. *Blood*, 84, 2840-2853.
- (13) Wood, G. W. (1980) Mononuclear phagocytes in the human placenta. *Placenta*, 1, 113-123.
- (14) Ovchinnikov, D. A. (2008) Macrophages in the embryo and beyond: much more than just giant phagocytes. *Genesis*, 46, 447-462.
- (15) Mosser, D. M., and Edwards, J. P. (2008) Exploring the full spectrum of macrophage activation. *Nature reviews. Immunology*, 8, 958-969.
- (16) Mackaness, G. B. (1977) Cellular immunity and the parasite. *Advances in experimental medicine and biology*, 93, 65-73.
- (17) Zhang, X., and Mosser, D. M. (2008) Macrophage activation by endogenous danger signals. *The Journal of pathology*, 214, 161-178.
- (18) Park, J. S., Svetkauskaite, D., He, Q., Kim, J. Y., Strassheim, D., Ishizaka, A., and Abraham, E. (2004) Involvement of toll-like receptors 2 and 4 in cellular activation by high mobility group box 1 protein. *J Biol Chem*, 279, 7370-7377.
- (19) West, A. P., Koblansky, A. A., and Ghosh, S. (2006) Recognition and signaling by toll-like receptors. *Annu Rev Cell Dev Biol*, 22, 409-437.
- (20) West, A. P., Brodsky, I. E., Rahner, C., Woo, D. K., Erdjument-Bromage, H., Tempst, P., Walsh, M. C., Choi, Y., Shadel, G. S., and Ghosh, S. (2011) TLR signalling augments macrophage bactericidal activity through mitochondrial ROS. *Nature*, 472, 476-480.
- (21) MacMicking, J. D., North, R. J., LaCourse, R., Mudgett, J. S., Shah, S. K., and Nathan, C. F. (1997) Identification of nitric oxide synthase as a protective locus against tuberculosis. *Proc Natl Acad Sci U S A*, 94, 5243-5248.
- (22) Rouzer, C. A., Scott, W. A., Kempe, J., and Cohn, Z. A. (1980) Prostaglandin synthesis by macrophages requires a specific receptor-ligand interaction. *Proc Natl Acad Sci U S A*, 77, 4279-4282.
- (23) Rouzer, C. A., Scott, W. A., Cohn, Z. A., Blackburn, P., and Manning, J. M. (1980) Mouse peritoneal macrophages release leukotriene C in response to a phagocytic stimulus. *Proc Natl Acad Sci U S A*, 77, 4928-4932.

- (24) McGrath, C. E., Tallman, K. A., Porter, N. A., and Marnett, L. J. (2011) Structure-activity analysis of diffusible lipid electrophiles associated with phospholipid peroxidation: 4-hydroxynonenal and 4-oxononenal analogues. *Chem Res Toxicol*, *24*, 357-370.
- (25) Nathan, C. F., Murray, H. W., Wiebe, M. E., and Rubin, B. Y. (1983) Identification of interferon-gamma as the lymphokine that activates human macrophage oxidative metabolism and antimicrobial activity. *J Exp Med*, *158*, 670-689.
- (26) Martinez, F. O., Sica, A., Mantovani, A., and Locati, M. (2008) Macrophage activation and polarization. *Frontiers in bioscience : a journal and virtual library*, *13*, 453-461.
- (27) Rouzer, C. A., Jacobs, A. T., Nirodi, C. S., Kingsley, P. J., Morrow, J. D., and Marnett, L. J. (2005) RAW264.7 cells lack prostaglandin-dependent autoregulation of tumor necrosis factor-alpha secretion. *J Lipid Res*, *46*, 1027-1037.
- (28) MacMicking, J., Xie, Q. W., and Nathan, C. (1997) Nitric oxide and macrophage function. *Annu Rev Immunol*, *15*, 323-350.
- (29) O'Shea, J. J., and Murray, P. J. (2008) Cytokine signaling modules in inflammatory responses. *Immunity*, *28*, 477-487.
- (30) Loke, P., Gallagher, I., Nair, M. G., Zang, X., Brombacher, F., Mohrs, M., Allison, J. P., and Allen, J. E. (2007) Alternative activation is an innate response to injury that requires CD4+ T cells to be sustained during chronic infection. *Journal of immunology*, *179*, 3926-3936.
- (31) Mosser, D. M. (2003) The many faces of macrophage activation. *J Leukoc Biol*, *73*, 209-212.
- (32) Gordon, S. (2003) Alternative activation of macrophages. *Nature reviews. Immunology*, *3*, 23-35.
- (33) Kreider, T., Anthony, R. M., Urban, J. F., Jr., and Gause, W. C. (2007) Alternatively activated macrophages in helminth infections. *Current opinion in immunology*, *19*, 448-453.
- (34) Gerber, J. S., and Mosser, D. M. (2001) Reversing lipopolysaccharide toxicity by ligating the macrophage Fc gamma receptors. *Journal of immunology*, *166*, 6861-6868.
- (35) Mantovani, A., Sica, A., Sozzani, S., Allavena, P., Vecchi, A., and Locati, M. (2004) The chemokine system in diverse forms of macrophage activation and polarization. *Trends in immunology*, *25*, 677-686.

- (36) Fadok, V. A., Bratton, D. L., Konowal, A., Freed, P. W., Westcott, J. Y., and Henson, P. M. (1998) Macrophages that have ingested apoptotic cells in vitro inhibit proinflammatory cytokine production through autocrine/paracrine mechanisms involving TGF-beta, PGE2, and PAF. *The Journal of clinical investigation*, 101, 890-898.
- (37) Strassmann, G., Patil-Koota, V., Finkelman, F., Fong, M., and Kambayashi, T. (1994) Evidence for the involvement of interleukin 10 in the differential deactivation of murine peritoneal macrophages by prostaglandin E2. *J Exp Med*, 180, 2365-2370.
- (38) Weber, C., Zernecke, A., and Libby, P. (2008) The multifaceted contributions of leukocyte subsets to atherosclerosis: lessons from mouse models. *Nature reviews. Immunology*, 8, 802-815.
- (39) Churg, A., Wang, R. D., Tai, H., Wang, X., Xie, C., Dai, J., Shapiro, S. D., and Wright, J. L. (2003) Macrophage metalloelastase mediates acute cigarette smoke-induced inflammation via tumor necrosis factor-alpha release. *American journal of respiratory and critical care medicine*, 167, 1083-1089.
- (40) D'Hulst A, I., Vermaelen, K. Y., Brusselle, G. G., Joos, G. F., and Pauwels, R. A. (2005) Time course of cigarette smoke-induced pulmonary inflammation in mice. *The European respiratory journal*, 26, 204-213.
- (41) Chen, X., Zhu, G., Jin, T., Gu, S., Xiao, H., and Qiu, J. (2011) Cadmium induces differentiation of RAW264.7 cells into osteoclasts in the presence of RANKL. *Food and chemical toxicology : an international journal published for the British Industrial Biological Research Association*, 49, 2392-2397.
- (42) Jomova, K., and Valko, M. (2011) Advances in metal-induced oxidative stress and human disease. *Toxicology*, 283, 65-87.
- (43) Tracy, R. P. (2006) The five cardinal signs of inflammation: Calor, Dolor, Rubor, Tumor ... and Penuria (Apologies to Aulus Cornelius Celsus, De medicina, c. A.D. 25). *J Gerontol A Biol Sci Med Sci*, 61, 1051-1052.
- (44) Nathan, C., and Ding, A. (2010) Nonresolving inflammation. *Cell*, 140, 871-882.
- (45) Karin, M., and Greten, F. R. (2005) NF-kappaB: linking inflammation and immunity to cancer development and progression. *Nature reviews. Immunology*, 5, 749-759.
- (46) Mercurio, F., Zhu, H., Murray, B. W., Shevchenko, A., Bennett, B. L., Li, J., Young, D. B., Barbosa, M., Mann, M., Manning, A., and Rao, A. (1997)

IKK-1 and IKK-2: cytokine-activated I $\kappa$ B kinases essential for NF- $\kappa$ B activation. *Science*, 278, 860-866.

- (47) Beg, A. A., and Baldwin, A. S., Jr. (1994) Activation of multiple NF- $\kappa$ B DNA-binding complexes by tumor necrosis factor. *Oncogene*, 9, 1487-1492.
- (48) Beinke, S., Robinson, M. J., Hugunin, M., and Ley, S. C. (2004) Lipopolysaccharide activation of the TPL-2/MEK/extracellular signal-regulated kinase mitogen-activated protein kinase cascade is regulated by I $\kappa$ B kinase-induced proteolysis of NF- $\kappa$ B1 p105. *Mol Cell Biol*, 24, 9658-9667.
- (49) Woronicz, J. D., Gao, X., Cao, Z., Rothe, M., and Goeddel, D. V. (1997) I $\kappa$ B kinase- $\beta$ : NF- $\kappa$ B activation and complex formation with I $\kappa$ B kinase- $\alpha$  and NIK. *Science*, 278, 866-869.
- (50) Suyang, H., Phillips, R., Douglas, I., and Ghosh, S. (1996) Role of unphosphorylated, newly synthesized I $\kappa$ B  $\beta$  in persistent activation of NF- $\kappa$ B. *Mol Cell Biol*, 16, 5444-5449.
- (51) DiDonato, J., Mercurio, F., Rosette, C., Wu-Li, J., Suyang, H., Ghosh, S., and Karin, M. (1996) Mapping of the inducible I $\kappa$ B phosphorylation sites that signal its ubiquitination and degradation. *Mol Cell Biol*, 16, 1295-1304.
- (52) Hayden, M. S., and Ghosh, S. (2004) Signaling to NF- $\kappa$ B. *Genes Dev*, 18, 2195-2224.
- (53) Delhase, M., Hayakawa, M., Chen, Y., and Karin, M. (1999) Positive and negative regulation of I $\kappa$ B kinase activity through IKK $\beta$  subunit phosphorylation. *Science*, 284, 309-313.
- (54) Lee, K. M., Kang, B. S., Lee, H. L., Son, S. J., Hwang, S. H., Kim, D. S., Park, J. S., and Cho, H. J. (2004) Spinal NF- $\kappa$ B activation induces COX-2 upregulation and contributes to inflammatory pain hypersensitivity. *The European journal of neuroscience*, 19, 3375-3381.
- (55) Xie, Q. W., Kashiwabara, Y., and Nathan, C. (1994) Role of transcription factor NF- $\kappa$ B/Rel in induction of nitric oxide synthase. *J Biol Chem*, 269, 4705-4708.
- (56) Malinin, N. L., Boldin, M. P., Kovalenko, A. V., and Wallach, D. (1997) MAP3K-related kinase involved in NF- $\kappa$ B induction by TNF, CD95 and IL-1. *Nature*, 385, 540-544.
- (57) Zhang, Y., Broser, M., and Rom, W. N. (1994) Activation of the interleukin 6 gene by Mycobacterium tuberculosis or lipopolysaccharide is mediated

by nuclear factors NF-IL6 and NF-kappa B. *Proc Natl Acad Sci U S A*, 91, 2225-2229.

- (58) Chen, C., Edelstein, L. C., and Gelinas, C. (2000) The Rel/NF-kappaB family directly activates expression of the apoptosis inhibitor Bcl-x(L). *Mol Cell Biol*, 20, 2687-2695.
- (59) Cheng, Q., Lee, H. H., Li, Y., Parks, T. P., and Cheng, G. (2000) Upregulation of Bcl-x and Bfl-1 as a potential mechanism of chemoresistance, which can be overcome by NF-kappaB inhibition. *Oncogene*, 19, 4936-4940.
- (60) Kim, Y. S., Schwabe, R. F., Qian, T., Lemasters, J. J., and Brenner, D. A. (2002) TRAIL-mediated apoptosis requires NF-kappaB inhibition and the mitochondrial permeability transition in human hepatoma cells. *Hepatology*, 36, 1498-1508.
- (61) Mattson, M. P., Goodman, Y., Luo, H., Fu, W., and Furukawa, K. (1997) Activation of NF-kappaB protects hippocampal neurons against oxidative stress-induced apoptosis: evidence for induction of manganese superoxide dismutase and suppression of peroxynitrite production and protein tyrosine nitration. *J Neurosci Res*, 49, 681-697.
- (62) Xu, Y., Kiningham, K. K., Devalaraja, M. N., Yeh, C. C., Majima, H., Kasarskis, E. J., and St Clair, D. K. (1999) An intronic NF-kappaB element is essential for induction of the human manganese superoxide dismutase gene by tumor necrosis factor-alpha and interleukin-1beta. *DNA Cell Biol*, 18, 709-722.
- (63) Okawa, H., Motohashi, H., Kobayashi, A., Aburatani, H., Kensler, T. W., and Yamamoto, M. (2006) Hepatocyte-specific deletion of the keap1 gene activates Nrf2 and confers potent resistance against acute drug toxicity. *Biochem Biophys Res Commun*, 339, 79-88.
- (64) Itoh, K., Chiba, T., Takahashi, S., Ishii, T., Igarashi, K., Katoh, Y., Oyake, T., Hayashi, N., Satoh, K., Hatayama, I., Yamamoto, M., and Nabeshima, Y. (1997) An Nrf2/small Maf heterodimer mediates the induction of phase II detoxifying enzyme genes through antioxidant response elements. *Biochem Biophys Res Commun*, 236, 313-322.
- (65) Kobayashi, A., Kang, M. I., Okawa, H., Ohtsuji, M., Zenke, Y., Chiba, T., Igarashi, K., and Yamamoto, M. (2004) Oxidative stress sensor Keap1 functions as an adaptor for Cul3-based E3 ligase to regulate proteasomal degradation of Nrf2. *Mol Cell Biol*, 24, 7130-7139.
- (66) McMahon, M., Itoh, K., Yamamoto, M., and Hayes, J. D. (2003) Keap1-dependent proteasomal degradation of transcription factor Nrf2



contributes to the negative regulation of antioxidant response element-driven gene expression. *J Biol Chem*, 278, 21592-21600.

- (67) Rachakonda, G., Xiong, Y., Sekhar, K. R., Stamer, S. L., Liebler, D. C., and Freeman, M. L. (2008) Covalent modification at Cys151 dissociates the electrophile sensor Keap1 from the ubiquitin ligase CUL3. *Chem Res Toxicol*, 21, 705-710.
- (68) Dinkova-Kostova, A. T., Holtzclaw, W. D., Cole, R. N., Itoh, K., Wakabayashi, N., Katoh, Y., Yamamoto, M., and Talalay, P. (2002) Direct evidence that sulfhydryl groups of Keap1 are the sensors regulating induction of phase 2 enzymes that protect against carcinogens and oxidants. *Proc Natl Acad Sci U S A*, 99, 11908-11913.
- (69) Hong, F., Freeman, M. L., and Liebler, D. C. (2005) Identification of sensor cysteines in human Keap1 modified by the cancer chemopreventive agent sulforaphane. *Chem Res Toxicol*, 18, 1917-1926.
- (70) Hong, F., Sekhar, K. R., Freeman, M. L., and Liebler, D. C. (2005) Specific patterns of electrophile adduction trigger Keap1 ubiquitination and Nrf2 activation. *J Biol Chem*, 280, 31768-31775.
- (71) Alam, J., Stewart, D., Touchard, C., Boinapally, S., Choi, A. M., and Cook, J. L. (1999) Nrf2, a Cap'n'Collar transcription factor, regulates induction of the heme oxygenase-1 gene. *J Biol Chem*, 274, 26071-26078.
- (72) Suh, J. H., Shenvi, S. V., Dixon, B. M., Liu, H., Jaiswal, A. K., Liu, R. M., and Hagen, T. M. (2004) Decline in transcriptional activity of Nrf2 causes age-related loss of glutathione synthesis, which is reversible with lipoic acid. *Proc Natl Acad Sci U S A*, 101, 3381-3386.
- (73) Thimmulappa, R. K., Mai, K. H., Srisuma, S., Kensler, T. W., Yamamoto, M., and Biswal, S. (2002) Identification of Nrf2-regulated genes induced by the chemopreventive agent sulforaphane by oligonucleotide microarray. *Cancer Res*, 62, 5196-5203.
- (74) Balkwill, F., and Mantovani, A. (2001) Inflammation and cancer: back to Virchow? *Lancet*, 357, 539-545.
- (75) Condeelis, J., and Pollard, J. W. (2006) Macrophages: obligate partners for tumor cell migration, invasion, and metastasis. *Cell*, 124, 263-266.
- (76) Biswas, S. K., Gangi, L., Paul, S., Schioppa, T., Sacconi, A., Sironi, M., Bottazzi, B., Doni, A., Vincenzo, B., Pasqualini, F., Vago, L., Nebuloni, M., Mantovani, A., and Sica, A. (2006) A distinct and unique transcriptional program expressed by tumor-associated macrophages (defective NF-kappaB and enhanced IRF-3/STAT1 activation). *Blood*, 107, 2112-2122.

- (77) Pollard, J. W. (2008) Macrophages define the invasive microenvironment in breast cancer. *J Leukoc Biol*, 84, 623-630.
- (78) Hagemann, T., Wilson, J., Kulbe, H., Li, N. F., Leinster, D. A., Charles, K., Klemm, F., Pukrop, T., Binder, C., and Balkwill, F. R. (2005) Macrophages induce invasiveness of epithelial cancer cells via NF-kappa B and JNK. *Journal of immunology*, 175, 1197-1205.
- (79) Pikarsky, E., Porat, R. M., Stein, I., Abramovitch, R., Amit, S., Kasem, S., Gutkovich-Pyest, E., Urieli-Shoval, S., Galun, E., and Ben-Neriah, Y. (2004) NF-kappaB functions as a tumour promoter in inflammation-associated cancer. *Nature*, 431, 461-466.
- (80) Wyckoff, J. B., Wang, Y., Lin, E. Y., Li, J. F., Goswami, S., Stanley, E. R., Segall, J. E., Pollard, J. W., and Condeelis, J. (2007) Direct visualization of macrophage-assisted tumor cell intravasation in mammary tumors. *Cancer Res*, 67, 2649-2656.
- (81) Greten, F. R., Eckmann, L., Greten, T. F., Park, J. M., Li, Z. W., Egan, L. J., Kagnoff, M. F., and Karin, M. (2004) IKKbeta links inflammation and tumorigenesis in a mouse model of colitis-associated cancer. *Cell*, 118, 285-296.
- (82) Akiyama, H., Barger, S., Barnum, S., Bradt, B., Bauer, J., Cole, G. M., Cooper, N. R., Eikelenboom, P., Emmerling, M., Fiebich, B. L., Finch, C. E., Frautschy, S., Griffin, W. S., Hampel, H., Hull, M., Landreth, G., Lue, L., Mrak, R., Mackenzie, I. R., McGeer, P. L., O'Banion, M. K., Pachter, J., Pasinetti, G., Plata-Salaman, C., Rogers, J., Rydel, R., Shen, Y., Streit, W., Strohmeyer, R., Tooyoma, I., Van Muiswinkel, F. L., Veerhuis, R., Walker, D., Webster, S., Wegrzyniak, B., Wenk, G., and Wyss-Coray, T. (2000) Inflammation and Alzheimer's disease. *Neurobiology of aging*, 21, 383-421.
- (83) McGeer, P. L., and McGeer, E. G. (2002) Innate immunity, local inflammation, and degenerative disease. *Sci Aging Knowledge Environ*, 2002, re3.
- (84) McGeer, P. L., and McGeer, E. G. (2004) Inflammation and neurodegeneration in Parkinson's disease. *Parkinsonism Relat Disord*, 10 Suppl 1, S3-7.
- (85) Manzano-Leon, N., Delgado-Coello, B., Guaderrama-Diaz, M., and Mas-Oliva, J. (2006) Beta-adaptin: key molecule for microglial scavenger receptor function under oxidative stress. *Biochem Biophys Res Commun*, 351, 588-594.
- (86) Gagliardi, S., Cova, E., Davin, A., Guareschi, S., Abel, K., Alvisi, E., Laforenza, U., Ghidoni, R., Cashman, J. R., Ceroni, M., and Cereda, C.

- (2010) SOD1 mRNA expression in sporadic amyotrophic lateral sclerosis. *Neurobiol Dis*, 39, 198-203.
- (87) Saeed, M., Yang, Y., Deng, H. X., Hung, W. Y., Siddique, N., Dellefave, L., Gellera, C., Andersen, P. M., and Siddique, T. (2009) Age and founder effect of SOD1 A4V mutation causing ALS. *Neurology*, 72, 1634-1639.
- (88) Wang, J., Slunt, H., Gonzales, V., Fromholt, D., Coonfield, M., Copeland, N. G., Jenkins, N. A., and Borchelt, D. R. (2003) Copper-binding-site-null SOD1 causes ALS in transgenic mice: aggregates of non-native SOD1 delineate a common feature. *Human molecular genetics*, 12, 2753-2764.
- (89) Bruijn, L. I., Houseweart, M. K., Kato, S., Anderson, K. L., Anderson, S. D., Ohama, E., Reaume, A. G., Scott, R. W., and Cleveland, D. W. (1998) Aggregation and motor neuron toxicity of an ALS-linked SOD1 mutant independent from wild-type SOD1. *Science*, 281, 1851-1854.
- (90) Fearnley, J. M., and Lees, A. J. (1991) Ageing and Parkinson's disease: substantia nigra regional selectivity. *Brain : a journal of neurology*, 114 ( Pt 5), 2283-2301.
- (91) Kim, W. G., Mohny, R. P., Wilson, B., Jeohn, G. H., Liu, B., and Hong, J. S. (2000) Regional difference in susceptibility to lipopolysaccharide-induced neurotoxicity in the rat brain: role of microglia. *The Journal of neuroscience : the official journal of the Society for Neuroscience*, 20, 6309-6316.
- (92) Liberatore, G. T., Jackson-Lewis, V., Vukosavic, S., Mandir, A. S., Vila, M., McAuliffe, W. G., Dawson, V. L., Dawson, T. M., and Przedborski, S. (1999) Inducible nitric oxide synthase stimulates dopaminergic neurodegeneration in the MPTP model of Parkinson disease. *Nat Med*, 5, 1403-1409.
- (93) Galkina, E., and Ley, K. (2009) Immune and inflammatory mechanisms of atherosclerosis (\*). *Annu Rev Immunol*, 27, 165-197.
- (94) Gerrity, R. G., Naito, H. K., Richardson, M., and Schwartz, C. J. (1979) Dietary induced atherogenesis in swine. Morphology of the intima in prelesion stages. *Am J Pathol*, 95, 775-792.
- (95) Hansson, G. K., and Libby, P. (2006) The immune response in atherosclerosis: a double-edged sword. *Nature reviews. Immunology*, 6, 508-519.
- (96) Bobryshev, Y. V. (2006) Monocyte recruitment and foam cell formation in atherosclerosis. *Micron*, 37, 208-222.

- (97) Stoneman, V., Braganza, D., Figg, N., Mercer, J., Lang, R., Goddard, M., and Bennett, M. (2007) Monocyte/macrophage suppression in CD11b diphtheria toxin receptor transgenic mice differentially affects atherogenesis and established plaques. *Circ Res*, 100, 884-893.
- (98) Byrne, G. I., and Kalayoglu, M. V. (1999) Chlamydia pneumoniae and atherosclerosis: links to the disease process. *American heart journal*, 138, S488-490.
- (99) Saederup, N., Chan, L., Lira, S. A., and Charo, I. F. (2008) Fractalkine deficiency markedly reduces macrophage accumulation and atherosclerotic lesion formation in CCR2<sup>-/-</sup> mice: evidence for independent chemokine functions in atherogenesis. *Circulation*, 117, 1642-1648.
- (100) Belton, O., Byrne, D., Kearney, D., Leahy, A., and Fitzgerald, D. J. (2000) Cyclooxygenase-1 and -2-dependent prostacyclin formation in patients with atherosclerosis. *Circulation*, 102, 840-845.
- (101) Cyrus, T., Witztum, J. L., Rader, D. J., Tangirala, R., Fazio, S., Linton, M. F., and Funk, C. D. (1999) Disruption of the 12/15-lipoxygenase gene diminishes atherosclerosis in apo E-deficient mice. *The Journal of clinical investigation*, 103, 1597-1604.
- (102) Febbraio, M., Podrez, E. A., Smith, J. D., Hajjar, D. P., Hazen, S. L., Hoff, H. F., Sharma, K., and Silverstein, R. L. (2000) Targeted disruption of the class B scavenger receptor CD36 protects against atherosclerotic lesion development in mice. *The Journal of clinical investigation*, 105, 1049-1056.
- (103) Porter, N. A., Caldwell, S. E., and Mills, K. A. (1995) Mechanisms of free radical oxidation of unsaturated lipids. *Lipids*, 30, 277-290.
- (104) Yin, H., Xu, L., and Porter, N. A. (2011) Free radical lipid peroxidation: mechanisms and analysis. *Chem Rev*, 111, 5944-5972.
- (105) Porter, N. A. (1986) Mechanisms for the autoxidation of polyunsaturated lipids. *Acc Chem Res*, 19, 262-268.
- (106) Brash, A. R. (2000) Autoxidation of methyl linoleate: Identification of the bis-allylic 11-hydroperoxide. *Lipids*, 35, 947-952.
- (107) Porter, N. A., and Wujek, J. S. (1987) Allylic Hydroperoxide Rearrangement - Beta-Scission or Concerted Pathway. *J Org Chem*, 52, 5085-5089.

- (108) Tallman, K. A., Pratt, D. A., and Porter, N. A. (2001) Kinetic products of linoleate peroxidation: rapid beta-fragmentation of nonconjugated peroxy radicals. *J Am Chem Soc*, 123, 11827-11828.
- (109) Tallman, K. A., Roschek, B., Jr., and Porter, N. A. (2004) Factors influencing the autoxidation of fatty acids: effect of olefin geometry of the nonconjugated diene. *J Am Chem Soc*, 126, 9240-9247.
- (110) Porter, N. A., Weber, B. A., Weenen, H., and Khan, J. A. (1980) Autoxidation of polyunsaturated lipids. Factors controlling the stereochemistry of product hydroperoxides. *J Am Chem Soc*, 102, 5597-5601.
- (111) Porter, N. A., and Wujek, D. G. (1984) Autoxidation of Poly-Unsaturated Fatty-Acids, an Expanded Mechanistic Study. *J Am Chem Soc*, 106, 2626-2629.
- (112) Garscha, U., Nilsson, T., and Oliw, E. H. (2008) Enantiomeric separation and analysis of unsaturated hydroperoxy fatty acids by chiral column chromatography-mass spectrometry. *Journal of chromatography. B, Analytical technologies in the biomedical and life sciences*, 872, 90-98.
- (113) Schneider, C., Pratt, D. A., Porter, N. A., and Brash, A. R. (2007) Control of oxygenation in lipoxygenase and cyclooxygenase catalysis. *Chem Biol*, 14, 473-488.
- (114) Hubke, H., Garbe, L. A., and Tressl, R. (2005) Characterization and quantification of free and esterified 9- and 13-hydroxyoctadecadienoic acids (HODE) in barley, germinating barley, and finished malt. *J Agric Food Chem*, 53, 1556-1562.
- (115) Schneider, C., Yu, Z., Boeglin, W. E., Zheng, Y., and Brash, A. R. (2007) Enantiomeric separation of hydroxy and hydroperoxy eicosanoids by chiral column chromatography. *Methods Enzymol*, 433, 145-157.
- (116) Porter, N. A., Lehman, L. S., Weber, B. A., and Smith, K. J. (1981) Unified Mechanism for Poly-Unsaturated Fatty-Acid Autoxidation - Competition of Peroxy Radical Hydrogen-Atom Abstraction, Beta-Scission, and Cyclization. *J Am Chem Soc*, 103, 6447-6455.
- (117) Morrow, J. D., Hill, K. E., Burk, R. F., Nammour, T. M., Badr, K. F., and Roberts, L. J., 2nd. (1990) A series of prostaglandin F<sub>2</sub>-like compounds are produced in vivo in humans by a non-cyclooxygenase, free radical-catalyzed mechanism. *Proc Natl Acad Sci U S A*, 87, 9383-9387.
- (118) Yin, H., Havrilla, C. M., Morrow, J. D., and Porter, N. A. (2002) Formation of isoprostane bicyclic endoperoxides from the autoxidation of cholesteryl arachidonate. *J Am Chem Soc*, 124, 7745-7754.

- (119) Yin, H., Havrilla, C. M., Gao, L., Morrow, J. D., and Porter, N. A. (2003) Mechanisms for the formation of isoprostane endoperoxides from arachidonic acid. "Dioxetane" intermediate versus beta-fragmentation of peroxy radicals. *J Biol Chem*, 278, 16720-16725.
- (120) Milne, G. L., Musiek, E. S., and Morrow, J. D. (2005) F2-isoprostanes as markers of oxidative stress in vivo: an overview. *Biomarkers : biochemical indicators of exposure, response, and susceptibility to chemicals*, 10 Suppl 1, S10-23.
- (121) Milne, G. L., Sanchez, S. C., Musiek, E. S., and Morrow, J. D. (2007) Quantification of F2-isoprostanes as a biomarker of oxidative stress. *Nat Protoc*, 2, 221-226.
- (122) Rouzer, C., and Marnett, L. (2003) Mechanism of free radical oxygenation of polyunsaturated fatty acids by cyclooxygenases. *Chem Rev*, 103, 2239-2304.
- (123) Hamberg, M., and Samuelsson, B. (1973) Detection and isolation of an endoperoxide intermediate in prostaglandin biosynthesis. *Proc Natl Acad Sci U S A*, 70, 899-903.
- (124) Fu, J. Y., Masferrer, J. L., Seibert, K., Raz, A., and Needleman, P. (1990) The induction and suppression of prostaglandin H2 synthase (cyclooxygenase) in human monocytes. *J Biol Chem*, 265, 16737-16740.
- (125) Hubbard, W. C., Hough, A. J., Jr., Brash, A. R., Watson, J. T., and Oates, J. A. (1980) Metabolism of linoleic and arachidonic acids in VX2 carcinoma tissue: identification of monohydroxy octadecadienoic acids and monohydroxy eicosatetraenoic acids. *Prostaglandins*, 20, 431-447.
- (126) Groeger, A. L., Cipollina, C., Cole, M. P., Woodcock, S. R., Bonacci, G., Rudolph, T. K., Rudolph, V., Freeman, B. A., and Schopfer, F. J. (2010) Cyclooxygenase-2 generates anti-inflammatory mediators from omega-3 fatty acids. *Nat Chem Biol*, 6, 433-441.
- (127) Kozak, K. R., Crews, B. C., Ray, J. L., Tai, H. H., Morrow, J. D., and Marnett, L. J. (2001) Metabolism of prostaglandin glycerol esters and prostaglandin ethanolamides in vitro and in vivo. *J Biol Chem*, 276, 36993-36998.
- (128) Stables, M. J., and Gilroy, D. W. (2011) Old and new generation lipid mediators in acute inflammation and resolution. *Prog Lipid Res*, 50, 35-51.
- (129) Jack, D. B. (1997) One hundred years of aspirin. *Lancet*, 350, 437-439.

- (130) Marnett, L. J., Rowlinson, S. W., Goodwin, D. C., Kalgutkar, A. S., and Lanzo, C. A. (1999) Arachidonic acid oxygenation by COX-1 and COX-2. Mechanisms of catalysis and inhibition. *J Biol Chem*, 274, 22903-22906.
- (131) Marnett, L. J., and Kalgutkar, A. S. (1999) Cyclooxygenase 2 inhibitors: discovery, selectivity and the future. *Trends Pharmacol Sci*, 20, 465-469.
- (132) FitzGerald, G. A., and Patrono, C. (2001) The coxibs, selective inhibitors of cyclooxygenase-2. *The New England journal of medicine*, 345, 433-442.
- (133) Sano, H., Kawahito, Y., Wilder, R. L., Hashiramoto, A., Mukai, S., Asai, K., Kimura, S., Kato, H., Kondo, M., and Hla, T. (1995) Expression of cyclooxygenase-1 and -2 in human colorectal cancer. *Cancer Res*, 55, 3785-3789.
- (134) Schonbeck, U., Sukhova, G. K., Graber, P., Coulter, S., and Libby, P. (1999) Augmented expression of cyclooxygenase-2 in human atherosclerotic lesions. *Am J Pathol*, 155, 1281-1291.
- (135) Sano, H., Hla, T., Maier, J. A., Crofford, L. J., Case, J. P., Maciag, T., and Wilder, R. L. (1992) In vivo cyclooxygenase expression in synovial tissues of patients with rheumatoid arthritis and osteoarthritis and rats with adjuvant and streptococcal cell wall arthritis. *The Journal of clinical investigation*, 89, 97-108.
- (136) Teismann, P., Tieu, K., Choi, D. K., Wu, D. C., Naini, A., Hunot, S., Vila, M., Jackson-Lewis, V., and Przedborski, S. (2003) Cyclooxygenase-2 is instrumental in Parkinson's disease neurodegeneration. *Proc Natl Acad Sci U S A*, 100, 5473-5478.
- (137) Dong, L., Vecchio, A. J., Sharma, N. P., Jurban, B. J., Malkowski, M. G., and Smith, W. L. (2011) Human cyclooxygenase-2 is a sequence homodimer that functions as a conformational heterodimer. *J Biol Chem*, 286, 19035-19046.
- (138) Prusakiewicz, J. J., Duggan, K. C., Rouzer, C. A., and Marnett, L. J. (2009) Differential sensitivity and mechanism of inhibition of COX-2 oxygenation of arachidonic acid and 2-arachidonoylglycerol by ibuprofen and mefenamic acid. *Biochemistry*, 48, 7353-7355.
- (139) Schneider, C., Boeglin, W. E., and Brash, A. R. (2004) Identification of two cyclooxygenase active site residues, Leucine 384 and Glycine 526, that control carbon ring cyclization in prostaglandin biosynthesis. *J Biol Chem*, 279, 4404-4414.
- (140) Schneider, C., and Brash, A. R. (2000) Stereospecificity of hydrogen abstraction in the conversion of arachidonic acid to 15R-HETE by aspirin-

treated cyclooxygenase-2. Implications for the alignment of substrate in the active site. *J Biol Chem*, 275, 4743-4746.

- (141) Malkowski, M. G., Ginell, S. L., Smith, W. L., and Garavito, R. M. (2000) The productive conformation of arachidonic acid bound to prostaglandin synthase. *Science*, 289, 1933-1937.
- (142) Rowlinson, S. W., Crews, B. C., Lanzo, C. A., and Marnett, L. J. (1999) The binding of arachidonic acid in the cyclooxygenase active site of mouse prostaglandin endoperoxide synthase-2 (COX-2). A putative L-shaped binding conformation utilizing the top channel region. *J Biol Chem*, 274, 23305-23310.
- (143) Kiefer, J. R., Pawlitz, J. L., Moreland, K. T., Stegeman, R. A., Hood, W. F., Gierse, J. K., Stevens, A. M., Goodwin, D. C., Rowlinson, S. W., Marnett, L. J., Stallings, W. C., and Kurumbail, R. G. (2000) Structural insights into the stereochemistry of the cyclooxygenase reaction. *Nature*, 405, 97-101.
- (144) Smith, W. L., and Lands, W. E. (1972) Oxygenation of unsaturated fatty acids by soybean lipoxygenase. *J Biol Chem*, 247, 1038-1047.
- (145) Losito, I., Conte, E., Introna, B., Megli, F. M., and Palmisano, F. (2011) Improved specificity of cardiolipin peroxidation by soybean lipoxygenase: a liquid chromatography - electrospray ionization mass spectrometry investigation. *Journal of mass spectrometry : JMS*, 46, 1255-1262.
- (146) Berger, W., De Chandt, M. T., and Cairns, C. B. (2007) Zileuton: clinical implications of 5-Lipoxygenase inhibition in severe airway disease. *International journal of clinical practice*, 61, 663-676.
- (147) Karelina, T. A., Zhudenkov, K. V., Demin, O. O., Svetlichny, D. V., Agoram, B., Fairman, D., and Demin, O. V. (2012) Regulation of leukotriene and 5oxoETE synthesis and the effect of 5-lipoxygenase inhibitors: a mathematical modeling approach. *BMC Syst Biol*, 6, 141.
- (148) Fischer, L., Hornig, M., Pergola, C., Meindl, N., Franke, L., Tanrikulu, Y., Dodt, G., Schneider, G., Steinhilber, D., and Werz, O. (2007) The molecular mechanism of the inhibition by licofelone of the biosynthesis of 5-lipoxygenase products. *Br J Pharmacol*, 152, 471-480.
- (149) Kenyon, V., Rai, G., Jadhav, A., Schultz, L., Armstrong, M., Jameson, J. B., 2nd, Perry, S., Joshi, N., Bougie, J. M., Leister, W., Taylor-Fishwick, D. A., Nadler, J. L., Holinstat, M., Simeonov, A., Maloney, D. J., and Holman, T. R. (2011) Discovery of potent and selective inhibitors of human platelet-type 12- lipoxygenase. *J Med Chem*, 54, 5485-5497.
- (150) Rai, G., Kenyon, V., Jadhav, A., Schultz, L., Armstrong, M., Jameson, J. B., Hoobler, E., Leister, W., Simeonov, A., Holman, T. R., and Maloney, D.



- J. (2010) Discovery of potent and selective inhibitors of human reticulocyte 15-lipoxygenase-1. *J Med Chem*, 53, 7392-7404.
- (151) Mikuni, M., Yoshida, M., Hellberg, P., Peterson, C. A., Edwin, S. S., Brannstrom, M., and Peterson, C. M. (1998) The lipoxygenase inhibitor, nordihydroguaiaretic acid, inhibits ovulation and reduces leukotriene and prostaglandin levels in the rat ovary. *Biol Reprod*, 58, 1211-1216.
- (152) Doderer, A., Kokkelink, I., van der Veen, S., Valk, B. E., Schram, A. W., and Douma, A. C. (1992) Purification and characterization of two lipoxygenase isoenzymes from germinating barley. *Biochim Biophys Acta*, 1120, 97-104.
- (153) Schneider, C., and Pozzi, A. (2011) Cyclooxygenases and lipoxygenases in cancer. *Cancer metastasis reviews*, 30, 277-294.
- (154) Boyington, J. C., Gaffney, B. J., and Amzel, L. M. (1997) The three-dimensional structure of soybean lipoxygenase-1: an arachidonic acid 15-lipoxygenase. *Advances in experimental medicine and biology*, 400A, 133-138.
- (155) Gardner, H. W. (1989) Soybean lipoxygenase-1 enzymically forms both (9S)- and (13S)-hydroperoxides from linoleic acid by a pH-dependent mechanism. *Biochim Biophys Acta*, 1001, 274-281.
- (156) Mulliez, E., Leblanc, J. P., Girerd, J. J., Rigaud, M., and Chottard, J. C. (1987) 5-Lipoxygenase from Potato-Tubers - Improved Purification and Physicochemical Characteristics. *Biochim Biophys Acta*, 916, 13-23.
- (157) Soumya, S. J., Binu, S., Helen, A., Anil Kumar, K., Reddanna, P., and Sudhakaran, P. R. (2012) Effect of 15-lipoxygenase metabolites on angiogenesis: 15(S)-HPETE is angiostatic and 15(S)-HETE is angiogenic. *Inflammation research : official journal of the European Histamine Research Society ... [et al.]*, 61, 707-718.
- (158) Sauer, L. A., Dauchy, R. T., Blask, D. E., Armstrong, B. J., and Scalici, S. (1999) 13-Hydroxyoctadecadienoic acid is the mitogenic signal for linoleic acid-dependent growth in rat hepatoma 7288CTC in vivo. *Cancer Res*, 59, 4688-4692.
- (159) Samuelsson, B. (1983) Leukotrienes: mediators of immediate hypersensitivity reactions and inflammation. *Science*, 220, 568-575.
- (160) Haeggstrom, J. Z., and Funk, C. D. (2011) Lipoxygenase and leukotriene pathways: biochemistry, biology, and roles in disease. *Chem Rev*, 111, 5866-5898.

- (161) Schaloske, R. H., and Dennis, E. A. (2006) The phospholipase A2 superfamily and its group numbering system. *Biochim Biophys Acta*, 1761, 1246-1259.
- (162) Dixon, R. A., Diehl, R. E., Opas, E., Rands, E., Vickers, P. J., Evans, J. F., Gillard, J. W., and Miller, D. K. (1990) Requirement of a 5-lipoxygenase-activating protein for leukotriene synthesis. *Nature*, 343, 282-284.
- (163) Evans, J. F., Ferguson, A. D., Mosley, R. T., and Hutchinson, J. H. (2008) What's all the FLAP about?: 5-lipoxygenase-activating protein inhibitors for inflammatory diseases. *Trends Pharmacol Sci*, 29, 72-78.
- (164) Rouzer, C. A., Matsumoto, T., and Samuelsson, B. (1986) Single protein from human leukocytes possesses 5-lipoxygenase and leukotriene A4 synthase activities. *Proc Natl Acad Sci U S A*, 83, 857-861.
- (165) Shimizu, T., Izumi, T., Seyama, Y., Tadokoro, K., Radmark, O., and Samuelsson, B. (1986) Characterization of leukotriene A4 synthase from murine mast cells: evidence for its identity to arachidonate 5-lipoxygenase. *Proc Natl Acad Sci U S A*, 83, 4175-4179.
- (166) Borgeat, P., and Samuelsson, B. (1979) Arachidonic acid metabolism in polymorphonuclear leukocytes: unstable intermediate in formation of dihydroxy acids. *Proc Natl Acad Sci U S A*, 76, 3213-3217.
- (167) Lam, B. K., and Austen, K. F. (2002) Leukotriene C4 synthase: a pivotal enzyme in cellular biosynthesis of the cysteinyl leukotrienes. *Prostaglandins & other lipid mediators*, 68-69, 511-520.
- (168) Lee, C. W., Lewis, R. A., Corey, E. J., and Austen, K. F. (1983) Conversion of leukotriene D4 to leukotriene E4 by a dipeptidase released from the specific granule of human polymorphonuclear leucocytes. *Immunology*, 48, 27-35.
- (169) Dahlen, S. E., Bjork, J., Hedqvist, P., Arfors, K. E., Hammarstrom, S., Lindgren, J. A., and Samuelsson, B. (1981) Leukotrienes promote plasma leakage and leukocyte adhesion in postcapillary venules: in vivo effects with relevance to the acute inflammatory response. *Proc Natl Acad Sci U S A*, 78, 3887-3891.
- (170) Klickstein, L. B., Shapleigh, C., and Goetzel, E. J. (1980) Lipoxygenation of arachidonic acid as a source of polymorphonuclear leukocyte chemotactic factors in synovial fluid and tissue in rheumatoid arthritis and spondyloarthritis. *The Journal of clinical investigation*, 66, 1166-1170.
- (171) Laursen, L. S., Naesdal, J., Bukhave, K., Lauritsen, K., and Rask-Madsen, J. (1990) Selective 5-lipoxygenase inhibition in ulcerative colitis. *Lancet*, 335, 683-685.

- (172) Israel, E., Dermarkarian, R., Rosenberg, M., Sperling, R., Taylor, G., Rubin, P., and Drazen, J. M. (1990) The effects of a 5-lipoxygenase inhibitor on asthma induced by cold, dry air. *The New England journal of medicine*, 323, 1740-1744.
- (173) Drazen, J. M., Israel, E., and O'Byrne, P. M. (1999) Treatment of asthma with drugs modifying the leukotriene pathway. *The New England journal of medicine*, 340, 197-206.
- (174) Esterbauer, H., Schaur, R. J., and Zollner, H. (1991) Chemistry and biochemistry of 4-hydroxynonenal, malonaldehyde and related aldehydes. *Free Radic Biol Med*, 11, 81-128.
- (175) Zhu, P., Jian, W., and Blair, I. A. (2009) A 4-oxo-2(E)-nonenal-derived glutathione adduct from 15-lipoxygenase-1-mediated oxidation of cytosolic and esterified arachidonic acid. *Free Radic Biol Med*, 47, 953-961.
- (176) Jian, W., Lee, S. H., Mesaros, C., Oe, T., Elipe, M. V., and Blair, I. A. (2007) A novel 4-oxo-2(E)-nonenal-derived endogenous thiadiazabicyclo glutathione adduct formed during cellular oxidative stress. *Chem Res Toxicol*, 20, 1008-1018.
- (177) Lee, S. H., Rangiah, K., Williams, M. V., Wehr, A. Y., DuBois, R. N., and Blair, I. A. (2007) Cyclooxygenase-2-mediated metabolism of arachidonic acid to 15-oxo-eicosatetraenoic acid by rat intestinal epithelial cells. *Chem Res Toxicol*, 20, 1665-1675.
- (178) Griesser, M., Boeglin, W. E., Suzuki, T., and Schneider, C. (2009) Convergence of the 5-LOX and COX-2 pathways: heme-catalyzed cleavage of the 5S-HETE-derived di-endoperoxide into aldehyde fragments. *J Lipid Res*, 50, 2455-2462.
- (179) Rindgen, D., Nakajima, M., Wehrli, S., Xu, K., and Blair, I. A. (1999) Covalent modifications to 2'-deoxyguanosine by 4-oxo-2-nonenal, a novel product of lipid peroxidation. *Chem Res Toxicol*, 12, 1195-1204.
- (180) Zhu, X., Tang, X., Anderson, V. E., and Sayre, L. M. (2009) Mass spectrometric characterization of protein modification by the products of nonenzymatic oxidation of linoleic acid. *Chem Res Toxicol*, 22, 1386-1397.
- (181) Lee, S. H., and Blair, I. A. (2000) Characterization of 4-oxo-2-nonenal as a novel product of lipid peroxidation. *Chem Res Toxicol*, 13, 698-702.
- (182) Gu, X., Zhang, W., and Salomon, R. G. (2007) Fe<sup>2+</sup> catalyzes vitamin E-induced fragmentation of hydroperoxy and hydroxy endoperoxides that generates gamma-hydroxy alkenals. *J Am Chem Soc*, 129, 6088-6089.

- (183) Lee, S. H., Oe, T., and Blair, I. A. (2001) Vitamin C-induced decomposition of lipid hydroperoxides to endogenous genotoxins. *Science*, 292, 2083-2086.
- (184) Liu, W., Porter, N., Schneider, C., Brash, A., and Yin, H. (2011) Formation of 4-hydroxynonenal from cardiolipin oxidation: intramolecular peroxy radical addition and decomposition. *Free Radic Biol Med*, 50, 166-178.
- (185) Hill, S., Lamberson, C. R., Xu, L., To, R., Tsui, H. S., Shmanai, V. V., Bekish, A. V., Awad, A. M., Marbois, B. N., Cantor, C. R., Porter, N. A., Clarke, C. F., and Shchepinov, M. S. (2012) Small amounts of isotope-reinforced polyunsaturated fatty acids suppress lipid autoxidation. *Free Radic Biol Med*, 53, 893-906.
- (186) Lamberson, C. R., Xu, L., Muchalski, H., Montenegro-Burke, J. R., Shmanai, V. V., Bekish, A. V., McLean, J. A., Clarke, C. F., Shchepinov, M. S., and Porter, N. A. (2014) Unusual kinetic isotope effects of deuterium reinforced polyunsaturated fatty acids in tocopherol-mediated free radical chain oxidations. *J Am Chem Soc*, 136, 838-841.
- (187) Yin, H., Vergeade, A., Shi, Q., Zackert, W. E., Gruenberg, K. C., Bokiej, M., Amin, T., Ying, W., Masterson, T. S., Zinkel, S. S., Oates, J. A., Boutaud, O., and Roberts, L. J., 2nd. (2012) Acetaminophen inhibits cytochrome c redox cycling induced lipid peroxidation. *Biochem Biophys Res Commun*, 423, 224-228.
- (188) Wei, C., Zhu, P., Shah, S. J., and Blair, I. A. (2009) 15-oxo-Eicosatetraenoic acid, a metabolite of macrophage 15-hydroxyprostaglandin dehydrogenase that inhibits endothelial cell proliferation. *Mol Pharmacol*, 76, 516-525.
- (189) Bronstein, J. C., and Bull, A. W. (1997) Substrate specificity and characterization of partially purified rat liver 13-hydroxyoctadecadienoic acid (13-HODE) dehydrogenase. *Arch Biochem Biophys*, 348, 219-225.
- (190) Hammond, V. J., Morgan, A. H., Lauder, S., Thomas, C. P., Brown, S., Freeman, B. A., Lloyd, C. M., Davies, J., Bush, A., Levonen, A. L., Kansanen, E., Villacorta, L., Chen, Y. E., Porter, N., Garcia-Diaz, Y. M., Schopfer, F. J., and O'Donnell, V. B. (2012) Novel keto-phospholipids are generated by monocytes and macrophages, detected in cystic fibrosis, and activate peroxisome proliferator-activated receptor-gamma. *J Biol Chem*, 287, 41651-41666.
- (191) Tyurina, Y. Y., Poloyac, S. M., Tyurin, V. A., Kapralov, A. A., Jiang, J., Anthonymuthu, T. S., Kapralova, V. I., Vikulina, A. S., Jung, M. Y., Epperly, M. W., Mohammadyani, D., Klein-Seetharaman, J., Jackson, T. C., Kochanek, P. M., Pitt, B. R., Greenberger, J. S., Vladimirov, Y. A.,

- Bayir, H., and Kagan, V. E. (2014) A mitochondrial pathway for biosynthesis of lipid mediators. *Nature chemistry*, 6, 542-552.
- (192) Milne, G. L., Yin, H., Hardy, K. D., Davies, S. S., and Roberts, L. J., 2nd. (2011) Isoprostane generation and function. *Chem Rev*, 111, 5973-5996.
- (193) Salomon, R. G., Miller, D. B., Zagorski, M. G., and Coughlin, D. J. (1984) Prostaglandin Endoperoxides Solvent-Induced Fragmentation of Prostaglandin Endoperoxides - New Aldehyde Products from Pgh2 and a Novel Intramolecular 1,2-Hydride Shift during Endoperoxide Fragmentation in Aqueous-Solution. *J Am Chem Soc*, 106, 6049-6060.
- (194) Boutaud, O., Li, J., Zagol, I., Shipp, E. A., Davies, S. S., Roberts, L. J., 2nd, and Oates, J. A. (2003) Levuglandinyl adducts of proteins are formed via a prostaglandin H2 synthase-dependent pathway after platelet activation. *J Biol Chem*, 278, 16926-16928.
- (195) Brame, C. J., Salomon, R. G., Morrow, J. D., and Roberts, L. J., 2nd. (1999) Identification of extremely reactive gamma-ketoaldehydes (isolevuglandins) as products of the isoprostane pathway and characterization of their lysyl protein adducts. *J Biol Chem*, 274, 13139-13146.
- (196) Fitzpatrick, F. A., and Wynalda, M. A. (1983) Albumin-catalyzed metabolism of prostaglandin D2. Identification of products formed in vitro. *J Biol Chem*, 258, 11713-11718.
- (197) Shibata, T., Kondo, M., Osawa, T., Shibata, N., Kobayashi, M., and Uchida, K. (2002) 15-deoxy-delta 12,14-prostaglandin J2. A prostaglandin D2 metabolite generated during inflammatory processes. *J Biol Chem*, 277, 10459-10466.
- (198) Chen, Y., Morrow, J. D., and Roberts, L. J., 2nd. (1999) Formation of reactive cyclopentenone compounds in vivo as products of the isoprostane pathway. *J Biol Chem*, 274, 10863-10868.
- (199) Shimozu, Y., Shibata, T., Ojika, M., and Uchida, K. (2009) Identification of advanced reaction products originating from the initial 4-oxo-2-nonenal-cysteine Michael adducts. *Chem Res Toxicol*, 22, 957-964.
- (200) Doorn, J. A., and Petersen, D. R. (2002) Covalent modification of amino acid nucleophiles by the lipid peroxidation products 4-hydroxy-2-nonenal and 4-oxo-2-nonenal. *Chem Res Toxicol*, 15, 1445-1450.
- (201) Hashimoto, M., Sibata, T., Wasada, H., Toyokuni, S., and Uchida, K. (2003) Structural basis of protein-bound endogenous aldehydes. Chemical and immunochemical characterizations of configurational isomers of a 4-hydroxy-2-nonenal-histidine adduct. *J Biol Chem*, 278, 5044-5051.

- (202) Oe, T., Lee, S. H., Silva Elipe, M. V., Arison, B. H., and Blair, I. A. (2003) A novel lipid hydroperoxide-derived modification to arginine. *Chem Res Toxicol*, *16*, 1598-1605.
- (203) Schopfer, F. J., Cipollina, C., and Freeman, B. A. (2011) Formation and signaling actions of electrophilic lipids. *Chem Rev*, *111*, 5997-6021.
- (204) Codreanu, S. G., Ullery, J. C., Zhu, J., Tallman, K. A., Beavers, W. N., Porter, N. A., Marnett, L. J., Zhang, B., and Liebler, D. C. (2014) Alkylation damage by lipid electrophiles targets functional protein systems. *Molecular & cellular proteomics : MCP*, *13*, 849-859.
- (205) Sayre, L. M., Lin, D., Yuan, Q., Zhu, X., and Tang, X. (2006) Protein adducts generated from products of lipid oxidation: focus on HNE and one. *Drug Metab Rev*, *38*, 651-675.
- (206) Boutaud, O., Brame, C. J., Salomon, R. G., Roberts, L. J., 2nd, and Oates, J. A. (1999) Characterization of the lysyl adducts formed from prostaglandin H2 via the levuglandin pathway. *Biochemistry*, *38*, 9389-9396.
- (207) Zagol-Ikapitte, I., Amarnath, V., Bala, M., Roberts, L. J., 2nd, Oates, J. A., and Boutaud, O. (2010) Characterization of scavengers of gamma-ketoaldehydes that do not inhibit prostaglandin biosynthesis. *Chem Res Toxicol*, *23*, 240-250.
- (208) Zhu, X., and Sayre, L. M. (2007) Long-lived 4-oxo-2-enal-derived apparent lysine michael adducts are actually the isomeric 4-ketoamides. *Chem Res Toxicol*, *20*, 165-170.
- (209) Zhang, W. H., Liu, J., Xu, G., Yuan, Q., and Sayre, L. M. (2003) Model studies on protein side chain modification by 4-oxo-2-nonenal. *Chem Res Toxicol*, *16*, 512-523.
- (210) Liu, Q., Ullery, J., Zhu, J., Liebler, D. C., Marnett, L. J., and Zhang, B. (2013) RNA-seq data analysis at the gene and CDS levels provides a comprehensive view of transcriptome responses induced by 4-hydroxynonenal. *Molecular bioSystems*, *9*, 3036-3046.
- (211) West, J. D., and Marnett, L. J. (2005) Alterations in gene expression induced by the lipid peroxidation product, 4-hydroxy-2-nonenal. *Chem Res Toxicol*, *18*, 1642-1653.
- (212) Luckey, S. W., Taylor, M., Sampey, B. P., Scheinman, R. I., and Petersen, D. R. (2002) 4-hydroxynonenal decreases interleukin-6 expression and protein production in primary rat Kupffer cells by inhibiting nuclear factor-kappaB activation. *The Journal of pharmacology and experimental therapeutics*, *302*, 296-303.

- (213) Ji, C., Kozak, K. R., and Marnett, L. J. (2001) I $\kappa$ B kinase, a molecular target for inhibition by 4-hydroxy-2-nonenal. *J Biol Chem*, 276, 18223-18228.
- (214) Marantos, C., Mukaro, V., Ferrante, J., Hii, C., and Ferrante, A. (2008) Inhibition of the lipopolysaccharide-induced stimulation of the members of the MAPK family in human monocytes/macrophages by 4-hydroxynonenal, a product of oxidized omega-6 fatty acids. *Am J Pathol*, 173, 1057-1066.
- (215) Straus, D. S., Pascual, G., Li, M., Welch, J. S., Ricote, M., Hsiang, C. H., Sengchanthalangsy, L. L., Ghosh, G., and Glass, C. K. (2000) 15-deoxy-delta 12,14-prostaglandin J2 inhibits multiple steps in the NF-kappa B signaling pathway. *Proc Natl Acad Sci U S A*, 97, 4844-4849.
- (216) Rossi, A., Kapahi, P., Natoli, G., Takahashi, T., Chen, Y., Karin, M., and Santoro, M. G. (2000) Anti-inflammatory cyclopentenone prostaglandins are direct inhibitors of I $\kappa$ B kinase. *Nature*, 403, 103-108.
- (217) Musiek, E. S., Brooks, J. D., Joo, M., Brunoldi, E., Porta, A., Zanoni, G., Vidari, G., Blackwell, T. S., Montine, T. J., Milne, G. L., McLaughlin, B., and Morrow, J. D. (2008) Electrophilic cyclopentenone neuroprostanes are anti-inflammatory mediators formed from the peroxidation of the omega-3 polyunsaturated fatty acid docosahexaenoic acid. *J Biol Chem*, 283, 19927-19935.
- (218) Cernuda-Morollon, E., Pineda-Molina, E., Canada, F. J., and Perez-Sala, D. (2001) 15-Deoxy-Delta 12,14-prostaglandin J2 inhibition of NF-kappaB-DNA binding through covalent modification of the p50 subunit. *J Biol Chem*, 276, 35530-35536.
- (219) Stavrovskaya, I. G., Baranov, S. V., Guo, X., Davies, S. S., Roberts, L. J., 2nd, and Kristal, B. S. (2010) Reactive gamma-ketoaldehydes formed via the isoprostane pathway disrupt mitochondrial respiration and calcium homeostasis. *Free Radic Biol Med*, 49, 567-579.
- (220) Shibata, T., Iio, K., Kawai, Y., Shibata, N., Kawaguchi, M., Toi, S., Kobayashi, M., Kobayashi, M., Yamamoto, K., and Uchida, K. (2006) Identification of a lipid peroxidation product as a potential trigger of the p53 pathway. *J Biol Chem*, 281, 1196-1204.
- (221) West, J. D., Ji, C., Duncan, S. T., Amarnath, V., Schneider, C., Rizzo, C. J., Brash, A. R., and Marnett, L. J. (2004) Induction of apoptosis in colorectal carcinoma cells treated with 4-hydroxy-2-nonenal and structurally related aldehydic products of lipid peroxidation. *Chem Res Toxicol*, 17, 453-462.

- (222) Kondo, M., Shibata, T., Kumagai, T., Osawa, T., Shibata, N., Kobayashi, M., Sasaki, S., Iwata, M., Noguchi, N., and Uchida, K. (2002) 15-Deoxy-Delta(12,14)-prostaglandin J(2): the endogenous electrophile that induces neuronal apoptosis. *Proc Natl Acad Sci U S A*, *99*, 7367-7372.
- (223) Shibata, T., Yamada, T., Kondo, M., Tanahashi, N., Tanaka, K., Nakamura, H., Masutani, H., Yodoi, J., and Uchida, K. (2003) An endogenous electrophile that modulates the regulatory mechanism of protein turnover: inhibitory effects of 15-deoxy-Delta 12,14-prostaglandin J2 on proteasome. *Biochemistry*, *42*, 13960-13968.
- (224) Codreanu, S. G., Zhang, B., Sobocki, S. M., Billheimer, D. D., and Liebler, D. C. (2009) Global analysis of protein damage by the lipid electrophile 4-hydroxy-2-nonenal. *Molecular & cellular proteomics : MCP*, *8*, 670-680.
- (225) Ishii, T., Sakurai, T., Usami, H., and Uchida, K. (2005) Oxidative modification of proteasome: identification of an oxidation-sensitive subunit in 26 S proteasome. *Biochemistry*, *44*, 13893-13901.
- (226) Toyoda, K., Nagae, R., Akagawa, M., Ishino, K., Shibata, T., Ito, S., Shibata, N., Yamamoto, T., Kobayashi, M., Takasaki, Y., Matsuda, T., and Uchida, K. (2007) Protein-bound 4-hydroxy-2-nonenal: an endogenous triggering antigen of anti-DNA response. *J Biol Chem*, *282*, 25769-25778.
- (227) Miyashita, H., Chikazawa, M., Otaki, N., Hioki, Y., Shimozu, Y., Nakashima, F., Shibata, T., Hagihara, Y., Maruyama, S., Matsumi, N., and Uchida, K. (2014) Lysine pyrrolation is a naturally-occurring covalent modification involved in the production of DNA mimic proteins. *Sci Rep*, *4*, 5343.
- (228) Davies, S. S., Amarnath, V., Montine, K. S., Bernoud-Hubac, N., Boutaud, O., Montine, T. J., and Roberts, L. J., 2nd. (2002) Effects of reactive gamma-ketoaldehydes formed by the isoprostane pathway (isoketals) and cyclooxygenase pathway (levuglandins) on proteasome function. *FASEB journal : official publication of the Federation of American Societies for Experimental Biology*, *16*, 715-717.
- (229) Shibata, T., Shimozu, Y., Wakita, C., Shibata, N., Kobayashi, M., Machida, S., Kato, R., Itabe, H., Zhu, X., Sayre, L. M., and Uchida, K. (2011) Lipid peroxidation modification of protein generates Nepsilon-(4-oxononanyl)lysine as a pro-inflammatory ligand. *J Biol Chem*, *286*, 19943-19957.
- (230) Kumagai, T., Matsukawa, N., Kaneko, Y., Kusumi, Y., Mitsumata, M., and Uchida, K. (2004) A lipid peroxidation-derived inflammatory mediator: identification of 4-hydroxy-2-nonenal as a potential inducer of cyclooxygenase-2 in macrophages. *J Biol Chem*, *279*, 48389-48396.



- (231) Uchida, K., and Kumagai, T. (2003) 4-hydroxy-2-nonenal as a COX-2 inducer. *Mol Aspects Med*, 24, 213-218.
- (232) Brunoldi, E. M., Zanoni, G., Vidari, G., Sasi, S., Freeman, M. L., Milne, G. L., and Morrow, J. D. (2007) Cyclopentenone prostaglandin, 15-deoxy-Delta12,14-PGJ2, is metabolized by HepG2 cells via conjugation with glutathione. *Chem Res Toxicol*, 20, 1528-1535.
- (233) Aldini, G., Vistoli, G., Regazzoni, L., Gamberoni, L., Facino, R. M., Yamaguchi, S., Uchida, K., and Carini, M. (2008) Albumin is the main nucleophilic target of human plasma: a protective role against pro-atherogenic electrophilic reactive carbonyl species? *Chem Res Toxicol*, 21, 824-835.
- (234) Diers, A. R., Higdon, A. N., Ricart, K. C., Johnson, M. S., Agarwal, A., Kalyanaraman, B., Landar, A., and Darley-Usmar, V. M. (2010) Mitochondrial targeting of the electrophilic lipid 15-deoxy-Delta12,14-prostaglandin J2 increases apoptotic efficacy via redox cell signalling mechanisms. *The Biochemical journal*, 426, 31-41.
- (235) Szapacs, M. E., Riggins, J. N., Zimmerman, L. J., and Liebler, D. C. (2006) Covalent adduction of human serum albumin by 4-hydroxy-2-nonenal: kinetic analysis of competing alkylation reactions. *Biochemistry*, 45, 10521-10528.
- (236) Ishii, T., Tatsuda, E., Kumazawa, S., Nakayama, T., and Uchida, K. (2003) Molecular basis of enzyme inactivation by an endogenous electrophile 4-hydroxy-2-nonenal: identification of modification sites in glyceraldehyde-3-phosphate dehydrogenase. *Biochemistry*, 42, 3474-3480.
- (237) Fukuda, A., Osawa, T., Hitomi, K., and Uchida, K. (1996) 4-Hydroxy-2-nonenal cytotoxicity in renal proximal tubular cells: protein modification and redox alteration. *Arch Biochem Biophys*, 333, 419-426.
- (238) Connor, R. E., Marnett, L. J., and Liebler, D. C. (2011) Protein-selective capture to analyze electrophile adduction of hsp90 by 4-hydroxynonenal. *Chem Res Toxicol*, 24, 1275-1282.
- (239) Isom, A. L., Barnes, S., Wilson, L., Kirk, M., Coward, L., and Darley-Usmar, V. (2004) Modification of Cytochrome c by 4-hydroxy-2-nonenal: evidence for histidine, lysine, and arginine-aldehyde adducts. *J Am Soc Mass Spectrom*, 15, 1136-1147.
- (240) Galligan, J. J., Fritz, K. S., Backos, D. S., Shearn, C. T., Smathers, R. L., Jiang, H., MacLean, K. N., Reigan, P. R., and Petersen, D. R. (2014) Oxidative stress-mediated aldehyde adduction of GRP78 in a mouse model of alcoholic liver disease: functional independence of ATPase activity and chaperone function. *Free Radic Biol Med*, 73, 411-420.

- (241) Fritz, K. S., Galligan, J. J., Smathers, R. L., Roede, J. R., Shearn, C. T., Reigan, P., and Petersen, D. R. (2011) 4-Hydroxynonenal inhibits SIRT3 via thiol-specific modification. *Chem Res Toxicol*, 24, 651-662.
- (242) Aluise, C. D., Rose, K., Boiani, M., Reyzer, M. L., Manna, J. D., Tallman, K., Porter, N. A., and Marnett, L. J. (2013) Peptidyl-prolyl cis/trans-isomerase A1 (Pin1) is a target for modification by lipid electrophiles. *Chem Res Toxicol*, 26, 270-279.
- (243) Landar, A., Zmijewski, J. W., Dickinson, D. A., Le Goffe, C., Johnson, M. S., Milne, G. L., Zanoni, G., Vidari, G., Morrow, J. D., and Darley-Usmar, V. M. (2006) Interaction of electrophilic lipid oxidation products with mitochondria in endothelial cells and formation of reactive oxygen species. *American journal of physiology. Heart and circulatory physiology*, 290, H1777-1787.
- (244) Shibata, T., Yamada, T., Ishii, T., Kumazawa, S., Nakamura, H., Masutani, H., Yodoi, J., and Uchida, K. (2003) Thioredoxin as a molecular target of cyclopentenone prostaglandins. *J Biol Chem*, 278, 26046-26054.
- (245) Mirzaei, H., and Regnier, F. (2005) Affinity chromatographic selection of carbonylated proteins followed by identification of oxidation sites using tandem mass spectrometry. *Anal Chem*, 77, 2386-2392.
- (246) Weerapana, E., Wang, C., Simon, G. M., Richter, F., Khare, S., Dillon, M. B., Bachovchin, D. A., Mowen, K., Baker, D., and Cravatt, B. F. (2010) Quantitative reactivity profiling predicts functional cysteines in proteomes. *Nature*, 468, 790-795.
- (247) Rostovtsev, V. V., Green, L. G., Fokin, V. V., and Sharpless, K. B. (2002) A stepwise Huisgen cycloaddition process: copper(I)-catalyzed regioselective "ligation" of azides and terminal alkynes. *Angewandte Chemie*, 41, 2596-2599.
- (248) Vila, A., Tallman, K., Jacobs, A., Liebler, D., Porter, N., and Marnett, L. (2008) Identification of protein targets of 4-hydroxynonenal using click chemistry for ex vivo biotinylation of azido and alkynyl derivatives. *Chem Res Toxicol*, 21, 432-444.
- (249) Kim, H., Tallman, K., Liebler, D., and Porter, N. (2009) An Azido-Biotin Reagent for Use in the Isolation of Protein Adducts of Lipid-derived Electrophiles by Streptavidin Catch and Photorelease. *Molecular & cellular proteomics : MCP*, 8, 2080-2089.
- (250) Dasari, S., Chambers, M. C., Codreanu, S. G., Liebler, D. C., Collins, B. C., Pennington, S. R., Gallagher, W. M., and Tabb, D. L. (2011) Sequence tagging reveals unexpected modifications in toxicoproteomics. *Chem Res Toxicol*, 24, 204-216.

- (251) Cummins, T. D., Higdon, A. N., Kramer, P. A., Chacko, B. K., Riggs, D. W., Salabei, J. K., Dell'Italia, L. J., Zhang, J., Darley-Usmar, V. M., and Hill, B. G. (2013) Utilization of fluorescent probes for the quantification and identification of subcellular proteomes and biological processes regulated by lipid peroxidation products. *Free Radic Biol Med*, 59, 56-68.
- (252) Szapacs, M. E., Kim, H. Y., Porter, N. A., and Liebler, D. C. (2008) Identification of proteins adducted by lipid peroxidation products in plasma and modifications of apolipoprotein A1 with a novel biotinylated phospholipid probe. *J Proteome Res*, 7, 4237-4246.
- (253) Itakura, A., Kurauchi, O., Takashima, S., Uchida, K., Ito, M., and Mizutani, S. (2002) Immunological detection of 4-hydroxynonenal protein adducts in developing pontine and Purkinje neurons and in karyorrhexis in pontosubicular neuronal necrosis. *Early Hum Dev*, 67, 19-28.
- (254) Shibata, N., Toi, S., Shibata, T., Uchida, K., Itabe, H., Sawada, T., Kawamata, T., Okada, Y., Uchiyama, S., and Kobayashi, M. (2009) Immunohistochemical detection of 13(R)-hydroxyoctadecadienoic acid in atherosclerotic plaques of human carotid arteries using a novel specific antibody. *Acta Histochem Cytochem*, 42, 197-203.
- (255) Galligan, J. J., Smathers, R. L., Fritz, K. S., Epperson, L. E., Hunter, L. E., and Petersen, D. R. (2012) Protein carbonylation in a murine model for early alcoholic liver disease. *Chem Res Toxicol*, 25, 1012-1021.
- (256) Kirabo, A., Fontana, V., de Faria, A. P., Loperena, R., Galindo, C. L., Wu, J., Bikineyeva, A. T., Dikalov, S., Xiao, L., Chen, W., Saleh, M. A., Trott, D. W., Itani, H. A., Vinh, A., Amarnath, V., Amarnath, K., Guzik, T. J., Bernstein, K. E., Shen, X. Z., Shyr, Y., Chen, S. C., Mernaugh, R. L., Laffer, C. L., Eljovich, F., Davies, S. S., Moreno, H., Madhur, M. S., Roberts, J., 2nd, and Harrison, D. G. (2014) DC isoketal-modified proteins activate T cells and promote hypertension. *The Journal of clinical investigation*, 124, 4642-4656.
- (257) Davies, S. S., Talati, M., Wang, X., Mernaugh, R. L., Amarnath, V., Fessel, J., Meyrick, B. O., Sheller, J., and Roberts, L. J., 2nd. (2004) Localization of isoketal adducts in vivo using a single-chain antibody. *Free Radic Biol Med*, 36, 1163-1174.
- (258) Carbone, D. L., Doorn, J. A., Kiebler, Z., Ickes, B. R., and Petersen, D. R. (2005) Modification of heat shock protein 90 by 4-hydroxynonenal in a rat model of chronic alcoholic liver disease. *The Journal of pharmacology and experimental therapeutics*, 315, 8-15.
- (259) Grimsrud, P. A., Picklo, M. J., Sr., Griffin, T. J., and Bernlohr, D. A. (2007) Carbonylation of adipose proteins in obesity and insulin resistance:

identification of adipocyte fatty acid-binding protein as a cellular target of 4-hydroxynonenal. *Molecular & cellular proteomics : MCP*, 6, 624-637.

- (260) Soreghan, B. A., Yang, F., Thomas, S. N., Hsu, J., and Yang, A. J. (2003) High-throughput proteomic-based identification of oxidatively induced protein carbonylation in mouse brain. *Pharm Res*, 20, 1713-1720.
- (261) Zhao, Y., Miriyala, S., Miao, L., Mitov, M., Schnell, D., Dhar, S. K., Cai, J., Klein, J. B., Sultana, R., Butterfield, D. A., Vore, M., Batinic-Haberle, I., Bondada, S., and St Clair, D. K. (2014) Redox proteomic identification of HNE-bound mitochondrial proteins in cardiac tissues reveals a systemic effect on energy metabolism after doxorubicin treatment. *Free Radic Biol Med*, 72, 55-65.
- (262) Di Domenico, F., Sultana, R., Ferree, A., Smith, K., Barone, E., Perluigi, M., Coccia, R., Pierce, W., Cai, J., Mancuso, C., Squillace, R., Wiengeler, M., Dalle-Donne, I., Wolozin, B., and Butterfield, D. A. (2012) Redox proteomics analyses of the influence of co-expression of wild-type or mutated LRRK2 and Tau on *C. elegans* protein expression and oxidative modification: relevance to Parkinson disease. *Antioxid Redox Signal*, 17, 1490-1506.
- (263) Di Domenico, F., Pupo, G., Tramutola, A., Giorgi, A., Schinina, M. E., Coccia, R., Head, E., Butterfield, D. A., and Perluigi, M. (2014) Redox proteomics analysis of HNE-modified proteins in Down syndrome brain: clues for understanding the development of Alzheimer disease. *Free Radic Biol Med*, 71, 270-280.
- (264) Reed, T., Perluigi, M., Sultana, R., Pierce, W. M., Klein, J. B., Turner, D. M., Coccia, R., Markesbery, W. R., and Butterfield, D. A. (2008) Redox proteomic identification of 4-hydroxy-2-nonenal-modified brain proteins in amnesic mild cognitive impairment: insight into the role of lipid peroxidation in the progression and pathogenesis of Alzheimer's disease. *Neurobiol Dis*, 30, 107-120.
- (265) Quehenberger, O., Armando, A. M., Brown, A. H., Milne, S. B., Myers, D. S., Merrill, A. H., Bandyopadhyay, S., Jones, K. N., Kelly, S., Shaner, R. L., Sullards, C. M., Wang, E., Murphy, R. C., Barkley, R. M., Leiker, T. J., Rietz, C. R., Guan, Z., Laird, G. M., Six, D. A., Russell, D. W., McDonald, J. G., Subramaniam, S., Fahy, E., and Dennis, E. A. (2010) Lipidomics reveals a remarkable diversity of lipids in human plasma. *J Lipid Res*, 51, 3299-3305.
- (266) Andreou, A., and Feussner, I. (2009) Lipoxygenases - Structure and reaction mechanism. *Phytochemistry*, 70, 1504-1510.

- (267) Buczynski, M. W., Dumlao, D. S., and Dennis, E. A. (2009) Thematic Review Series: Proteomics. An integrated omics analysis of eicosanoid biology. *J Lipid Res*, 50, 1015-1038.
- (268) Coffa, G., Schneider, C., and Brash, A. R. (2005) A comprehensive model of positional and stereo control in lipoxygenases. *Biochem Biophys Res Commun*, 338, 87-92.
- (269) Davis, T. A., Gao, L., Yin, H., Morrow, J. D., and Porter, N. A. (2006) In vivo and in vitro lipid peroxidation of arachidonate esters: the effect of fish oil omega-3 lipids on product distribution. *J Am Chem Soc*, 128, 14897-14904.
- (270) Porter, N. A., and Wujek, D. G. (1984) Autoxidation of polyunsaturated fatty acids, an expanded mechanistic study. *J Am Chem Soc*, 106, 2626-2629.
- (271) Porter, N., Caldwell, S., and Mills, K. (1995) Mechanisms of free radical oxidation of unsaturated lipids. *Lipids*, 30, 277-290.
- (272) Esterbauer, H. (1996) Estimation of peroxidative damage. A critical review. *Pathologie-biologie*, 44, 25-28.
- (273) Esterbauer, H., and Cheeseman, K. H. (1990) Determination of aldehydic lipid peroxidation products: malonaldehyde and 4-hydroxynonenal. *Methods Enzymol*, 186, 407-421.
- (274) Esterbauer, H., and Zollner, H. (1989) Methods for determination of aldehydic lipid peroxidation products. *Free Radic Biol Med*, 7, 197-203.
- (275) Milne, S., Ivanova, P., Forrester, J., and Alex Brown, H. (2006) Lipidomics: an analysis of cellular lipids by ESI-MS. *Methods*, 39, 92-103.
- (276) Berliner, J. A., and Zimman, A. (2007) Future of toxicology--lipidomics, an important emerging area for toxicologists: focus on lipid oxidation products. *Chem Res Toxicol*, 20, 849-853.
- (277) Brown, H. A., and Murphy, R. C. (2009) Working towards an exegesis for lipids in biology. *Nat Chem Biol*, 5, 602-606.
- (278) Rouzer, C., Ivanova, P., Byrne, M., Milne, S., Marnett, L., and Brown, H. (2006) Lipid Profiling Reveals Arachidonate Deficiency in RAW264. 7 Cells: Structural and Functional Implications†. *Biochemistry*, 45, 14795-14808.
- (279) Myers, D. S., Ivanova, P. T., Milne, S. B., and Brown, H. A. (2011) Quantitative analysis of glycerophospholipids by LC-MS: acquisition, data handling, and interpretation. *Biochim Biophys Acta*, 1811, 748-757.

- (280) Milne, S., Tallman, K., Serwa, R., Rouzer, C., Armstrong, M., Marnett, L., Lukehart, C., Porter, N., and Brown, H. (2010) Capture and release of alkyne-derivatized glycerophospholipids using cobalt chemistry. *Nat Chem Biol*, *6*, 205-207.
- (281) Tallman, K., Armstrong, M., Milne, S., Marnett, L., Brown, H., and Porter, N. (2013) Cobalt carbonyl complexes as probes for alkyne-tagged lipids. *J Lipid Res*, *54*, 859-868.
- (282) Windsor, K., Genaro-Mattos, T., Kim, H., Liu, W., Tallman, K., Miyamoto, S., Korade, Z., and Porter, N. (2013) Probing lipid-protein adduction with alkynyl surrogates: application to Smith-Lemli-Opitz syndrome. *J Lipid Res*, *54*, 2842-2850.
- (283) Punta, C., Rector, C. L., and Porter, N. A. (2005) Peroxidation of polyunsaturated fatty acid methyl esters catalyzed by N-methyl benzohydroxamic acid: a new and convenient method for selective synthesis of hydroperoxides and alcohols. *Chem Res Toxicol*, *18*, 349-356.
- (284) Liu, W., Yin, H., Akazawa, Y. O., Yoshida, Y., Niki, E., and Porter, N. A. (2010) Ex vivo oxidation in tissue and plasma assays of hydroxyoctadecadienoates: Z,E/E,E stereoisomer ratios. *Chem Res Toxicol*, *23*, 986-995.
- (285) Van Harken, D., Dixon, C., and Heimberg, M. (1969) Hepatic lipid metabolism in experimental diabetes. *J Biol Chem*, *244*, 2278.
- (286) Raetz, C., Garrett, T., Reynolds, C., Shaw, W., Moore, J., Smith, D., Ribeiro, A., Murphy, R., Ulevitch, R., and Fearn, C. (2006) Kdo2-Lipid A of *Escherichia coli*, a defined endotoxin that activates macrophages via TLR-4. *J Lipid Res*, *47*, 1097.
- (287) Morrow, J. D. (2000) The isoprostanes: their quantification as an index of oxidant stress status in vivo. *Drug Metab Rev*, *32*, 377-385.
- (288) Morrow, J. D., Awad, J. A., Boss, H. J., Blair, I. A., and Roberts, L. J., 2nd. (1992) Non-cyclooxygenase-derived prostanoids (F2-isoprostanes) are formed in situ on phospholipids. *Proc Natl Acad Sci U S A*, *89*, 10721-10725.
- (289) Morrow, J. D., Minton, T. A., and Roberts, L. J., 2nd. (1992) The F2-isoprostane, 8-epi-prostaglandin F2 alpha, a potent agonist of the vascular thromboxane/endoperoxide receptor, is a platelet thromboxane/endoperoxide receptor antagonist. *Prostaglandins*, *44*, 155-163.

- (290) Morrow, J. D., and Roberts, L. J., 2nd. (1999) Mass spectrometric quantification of F2-isoprostanes in biological fluids and tissues as measure of oxidant stress. *Methods Enzymol*, 300, 3-12.
- (291) Yin, H., and Porter, N. A. (2005) New insights regarding the autoxidation of polyunsaturated fatty acids. *Antioxid Redox Signal*, 7, 170-184.
- (292) Schneider, C., Porter, N., and Brash, A. (2008) Routes to 4-hydroxynonenal: fundamental issues in the mechanisms of lipid peroxidation. *J Biol Chem*, 283, 15539-15543.
- (293) Roschek, B., Jr., Tallman, K. A., Rector, C. L., Gillmore, J. G., Pratt, D. A., Punta, C., and Porter, N. A. (2006) Peroxyl radical clocks. *J Org Chem*, 71, 3527-3532.
- (294) Porter, N., Logan, J., and Kontoyiannidou, V. (1979) Preparation and purification of arachidonic acid hydroperoxides of biological importance. *J Org Chem*, 44, 3177-3181.
- (295) Yin, H., Gao, L., Tai, H. H., Murphey, L. J., Porter, N. A., and Morrow, J. D. (2007) Urinary prostaglandin F2 $\alpha$  is generated from the isoprostane pathway and not the cyclooxygenase in humans. *J Biol Chem*, 282, 329-336.
- (296) Porter, N., and Nixon, J. (1978) Stereochemistry of free-radical substitution on the peroxide bond. *J Am Chem Soc*, 100, 7116-7117.
- (297) Zhang, J. Y., Prakash, C., Yamashita, K., and Blair, I. A. (1992) Regiospecific and enantioselective metabolism of 8,9-epoxyeicosatrienoic acid by cyclooxygenase. *Biochem Biophys Res Commun*, 183, 138-143.
- (298) Homma, T., Zhang, J. Y., Shimizu, T., Prakash, C., Blair, I. A., and Harris, R. C. (1993) Cyclooxygenase-derived metabolites of 8,9-epoxyeicosatrienoic acid are potent mitogens for cultured rat glomerular mesangial cells. *Biochem Biophys Res Commun*, 191, 282-288.
- (299) Vecchio, A., and Malkowski, M. (2011) The structural basis of endocannabinoid oxygenation by cyclooxygenase-2. *J Biol Chem*, 1-10.
- (300) Kozak, K. R., Rowlinson, S. W., and Marnett, L. J. (2000) Oxygenation of the endocannabinoid, 2-arachidonylglycerol, to glyceryl prostaglandins by cyclooxygenase-2. *J Biol Chem*, 275, 33744-33749.
- (301) Bailey, J. M., Bryant, R. W., Whiting, J., and Salata, K. (1983) Characterization of 11-HETE and 15-HETE, together with prostacyclin, as major products of the cyclooxygenase pathway in cultured rat aorta smooth muscle cells. *J Lipid Res*, 24, 1419-1428.

- (302) Buczynski, M. W., Stephens, D. L., Bowers-Gentry, R. C., Grkovich, A., Deems, R. A., and Dennis, E. A. (2007) TLR-4 and sustained calcium agonists synergistically produce eicosanoids independent of protein synthesis in RAW264.7 cells. *J Biol Chem*, 282, 22834-22847.
- (303) Dennis, E. A., Deems, R. A., Harkewicz, R., Quehenberger, O., Brown, H. A., Milne, S. B., Myers, D. S., Glass, C. K., Hardiman, G., Reichart, D., Merrill, A. H., Jr., Sullards, M. C., Wang, E., Murphy, R. C., Raetz, C. R., Garrett, T. A., Guan, Z., Ryan, A. C., Russell, D. W., McDonald, J. G., Thompson, B. M., Shaw, W. A., Sud, M., Zhao, Y., Gupta, S., Maurya, M. R., Fahy, E., and Subramaniam, S. (2010) A mouse macrophage lipidome. *J Biol Chem*, 285, 39976-39985.
- (304) Norris, P. C., Reichart, D., Dumlao, D. S., Glass, C. K., and Dennis, E. A. (2011) Specificity of eicosanoid production depends on the TLR-4-stimulated macrophage phenotype. *J Leukoc Biol*, 90, 563-574.
- (305) Liu, X., Zhang, S., Arora, J. S., Snyder, N. W., Shah, S. J., and Blair, I. A. (2011) 11-Oxoeicosatetraenoic acid is a cyclooxygenase-2/15-hydroxyprostaglandin dehydrogenase-derived antiproliferative eicosanoid. *Chem Res Toxicol*, 24, 2227-2236.
- (306) Snyder, N. W., Revello, S. D., Liu, X., Zhang, S., and Blair, I. A. (2013) Cellular uptake and antiproliferative effects of 11-oxo-eicosatetraenoic acid. *J Lipid Res*, 54, 3070-3077.
- (307) West, J. D., and Marnett, L. J. (2006) Endogenous reactive intermediates as modulators of cell signaling and cell death. *Chem Res Toxicol*, 19, 173-194.
- (308) Galligan, J. J., Rose, K. L., Beavers, W. N., Hill, S., Tallman, K. A., Tansey, W. P., and Marnett, L. J. (2014) Stable Histone Adduction by 4-Oxo-2-nonenal: A Potential Link between Oxidative Stress and Epigenetics. *J Am Chem Soc*.
- (309) Wang, C., Weerapana, E., Blewett, M. M., and Cravatt, B. F. (2014) A chemoproteomic platform to quantitatively map targets of lipid-derived electrophiles. *Nat Methods*, 11, 79-85.
- (310) Kim, H. Y., Tallman, K. A., Liebler, D. C., and Porter, N. A. (2009) An azido-biotin reagent for use in the isolation of protein adducts of lipid-derived electrophiles by streptavidin catch and photorelease. *Molecular & cellular proteomics : MCP*, 8, 2080-2089.
- (311) Beavers, W. N., Serwa, R., Shimozu, Y., Tallman, K. A., Vaught, M., Dalvie, E. D., Marnett, L. J., and Porter, N. A. (2014) omega-Alkynyl Lipid Surrogates for Polyunsaturated Fatty Acids: Free Radical and Enzymatic Oxidations. *J Am Chem Soc*, 136, 11529-11539.



- (312) Mann, M. (2014) Fifteen years of Stable Isotope Labeling by Amino Acids in Cell Culture (SILAC). *Methods in molecular biology*, 1188, 1-7.
- (313) Deeb, S. J., D'Souza, R. C., Cox, J., Schmidt-Supprian, M., and Mann, M. (2012) Super-SILAC allows classification of diffuse large B-cell lymphoma subtypes by their protein expression profiles. *Molecular & cellular proteomics : MCP*, 11, 77-89.
- (314) Zanivan, S., Krueger, M., and Mann, M. (2012) In vivo quantitative proteomics: the SILAC mouse. *Methods in molecular biology*, 757, 435-450.
- (315) Geiger, T., Cox, J., Ostasiewicz, P., Wisniewski, J. R., and Mann, M. (2010) Super-SILAC mix for quantitative proteomics of human tumor tissue. *Nat Methods*, 7, 383-385.
- (316) Graumann, J., Hubner, N. C., Kim, J. B., Ko, K., Moser, M., Kumar, C., Cox, J., Scholer, H., and Mann, M. (2008) Stable isotope labeling by amino acids in cell culture (SILAC) and proteome quantitation of mouse embryonic stem cells to a depth of 5,111 proteins. *Molecular & cellular proteomics : MCP*, 7, 672-683.
- (317) Ong, S. E., Blagoev, B., Kratchmarova, I., Kristensen, D. B., Steen, H., Pandey, A., and Mann, M. (2002) Stable isotope labeling by amino acids in cell culture, SILAC, as a simple and accurate approach to expression proteomics. *Molecular & cellular proteomics : MCP*, 1, 376-386.
- (318) Udeshi, N. D., Mani, D. R., Eisenhaure, T., Mertins, P., Jaffe, J. D., Clauser, K. R., Hachohen, N., and Carr, S. A. (2012) Methods for quantification of in vivo changes in protein ubiquitination following proteasome and deubiquitinase inhibition. *Molecular & cellular proteomics : MCP*, 11, 148-159.
- (319) Ong, S. E., and Mann, M. (2006) A practical recipe for stable isotope labeling by amino acids in cell culture (SILAC). *Nat Protoc*, 1, 2650-2660.
- (320) Cox, J., and Mann, M. (2008) MaxQuant enables high peptide identification rates, individualized ppb-range mass accuracies and proteome-wide protein quantification. *Nat Biotechnol*, 26, 1367-1372.
- (321) Cox, J., Neuhauser, N., Michalski, A., Scheltema, R. A., Olsen, J. V., and Mann, M. (2011) Andromeda: a peptide search engine integrated into the MaxQuant environment. *J Proteome Res*, 10, 1794-1805.
- (322) Zhang, B., Kirov, S., and Snoddy, J. (2005) WebGestalt: an integrated system for exploring gene sets in various biological contexts. *Nucleic Acids Res*, 33, W741-748.

- (323) Schneider, C. A., Rasband, W. S., and Eliceiri, K. W. (2012) NIH Image to ImageJ: 25 years of image analysis. *Nat Methods*, 9, 671-675.
- (324) Mead, J. F., and Howton, D. R. (1957) Metabolism of essential fatty acids. VII. Conversion of gamma-linolenic acid to arachidonic acid. *J Biol Chem*, 229, 575-582.
- (325) Steinberg, G., Slaton, W. H., Jr., Howton, D. R., and Mead, J. F. (1957) Metabolism of essential fatty acids. V. Metabolic pathway of linolenic acid. *J Biol Chem*, 224, 841-849.
- (326) Michelucci, A., Cordes, T., Ghelfi, J., Pailot, A., Reiling, N., Goldmann, O., Binz, T., Wegner, A., Tallam, A., Rausell, A., Buttini, M., Linster, C. L., Medina, E., Balling, R., and Hiller, K. (2013) Immune-responsive gene 1 protein links metabolism to immunity by catalyzing itaconic acid production. *Proc Natl Acad Sci U S A*, 110, 7820-7825.
- (327) Dikalov, S. (2011) Cross talk between mitochondria and NADPH oxidases. *Free Radic Biol Med*, 51, 1289-1301.
- (328) Groeger, A. L., and Freeman, B. A. (2010) Signaling actions of electrophiles: anti-inflammatory therapeutic candidates. *Mol Interv*, 10, 39-50.
- (329) Sharif, O., Bolshakov, V. N., Raines, S., Newham, P., and Perkins, N. D. (2007) Transcriptional profiling of the LPS induced NF-kappaB response in macrophages. *BMC Immunol*, 8, 1.
- (330) MacGarvey, N. C., Suliman, H. B., Bartz, R. R., Fu, P., Withers, C. M., Welty-Wolf, K. E., and Piantadosi, C. A. (2012) Activation of mitochondrial biogenesis by heme oxygenase-1-mediated NF-E2-related factor-2 induction rescues mice from lethal *Staphylococcus aureus* sepsis. *American journal of respiratory and critical care medicine*, 185, 851-861.
- (331) Cherry, A. D., and Piantadosi, C. A. (2015) Regulation of mitochondrial biogenesis and its intersection with inflammatory responses. *Antioxid Redox Signal*, 22, 965-976.
- (332) Piantadosi, C. A., Withers, C. M., Bartz, R. R., MacGarvey, N. C., Fu, P., Sweeney, T. E., Welty-Wolf, K. E., and Suliman, H. B. (2011) Heme oxygenase-1 couples activation of mitochondrial biogenesis to anti-inflammatory cytokine expression. *J Biol Chem*, 286, 16374-16385.
- (333) Murphy, M. P. (2009) How mitochondria produce reactive oxygen species. *The Biochemical journal*, 417, 1-13.
- (334) Miller, A. F. (2012) Superoxide dismutases: ancient enzymes and new insights. *FEBS Lett*, 586, 585-595.

- (335) Zelko, I. N., Mariani, T. J., and Folz, R. J. (2002) Superoxide dismutase multigene family: a comparison of the CuZn-SOD (SOD1), Mn-SOD (SOD2), and EC-SOD (SOD3) gene structures, evolution, and expression. *Free Radic Biol Med*, 33, 337-349.
- (336) Landino, L. M., Crews, B. C., Timmons, M. D., Morrow, J. D., and Marnett, L. J. (1996) Peroxynitrite, the coupling product of nitric oxide and superoxide, activates prostaglandin biosynthesis. *Proc Natl Acad Sci U S A*, 93, 15069-15074.
- (337) Tao, R., Coleman, M. C., Pennington, J. D., Ozden, O., Park, S. H., Jiang, H., Kim, H. S., Flynn, C. R., Hill, S., Hayes McDonald, W., Olivier, A. K., Spitz, D. R., and Gius, D. (2010) Sirt3-mediated deacetylation of evolutionarily conserved lysine 122 regulates MnSOD activity in response to stress. *Mol Cell*, 40, 893-904.
- (338) Qiu, X., Brown, K., Hirschey, M. D., Verdin, E., and Chen, D. (2010) Calorie restriction reduces oxidative stress by SIRT3-mediated SOD2 activation. *Cell Metab*, 12, 662-667.
- (339) Zhu, Y., Park, S. H., Ozden, O., Kim, H. S., Jiang, H., Vassilopoulos, A., Spitz, D. R., and Gius, D. (2012) Exploring the electrostatic repulsion model in the role of Sirt3 in directing MnSOD acetylation status and enzymatic activity. *Free Radic Biol Med*, 53, 828-833.
- (340) Carlioz, A., and Touati, D. (1986) Isolation of superoxide dismutase mutants in Escherichia coli: is superoxide dismutase necessary for aerobic life? *EMBO J*, 5, 623-630.
- (341) Lebovitz, R. M., Zhang, H., Vogel, H., Cartwright, J., Jr., Dionne, L., Lu, N., Huang, S., and Matzuk, M. M. (1996) Neurodegeneration, myocardial injury, and perinatal death in mitochondrial superoxide dismutase-deficient mice. *Proc Natl Acad Sci U S A*, 93, 9782-9787.
- (342) Visner, G. A., Dougall, W. C., Wilson, J. M., Burr, I. A., and Nick, H. S. (1990) Regulation of manganese superoxide dismutase by lipopolysaccharide, interleukin-1, and tumor necrosis factor. Role in the acute inflammatory response. *J Biol Chem*, 265, 2856-2864.
- (343) Davies, S. S., Amarnath, V., Brame, C. J., Boutaud, O., and Roberts, L. J., 2nd. (2007) Measurement of chronic oxidative and inflammatory stress by quantification of isoketal/levuglandin gamma-ketoaldehyde protein adducts using liquid chromatography tandem mass spectrometry. *Nat Protoc*, 2, 2079-2091.
- (344) Baker, L. M., Baker, P. R., Golin-Bisello, F., Schopfer, F. J., Fink, M., Woodcock, S. R., Branchaud, B. P., Radi, R., and Freeman, B. A. (2007) Nitro-fatty acid reaction with glutathione and cysteine. Kinetic analysis of

thiol alkylation by a Michael addition reaction. *J Biol Chem*, 282, 31085-31093.

- (345) Markesbery, W. R., and Lovell, M. A. (1998) Four-hydroxynonenal, a product of lipid peroxidation, is increased in the brain in Alzheimer's disease. *Neurobiology of aging*, 19, 33-36.
- (346) Porter, N. A. (1986) Mechanisms for the Autoxidation of Polyunsaturated Lipids. *Accounts of Chemical Research*, 19, 262-268.
- (347) Otteneder, M. B., Knutson, C. G., Daniels, J. S., Hashim, M., Crews, B. C., Rimmel, R. P., Wang, H., Rizzo, C., and Marnett, L. J. (2006) In vivo oxidative metabolism of a major peroxidation-derived DNA adduct, M1dG. *Proc Natl Acad Sci U S A*, 103, 6665-6669.
- (348) Marnett, L. J. (1999) Lipid peroxidation-DNA damage by malondialdehyde. *Mutation research*, 424, 83-95.
- (349) Kusunoki, N., Yamazaki, R., and Kawai, S. (2002) Induction of apoptosis in rheumatoid synovial fibroblasts by celecoxib, but not by other selective cyclooxygenase 2 inhibitors. *Arthritis and rheumatism*, 46, 3159-3167.
- (350) Hata, A. N., and Breyer, R. M. (2004) Pharmacology and signaling of prostaglandin receptors: multiple roles in inflammation and immune modulation. *Pharmacol Ther*, 103, 147-166.
- (351) Yao, C., Sakata, D., Esaki, Y., Li, Y., Matsuoka, T., Kuroiwa, K., Sugimoto, Y., and Narumiya, S. (2009) Prostaglandin E2-EP4 signaling promotes immune inflammation through Th1 cell differentiation and Th17 cell expansion. *Nat Med*, 15, 633-640.
- (352) Aldrovandi, M., Hammond, V. J., Podmore, H., Hornshaw, M., Clark, S. R., Marnett, L. J., Slatter, D. A., Murphy, R. C., Collins, P. W., and O'Donnell, V. B. (2013) Human platelets generate phospholipid-esterified prostaglandins via cyclooxygenase-1 that are inhibited by low dose aspirin supplementation. *J Lipid Res*, 54, 3085-3097.
- (353) Kozak, K. R., Prusakiewicz, J. J., Rowlinson, S. W., Schneider, C., and Marnett, L. J. (2001) Amino acid determinants in cyclooxygenase-2 oxygenation of the endocannabinoid 2-arachidonylglycerol. *J Biol Chem*, 276, 30072-30077.
- (354) Manna, J. D., Wepy, J. A., Hsu, K. L., Chang, J. W., Cravatt, B. F., and Marnett, L. J. (2014) Identification of the major prostaglandin glycerol ester hydrolase in human cancer cells. *J Biol Chem*, 289, 33741-33753.
- (355) Aluri, H. S., Simpson, D. C., Allegood, J. C., Hu, Y., Szczepanek, K., Gronert, S., Chen, Q., and Lesnefsky, E. J. (2014) Electron flow into

cytochrome c coupled with reactive oxygen species from the electron transport chain converts cytochrome c to a cardiolipin peroxidase: role during ischemia-reperfusion. *Biochim Biophys Acta*, 1840, 3199-3207.

- (356) Sherer, T. B., Betarbet, R., Testa, C. M., Seo, B. B., Richardson, J. R., Kim, J. H., Miller, G. W., Yagi, T., Matsuno-Yagi, A., and Greenamyre, J. T. (2003) Mechanism of toxicity in rotenone models of Parkinson's disease. *The Journal of neuroscience : the official journal of the Society for Neuroscience*, 23, 10756-10764.
- (357) Tanner, C. M., Kamel, F., Ross, G. W., Hoppin, J. A., Goldman, S. M., Korell, M., Marras, C., Bhudhikanok, G. S., Kasten, M., Chade, A. R., Comyns, K., Richards, M. B., Meng, C., Priestley, B., Fernandez, H. H., Cambi, F., Umbach, D. M., Blair, A., Sandler, D. P., and Langston, J. W. (2011) Rotenone, paraquat, and Parkinson's disease. *Environ Health Perspect*, 119, 866-872.
- (358) Alam, M., and Schmidt, W. J. (2002) Rotenone destroys dopaminergic neurons and induces parkinsonian symptoms in rats. *Behavioural brain research*, 136, 317-324.
- (359) Abou-Sleiman, P. M., Muqit, M. M., and Wood, N. W. (2006) Expanding insights of mitochondrial dysfunction in Parkinson's disease. *Nat Rev Neurosci*, 7, 207-219.
- (360) Greenamyre, J. T., MacKenzie, G., Peng, T. I., and Stephans, S. E. (1999) Mitochondrial dysfunction in Parkinson's disease. *Biochemical Society symposium*, 66, 85-97.
- (361) Trnka, J., Blaikie, F. H., Smith, R. A., and Murphy, M. P. (2008) A mitochondria-targeted nitroxide is reduced to its hydroxylamine by ubiquinol in mitochondria. *Free Radic Biol Med*, 44, 1406-1419.
- (362) Shaw, G., Morse, S., Ararat, M., and Graham, F. L. (2002) Preferential transformation of human neuronal cells by human adenoviruses and the origin of HEK 293 cells. *FASEB journal : official publication of the Federation of American Societies for Experimental Biology*, 16, 869-871.
- (363) Lim, G. P., Calon, F., Morihara, T., Yang, F., Teter, B., Ubeda, O., Salem, N., Jr., Frautschy, S. A., and Cole, G. M. (2005) A diet enriched with the omega-3 fatty acid docosahexaenoic acid reduces amyloid burden in an aged Alzheimer mouse model. *The Journal of neuroscience : the official journal of the Society for Neuroscience*, 25, 3032-3040.
- (364) Prickett, J. D., Robinson, D. R., and Steinberg, A. D. (1981) Dietary enrichment with the polyunsaturated fatty acid eicosapentaenoic acid prevents proteinuria and prolongs survival in NZB x NZW F1 mice. *The Journal of clinical investigation*, 68, 556-559.

- (365) Rudel, L. L., Kelley, K., Sawyer, J. K., Shah, R., and Wilson, M. D. (1998) Dietary monounsaturated fatty acids promote aortic atherosclerosis in LDL receptor-null, human ApoB100-overexpressing transgenic mice. *Arteriosclerosis, thrombosis, and vascular biology*, 18, 1818-1827.
- (366) Taki, H., Nakamura, N., Hamazaki, T., and Kobayashi, M. (1993) Intravenous injection of tridihomo-gamma-linolenoyl-glycerol into mice and its effects on delayed-type hypersensitivity. *Lipids*, 28, 873-876.
- (367) Vinh, A., Chen, W., Blinder, Y., Weiss, D., Taylor, W. R., Goronzy, J. J., Weyand, C. M., Harrison, D. G., and Guzik, T. J. (2010) Inhibition and genetic ablation of the B7/CD28 T-cell costimulation axis prevents experimental hypertension. *Circulation*, 122, 2529-2537.